Title

Development of Selective C—C and C—N Bond-Forming Reactions Using Metals and Enzymes

ISBN

9798288863233

Author

Nicolai, Jeremy

Publication Date

2025-05-15

Peer reviewed|Thesis/dissertation

Development of Selective C–C and C–N Bond-Forming Reactions Using Metals and Enzymes

By

Jeremy Nicolai

A dissertation submitted in partial satisfaction of the

requirements for the degree of

Doctor of Philosophy

in

Chemistry

in the

Graduate Division

of the

University of California, Berkeley

Committee in Charge:

Professor John F. Hartwig, Chair

Professor Richmond Sarpong

Professor Alexis T. Bell

Spring 2025

Abstract

Development of Selective C–C and C–N Bond-Forming Reactions Using Metals and Enzymes

by

Jeremy Nicolai

Doctor of Philosophy in Chemistry

University of California, Berkeley

Professor John F. Hartwig, Chair

The following Dissertation discusses the use of transition metals to enable the installation and modification of benzylic difluoromethylene units and the use of homogenous, heterogenous, and chemo-enzymatic catalysts to enable the selective functionalization of olefins.

Chapter 1 reviews recent applications of biocatalysis in the pharmaceutical industry during the period 2020–2025. The application of biocatalysis to industrial chemistry has been a longstanding challenge, and has been historically limited due to the small amounts of enzyme that were typically available. Over the last 70 years, major advances in technology in the fields of proteomics, enzyme engineering, chemical biology, and process engineering have reduced the barrier to entry for the use of biocatalysis. These technological improvements have enabled the efficient and sustainable synthesis biocatalysts that are capable of transformations relevant to the synthesis of active pharmaceutical ingredients, key intermediates, and valuable chemical building blocks under mild, often aqueous conditions and with minimal environmental impact. Case studies; including the synthesis of Esomeprazole, Nemtabrutinib, Belzutifan, Molnupiravir, and Uvelostinag; illustrate the transformation of traditional chemical manufacturing routes into processes that integrate biocatalytic transformations. These examples, and others, highlight the successful application of enzymes to the synthesis of biologically-active compounds in the pharmaceutical industry. Key to the success of biocatalytic methods is the strategic use of enzyme engineering to enhance activity and selectivity, and the development of robust multi-enzyme cascades that streamline manufacturing while reducing waste and energy demand.

Chapter 2 describes the development of a sequential chemoenzymatic method to form linear, primary amines from olefins. Methods that form amines from feedstock chemicals are an important component of industrial chemistry. Many methods for the synthesis of amines yield mixtures of primary, secondary, and tertiary amines, necessitating costly downstream separations. We present a chemoenzymatic approach to hydroaminomethylation that addresses these challenges by combining hydroformylation catalyzed by a phosphine-bound rhodium complex with enzymatic transamination catalyzed by an ω-transaminase from *Vibrio fluvialis* (*Vf*TA). This sequential chemoenzymatic hydroaminomethylation reaction converts olefins to linear primary amines with high regioselectivity and chemoselectivity for the linear primary amine, and we demonstrate that this process occurs with a series of olefins with varying structures. Furthermore, we report progress toward a tandem process that incorporates a biocatalytic cascade for recycling an intermediate amine donor, which is required for the transaminase enzyme to use an ammonium salt as the terminal nitrogen source. This study illustrates the potential to combine chemo- and biocatalytic

reactions to produce valuable materials from readily available feedstocks in both tandem and sequential processes, with selectivities that have not been achieved with transition-metal catalysts.

Chapter 3 describes the development of a tandem chemoenzymatic method to achieve the synthesis of linear, primary amines from olefins using feedstock reagents and mild conditions. Linear primary amines serve as crucial building blocks in pharmaceuticals, fine chemicals, polymers, and surfactants. Despite their importance, conventional methods for the synthesis of linear primary amines often suffer from overalkylation and the requirement for elevated temperatures and pressures. Herein, we report a tandem chemoenzymatic hydroaminomethylation strategy that converts terminal olefins into linear primary amines under mild conditions by integrating a Rh/DPPon-catalyzed hydroformylation performed in surfactant micelles with a wild-type ω-transaminase from wild-type *Vibrio fluvialis* (WT-*Vf*TA) and an amine donor recycling system composed of wild-type alanine dehydrogenase (WT-AlaDH) and wild-type glucose dehydrogenase (WT-GDH) enzymes. This cooperative cascade uses inexpensive feedstock reagents—including ammonium salts, alanine, carbon monoxide, hydrogen, and glucose—to achieve high selectivity for primary amines without the formation of secondary and tertiary amine byproducts. Moreover, the system's versatility is demonstrated by the synthesis of ^{15}N-labeled primary amines and biologically relevant compounds containing linear primary amines, underscoring the potential of this integrated tandem process and other chemoenzymatic methods for applications ranging from medicinal chemistry to industrial manufacturing.

Chapter 4 describes the development of a copper-mediate C–C bond-forming reaction that installs a cyanodifluoromethyl group in the place of (hetero)aryl iodides and bromides. The cyanodifluoromethyl group is unique because its size is closer than that of any other substituted difluoromethyl group to the size of the trifluoromethyl group, but its electronic properties are distinct from those of the trifluoromethyl group. In addition, the presence of the cyano group provides synthetic entry to a wide range of substituted difluoromethyl groups. However, the synthesis of cyanodifluoromethyl compounds requires multiple steps, highly reactive reagents (such as DAST, NSFI, or IF_5), or specialized starting materials (such as α,α-dichloroacetonitriles or α-mercaptoacetonitriles). Herein, we report a copper-mediated cyanodifluoromethylation of aryl and heteroaryl iodides and activated aryl and heteroaryl bromides with $TMSCF_2CN$. This cyanodifluoromethylation tolerates an array of functional groups, is applicable to late-stage functionalization of complex molecules, yields analogues of FDA-approved pharmaceuticals and fine chemicals, and enables the synthesis of a range of complex molecules bearing a difluoromethylene unit by transformations of the electron-poor CN unit. Calculations of selected steps of the reaction mechanism by Density Functional Theory indicate that the barriers for both the oxidative addition of iodobenzene to $[(DMF)CuCF_2CN]$ and the reductive elimination of the fluoroalkyl product from the fluoroalkyl copper intermediate lie in between those of $[(DMF)CuCF_3]$ and $[(DMF)CuCF_2C(O)NMe_2]$.

Chapter 5 describes the development of a palladium-catalyzed desymmetrization reaction of benzylic difluoromethylene units. Molecules containing fluorine are widespread in modern materials, agrochemicals, and pharmaceuticals because the inclusion of fluorine in a molecule can beneficially modulate the physiochemical properties of the parent molecule. Stereocenters bearing fluorine are particularly valuable as bio-isosteres of alcohols and of C(sp^3)-H bonds. Preparing different isomers of secondary and tertiary benzylic fluorides can affect molecular conformation and modulate biological activity; however, synthesizing these chiral alkyl fluorides from non-chiral starting materials is challenging. We report a palladium-catalyzed desymmetrization strategy

for the alkylation of (hetero)aryl-α,α-difluoromethylene units that enables the synthesis of enantioenriched 2° and 3° C(sp^3) stereocenters bearing fluorine. The use of $Ba(OTf)_2$ as Lewis acid, Li*O*t*Bu as base, and the novel germanium-containing bisphosphine ligand (*R*)-DTMGM-BINAP (DTMGM = 3,5-(trimethylgermanyl)-4-methoxyphenyl), enables the desymmetrization of (hetero)aryl-α,α-difluorides in high yields and in high enantioselectivities under mild conditions. We demonstrate that a wide range of carbon nucleophiles and a wide range of benzylic difluorides react under the developed conditions. Additionally, the use of a masked acyl cyanide nucleophile enables rapid functionalization of the fluorinated products to form stereo-defined α-fluorinated carbonyl compounds.

Acknowledgements

Obtaining a PhD in chemistry from UC Berkeley is an honor, and I would not have been able to achieve this goal without the support of a large cast of impactful people. While I cannot thank everyone who has helped, influenced, or inspired me along my journey (there simply is not enough room on the page), I will do my best to thank as many of those individuals as I can. Nonetheless, it goes without saying that this list is incomplete.

First and foremost, I want to thank my parents, Jim Nicolai and Erin Whitney. Without their tireless patience and unending support during my entire journey, I would not be where I am today. I cannot thank you enough for everything you have sacrificed for me and for my brother over the years, but I can express my gratitude. *Thank you.*

I thank my late Aunt Nancy, whose PhD celebration party I remember fondly, for earnestly sharing her love of nature with all who would listen. I thank my late grandparents, Art and Glennis Nicolai, for their love and support, and for the letters we sent back and forth while I was an undergraduate student at UT Austin. To my extended family: Jon Berman, Greg and Pam Rudebusch, Sara and Michael Miller, my grandmother Arlis White; and my cousins Rachel, Brook, Mitchell, and Carly; thank you for celebrating the milestones in my life, and for supporting me from coast to coast. Literally.

Graduate school is challenging, and without my beautiful, brilliant, loving partner, Caitilin Vaille, it would have been a journey fraught with countless more difficulties. I am grateful for your support each and every day. I am inspired by your joy in the face of fear, your strength in the face of despair, and your love in the face of grief, to be to be the best version of myself that I can be. I cannot wait to write more chapters of our story together.

I would also like to thank the myriads of talented chemists that have inspired me along the way. First, I must thank both of my mentors in the Krische Lab, Dr. James Cabrera and Dr. Nancy Hyunh. Not only did they teach me the techniques that have served me well throughout my graduate career, but they also showed me what effective, positive mentorship looks like, and opened my eyes to the possibility of going to graduate school. I would be remiss to not mention Terry Crawford, my manager at Genentech, who helped me to grow and learn in an industrial setting. My experience at Genentech was truly life-changing, and showed me why I wanted to go to grad school – to be in an energetic, innovative, and caring environment like the one at Genentech.

I would not have made it through the gauntlet of graduate school if it were not for the spectacular people and chemists that make the Hartwig group greater than the sum of its parts. Specifically, I would like to thank John Brunn and Christina Pierson for the many conversations we have had about chemistry, life, and everything in-between. If not for our coffee breaks (even if we were already caffeinated) and for the support and advice that both JB and Christina have provided to me, I would not be the person or chemist that I am today. I would be remiss if I did not thank the other members of my cohort; Nico Ciccia, Jenna Manske, and Isaac Joyner; for their support, mentorship, and advice over the years.

My time here has also been enriched by several visiting and post-doctoral scholars. I cannot thank Dr. Nils Ansmann, Dr. Tommaso Fantoni, Teresa Horak, Prof. Connor Delaney, and Prof. Masha

Elkin enough for the friendship, energy, and humor that they brought to Latimer Hall, and for teaching me so much about chemistry, friendship, and the world at large.

Finally, I want to thank all the members of Latimer 707 – my home for five years – for keeping morale high despite a severe lack of windows. To the other members of the Hartwig group that I have not mentioned, thank you for making the lab an exciting place to be.

Table of Contents

CHAPTER ONE

Recent Developments in Biocatalysis in the Pharmaceutical Industry (2020 – 2025)

1.1 Abstract

The application of biocatalysis to industrial chemistry has been a longstanding challenge, and has been historically limited due to the small amounts of enzyme that were typically available. Over the last 70 years, major advances in technology in the fields of proteomics, enzyme engineering, chemical biology, and process engineering have reduced the barrier to entry for the use of biocatalysis. These technological improvements have enabled the efficient and sustainable synthesis biocatalysts that are capable of transformations relevant to the synthesis of active pharmaceutical ingredients, key intermediates, and valuable chemical building blocks under mild, often aqueous conditions and with minimal environmental impact. Case studies; including the synthesis of Esomeprazole, Nemtabrutinib, Belzutifan, Molnupiravir, and Uvelostinag; illustrate the transformation of traditional chemical manufacturing routes into processes that integrate biocatalytic transformations. These examples, and others, highlight the successful application of enzymes to the synthesis of biologically-active compounds in the pharmaceutical industry. Key to the success of biocatalytic methods is the strategic use of enzyme engineering to enhance activity and selectivity, and the development of robust multi-enzyme cascades that streamline manufacturing while reducing waste and energy demand.

1.2 Introduction

In the past 70 years, the field of biochemistry has advanced to the point that enzymes are now used in large-scale applications for the bulk synthesis of fine chemicals. The industrial adoption of methods that harness the selectivity and reactivity of enzymes has been aided by the development of new technologies that have made the discovery and production of new enzymes viable for the chemical industry. This chapter will examine recent implementations of biocatalysis in the pharmaceutical industry from 2020 – 2025. This chapter also will summarize technologies that have allowed for the adoption of such techniques in an industrial setting and examine several case studies involving the large-scale application of biocatalysis for the synthesis of active pharmaceutical ingredients (APIs), of intermediates, and of chemical building blocks.

Environmental considerations have increasingly influenced the direction of industrial chemistry since the introduction of the concept of green chemistry in the 1990s.[1-2] Hazardous reagents and multi-step chemical sequences are now being replaced with streamlined enzymatic cascades that lower process mass intensity, input cost, and energy expenditure. The use of engineered enzymes under mild aqueous conditions also reduces the need for organic solvents and typically simplifies purification procedures. These greener pathways also contribute to a safer working environment and improved sustainability, aspects that have received growing attention from regulatory bodies and industry alike.[3-4]

More recently, advances in automation, high-throughput screening, and computational modeling have markedly accelerated the discovery and development of novel biocatalysts (see section 1.2). Integrated workflows combine automated reaction setup, data collection, and data analysis with deep-learning–driven structure prediction to generate enzyme variants that exhibit improved stability and selectivity. Interdisciplinary collaborations among chemists, molecular biologists, and engineers have enabled rapid cycle times in design, evolution, and testing, which, together with innovations in enzyme engineering, continuous-flow processing, and advanced cofactor recycling strategies, promise further transformation of industrial synthesis. These developments have

streamlined process optimization and reduced reliance on traditional, resource-intensive methods, while improvements in enzyme immobilization and cascade reactions have enabled scalable processes that maintain high stereoselectivity and yield. Such robust methodologies are expected to extend the use of biocatalysis into earlier stages of pharmaceutical development and fine chemical manufacturing,[5] thereby supporting a transition to more sustainable, cost-effective production practices in the chemical industry.

1.3 Historical Context for the Adoption of Biocatalysis in Industry

1.3.1 Technological Advancements that Enabled Wider Adoption

Since the 1833 discovery of the enzyme "diastase" by Payen and Persoz,[6] the field of biocatalysis has advanced considerably. The 1897 discovery by Buchner that enzymes can perform biochemical transformations outside of their host cell (described as "cell-free fermentation"),[7-8] and the discovery by Harden[9] and von Euler-Chelpin[10] that these fermenting enzymes are dependent on phosphate and a "cozymase," improved our understanding of enzymes and how they function. It was not until 1926—nearly 100 years since the discovery of diastase—that James Sumner crystallized an enzyme, urease, for the first time, and confirming that enzymes are a type of protein.[11] Sumner and Northrop soon crystallized a series of enzymes, among them pepsin and chymotrypsin,[12] lending structural knowledge to the field of biochemistry. By the late 1940s a series of enzymes had been structurally characterized, but the mechanism by which they accomplished chemical transformations remained unknown.[13] In 1951, the amino acid sequence of insulin was determined by Sanger, showing with certainty for the first time that proteins, and therefore enzymes, were composed of a well-defined sequence of amino acids.[14-15]

Early attempts to adapt biocatalysis to industry were severely limited by the small quantities of enzyme available, the substrate specificity of wild-type (WT) enzymes, and an inability to systematically modify the amino acid sequence of enzymes catalysts. In the 1950s, the technique of enzyme immobilization was developed, allowing for the reuse and recycling of enzymes without a loss of their activity.[13] This technology allowed for a reduction in the quantity of enzyme required for chemical transformations, making the overall process more economically viable. By the 1970s, the use of immobilized glucose isomerase had become the dominant method for the conversion of dextrose to fructose in the synthesis of high-fructose corn syrup.[16] The widespread use of biocatalysis in industry, however, was still limited by the amount of enzyme that was able to be produced and the substrate specificity of WT enzymes.

Beginning in the mid twentieth century, molecular biologists began researching and developing new methods for the transmission and transcription of genetic information. In the 1960s, it was found that DNA encodes amino acid sequences and that amino acid sequence alone determines the structure of proteins.[17] These findings set the stage for systematic structural modification of enzymes if adequate molecular biology and analytical tools could be developed. More efficient methods of genome sequencing were soon developed, including capillary electrophoresis.[18] Also of impact was the invention of dyes based on energy transfer,[19-20] not radioactivity. These technologies enabled the automated high-throughput sequencing of DNA. In the early 2000s, next generation sequencing (NGS) techniques were introduced that took advantage of the growing power of computers to more efficiently and rapidly sequence genomes,[21] resulting in a precipitous

drop in the price of DNA sequencing and a lower barrier to entry for companies considering biocatalysis.

The research of the mid twentieth century also led to the discovery of restriction enzymes, which soon become invaluable in the development of recombinant DNA technologies.[22] Recombinant DNA techniques rely upon the action of DNA ligase, guided by restriction enzymes, to allow researchers to cut and paste DNA fragments into a larger sequence.[23] These DNA sequences can then be implanted into an organism, such as *E. coli*; the proteins encoded in those DNA sequences can then be expressed by that organism. This process, the propagation of recombinant DNA in a new host, is known as cloning. Further developments in the 1980s resulted in strains of *E. coli* that contained a T7 promoter, which allows for amplified and selective expression of the inserted DNA.[24]

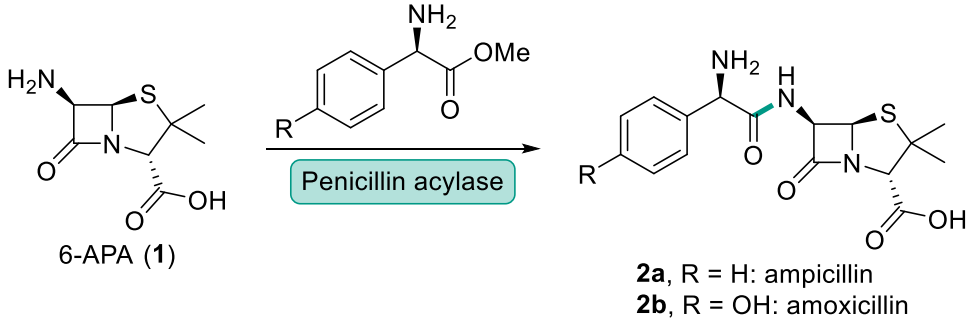

Figure 1.1. Use of penicillin acylase to synthesize beta-lactam antibiotics from 6-APA (**1**).

With new proteomic and molecular biology tools available, the genome of a new enzyme could now be rapidly discovered, sequenced, and cloned. Human insulin, the first recombinant protein to be produced in 1978, began commercial-scale production in 1982.[25] This production allowed for the supply of insulin to become stable becuase it was no longer derived from livestock animals.[13] In addition, these new techniques, in combination with enzyme immobilization, allowed for the enzyme penicillin acylase (PA) to be produced using recombinant methods by 1979 in industrially-relevant quantities. The increased production of PA lowed the price, enabling the application of PA to the synthesis penicillin-type antibiotics (Figure 1.1) such as ampicillin (**2a**) or amoxicillin (**2b**) from 6-aminopenicillanic acid (6-APA, **1**).[26-27] Throughout this chapter, enzymes that have undergone rounds of enzyme engineering from an initial WT or commercial starting enzyme will be highlighted in gold, while enzymes used without modification will be highlighted in teal. In addition, the stereocenter(s) and bond(s) formed by biocatalytic methods will be either highlighted (for stereocenters) or bold (for bonds) and colored teal.

Despite the advances in genomics and analytical methods available to study and clone natural enzymes, tools for the selective modification of these enzymes were lacking. Despite their utility, WT enzymes are often unsuitable for industrial chemistry because of a lack of thermostability, incompatibility with organic solvents, and low reactivity with non-native substrates. Initial efforts to modify enzymes employed mutagenesis induced by radiation or chemical reagents, followed by phenotypic screening of the resulting enzymes for the desired activity.[28] These methods for introducing random mutations into the DNA were slow, imprecise, and difficult to control. In 1978, Smith and coworkers introduced site-directed mutagenesis, enabling the targeted introduction of DNA mutations, which allowed for thorough investigation of the role of catalytic residues in enzymes.[29] The development of the polymerase chain reaction (PCR) by Mullis and coworkers in

the 1980s enabled researchers to copy a DNA "template" and produce a large number of copies of that template.[30] By adjusting the polymerase, random mutations could be introduced to the template copies to provide a large number of variants of the enzyme; this techniques is known as error-prone PCR (epPCR).

The technique of epPCR was employed to enable the breakthrough of directed evolution. First reported by Arnold and coworkers in 1993,[31] directed evolution enabled the selection of enzyme variants with improved properties by iterative rounds of random mutations, created by epPCR, and phenotypic screening of the resulting variants. The best performing variants from the first round were then subjected to a second round of epPCR, and the process was continued until the desired outcome was achieved. Directed evolution allowed for the relatively rapid and semi-rational creation of enzymes with increased activity, stability, and reactivity with non-native substrates and of enzymes that could tolerate organic solvents or catalyze reactions not known to nature. In 2018, Frances Arnold received the Nobel Prize in Chemistry for the development of directed evolution. The ability to evolve enzymes rapidly and cheaply for a specific function opened the doors to more extensive use of enzymes in industry.

For newly emerging technologies to be implemented widely and at scale, they must accelerate the design-evolve-test cycle of developing biocatalysts while simultaneously lowering the cost to do so. Computer-aided *de novo* protein design is one emerging technology poised to accelerate biocatalyst discovery by reducing the amount of time spent on the design and evolve phases of the cycle. The *de novo* design of proteins and the *de novo* prediction of protein structures by computational methods have been sought for many years, and some computational models, often, are now on par with the spatial accuracy of protein structures determined experimentally using X-ray diffraction.[32] Particularly, the recent development and implantation of deep-learning models has aided the advancement of *de novo* protein design and structure prediction. There are now several software packages, some of which are freely available, that are capable of these types of *de novo* predictions, such as AlphaFold,[33-34] Rosetta3,[35] and RFdiffusion.[36]

AlphaFold, developed by Google DeepMind and currently in its third iteration, has consistently demonstrated much higher accuracies (typically within 1.5 A for all atoms) than competing software packages (typically within 3.5 A for all atoms).[33] AlphaFold3 makes end-to-end structure predictions, meaning it predicts the structure of a protein based on a sequential reading of the amino acid sequence using a single neural network with multiple layers that can cross-communicate. DeepMind's approach, when compared to the traditional approach of using multiple neural networks, shortened the amount of time required for structure prediction of small protein fragments (hundreds of residues) from hours to minutes,[33] and it was used to predict the structure of the human proteome (98.5% of human proteins, approximately 12 million residues[37]) in 930 GPU days.[38] AphaFold3 is also capable of modeling complex interactions (protein-ligand, protein-nucleic acid, antibody-antigen, etc.) with accuracies that rival other, more specialized computational biology tools.[39]

Another tool— the Rosetta software suite—was originally developed by Baker and coworkers at the University of Washington for the *de novo* design of protein structures.[40] This software has since expanded to a GUI-based package capable of structure prediction, the modeling of protein-ligand interactions, and other advanced features. The modern implementation, RoseTTAfold,[41] employs deep learning techniques inspired by those developed by DeepMind and exhibits large improvements in speed and efficiency over its predecessor(s). As a powerful demonstration of its

utility, RoseTTAfold was used to design Top7,[42] a 93-residue protein containing a fold structure unknown to nature. The gene sequence for Top7 was then inserted into a plasmid and expressed in *E. coli*; subsequent recrystallization and X-ray diffraction of the protein showed remarkable agreement between the computational and experimental structures of Top7.[42]

The continued development of computational tools like RoseTTAfold and AlphaFold will continue to increase the efficiency and speed of computational protein structure prediction, allowing for the increased integration of biocatalysis into the production of industrial and fine chemicals. In recognition of their groundbreaking work, the 2024 Nobel Prize in chemistry was awarded to David Baker of UW Madison "for computational protein design," along with Demis Hassabis and John Jumper of Google DeepMind "for protein structure prediction."[43]

The discovery of new endonucleases and other enzymes will most likely utilize high-throughput assay technology to rapidly assess the outcome of experiments. High-throughput technologies have become widely utilized in the pharmaceutical industry, from early discovery to process development, and have allowed for the rapid identification of optimal reaction conditions for chemical[44] and biocatalytic[45] reactions alike. These high-throughput methods, when combined with emerging fields of automation,[46] microfluidics,[47] and robotics[48] in chemistry, have the potential to rapidly increase the pace and decrease the cost of biocatalyst discovery, design, and testing. There are now many well-established companies, such as Codexis[49] in the U.S. and Novonesis in Denmark,[50] which provide robust biocatalysis development services, further lowering the barrier to entry for companies who are willing to outsource the development of such catalysts.

1.3.2 Early Applications of Biocatalysis in Industry

As of the 1940s, only a limited number of processes catalyzed by enzymes had been developed. For example, in 1949, 26 million pounds of citric acid was produced in the United States, almost exclusively by fermentation using the fungus *A. niger*.[13] In addition, in the 1934 patent for the synthesis of the decongestant L-ephedrine, an enzymatic cascade with whole yeast as a catalyst for the condensation of acetaldehyde (derived *in situ* from glucose) with benzaldehyde was disclosed.[51] This procedure is still used today, showing the power of a highly optimized biocatalytic method.[52]

The adoption of biocatalytic methods began to accelerate in the 1990s, alongside the rapid development of new techniques in molecular biology, genomics, and enzyme engineering (see *section 1.2.2*). In addition, the growing global consensus on the value of environmental conservation led to an interest in "green chemistry,"[53] with the 12 principles of green chemistry[2] still used today introduced by Anastas and Warner in 1998.[1] Biocatalysis has long been viewed as an ideal solution to achieving the lofty goals required to render industrial and fine chemical synthesis environmentally sustainable. These goals include the prevention of waste instead of waste remediation, the design of atom-economical routes that utilize non-toxic and environmentally benign reagents, the use of renewable feedstocks, and an emphasis on catalysis, analytical method development, and avoiding harmful end-of-life breakdown products. Biocatalysts often operate under mild reaction conditions in aqueous environments and can be engineered to react with high turnover numbers (TONs), selectivity, and chemical robustness. In

addition, the enzymes used for biocatalysis and many of their inputs (glucose, alanine, etc.) and outputs (gluconolactone, oxalic acid, etc.) are environmentally benign and renewable.

These technological and societal innovations set the stage for the widespread adoption of biocatalytic methods in the pharmaceutical industry. Between 2010 and 2020, the syntheses of atorvastatin[54] (Lipitor) and sitagliptin[55] (Januvia) on commercial scales by Pfizer and Merck, respectively, employed engineered enzymes to great effect. These examples demonstrated the utility of biocatalysis in large-scale drug production, and demonstrated how biocatalysis could be used to reduce production costs and to reduce the impact of fine chemical synthesis on the environment.

1.4 Applications in the Pharmaceutical Industry and Case Studies, 2020 – 2025

Section 1.4 will present case studies of the adoption of biocatalysis in (discovery) process chemistry in the pharmaceutical industry disclosed from 2020 to 2025. The evolution of the synthetic routes towards five lead compounds that have either been approved by the FDA or are currently undergoing clinical trials will be examined as they evolved to include biocatalytic transformations. These examples highlight the transformative role of biocatalysis in the large-scale synthesis of complex molecules.

1.4.1 Esomeprazole – Disclosed 2021

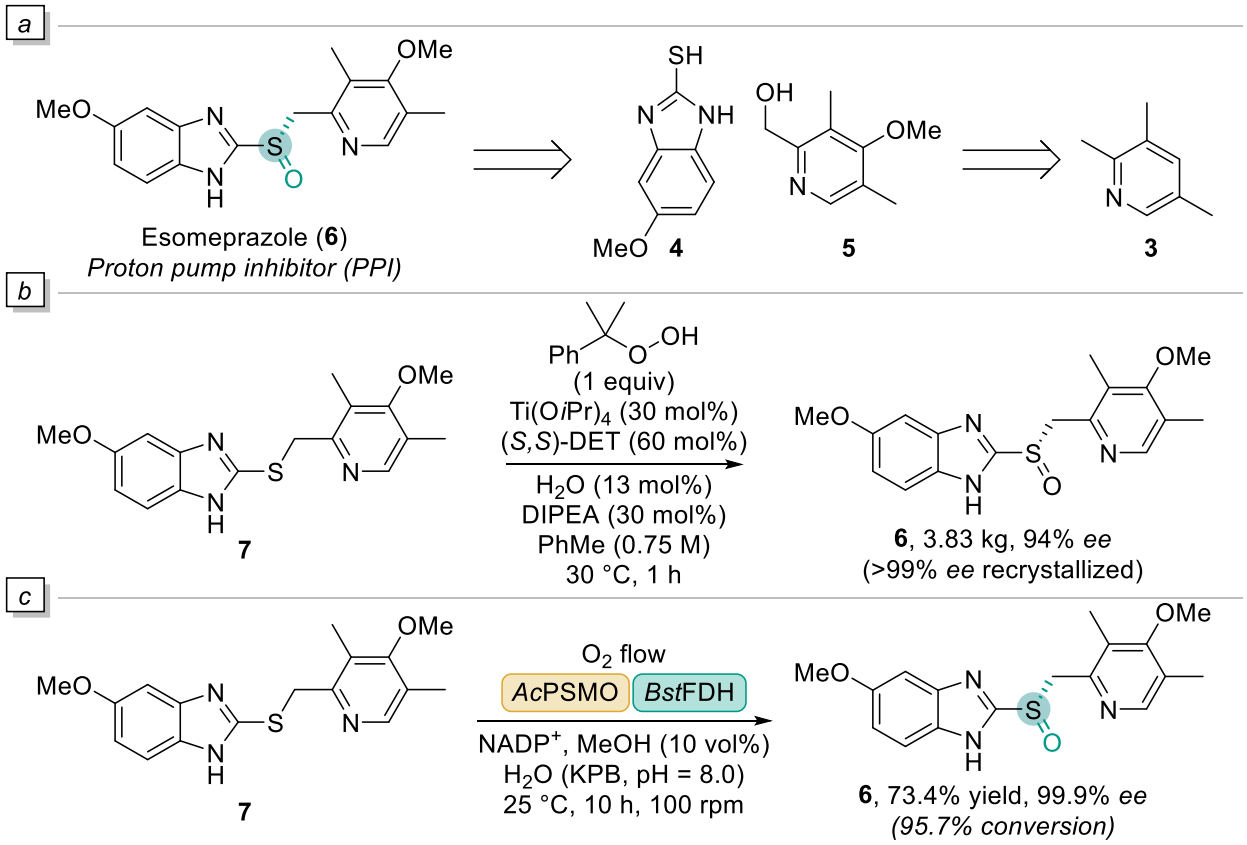

Figure 1.2. (a) Structure and retrosynthesis **6**, (b) initial process route for the oxidation of **7**, and (c) biocatalytic process for the oxidation of **7**.

Esomeprazole (**6**) is a proton pump inhibitor (PPI) marketed by AstraZeneca that is used to treat gastroesophageal reflux disease (Figure 1.2a). The initial synthetic route prior to the introduction of biocatalysis involved the synthesis of tetrasubstituted pyridine **5** from pyridine **3**. Pyridine **5** was then coupled with thiol **4** by an S_NAr reaction. Esomeprazole (**6**) was produced from the intermediate thioester **7** *via* a titanium-catalyzed asymmetric oxidation reaction with (*S,S*)-DET (DET = diethyl tartrate) as the chiral ligand and cumyl hydroperoxide as the oxidant (Figure 1.2b).[56] Despite the high enantioselectivity observed, this process had a number of shortcomings on process scale; for example, formation of the titanium catalyst required precise conditions, a high *%ee* required high catalyst loadings for the process to be robust, the enantioselectivity of the transformation was sensitive to the concentration of water, and the waste generated from the reaction included organic solvent, peroxides, and heavy metals.

To overcome the shortcomings of the metal-catalyzed route and to develop a more environmentally-benign oxidation method, scientists at Jiangsu Aosaikang Pharmaceutical Co., Ltd., and the East China University of Science and Technology (ECUST) sought to develop a biocatalytic method for the synthesis of non-racemic, chiral sulfoxides using molecular oxygen as the oxidant and water as solvent (Figure 1.2c.[57] The researchers used structure-based protein engineering to create a variant of cyclohexane monooxygenase enzyme from *Acinetobacter calcoacetius* (*Ac*PSMO) that had been modified to accept the pyrmetazole starting material **7**.

The authors identified several challenges to the scale-up of this biocatalytic process. First, the NADPH cofactor required by *Ac*PSMO is economically prohibitive to use in stoichiometric quantities; therefore, the authors chose an NADP+/NADPH recycling system wherein a formate dehydrogenase enzyme from *Bacillus megaterium* (*Bst*FDH) regenerates NADPH from NADP+ when exposed to sodium formate, releasing CO_2 as the byproduct. Because **7** is poorly soluble in water (<0.1 g/L), an organic cosolvent was required. The researchers used 10% MeOH (v/v) as the cosolvent beause it solubilized the substrate (0.27 g/L), did not denature the enzymes, and had a boiling point low enough that evaporation of the solvent was would occur below the decomposition temperature of the product **6** (40 °C). The initial reactions were developed on a 10 mL scale; when scaled to 1.0 L scale, a conversion of only 48.9% was observed, compared to 98.5% on 10 mL scale. When investigating in detail the parameters of the reaction, the authors found that the mass transfer of oxygen into the aqueous media limited the rate of the enzymatic reaction. This challenge was overcome by adjusting the flow rate of oxygen and the stirring speed. The authors also found significant deactivation of *Ac*PSMO over the course of the reaction, as well as degradation of NADP+ under alkaline conditions (pH = 9.0); thus, an operating pH of 8.0 was selected. With these modifications, the scale of the biocatalytic reaction was increased to 300 L, while achieving a conversion of 95.9%. The resulting product was extracted from the reaction medium using membrane ultrafiltration, further decreasing the quantity of solvent required.

By these process improvements, the chemists at Jiangsu Aosaikang Pharmaceutical Co., Ltd and ECUST addressed the shortcomings of the initial titanium-catalyzed oxidation, including the need for heavy metal waste remediation, the environmental burdens introduced by the use of peroxides and organic solvents, and the high sensitivity of the reaction. Their biocatalytic approach employed an engineered *Ac*PSMO enzyme and a cofactor recycling system comprising molecular oxygen in water, thereby significantly reducing chemical waste. Process challenges, such as enzyme stability, substrate solubility, and oxygen mass transfer, were systematically overcome, enabling reactions to be conducted in a 300 L reactor.

1.4.2 Nemtabrutinib – Disclosed 2023

Nemtabrutinib (**11**) is a reversible Bruton tyrosine kinase (BTK) inhibitor that exhibits therapeutic effects across various hematologic malignancies, such as leukemia and lymphoma (Figure 1.3a).[58-59] The C(sp^2)–N bond in Nemtabrutinib first was forged by an S_NAr reaction between aminopyran **8** and the biaryl ketone formed by sequential bromination and metalation of indole **9**, followed by treatment of **9** with ester **10**.[60]

The HCl salt of **8** was used initially for the S_NAr reaction and was originally prepared by scientists at Actelion Pharmaceuticals, Ltd. in a 9-step sequence from tri-*O*-acetyl-D-glucal **12** (Figure 1.3b).[61] To accomplish the synthesis of **8•HCl**, **12** was subjected to a Ferrier rearrangement in the presence of triethylsilane, followed by global deprotection and TBS re-protection of the primary alcohol. Alcohol **13** was then converted to trichloroacetimidate **14**, which was heated in the presence of base to affect the formation of **15** by a thermal Overmann rearrangement. Reduction of the remaining alkene and global deprotection provided ammonium salt **8•HCl** in 32% overall yield from **7**.

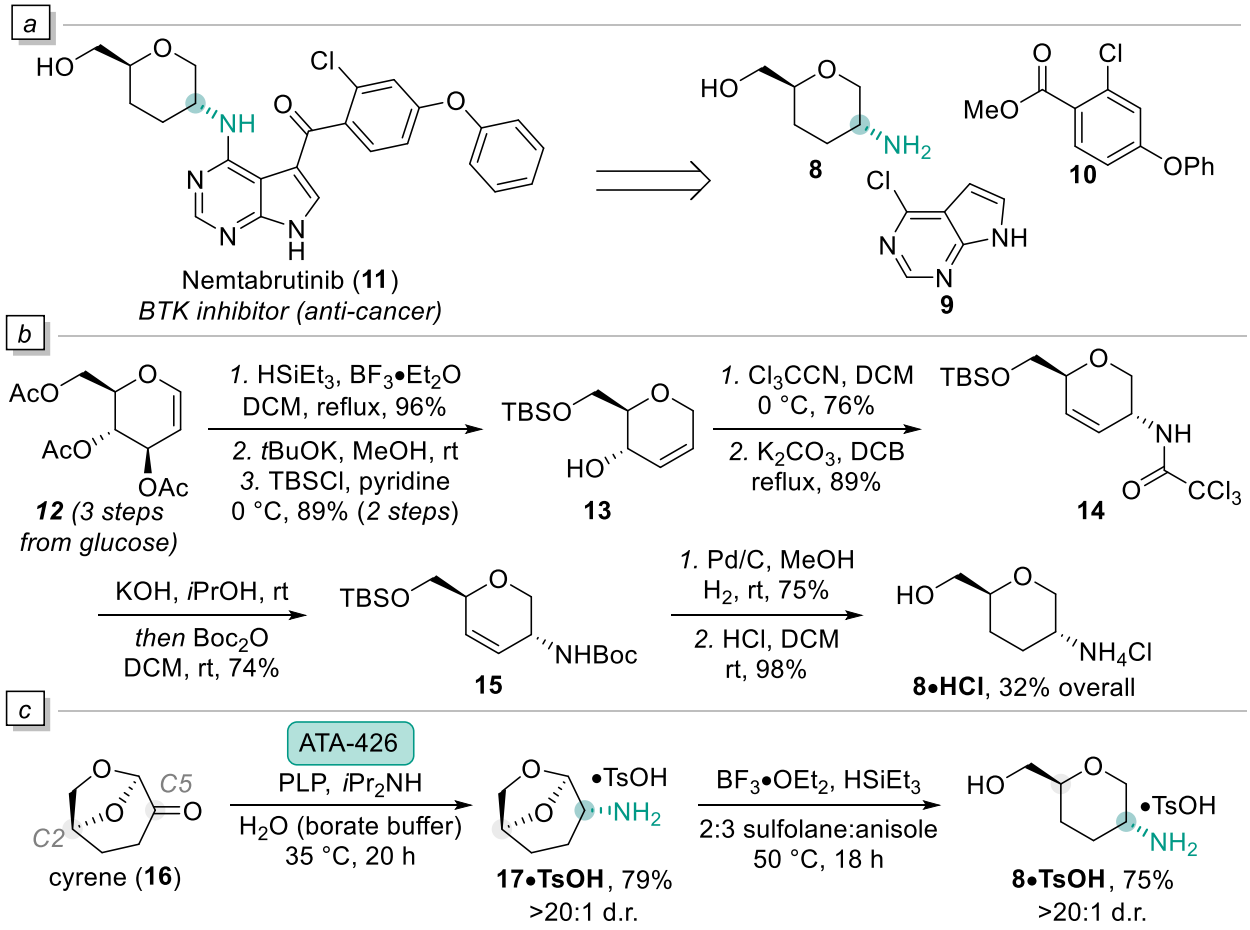

Figure 1.3. (a) Structure and retrosynthesis of Nemtabrutinib, (b) initial process route to fragment **2**, and (3) revised route to **2** involving biocatalytic transamination.

After the API was acquired by Merck in 2019, Merck scientists identified numerous process challenges with the discovery route. The sequence is lengthy, requires hazardous reagents, and

employs multiple solvent-intensive workups and purifications. Scientists at Merck pursued a biocatalytic route to **8** with the objective of decreasing step count and waste, while increasing the overall yield and sustainability of the reaction.[62] Merck researchers were drawn to Cyrene™ (**16**), a commercially-available, bio-based, and biodegradable solvent, because it already possessed the desired configuration at C2 and possessed a ketone that could be functionalized at the C5 position (Figure 1.3c). To accomplish the conversion of Cyrene™ to **8**, the researchers envisioned a diastereoselective reductive amination of the C5 ketone to form amine **17**, followed by reduction of the acetal; however, the thermodynamically favored product of reductive amination by chemical methods gave the undesired epimer of **17** in a 3.4:1 **17'**:**17** ratio. To overcome the inherent thermodynamic preference of this transformation, and to avoid the use of transition metals, transaminase enzymes were investigated for the conversion of **16** to **17**.

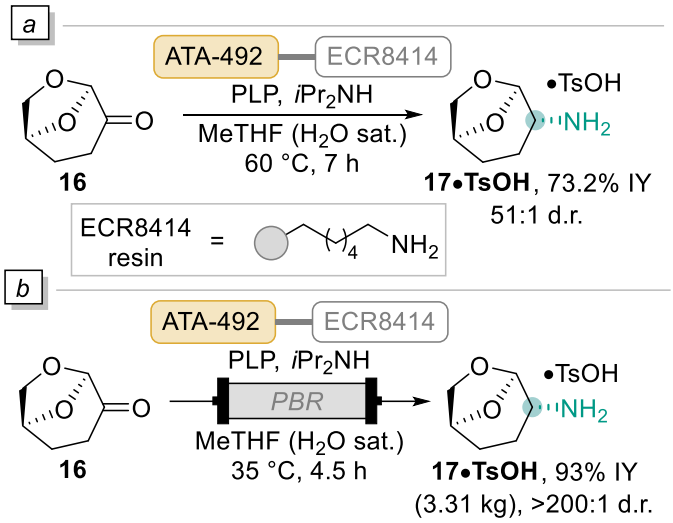

Figure 1.4 (a) Second-generation biocatalytic process for the synthesis of **17** using evolved, immobilized enzymes, and (b) third-generation process using flow chemistry for biocatalysis in a packed bed reactor (PBR).

A commercial-available transaminase enzyme from Codexis, ATA-426 formed the desired product in 17:1 d.r. (**17**:**17'** ratio) and 71% yield. After further optimization to limit the formation of an aldol byproduct with acetone (acetone is formed *in situ* by transamination of ispopropylamine), the d.r. was increased to 24:1 with a yield of 91%. A solvent swap to 2-methyl THF and recrystallization in the presence of TsOH yielded **17•TsOH** in 79% yield. This material was subsequently subjected to chemical reduction with BF_3•OEt_2 and triethylsilane to provide **8•TsOH** in 75% yield and >20:1 d.r. after direct recrystallization from the reaction mixture. By this new procedure, the overall yield of **8** was increased by more than 27% over the original route, with a concomitant reduction in process mass intensity (PMI), energy use, and global warming potential (kg CO_2 equiv) of 94%. In addition, the number of steps was reduced from 9 to 2, and chromatographic separations were eliminated from the process entirely.

Further improvements to the biocatalytic process were then made by Merck Process to enable kilogram- and multikilogram-scale batch deliveries of **11**.[63] The first-generation biocatalytic process required a slight vacuum and N_2 sweep to remove acetone,[62] and the free enzyme employed required careful control of the solution pH to avoid deactivation.[63] Immobilization of the enzyme on an amine-based resin, ECR8414, coupled with process optimization and four rounds of directed evolution to create ATA-492, enabled formation of the desired product in 98% yield and >50:1 d.r. after 7 h without the need for continuous acetone removal or *p*H maintenance. In addition, the reaction could now be run in water-saturated 2-methyl THF, eliminating the need for a solvent swap and enabling recrystallization of **17•TsOH** in 73% yield and 51:1 d.r. after filtration to remove the immobilized enzyme (Figure 1.4a). For the delivery of multikilogram batches of **11**,

Merck Process later deployed these immobilized enzymes in a flow process, in which the immobilized enzymes were loaded into a packed bed reactor (PBR).[64] This flow-based approach, after minimal evolution of the enzyme, delivers **17•TsOH** in 93% isolated yield and >200:1 d.r. and was demonstrated on multi-kilogram scale (Figure 1.4b).

Initially, the synthesis of aminopyran intermediate **8** involved a complex, hazardous, and low-yielding nine-step process. Merck researchers addressed these challenges by adopting a transaminase-catalyzed synthesis from the bio-based solvent Cyrene™, reducing step count from nine to two and significantly enhancing yield, selectivity, and sustainability. Further optimization involved enzyme immobilization and directed evolution, enabling the process to be conducted efficiently on kilogram-scale without complex operational controls. Ultimately, adopting immobilized enzymes in a flow chemistry processes enabled multikilogram production with exceptional stereoselectivity, yield, and environmental performance. This example showcases the power of biocatalysis for the reduction of waste and the number of synthetic steps, while maintaining high yields and selectivities.

1.4.3 *Belzutifan – Disclosed 2024*

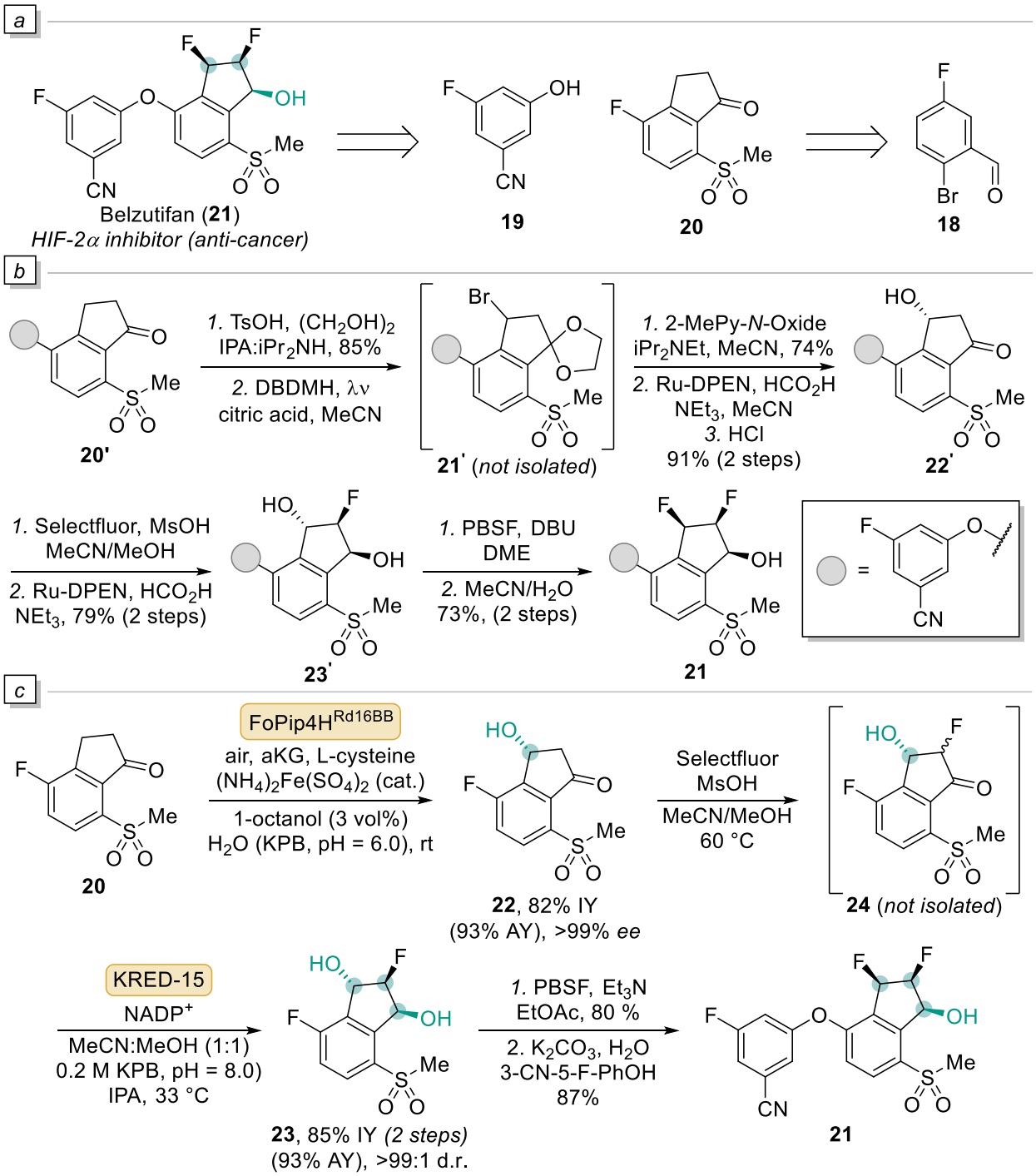

Figure 1.5. (a) Structure and retrosynthesis of **21**, (b) initial process route to Benzultifan from **20'** utilizing chemocatalysis, and (c) optimized route to **21** from **20** involving biocatalytic transformations. DBDMH = 1,3-Dibromo-5,5-dimethylimidazolidine-2,4-dione; PBSF = 1,1,2,2,3,3,4,4,4-nonafluorobutane-1-sulfonyl fluoride.

Belzutifan (**21**) is a selective, orally-available HIF-2α inhibitor that exhibits anti-cancer properties and was approved in the U.S. in 2021 for the treatment of various cancers (Figure 1.5a).[65] Merck

acquired the molecule in 2019 from Peloton and developed process routes for clinical delivery and for commercialization.

Table 1.1. Initial Investigation of Biocatalytic Asymmetric Benzylic Oxidation Conditions

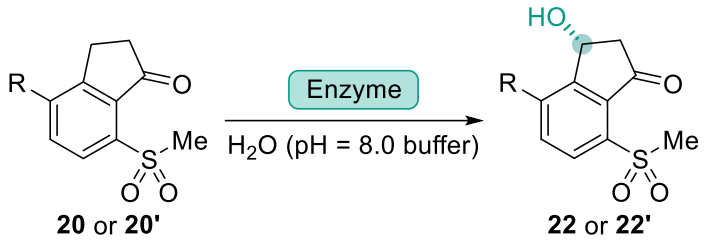

20 or **20'** → **22** or **22'**

Entry	R =	Enzyme	Conv. (%)	%ee
1	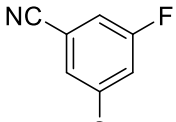	MCYP0150 [NADPH/PtDH, KPt buffer]	0%	*n.d.*
2	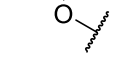 **20'**	FoPip4H, O_2 [αKG, ascorbate Fe^{2+}, KPi buffer]	0%	*n.d.*
3		MCYP0150 [NADPH/PtDH]	95%	-47%
4	**20**	FoPip4H, O_2 [αKG, ascorbate Fe^{2+}, KPi buffer]	12%	60%

PtDH = phosphite dehydrogenase ; αKG = α-ketoglutarate

The first-generation process route to **21** devised by Merck (Figure 1.5b) offered several improvements over the sequence used for clinical deliveries (not shown). The clinical supply route consisted of 16 steps (LLS), which provided the API in 4% overall yield (PMI = 2039).[65] The improved route shown in Figure 1.5b is a 14 step (LLS) sequence that delivered the desired API in 19% overall yield (PMI = 761),[65] and a reduction in raw material cost by greater than 80%.[66] In addition to these improvements, a number of toxic and/or costly reagents were eliminated from the route; however, there were still several improvements that Merck Process envisioned would further increase the sustainability and efficiency of the synthesis of **21**. Two key areas were identified by researchers at Merck to show potential for the use of biocatalysis: first, a direct method for the enantioselective synthesis of β-hydroxyketone **22'** from ketone **20'** was desired, as opposed to the four-step sequence to install the benzylic alcohol in **22'**. Second, the researchers envisioned the use of a ketoreductase (KRED) instead of a rhodium catalyst to set the final two contiguous stereocenters in **23'** by dynamic kinetic resolution (DKR) of the intermediate α-fluoroketone. Making the switch to biocatalysis in these cases would eliminate the use of third-row transition metals, reduce step count, and simplify product purification.

Merck began by investigating the enantioselective benzylic oxidation of ketone **20'** to form **22'** to bypass the previously established protection, bromination, oxidation, and asymmetric reduction sequence (Figure 1.5b, top). In addition, chemical methods of oxidation did not produce the desired enantiomer of **22'** during initial development.[65]

The initial high-throughput screening process for biocatalytic activity used commercially available enzymes. The enzymes tested were inactive for the oxidation of biaryl ether **20'** (Table 1.1, entries 1-2); however, cytochrome P450 150 enzyme (MCYP0150) and the α-ketoglutarate-dependent dioxygenase (αKGD) enzyme pipecolic acid 4-hydroxylase from *Fusarium oxysporum* (FoPip4H) catalyzed the benzylic hydroxylation of aryl fluoride **20** (95% and 12% conversion, respectively). Despite the higher activity of MCYP0150, FoPip4H was selected for future evaluation because it produced the desired *R*-enantiomer in 60% *ee* (Table 1.1, entry 4). The family of αKGDs enzymes are known to catalyze oxidation of C(sp^3)–H bonds at the benzylic position through the

intermediacy of an Fe(IV)-oxo species, but αKGDs typically suffer from poor turnover numbers, poor thermostability, and a propensity to self-hydroxylate.[67] After fifteen rounds of directed evolution, FoPip4H^{Rd16BB} catalyzed the conversion of **20** to **22** in 92% assay yield and 99% ee with a TON >15,000 on 1.5 kg scale. Key to the success of this directed evolution campaign were mutations that increased activity, thermal stability, oxidative stability, and selectivity.[67]

Researchers at Merck then sought to eliminate the use of the aforementioned ruthenium catalyst in the DKR of synthetic intermediate **22** (Figure 1.5c, bottom).[68] While the transition-metal catalyzed process was effective, the process group was concerned about the price and supply volatility of ruthenium and, therefore, sought to conduct this transformation using a DKR facilitated by a KRED enzyme. A key challenge was that the enzymatic process must tolerate byproducts from the preceding fluorination reaction (selectfluor, acetonitrile, etc.) to be a viable replacement, as the two steps were telescoped on production scale to avoid decomposition of the α-fluoroketone **24**. An initial HTE campaign with independently synthesized and purified intermediate **24** identified KRED-1 as a promising starting point. This enzyme enabled the production of **23** in 95% conversion and 3:1 d.r. (Figure 1.6a, top). Despite the high conversion, this initial hit presented several challenges: KRED-1 did not tolerate direct telescoping from the fluorination reaction (Figure 1.6a, bottom), 100 wt% of enzyme was required, and **23** was formed with a low diastereomeric ratio. The process team at Merck subjected KRED-1 to 14 rounds of directed evolution, producing KRED-15, which was capable of tolerating byproducts from the fluorination reaction while delivering the desired product **23** in 85% isolated yield and >99:1 d.r over two steps (Figure 1.6b).[68]

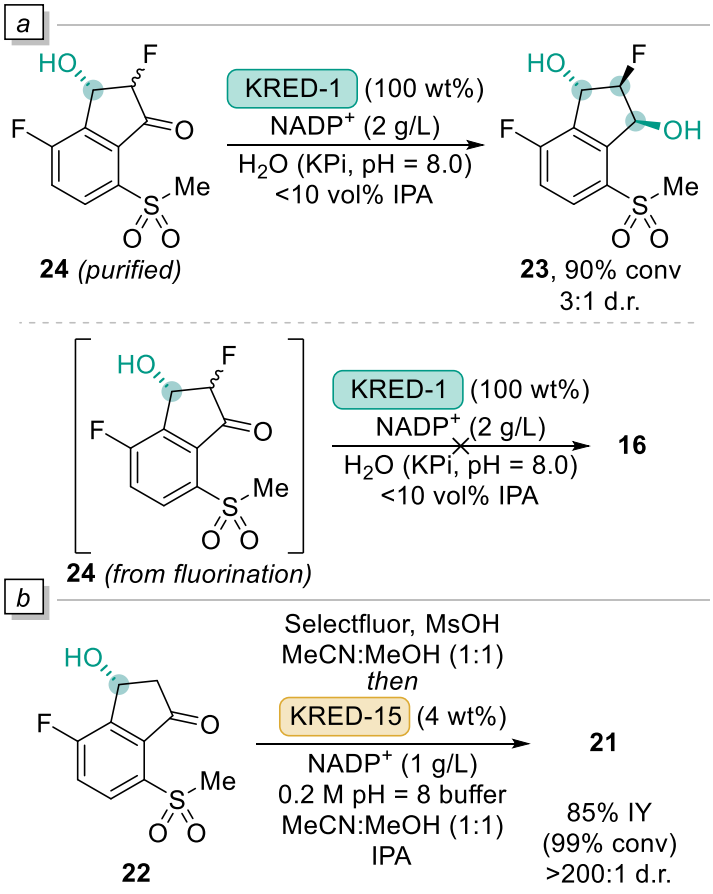

Figure 1.6. (a) initial hit for KRED-mediated DKR of 24 using a commercial enzyme and (b) final biocatalytic process using an engineered KRED enzyme.

The development of Belzutifan at Merck exemplifies the benefits gained from integrating biocatalysis into a process chemistry route. The use of biocatalytic transformations resulted in a more efficient and environmentally-friendly process, and the directed evolution of enzymes FoPip4H and KRED-1 yielded robust catalysts FoPip4H^{Rd16BB} and KRED-15 that were used to set three contiguous stereocenters with high selectivity (>99% ee and >99:1 d.r.) and efficiency (>90% assay yield). These enzymatic methods eliminated the need for a bromination step and two

ruthenium-catalyzed transfer hydrogenation reactions, lowered the step count, increased enantiopurity of the API, and enhanced overall yield. This example clearly demonstrates the potential of biocatalysis to improve the sustainability, cost-effectiveness, and efficiency of manufacturing routes.

1.4.4 Molnupiravir – Disclosed 2021

Molnupiravir (**28**, Figure 1.7a) is an orally available prodrug of a nucleoside antiviral developed by Merck for the treatment of adults with moderate-to-severe COVID-19; compound **28** is currently available under an Emergency Use Authorization (EUA) from the FDA[69] and is undergoing Phase III clinical trials en route to regulatory approval.[70] In the body, the alcohol at the 5′ position of the sugar backbone is deprotected and phosphorylated, generating the relevant active compound.[71] When Merck partnered with Ridgeback Biotherapeutics in 2020 to advance molnupiravir through clinical trials, the Merck process group inherited a five-step route from uridine **27** (Figure 1.7b) that produced high-quality material on pilot scale but faced a number of issues concerning robustness and feasibility for scale-up.

The inherited pilot-scale route comprised a 5-step synthesis of uridine (**27**) from ribose (**26**) and uracil (**25**). Protection of the vicinal alcohols of **27**, followed by isobutyrylation of the 5′ alcohol, formed acetal **29**, which was used directly as a solution in acetonitrile. The solution of **29** was coupled with 1-*H*-1,2,4-triazole mediated by $POCl_3$, resulting in the formation of triazole **30** in 82% yield after two steps. Displacement of the triazole by NH_2OH, followed by deprotection of the acetal, provided molnupiravir **28** in 36% overall yield from uridine (<10% overall when starting from uracil and ribose).[71]

While Merck process improved this original route and alleviated many concerns of technology transfer and reproducibility with a chemical synthesis (not shown) to conduct the synthesis on multi-ton scale,[71] they also investigated an enzymatic cascade for a more ideal assembly of **28** directly from ribose and uracil (Figure 1.7c).[72] The process group envisioned that an ideal synthesis of molnupiravir would consist of three steps: acylation of the primary alcohol, installation of the nucleobase, and formation of the oxime.

At the time, biocatalytic synthesis of nucleosides with sugars modified at the 5′ position was unknown; therefore, the scientists envisioned modifying the native reactivity of the 5-*S*-methylthioribose (MTR) kinase, whose native function is the direct 1-phosphorylation of **34**, which contains a thioether at the 5′ position (Figure 1.8a). If an MTR kinase could be modified to accept **31** as the substrate, researchers envisioned that the resulting phosphorylated ribose derivative **31•P** could be acted upon by a uridine phosphorylase (URP) to install the desired nucleobase.

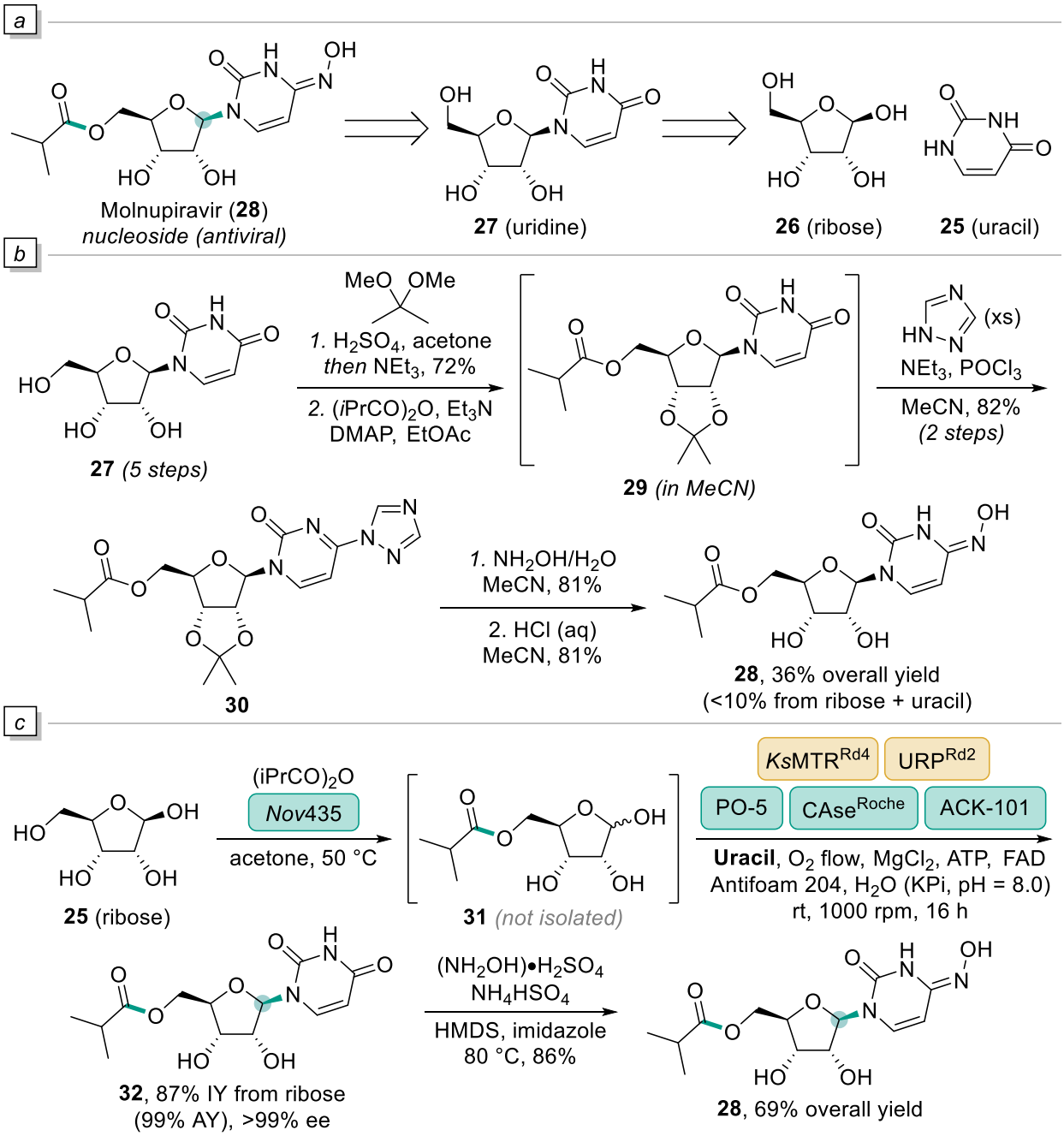

Figure 1.7. (a) Structure and retrosynthetic analysis of **28**, (b) initial route to **28** starting from uridine, and (c) biocatalytic cascade route to **28** from ribose.

MTR kinases are ATP-dependent. Although a stoichiometric phosphate donor could be employed,it was envisioned that a recycling cascade with the pyruvate oxidase (PO) enzyme could be constructed (Figure 1.9). PO catalyzes the formation of acetyl phosphate from pyruvic acid and an inorganic phosphate, producing CO_2 and H_2O_2 as byproducts. Because inorganic phosphate is the byproduct of the nucleobase coupling reaction, the researchers envisioned that this enzyme could enable ATP recycling if coupled with a catalase to decompose the generated hydrogen peroxide. If the product of phosphorylation, **31•P**, could be intercepted by the URP enzyme, the desired unnatural nucleobase **32** could be synthesized in a cascade fashion.

Directed evolution was used to modify initial hits from commercial panels of MTR kinases and URP enzymes, resulting in KsMTR andRd4 and URPRd2, which were capable of stereoselective phosphorylation in >90% conversion and stereo-invertive uridination in >99% conversion, respectively. In the final process, acylation was accomplished with the commercially available Novozym 435 (*Nov*435) to form **31** in 94% assay yield; the crude product of this reaction was then extracted into water and subjected directly to the biocatalytic cascade, resulting in the formation of **32** in 87% isolated yield and >99% ee (Figure 1.7c). Chemical formation of the oxime proceeded with NH_2OH to deliver molnupiravir in 69% overall yield from ribose using this biocatalytic cascade sequence.

The researchers at Merck overcame significant scaling and robustness challenges associated with the initial chemical route by designing an alternative biocatalytic route to molnupiravir. Modification of an MTR kinase enzyme enabled the direct stereoselective phosphorylation of an unnatural ribose derivative, which was coupled with a highly efficient engineered phosphorylase and an enzymatic ATP recycling system. This biocatalytic system significantly reduced the synthetic complexity of the manufacturing route and decreased the step count from ten steps to two, while improving the overall yield by >50%. This biocatalytic cascade exemplifies how enzyme engineering and pathway integration provide effective and sustainable alternatives to traditional chemical synthesis.

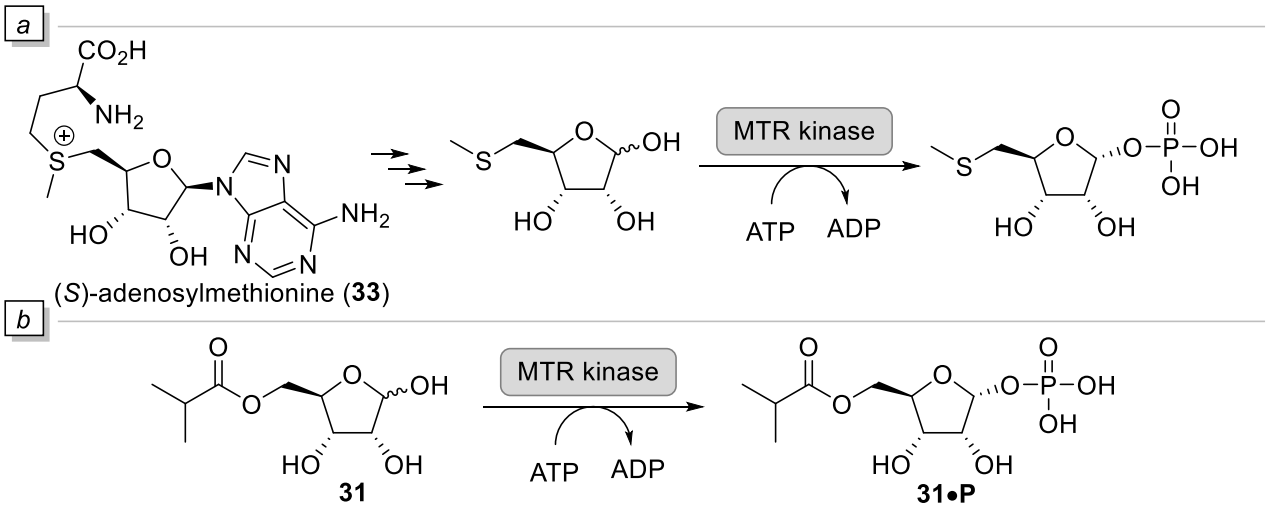

Figure 1.8. Comparison of the native function of MTR kinase with the desired reaction.

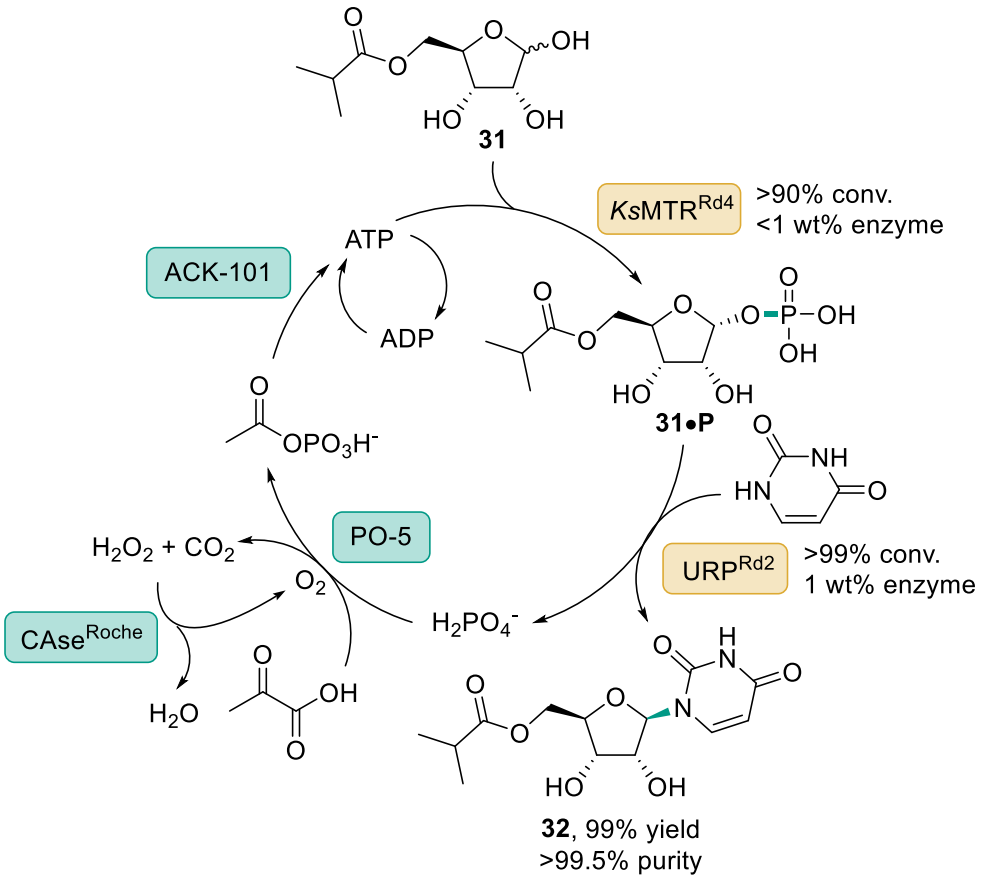

Figure 1.9. Biocatalytic cascade for the synthesis of **24** from **23**

1.4.5 Uvelostinag (MK-1454) – Disclosed 2022

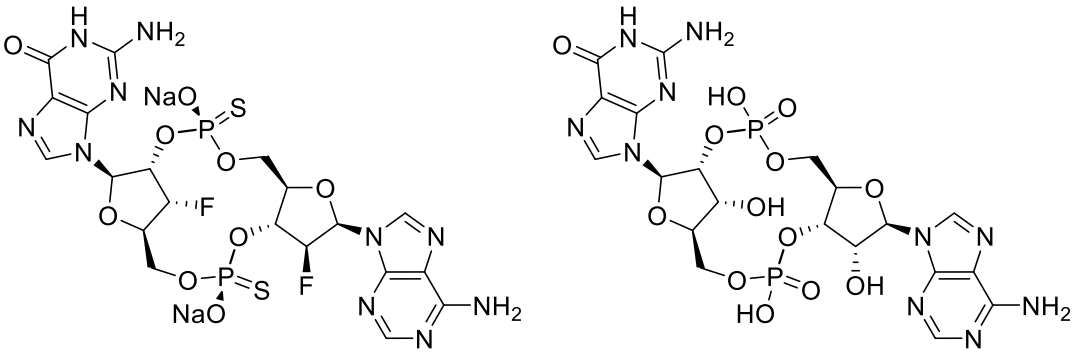

Figure 1.10. Structures of **33** and **34**.

Uvelostinag/MK-1454 (**33**) is an orally-available cyclic dinucleotide (CDN) that acts as an agonist for the Stimulator of Interferon Genes (STING) protein (Figure 1.10).[73] The STING protein is a receptor for endogenous 2',3'-cyclic guanosine monophosphate adenosine monophosphate (cGAMP, **34**, Figure 1.10). Upon binding, the STING-cGAMP complex undergoes a

confirmational change (e.g. from an "open" form to a "closed" form), causing a series of signaling cascades that eventually results in the production of cytokines and the recruitment of immune cells to attack tumor tissue.[73]

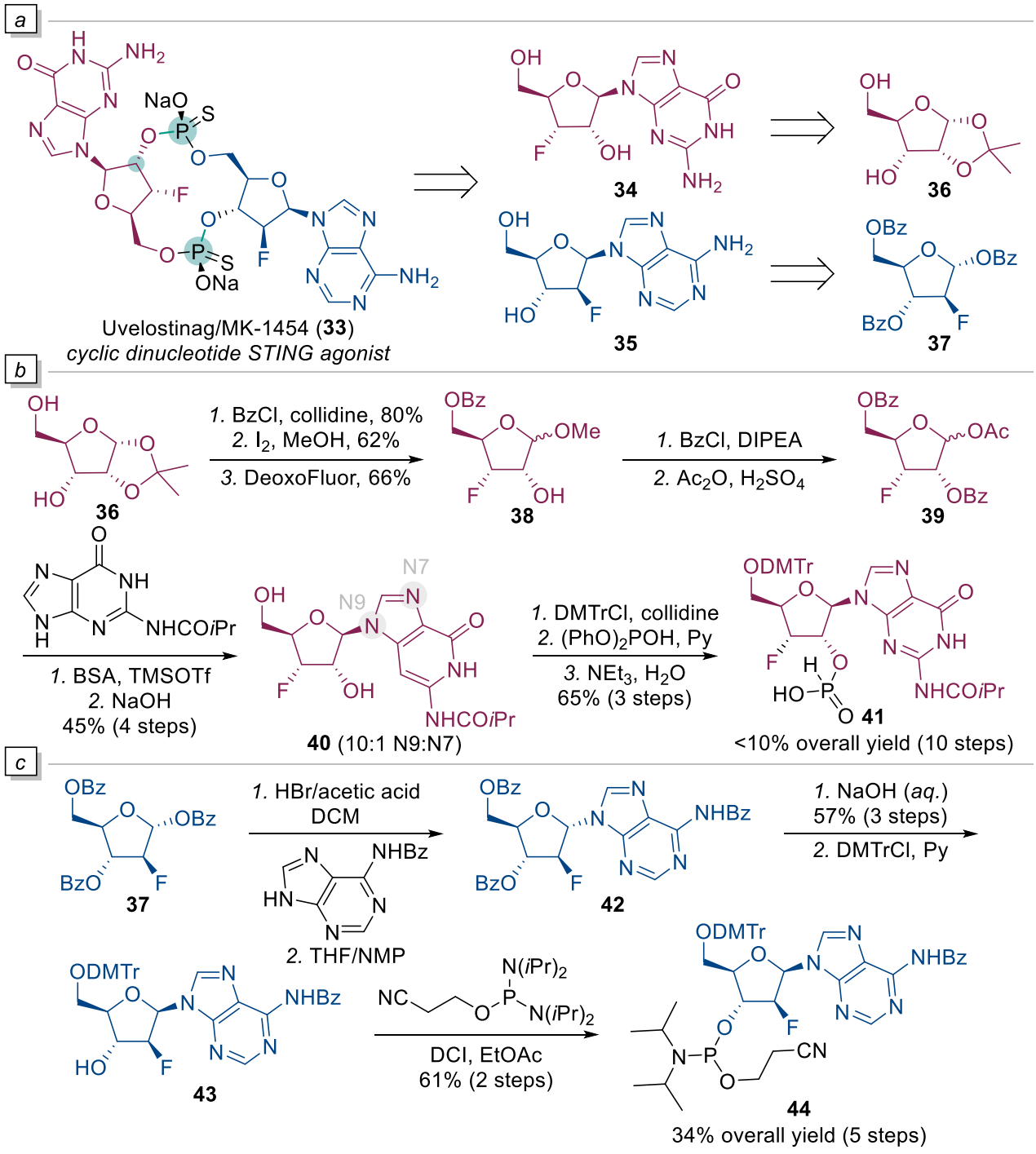

Figure 1.11. (a) structure and initial retrosynthetic analysis of **33**, (b) first-generation GMP synthesis of activated sugar **41**, and (c) first-generation GMP synthesis of activated sugar **44**.

MK-1454 was initially discovered by scientists at Novartis and Aduro, who initiated a collaboration in 2015 to develop and evaluate preclinical STING agonists. Researchers found that replacing the phosphodiester linkages with phosphorothioate linkages improved the pharmacology of STING agonists. Thus, Merck scientists began investigating cGAMP analogues as STING agonists, culminating in the development of Uvelostinag.

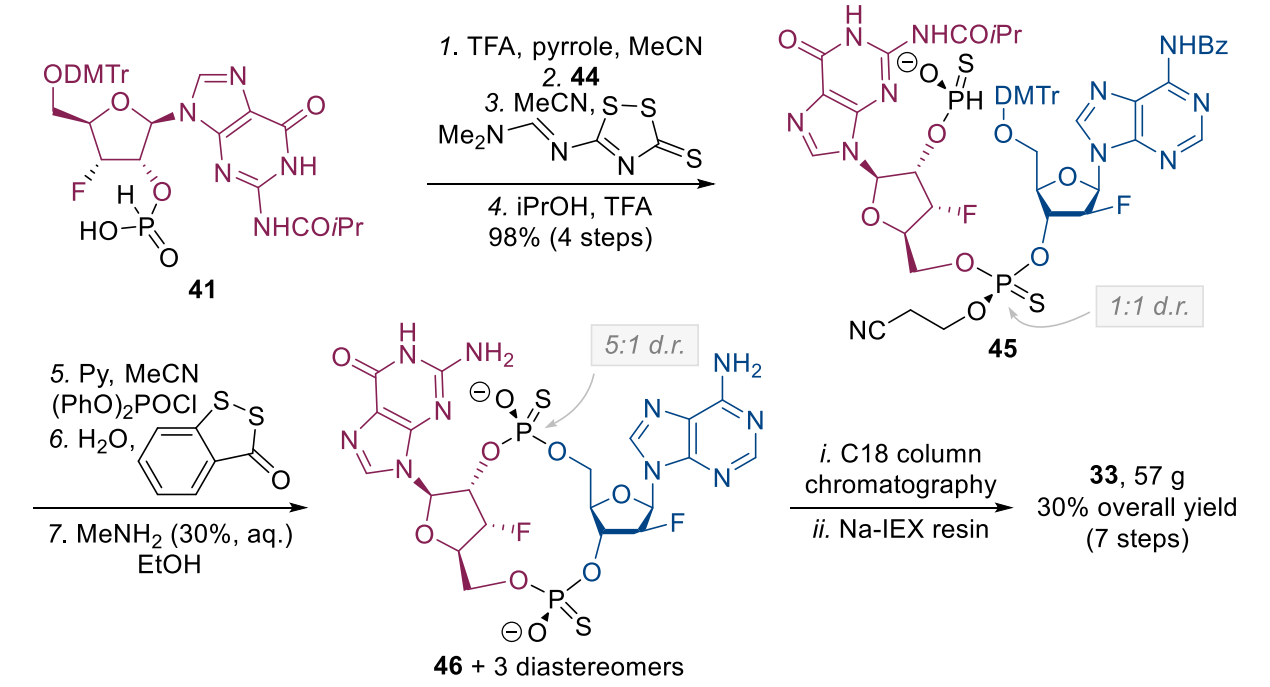

Figure 1.12. First-generation GMP dimerization route to MK-1454 from **41** and **44**.

The medicinal chemistry route to **33** consisted of the synthesis of activated analogues of the unnatural nucleosides **34** and **35** from the commercially available compounds **36** and **37**, respectively (Figure 1.11a). The synthesis of the western (red) fragment began with the commercially available acetal **36** (Figure 1.11b). After global protection of the free alcohols, the acetal was opened with iodine in methanol, and the resulting compound was subjected to deoxyfluorination using Deoxo-Fluor to provide 3'-fluorinated riboside **38**. Protecting group manipulation yielded **39** as an anomeric mixture, which then underwent a benzoate ester-directed β-selective diastereoconvergent glycosylation reaction with *iso*-butyryl guanidine to deliver compound **40** in 45% yield as a 10:1 mixture of N9:N7 isomers. Selective protection of the primary alcohol with 4,4′-dimethoxytriphenylmethyl chloride (DMTrCl), P–O coupling, and hydrolysis delivered the fully functionalized western fragment **41t** in <10% yield from the starting acetal.

Synthesis of the activated eastern (blue) fragment began with the commercially available fluoride **37** (Figure 1.11c). Bromination of the 1' position, followed by treatment with *N*-benzoyladenine in a 20:1 THF:NMP mixture, formed compound **42** w 14:1 β:α selectivity. Global alcohol deprotection, followed by selective protection of the primary alcohol with DMTrCl, gave compound **43**. Subsequent P–O coupling with 3-((bis(diisopropylamino)phosphaneyl)oxy)propanenitrile delivered functionalized fragment **44** in 34% overall yield from **37**.

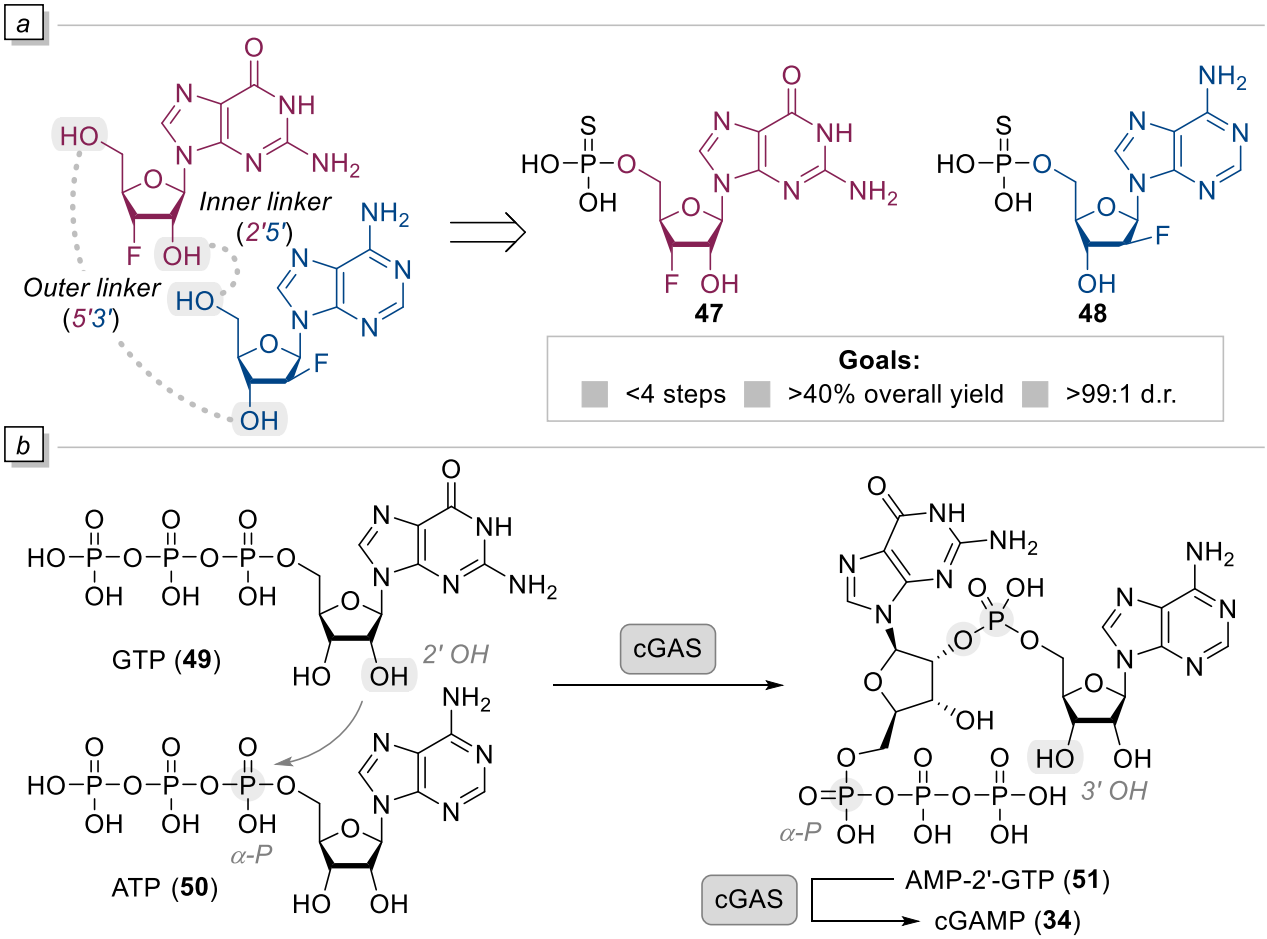

Figure 1.13. (a) depiction of linkages in **33**, retrosynthetic analysis, and design goals for a biocatalytic process, and (b) first step of the stepwise dimerization of ATP and GTP catalyzed by cGAS, producing AMP-2'-GTP.

The medicinal chemistry route to MK-1454 consisted of four steps from slightly different monomers and generated **33** in ~4% yield (not shown).[73] After significant reaction optimization to enable rapid delivery of material for early clinical supply, a first-generation good manufacturing practices (GMP) route was developed (Figure 1.12). Assembly of the two fragments began with deprotection of the primary alcohol of **41**, followed by P–O bond formation with phosphoramidite **44**. Sulfurization with 3-((dimethylaminomethylidene)-amino)-3*H*-1,2,4-dithiazole-5-thione (DDTT) delivered mono coupled product **45** in a 1:1 ratio of diastereomers at phosphorous. The sulfur-containing compound **45** was then treated with TFA to remove the remaining DMTr group, and the remaining P–O bond was formed with a 5:1 d.r. at phosphorous under substrate control with the desired stereochemistry. Global deprotection yielded a slurry of **46** and three undesired diastereomers of MK-1454; an ethanol wash was then used to upgrade the purity of the desired diastereomer. Despite this wash, 153 g of the crude API was purified by reverse-phase chiral prep-HPLC. This process r approximately 120 h of machine time and resulted in 140 L of fractions containing the pure API bis-ammonium salt of the API.[73] This material was passed through a sodium ion-exchange column to yield 57 g (30% overall yield) of **33**.

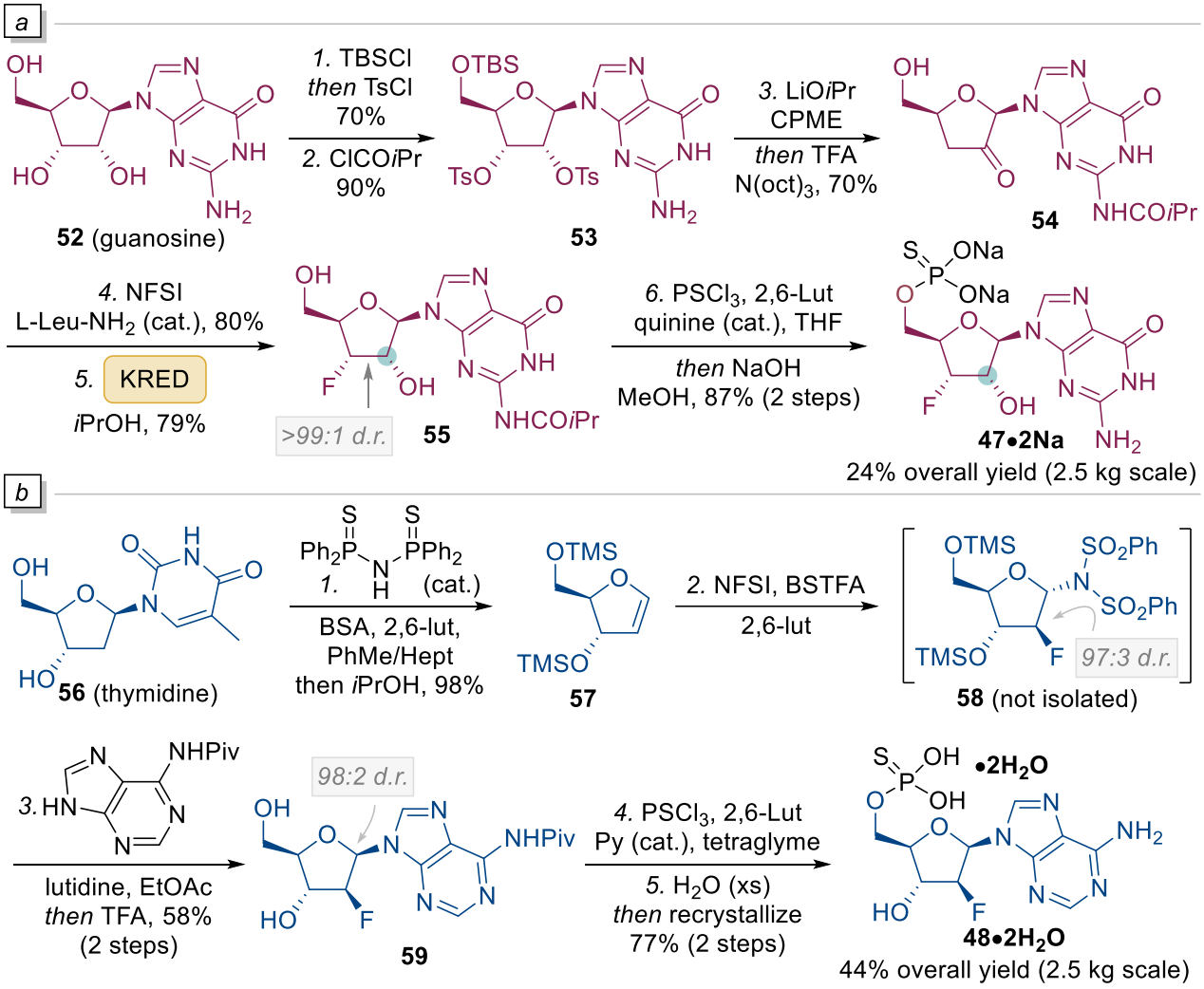

Figure 1.14. (a) Commercial supply route to CDN monomer **47** involving biocatalysis and (b) commercial supply route to CDN monomer **48**.

While this route was acceptable for preclinical supply, it was clear that a commercial-scale supply route would require multiple improvements. Besides the high step count (>20), high PMI (>9000) and low overall yield (~10%), the lack of stereocontrol at the phosphorous linkages, the reverse-phase purification and lyophilization and the lack of a crystalline form of MK-1454 were identified as critical issues. The uses of DeoxoFluor and diphenylphosporyl chloride on production scale were also considered too hazardous; therefore, new methods for enantioselective fluorination and for the installation of phosphorous to the sugar subunits would be required. To address the step count, yield, and lack of stereo-control, numerous avenues were considered, including modulation of the coupling order, the use of enantiopure P(III) or P(V) reagents and chiral auxiliaries, and the use of substrate-directed stereocontrol. This research culminated in a second-generation GMP route (not shown) that delivered material for the development process, but this approach would not create a robust commercial supply route.

To create a robust, sustainable process for long-term commercial production, the process chemists at Merck turned to biocatalysis, specifically the cyclic guanosine adenosine synthase (cGAS)

enzyme, They envisioned this enzyme could form the desired 2'5' inner linkage and/or the desired 5'3' outer linkage (Figure 1.13a) selectively from nucleotides that would ideally be generated from **47** and **48**. The endogenous function of cGAS is to catalyze the attack of the GTP 2' alcohol on the 5′-phosphorous of ATP (Figure 1.13b), forming AMP-2'-GTP (**51**). Compound **51** is then converted to cGAMP (**34**) by attack of the AMP 3' alcohol on the α-phosphorous of GTP in a stepwise dimerization sequence.[74] Leveraging experience with cGAS from the discovery effort, a high-throughput campaign was initiated to identify a cGAS variant that could catalyze diastereoselective phosphorothiolation between monomers.[75] To enable this high-throughput campaign, efficient syntheses of **47** and **48** were required.

Synthesis of the western (red) fragment begins with guanosine (**52**) as the starting material, as opposed to acetal **28** in the initial GMP route (Figure 1.14a). To enable an electrophilic fluorination with NFSI as the fluorine source, the α-fluorination would be conducted on a ketone derived from **52**. To this end, guanosine was protected at the 5′ position with TBSCl, and the vicinal diol motif was bis-tosylated to give **53**. Treatment of **53** with base followed by protonation provided ketone **54**, which was subsequently subjected to a diastereoselective fluorination using NFSI under enamine catalysis with the L-Leu-NH_2 as a chiral amine catalyst to provide catalyst control over the diastereoselectivity. This fluorination formed the desired C–F bond in >99:1 d.r. with a geminal diol at the 3′ position (not shown). This diol was converted to alcohol **55** in >99:1 d.r. using a highly-evolved KRED enzyme.[76] The initial active enzyme for this deoxygenation reaction came from a HTE campaign and produced the desired isomer in 3:1 d.r. and 0.1% conversion, while the evolved KRED enzyme produced **55** in >100:1 dr and 95% conversion, an improvement in activity of greater than 30,000-fold.[73] Thiophosphorylation of **55** with $PSCl_3$, 2,6-lutidine, and catalytic quinine formed the desired product **47•2Na** in 87% yield on 2.5 kg scale after deprotection and recrystallization from the reaction mixture.

For the eastern (blue) fragment (Figure 1.14b), pyrimidine nucleoside thymidine (**56)** was selected as the initial starting material. It was envisioned that β-fluorination and subsequent adenylation of a 1,2-glycal derived from **56** could deliver the desired fluorinated material with high selectivity. After extensive process development, researchers found that treatment of **56** with N,O-bis(trimethylsilyl)-acetamide (BSA) and lutidine in the presence of catalytic amounts of N-(diphenylphosphorothioyl)-P,P-diphenylphosphinothioic amide formed glycal **57** in 98% yield. Fluoro-adenylation was accomplished by a double-displacement strategy by first treating **57** with NFSI and bis(trimethylsilyl)trifluoroacetamide (BSTFA) to form fluorosugar **58**, and then N-piv-adenosine. Treatment of the resulting material with TFA delivered compound **59** in 58% yield with high diastereoselectivity over 2 steps. Compound **59** was thiophosphorylated in a manner similar to that of **55**, albeit with catalytic pyridine and a combination of 2,6-lutidine and triethylphosphate (TEP) as the base. This modified process delivered **48•2H_2O** in 77% yield on 2.5 kg scale after quench, deprotection, and recrystallization.

With nucleotides in hand, effort was undertaken to identify a suitable enzyme for enantioselective dimerization of phosphorylated derivatives of **47** and **48** ((*Sp*)-**60** and (*Sp*)-**61**, respectfully) to form MK-1454 (Figure 1.15). Initial screening of human cGAS enzymes with monothiolated analogues of (*S*p)-ATP and (*S*p)-GTP as model compounds led only to undesired stereoisomers of the CDN,

due to coordination of the phosphorous atoms of the nucleotides with the native magnesium metal cofactor in cGAS.[75]

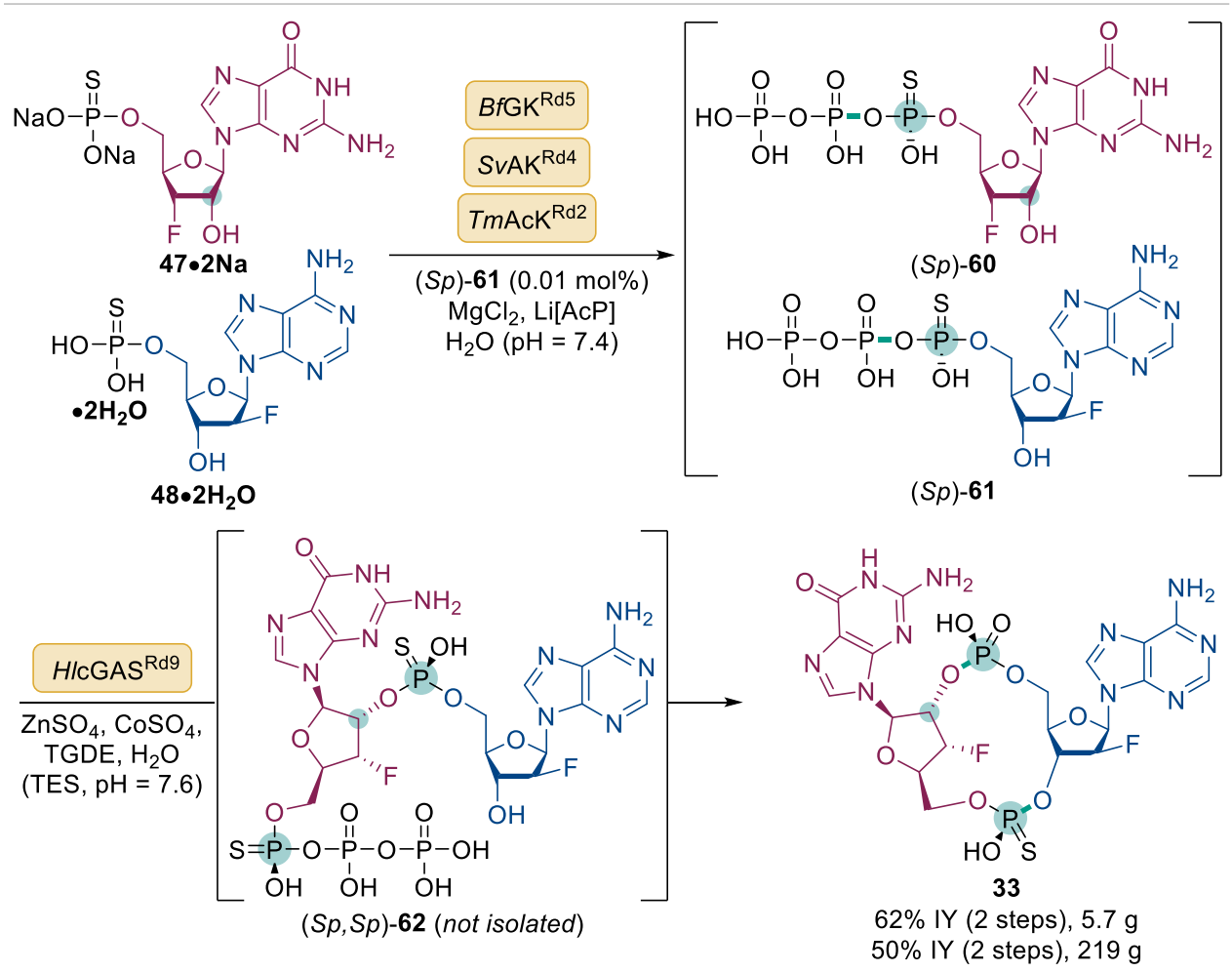

Figure 1.15. Commercial biocatalytic process for the synthesis of 33 from monomers **47** and **48** utilizing a biocatalytic cascade reaction.

Replacement of magnesium with cobalt in the cofactor coupled with the selection of a cGAS enzyme from *Haliaeetus leucocephalus* (bald eagle) yielded a starting enzyme that produced trace amounts of the desired coupled product with the correct configuration at phosphorous. Nine rounds of directed evolution, extensive reaction profiling, and the addition of a second metal (Zn) to accelerate the first coupling step produced, *Hl*cGAS^{Rd9}, which produced the desired CDN in approximately 80% assay yield. To produce the 1-thitriphosphates of **47** and **48** that are required for *Hl*cGAS^{Rd9} enantioselectively, the chemists at Merck again desired to implement a biocatalytic method. The method they devised involved enzymatic desymmetrization of (*rac*)-**47** and (*rac*)-**48** by DKR using an adenylase kinase from *Saccharomyces verevisiae* (*Sv*AK) and a guanylate kinase enzyme from *Branchistoma floridae* (*Bf*GK) to transiently generate both enantiomers of both of the nucleosides, followed by stereoselective phosphorylation of only the desired enantiomer using an acetate kinase enzyme from *Thermotaga maritima* (*Tm*AcK) (Figure 1.15, top). To avoid formation of CDNs containing ATP-derived byproducts (ATP is the natural cofactor of *Sv*AK and

*Bf*GK), these enzymes were evolved to use the unnatural fluorinated monomer (*Sp*)-**61** as the cofactor to avoid side products resulting from heterodimerization with ATP, resulting in *Bf*GK^{Rd5}, *Sv*AK^{Rd6}, and *Tm*AcK^{Rd2} after five, four, and two rounds of directed evolution, respectively. The phosphorylation of (*rac*)-**47** and (*rac*)-**48** and their subsequent dimerization to form **33** also could be merged into a single cascade, despite the presence of multiple different metal cofactors. Initial runs on gram scale provided MK-1454 in 62% isolated yield as a single diastereomer without the need for protecting groups, chiral auxiliaries, or chromatographic separation. Subsequent scale-up yielded MK-1454 in 50% yield over the two steps as a single diastereomer on hundred-gram scale. In the large-scale process, the three evolved phosphorylation enzymes were immobilized on a metal affinity resin to facilitate separation of the product from the enzymes and to facilitate recovery of the enzymes.[73]

The development of the commercial supply route to **33** illustrates how innovations in biocatalysis can profoundly impact process chemistry, particularly for the synthesis of CDNs. The evolution of synthetic routes—from initial medicinal chemistry strategies through first-generation GMP delivery to advanced biocatalytic methods—demonstrates the power of enzymatic catalysis to overcome significant synthetic challenges. By employing enzyme engineering, Merck researchers successfully replaced hazardous reagents, improved stereochemical control, and achieved remarkable reductions in step count, process mass intensity (PMI), and purification complexity. The final biocatalytic cascade, comprising evolved kinase enzymes and an engineered cGAS variant, exemplifies a robust, sustainable, and scalable approach for the commercial production of MK-1454. This example underscores the broader potential of biocatalysis as a pivotal strategy in the pharmaceutical industry.

1.5 Examples of Biocatalysis in the Early Stages of Development in the Pharmaceutical Industry (2020 – 2025)

Section 1.5 will briefly examine case studies of the adoption of biocatalysis in smaller-scale capacities, such as the synthesis of key intermediates or building blocks, in discovery chemistry and medicinal chemistry scale-up applications, disclosed from 2020 to 2025. These examples provide a brief overview of additional transformations that can be accomplished by biocatalysis.

1.5.1 Recent Examples Employing KRED Enzymes

During a recent medicinal chemistry campaign, researchers at Vertex Pharmaceuticals sought both isomers of cyclobutene **63** (Figure 1.16a), but the initial chemical route required 4 steps (18% overall yield for *trans*-***63***; 15% overall for *cis*-***63***).[77] Investigation of a panel of 120 commercially-available ketoreductase (KRED) enzymes revealed that KRED-A7 selectively gave *trans*-**63** and that KRED-B5 selectively formed the opposite isomer, *cis*-**63** from achiral ketone **64** (Figure 1.16b). Both of these reactions were conducted on >100g scale, providing material that was obtained in high purity without chromatography.

In 2022, researchers at Genentech and Roche disclosed the use of a KRED enzyme to form the 1,4-trans-cyclohexanol unit in Navoximod (**67**) *via* deracemization of **65** (Figure 1.16c).[78] After evaluation of >500 commercial enzymes, KRED ADH 430 was identified, which gave (*rac*)-**66** in 95% yield with a 99.6:0.4 *trans*:*cis* ratio after minimal reaction optimization. The benzylic stereocenter was desymmetrized by a crystallization-induced dynamic resolution (CIDR) that employed L-DBTA.[78] During their process development, the researchers noted that none of the

KRED enzymes tested catalyzed the reaction of the more hindered central ketone in **65** or **66**, exposing a gap in current KRED methodology.[5] Reduction of the more congested ketone was accomplished by chemical methods. The KRED-catalyzed construction of the 1,4-*trans*-cyclohexanol motif in **67** allowed for the removal of SFC separation that was present in the enabling route.

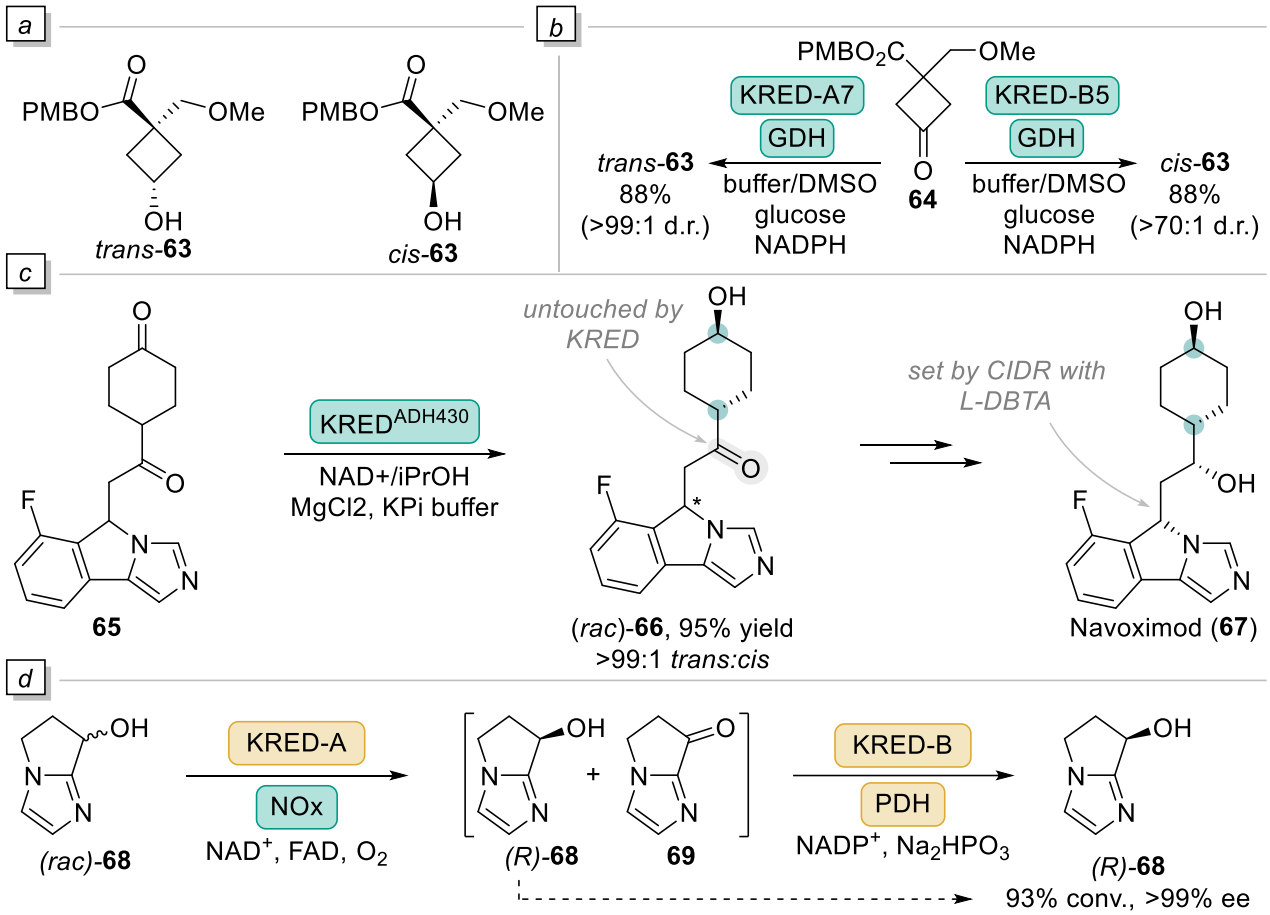

Figure 1.16. Additional examples of biocatalytic transformations in the pharmaceutical industry that employ KRED enzymes.

In 2020, Merck chemists disclosed in a patent the KRED-enabled DKR of (*rac*)-**68** to form enantiopure (*R*)-**68** using two separate engineered KRED enzymes with orthogonal cofactor recycling systems (Figure 1.16d).[5] In this cascade process, KRED-A selectively oxidizes (*S*)-**68** to ketone **69**, while KRED-B selectively reduces ketone **69** to alcohol (*R*)-**68**. What allows these two enzymes to run concurrently is their different cofactor preferences: KRED-A utilizes an NAD+/NADH couple, which is turned over by the NADH oxidase (NOx) enzyme, while KRED-B utilizes an NADP+/NADPH couple that is turned over by a phosphite dehydrogenase (PDH) system. Using this strategy, researchers at Merck conducted the DKR of (*rac*)-**68** to (*R*)-**68** with 93% conversion and >99% ee.

1.5.2 Recent Examples Employing Transaminase Enzymes

Scientists at Merck recently reported a biocatalytic dynamic amination in the synthesis of **71** for the CGRP receptor antagonists **72**, which has exhibited clinically relevant results for treating migrane.[79] After initially scouting a route to **71** involving metal-catalyzed asymmetric hydrogenation, they sought a more sustainable biocatalytic route to their desired intermediate (Figure 1.17a). Until this work, the transamination of ketones bearing an α-fluorine atom had not been reported, and scientists at Merck envisioned that the lability of the proton geminal to fluorine would enable a dynamic transamination that would set two stereocenters at a high pH.[5] An investigation of commercially available enzymes, both immobilized and as the lyophilized powder, was conducted, and lyophilized ATA-303 from Codexis (immobilized ATA-303 formed **71** in reduced enantioselectivity) formed the desired amine **71** from ketone **70** in 94% yield and 96% ee after process optimization. In addition, control of the pH to maintain a pH > 9.5 eliminated the defluorinated byproducts, simplifying purification. The biocatalytic system enabled the elimination of transition metals in the route and eliminated the formation of a defluorinated byproduct often formed from the asymmetric hydrogenation.[79]

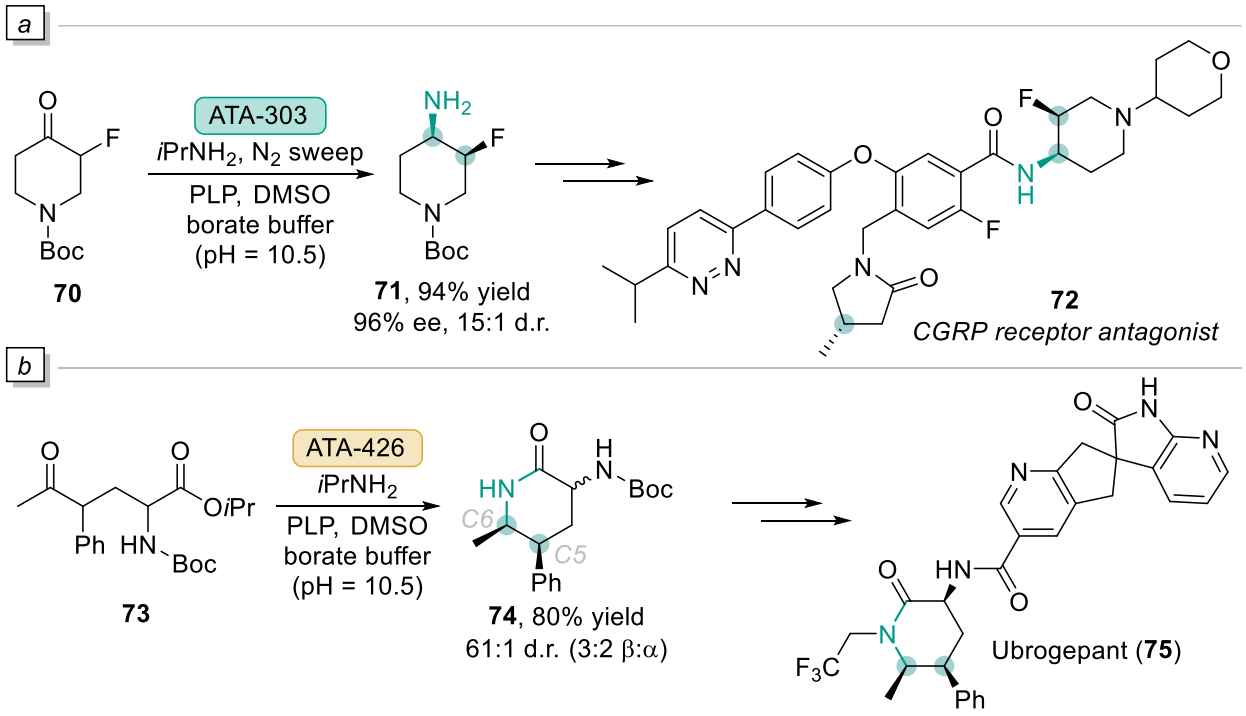

Figure 1.17. Additional examples of biocatalytic transformations in the pharmaceutical industry that employ transaminase enzymes.

For the synthesis of Ubrogepant (**75**), another CGRP receptor antagonist in development at Merck, scientists envisioned using biocatalysis to form chiral lactam **74** by a DKR process from diketone **73** (Figure 1.17b).[80] To accomplish this reaction, Merck partnered with Codexis to evaluate a series of enzymes for the desired reactivity at a pH of 10.5 that would lead to epimerization of the benzylic stereocenter.[5] The most promising enzyme, ATA-301, was subjected to multiple rounds of directed evolution, improving the stereoselectivity for the formation of the C5 and C6 stereocenters in lactam **74**, increasing enzyme reactivity, and increasing stability towards organic

cosolvents and higher temperatures. The final enzyme, ATA-426, delivered **74** in 80% yield (95% conversion) and 61:1 diastereomeric ratio.

1.5.3 Recent Examples Employing Other Enzymes

Abrocitinib (**78**) is a Janus kinase type 1 (JAK1) inhibitor that was approved by the FDA for the treatment of autoimmune disorders (Figure 1.18a).[81] During Phase III trials, the Pfizer process team began investigating potential routes for commercial production of the API, eventually choosing a biocatalytic route to *cis*-1,3-disubstituted cyclobutene **77** after chemical routes proved laborious. Researchers found that a commercially available wild-type reductive aminase from *Streptomyces purpureus* (WT-*Sp*RedAm) selectively (>99:1 d.r.) catalyzed reduction the imine generated from ketone **76** and methylamine *in situ*, albeit with just 0.75% conversion.[82] Multiple rounds of enzyme engineering yielded a new enzyme, *Sp*RedAm-R3-V6 that catalyzed the formation of **77** in 73% isolated yield and >99:1 d.r. (TON > 36,500) on 230 kg scale after process optimization. The reaction of glucose ith NADP+ catalyzed by GDH regenerated the NADPH required by *Sp*RedAm-R3-V6.

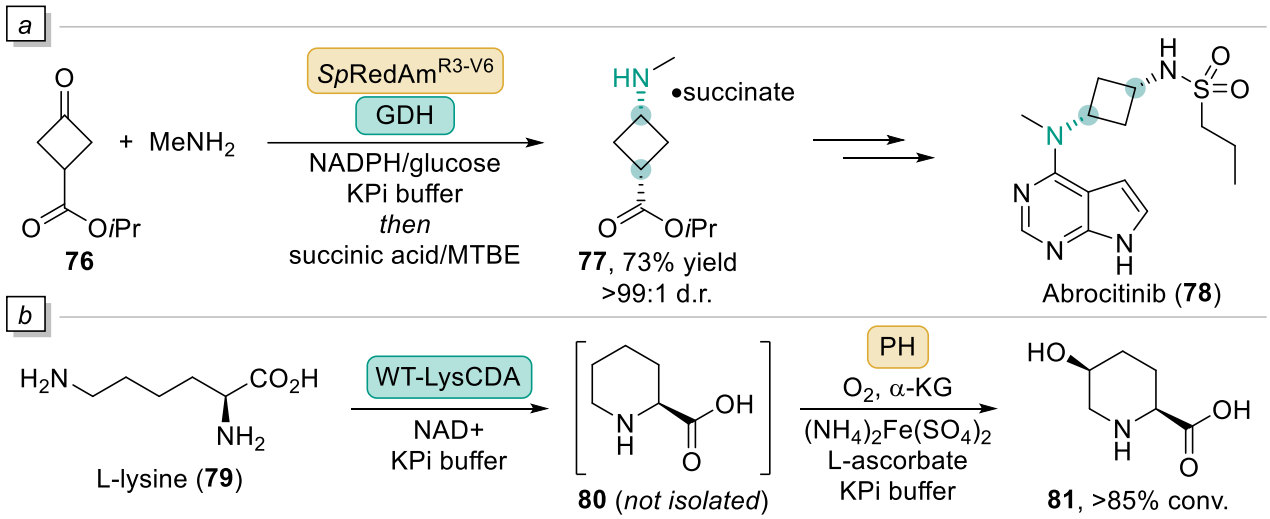

Figure 1.18. Additional examples of biocatalytic transformations in the pharmaceutical industry that employ enzymes not yet discussed in this chapter.

Finally, in a recent patent, researchers from Merck and Codexis disclosed a two-enzyme cascade to access hydroxyacid **81** from lysine (**79**, Figure 1.18b). To enable this transformation, the researchers employed a wild-type Lysine cyclodeaminase (WT-LysCDA) to form the desired enantiomer of pipecolic acid **80**. A wild-type enzyme was able to be used because it was acting upon its native substrate and already reacted with high activity and selectivity for the desired transformation. This cyclization was coupled with an enzymatic hydroxylation catalyzed by a proline hydroxylase (PH) that had been evolved for increased selectivity and activity on pipecolic acid. Mohr's salt was used to provide Fe^{2+} for the iron-dependent PH, and molecular oxygen was sparged through the reaction solution to enable the oxidation, delivering **81** on 13.6 g scale in over 85% conversion.

While there are many additional examples of biocatalysis in industry,[83] the above examples illustrate the synthetic utility of enzymes for the production of APIs, building blocks, and other

fine chemicals. With the increasing business interest, capital investment, and economic viability of biocatalysis, the implementation of biocatalytic routes should continue to expand and to reach further into earlier stages of pharmaceutical development as the time, labor, and capital required to generate new catalysts decreases.

1.6 Conclusion

The evolution of biocatalysis, from the discovery of diastase in 1833 to contemporary implementations at multinational pharmaceutical companies in 2025, illustrates a steady progression toward greater sustainability and process efficiency in chemical synthesis. Fundamental understanding of enzyme structure and function, as well as early breakthroughs in enzyme isolation and immobilization, paved the way for the adoption of biocatalytic methods in large-scale production, while subsequent developments in molecular biology, protein engineering, and computational modeling expanded the range of transformations amenable to enzyme-catalyzed reactions. The case studies of Esomeprazole, Nemtabrutinib, Belzutifan, Molnupiravir, and Uvelostinag demonstrate the potential of biocatalysis to reduce synthetic complexity, lower environmental impact, and improve product yield and selectivity on large scale. Biocatalytic routes are now commonly employed by process chemists to replace hazardous reagents and cumbersome purification steps that are often used in discovery chemistry, while simultaneously reducing the number of reaction steps. The use of directed evolution in conjunction with high-throughput screening and computational tools has resulted in the ability to design enzymatic catalysts that exhibit high stability, along with robust performance. The examples presented in this chapter highlight the benefits of integrating biocatalysis into process chemistry. The improved yields, reduced process mass intensity, and enhanced environmental profiles achieved in these case studies serve as benchmarks for the development of future industrial routes to fine chemicals. The continued convergence of enzyme engineering, computational design, and automation will only further lower the barrier to entry for biosynthesis in industry. The success of recent and current biocatalytic processes reinforces the view that biocatalytic strategies are not merely alternatives to chemical routes but are increasingly the preferred routes for sustainable chemical synthesis. Continued interdisciplinary efforts will ensure that biocatalysis remains a pivotal strategy for developing cleaner and more cost-effective synthetic routes in the years to come.

1.7 References

(1) Anastas, P. W., J. C., *Green Chemistry: Theory and Practice*. Oxford University Press: 1998.
(2) 12 Principles of Green Chemistry. https://www.acs.org/green-chemistry-sustainability/principles/12-principles-of-green-chemistry.html.
(3) Ganesh, K. N.; Zhang, D.; Miller, S. J.; Rossen, K.; Chirik, P. J.; Kozlowski, M. C.; Zimmerman, J. B.; Brooks, B. W.; Savage, P. E.; Allen, D. T.; Voutchkova-Kostal, A. M. *Org. Process Res. Dev.* **2021**, *25*, 1455-1459.
(4) Commission, E. Chemicals Strategy for Sustainability. https://environment.ec.europa.eu/strategy/chemicals-strategy_en.
(5) France, S. P.; Lewis, R. D.; Martinez, C. A. *JACS Au* **2023**, *3*, 715-735.
(6) Armstrong, E. F. *Nature* **1933**, *131*, 535-537.

(7) Kohler, R. *J. Hist. Biol.* **1971**, *4*, 35-61.
(8) Büchner, E., Eduard Büchner Nobel Lecture: Cell-Free Fermentation. 1907.
(9) Harden, A., Arthur Harden Nobel Lecture: The Function of Phosphate in Alcoholic Fermentation. 1929.
(10) Euler-Chelpin, H. v., Hans von Euler-Chelpin Nobel Lecture: Fermentation of Sugars and Fermentative Enzymes. 1930.
(11) Sumner, J. B., James B. Sumner Nobel Lecture: The Chemical Nature of Enzymes. 1946.
(12) Northrop, J. H., John H. Northrop Nobel Lecture: The Preparation of Pure Enzymes and Virus Proteins. 1946.
(13) Heckmann, C. M.; Paradisi, F. *ChemCatChem* **2020**, *12*, 6082-6102.
(14) Sanger, F.; Thompson, E. O. P. *Biochem. J.* **1953**, *53*, 353-366.
(15) Sanger, F.; Tuppy, H. *Biochem. J.* **1951**, *49*, 481-490.
(16) Hanover, L. M.; White, J. S. *Am. J. Clin. Nutr.* **1993**, *58*, 724S-732S.
(17) Anfinsen, C. B.; Haber, E.; Sela, M.; White, F. H. *Proc. Natl. Acad. Sci. USA* **1961**, *47*, 1309-1314.
(18) Jorgenson, J. W.; Lukacs, K. D. *Science* **1983**, *222*, 266-272.
(19) Lee, L. G.; Spurgeon, S. L.; Heiner, C. R.; Benson, S. C.; Rosenblum, B. B.; Menchen, S. M.; Graham, R. J.; Constantinescu, A.; Upadhya, K. G.; Cassel, J. M. *Nucleic Acids Res.* **1997**, *25*, 2816-2822.
(20) Rosenblum, B. B.; Lee, L. G.; Spurgeon, S. L.; Khan, S. H.; Menchen, S. M.; Heiner, C. R.; Chen, S. M. *Nucleic Acids Res.* **1997**, *25*, 4500-4504.
(21) Goodwin, S.; McPherson, J. D.; McCombie, W. R. *Nat. Rev. Genet.* **2016**, *17*, 333-351.
(22) Berg, P.; Mertz, J. E. *Genetics* **2010**, *184*, 9-17.
(23) Lobban, P. E.; Kaiser, A. D. *J. Mol. Biol.* **1973**, *78*, 453-471.
(24) Terpe, K. *Appl. Microbiol. Biotechnol.* **2006**, *72*, 211-222.
(25) Johnson, I. S. *Science* **1983**, *219*, 632-637.
(26) Bruggink, A.; Roos, E. C.; de Vroom, E. *Org. Process Res. Dev.* **1998**, *2*, 128-133.
(27) Marsden, S. R.; Mestrom, L.; McMillan, D. G. G.; Hanefeld, U. *ChemCatChem* **2020**, *12*, 426-437.
(28) Witkin, E. M. *Bacteriol. Rev.* **1976**, *40*, 869-907.
(29) Smith, M. *Trends Biochem. Sci* **1982**, *7*, 440-442.
(30) Mullis K Fau - Faloona, F.; Faloona F Fau - Scharf, S.; Scharf S Fau - Saiki, R.; Saiki R Fau - Horn, G.; Horn G Fau - Erlich, H.; Erlich, H. *Cold Spring Harb. Symp. Quant. Biol.* **1986**, *51*, 263-273.
(31) Chen, K.; Arnold, F. H. *Proc. Natl. Acad. Sci. USA* **1993**, *90*, 5618-5622.
(32) 2021 Breakthrough of the Year. https://www.science.org/content/article/breakthrough-2021#section_breakthrough.
(33) Jumper, J.; Evans, R.; Pritzel, A.; Green, T.; Figurnov, M.; Ronneberger, O.; Tunyasuvunakool, K.; Bates, R.; Žídek, A.; Potapenko, A.; Bridgland, A.; Meyer, C.; Kohl, S. A. A.; Ballard, A. J.; Cowie, A.; Romera-Paredes, B.; Nikolov, S.; Jain, R.; Adler, J.; Back, T.; Petersen, S.; Reiman, D.; Clancy, E.; Zielinski, M.; Steinegger, M.; Pacholska, M.; Berghammer, T.; Bodenstein, S.; Silver, D.; Vinyals, O.; Senior, A. W.; Kavukcuoglu, K.; Kohli, P.; Hassabis, D. *Nature* **2021**, *596*, 583-589.
(34) Yeh, A. H.-W.; Norn, C.; Kipnis, Y.; Tischer, D.; Pellock, S. J.; Evans, D.; Ma, P.; Lee, G. R.; Zhang, J. Z.; Anishchenko, I.; Coventry, B.; Cao, L.; Dauparas, J.; Halabiya, S.; DeWitt, M.; Carter, L.; Houk, K. N.; Baker, D. *Nature* **2023**, *614*, 774-780.

(35) Richter, F.; Leaver-Fay, A.; Khare, S. D.; Bjelic, S.; Baker, D. *PLOS ONE* **2011**, *6*, e19230.
(36) Watson, J. L.; Juergens, D.; Bennett, N. R.; Trippe, B. L.; Yim, J.; Eisenach, H. E.; Ahern, W.; Borst, A. J.; Ragotte, R. J.; Milles, L. F.; Wicky, B. I. M.; Hanikel, N.; Pellock, S. J.; Courbet, A.; Sheffler, W.; Wang, J.; Venkatesh, P.; Sappington, I.; Torres, S. V.; Lauko, A.; De Bortoli, V.; Mathieu, E.; Ovchinnikov, S.; Barzilay, R.; Jaakkola, T. S.; DiMaio, F.; Baek, M.; Baker, D. *Nature* **2023**, *620*, 1089-1100.
(37) Sinitcyn, P.; Richards, A. L.; Weatheritt, R. J.; Brademan, D. R.; Marx, H.; Shishkova, E.; Meyer, J. G.; Hebert, A. S.; Westphall, M. S.; Blencowe, B. J.; Cox, J.; Coon, J. J. *Nat. Biotechnol.* **2023**, *41*, 1776-1786.
(38) Tunyasuvunakool, K.; Adler, J.; Wu, Z.; Green, T.; Zielinski, M.; Žídek, A.; Bridgland, A.; Cowie, A.; Meyer, C.; Laydon, A.; Velankar, S.; Kleywegt, G. J.; Bateman, A.; Evans, R.; Pritzel, A.; Figurnov, M.; Ronneberger, O.; Bates, R.; Kohl, S. A. A.; Potapenko, A.; Ballard, A. J.; Romera-Paredes, B.; Nikolov, S.; Jain, R.; Clancy, E.; Reiman, D.; Petersen, S.; Senior, A. W.; Kavukcuoglu, K.; Birney, E.; Kohli, P.; Jumper, J.; Hassabis, D. *Nature* **2021**, *596*, 590-596.
(39) Abramson, J.; Adler, J.; Dunger, J.; Evans, R.; Green, T.; Pritzel, A.; Ronneberger, O.; Willmore, L.; Ballard, A. J.; Bambrick, J.; Bodenstein, S. W.; Evans, D. A.; Hung, C.-C.; O'Neill, M.; Reiman, D.; Tunyasuvunakool, K.; Wu, Z.; Žemgulytė, A.; Arvaniti, E.; Beattie, C.; Bertolli, O.; Bridgland, A.; Cherepanov, A.; Congreve, M.; Cowen-Rivers, A. I.; Cowie, A.; Figurnov, M.; Fuchs, F. B.; Gladman, H.; Jain, R.; Khan, Y. A.; Low, C. M. R.; Perlin, K.; Potapenko, A.; Savy, P.; Singh, S.; Stecula, A.; Thillaisundaram, A.; Tong, C.; Yakneen, S.; Zhong, E. D.; Zielinski, M.; Žídek, A.; Bapst, V.; Kohli, P.; Jaderberg, M.; Hassabis, D.; Jumper, J. M. *Nature* **2024**, *630*, 493-500.
(40) Rohl, C. A.; Strauss, C. E. M.; Misura, K. M. S.; Baker, D., Protein Structure Prediction Using Rosetta. In *Methods Enzymol.*, Academic Press: 2004; Vol. 383, pp 66-93.
(41) Baek, M.; DiMaio, F.; Anishchenko, I.; Dauparas, J.; Ovchinnikov, S.; Lee, G. R.; Wang, J.; Cong, Q.; Kinch, L. N.; Schaeffer, R. D.; Millán, C.; Park, H.; Adams, C.; Glassman, C. R.; DeGiovanni, A.; Pereira, J. H.; Rodrigues, A. V.; van Dijk, A. A.; Ebrecht, A. C.; Opperman, D. J.; Sagmeister, T.; Buhlheller, C.; Pavkov-Keller, T.; Rathinaswamy, M. K.; Dalwadi, U.; Yip, C. K.; Burke, J. E.; Garcia, K. C.; Grishin, N. V.; Adams, P. D.; Read, R. J.; Baker, D. *Science* **2021**, *373*, 871-876.
(42) Kuhlman, B.; Dantas, G.; Ireton, G. C.; Varani, G.; Stoddard, B. L.; Baker, D. *Science* **2003**, *302*, 1364-1368.
(43) NobelPrize.org, The Nobel Prize in Chemistry 2024. 2024.
(44) Mennen, S. M.; Alhambra, C.; Allen, C. L.; Barberis, M.; Berritt, S.; Brandt, T. A.; Campbell, A. D.; Castañón, J.; Cherney, A. H.; Christensen, M.; Damon, D. B.; Eugenio de Diego, J.; García-Cerrada, S.; García-Losada, P.; Haro, R.; Janey, J.; Leitch, D. C.; Li, L.; Liu, F.; Lobben, P. C.; MacMillan, D. W. C.; Magano, J.; McInturff, E.; Monfette, S.; Post, R. J.; Schultz, D.; Sitter, B. J.; Stevens, J. M.; Strambeanu, I. I.; Twilton, J.; Wang, K.; Zajac, M. A. *Org. Process Res. Dev.* **2019**, *23*, 1213-1242.
(45) Kumar, R. A.; Clark, D. S. *Curr. Opin. Chem. Biol.* **2006**, *10*, 162-168.
(46) Orsi, E.; Schada von Borzyskowski, L.; Noack, S.; Nikel, P. I.; Lindner, S. N. *Nat. Commun.* **2024**, *15*, 3447.
(47) Hajam, M. I.; Khan, M. M. *Biomater. Sci.* **2024**, *12*, 218-251.
(48) Norton-Baker, B.; Denton, M. C. R.; Murphy, N. P.; Fram, B.; Lim, S.; Erickson, E.; Gauthier, N. P.; Beckham, G. T. *Sci. Rep.* **2024**, *14*, 14449.
(49) CodeEvolver Platform. https://www.codexis.com/technology/codeevolver-platform.

(50) Biocatalysis. https://www.novonesis.com/en/biosolutions/industrial-bioprocessing/fine-chemicals/biocatalysis/solutions.
(51) Wilfrid, H. G. K. Manufacture of laevo-1-phenyl-2-methylaminopropanol-1. US1956950A, 1934.
(52) Maroney, K. A. N.; Culshaw, P. N.; Wermuth, U. D.; Cresswell, S. L. *Forensic Sci. Int.* **2014**, *235*, 52-61.
(53) de Marco, B. A.; Rechelo, B. S.; Tótoli, E. G.; Kogawa, A. C.; Salgado, H. R. N. *Saudi Pharm. J.* **2019**, *27*, 1-8.
(54) Patel, J. M. *J. Mol. Catal. B: Enzym.* **2009**, *61*, 123-128.
(55) Savile, C. K.; Janey, J. M.; Mundorff, E. C.; Moore, J. C.; Tam, S.; Jarvis, W. R.; Colbeck, J. C.; Krebber, A.; Fleitz, F. J.; Brands, J.; Devine, P. N.; Huisman, G. W.; Hughes, G. J. *Science* **2010**, *329*, 305-309.
(56) Cotton, H.; Elebring, T.; Larsson, M.; Li, L.; Sörensen, H.; von Unge, S. *Tetrahedron Asymmetry* **2000**, *11*, 3819-3825.
(57) Xu, N.; Zhu, J.; Wu, Y.-Q.; Zhang, Y.; Xia, J.-Y.; Zhao, Q.; Lin, G.-Q.; Yu, H.-L.; Xu, J.-H. *Org. Process Res. Dev.* **2020**, *24*, 1124-1130.
(58) Amann, F.; Frank, M.; Rhodes, R.; Robinson, A.; Kesselgruber, M.; Abele, S. *Org. Process Res. Dev.* **2016**, *20*, 446-451.
(59) Woyach, J. A.; Stephens, D. M.; Flinn, I. W.; Bhat, S. A.; Savage, R. E.; Chai, F.; Eathiraj, S.; Reiff, S. D.; Muhowski, E. M.; Granlund, L.; Szuszkiewicz, L.; Wang, W.; Schwartz, B.; Ghori, R.; Farooqui, M. Z. H.; Byrd, J. C. *Cancer Discov.* **2024**, *14*, 66-75.
(60) Deprez, N. R.; Rose, H. B.; Peters, B. K.; Diaz-Santana, A.; Liu, Z.; Kuhl, N.; Chung, C. K.; Liu, Z.; Newman, J. A.; Corry, J.; Guetschow, E. D.; Hoyt, E.; Jellett, L.; Kapil, S.; Poirier, M.; Shevlin, M.; Sirota, E.; Solovyov, A.; Sun, A. C.; Thaisrivongs, D. A. *Org. Process Res. Dev.* **2023**, *27*, 1965-1974.
(61) Kriek, Nicole M. A. J.; Hout, Elise van d.; Kelly, P.; Meijgaarden, Krista E. v.; Geluk, A.; Ottenhoff, Tom H. M.; Marel, Gijs A. van d.; Overhand, M.; Boom, Jacques H. v.; Valentijn, A. Rob P. M.; Overkleeft, Herman S. *Eur. J. Org. Chem.* **2003**, *2003*, 2418-2427.
(62) Kuhl, N.; Turnbull, B. W. H.; Ji, Y.; Larson, R. T.; Shevlin, M.; Prier, C. K.; Chung, C. K.; Desmond, R.; Guetschow, E.; He, C. Q.; Itoh, T.; Kuethe, J. T.; Newman, J. A.; Reibarkh, M.; Rivera, N. R.; Shang, G.; Wang, Z.; Zewge, D.; Thaisrivongs, D. A. *Green Chem.* **2023**, *25*, 606-613.
(63) Prier, C. K.; Camacho Soto, K.; Forstater, J. H.; Kuhl, N.; Kuethe, J. T.; Cheung-Lee, W. L.; Di Maso, M. J.; Eberle, C. M.; Grosser, S. T.; Ho, H.-I.; Hoyt, E.; Maguire, A.; Maloney, K. M.; Makarewicz, A.; McMullen, J. P.; Moore, J. C.; Murphy, G. S.; Narsimhan, K.; Pan, W.; Rivera, N. R.; Saha-Shah, A.; Thaisrivongs, D. A.; Verma, D.; Wyatt, A.; Zewge, D. *ACS Catal.* **2023**, *13*, 7707-7714.
(64) Di Maso, M. J.; Kuethe, J. T.; Narsimhan, K.; Burris, M.; Chung, C. K.; DiBenedetto, M.; Forstater, J. H.; Grosser, S. T.; Kuhl, N.; Lévesque, F.; Maguire, A.; Maloney, K. M.; McMullen, J. P.; Prier, C. K.; Qi, J.; Rivera, N. R.; Wang, Z.; Wyvratt, B. M.; Zewge, D. *Org. Process Res. Dev.* **2024**, *28*, 1764-1772.
(65) DiRocco, D. A.; Zhong, Y.-L.; Le, D. N.; McCann, S. D.; Hethcox, J. C.; Kim, J.; Kolev, J. N.; Kosjek, B.; Dalby, S. M.; McMullen, J. P.; Gangam, R.; Morris, W. J. *Org. Process Res. Dev.* **2024**, *28*, 404-412.
(66) Peng, F.; Tan, L.; Chen, L.; Dalby, S. M.; DiRocco, D. A.; Duan, J.; Feng, M.; Gong, G.; Guo, H.; Hethcox, J. C.; Jin, L.; Johnson, H. C.; Kim, J.; Le, D.; Lin, Y.; Liu, W.; Shen, J.; Wan,

Y.; Xiao, C.; Xiang, B.; Xiang, Q.; Xu, J.; Yan, L.; Yang, W.; Ye, H.; Yu, Y.; Zhang, J. *Org. Process Res. Dev.* **2022**, *26*, 508-515.
(67) Cheung-Lee, W. L.; Kolev, J. N.; McIntosh, J. A.; Gil, A. A.; Pan, W.; Xiao, L.; Velásquez, J. E.; Gangam, R.; Winston, M. S.; Li, S.; Abe, K.; Alwedi, E.; Dance, Z. E. X.; Fan, H.; Hiraga, K.; Kim, J.; Kosjek, B.; Le, D. N.; Marzijarani, N. S.; Mattern, K.; McMullen, J. P.; Narsimhan, K.; Vikram, A.; Wang, W.; Yan, J.-X.; Yang, R.-S.; Zhang, V.; Zhong, W.; DiRocco, D. A.; Morris, W. J.; Murphy, G. S.; Maloney, K. M. *Angew. Chem. Int. Ed.* **2024**, *63*, e202316133.
(68) McCann, S. D.; Dubina, S. H.; Kosjek, B.; Alwedi, E.; Behre, T.; Burgess, S. A.; Dal Poggetto, G.; DiRocco, D. A.; Hartmanshenn, C.; McMullen, J. P.; Padivitage, N.; Sun, A. C. *Org. Process Res. Dev.* **2024**, *28*, 441-450.
(69) FDA Lagevrio Letter of Authorization. https://www.fda.gov/media/155053/download.
(70) Merck Merck and Ridgeback Biotherapeutics Announce Initiation of Phase 3 Study (MOVe-NOW) Evaluating LAGEVRIO™ (molnupiravir) for the Treatment of COVID-19 in High-Risk Adults. https://www.merck.com/news/merck-and-ridgeback-biotherapeutics-announce-initiation-of-phase-3-study-move-now-evaluating-lagevrio-molnupiravir-for-the-treatment-of-covid-19-in-high-risk-adults/.
(71) Fier, P. S.; Xu, Y.; Poirier, M.; Brito, G.; Zheng, M.; Bade, R.; Sirota, E.; Stone, K.; Tan, L.; Humphrey, G. R.; Chang, D.; Bothe, J.; Zhang, Y.; Bernardoni, F.; Castro, S.; Zompa, M. A.; Taylor, J.; Sirk, K. M.; Diaz-Santana, A.; Diribe, I.; Emerson, K. M.; Krishnamurthi, B.; Zhao, R.; Ward, M.; Xiao, C.; Ouyand, H.; Zhan, J.; Morris, W. J. *Org. Process Res. Dev.* **2021**, *25*, 2806-2815.
(72) McIntosh, J. A.; Benkovics, T.; Silverman, S. M.; Huffman, M. A.; Kong, J.; Maligres, P. E.; Itoh, T.; Yang, H.; Verma, D.; Pan, W.; Ho, H.-I.; Vroom, J.; Knight, A. M.; Hurtak, J. A.; Klapars, A.; Fryszkowska, A.; Morris, W. J.; Strotman, N. A.; Murphy, G. S.; Maloney, K. M.; Fier, P. S. *ACS Cent. Sci.* **2021**, *7*, 1980-1985.
(73) Maddess, M.; McIntosh, J.; Chang, W., Discovery and Chemical Development of Uvelostinag (MK-1454): A Therapeutic Cyclic Dinucleotide Agonist of the Stimulator of Interferon Gene. In *Complete Accounts of Integrated Drug Discovery and Development: Recent Examples from the Pharmaceutical Industry. Volume 4*, American Chemical Society: 2022; Vol. 1423, pp 1-94.
(74) Hall, J.; Ralph, E. C.; Shanker, S.; Wang, H.; Byrnes, L. J.; Horst, R.; Wong, J.; Brault, A.; Dumlao, D.; Smith, J. F.; Dakin, L. A.; Schmitt, D. C.; Trujillo, J.; Vincent, F.; Griffor, M.; Aulabaugh, A. E. *Protein Sci.* **2017**, *26*, 2367-2380.
(75) McIntosh, J. A.; Liu, Z.; Andresen, B. M.; Marzijarani, N. S.; Moore, J. C.; Marshall, N. M.; Borra-Garske, M.; Obligacion, J. V.; Fier, P. S.; Peng, F.; Forstater, J. H.; Winston, M. S.; An, C.; Chang, W.; Lim, J.; Huffman, M. A.; Miller, S. P.; Tsay, F.-R.; Altman, M. D.; Lesburg, C. A.; Steinhuebel, D.; Trotter, B. W.; Cumming, J. N.; Northrup, A.; Bu, X.; Mann, B. F.; Biba, M.; Hiraga, K.; Murphy, G. S.; Kolev, J. N.; Makarewicz, A.; Pan, W.; Farasat, I.; Bade, R. S.; Stone, K.; Duan, D.; Alvizo, O.; Adpressa, D.; Guetschow, E.; Hoyt, E.; Regalado, E. L.; Castro, S.; Rivera, N.; Smith, J. P.; Wang, F.; Crespo, A.; Verma, D.; Axnanda, S.; Dance, Z. E. X.; Devine, P. N.; Tschaen, D.; Canada, K. A.; Bulger, P. G.; Sherry, B. D.; Truppo, M. D.; Ruck, R. T.; Campeau, L.-C.; Bennett, D. J.; Humphrey, G. R.; Campos, K. R.; Maddess, M. L. *Nature* **2022**, *603*, 439-444.
(76) Benkovics, T.; Peng, F.; Phillips, E. M.; An, C.; Bade, R. S.; Chung, C. K.; Dance, Z. E. X.; Fier, P. S.; Forstater, J. H.; Liu, Z.; Liu, Z.; Maligres, P. E.; Marshall, N. M.; Salehi Marzijarani, N.; McIntosh, J. A.; Miller, S. P.; Moore, J. C.; Neel, A. J.; Obligacion, J. V.; Pan, W.; Pirnot, M.

T.; Poirier, M.; Reibarkh, M.; Sherry, B. D.; Song, Z. J.; Tan, L.; Turnbull, B. W. H.; Verma, D.; Waldman, J. H.; Wang, L.; Wang, T.; Winston, M. S.; Xu, F. *J. Am. Chem. Soc.* **2022**, *144*, 5855-5863.
(77) O'Dowd, H.; Morales, O. M. *Org. Process Res. Dev.* **2024**, *28*, 2789-2793.
(78) St-Jean, F.; Angelaud, R.; Bachmann, S.; Carrera, D. E.; Remarchuk, T.; Piechowicz, K. A.; Niedermann, K.; Iding, H.; Meier, R.; Hou, H.; Sirois, L. E.; Xu, J.; Olbrich, M.; Rege, P.; Guillemot-Plass, M.; Gosselin, F. *J. Org. Chem.* **2022**, *87*, 4955-4960.
(79) Molinaro, C.; Phillips, E. M.; Xiang, B.; Milczek, E.; Shevlin, M.; Balsells, J.; Ceglia, S.; Chen, J.; Chen, L.; Chen, Q.; Fei, Z.; Hoerrner, S.; Qi, J.; de Lera Ruiz, M.; Tan, L.; Wan, B.; Yin, J. *J. Org. Chem.* **2019**, *84*, 8006-8018.
(80) Yasuda, N.; Cleator, E.; Kosjek, B.; Yin, J.; Xiang, B.; Chen, F.; Kuo, S.-C.; Belyk, K.; Mullens, P. R.; Goodyear, A.; Edwards, J. S.; Bishop, B.; Ceglia, S.; Belardi, J.; Tan, L.; Song, Z. J.; DiMichele, L.; Reamer, R.; Cabirol, F. L.; Tang, W. L.; Liu, G. *Org. Process Res. Dev.* **2017**, *21*, 1851-1858.
(81) Connor, C. G.; DeForest, J. C.; Dietrich, P.; Do, N. M.; Doyle, K. M.; Eisenbeis, S.; Greenberg, E.; Griffin, S. H.; Jones, B. P.; Jones, K. N.; Karmilowicz, M.; Kumar, R.; Lewis, C. A.; McInturff, E. L.; McWilliams, J. C.; Mehta, R.; Nguyen, B. D.; Rane, A. M.; Samas, B.; Sitter, B. J.; Ward, H. W.; Webster, M. E. *Org. Process Res. Dev.* **2021**, *25*, 608-615.
(82) Kumar, R.; Karmilowicz, M. J.; Burke, D.; Burns, M. P.; Clark, L. A.; Connor, C. G.; Cordi, E.; Do, N. M.; Doyle, K. M.; Hoagland, S.; Lewis, C. A.; Mangan, D.; Martinez, C. A.; McInturff, E. L.; Meldrum, K.; Pearson, R.; Steflik, J.; Rane, A.; Weaver, J. *Nat. Catal.* **2021**, *4*, 775-782.
(83) Kleinbeck, F.; Mahut, M.; Schlama, T., Industrial Processes Using Biocatalysts. In *Biocatalysis for Practitioners*, 2021; pp 427-465.

CHAPTER TWO

A Chemoenzymatic Hydroaminomethylation Strategy for the Selective Synthesis of Linear Primary Amines from Olefins by Sequential and Tandem Processes

2.1 Abstract

Methods that form amines from feedstock chemicals are an important component of industrial chemistry. Many methods for the synthesis of amines yield mixtures of primary, secondary, and tertiary amines, necessitating costly downstream separations. We present a chemoenzymatic approach to hydroaminomethylation that addresses these challenges by combining hydroformylation catalyzed by a phosphine-bound rhodium complex with enzymatic transamination catalyzed by an ω-transaminase from *Vibrio fluvialis* (*Vf*TA). This sequential chemoenzymatic hydroaminomethylation reaction converts olefins to linear primary amines with high regioselectivity and chemoselectivity for the linear primary amine, and we demonstrate that this process occurs with a series of olefins with varying structures. Furthermore, we report progress toward a tandem process that incorporates a biocatalytic cascade for recycling an intermediate amine donor, which is required for the transaminase enzyme to use an ammonium salt as the terminal nitrogen source. This study illustrates the potential to combine chemo- and biocatalytic reactions to produce valuable materials from readily available feedstocks in both tandem and sequential processes, with selectivities that have not been achieved with transition-metal catalysts.

2.2 Introduction

Linear primary amines are important intermediates and products for the production of many industrial and fine chemicals (Figure 1a).[1] At large scales, primary amines are commonly synthesized by the amination of alcohols, the reductive amination of ketones or aldehydes, or the reduction of nitriles.[2] These transformations yield mixtures of primary, secondary, and tertiary amines, which often necessitate costly and inefficient downstream separations to isolate the desired primary amine.[2] These methods may also require prior functionalization of feedstock chemicals to incorporate an alcohol, carbonyl group, or nitrile selectively at the terminal position.

Hydroaminomethylation is an alternative technique that can be harnessed to synthesize primary amines. In the desired reaction, an olefin is directly converted to a primary amine by sequential hydroformylation and reductive amination. However, there are many challenges to developing selective methods for hydroaminomethylation (Figure 1b): typical systems require high temperatures and pressures and, critically, suffer from overalkylation of the desired primary amine.[3-5] Without the proper choice of conditions, side reactions, such as reduction of the olefin or of the intermediate aldehyde, can also occur.

Previous work on hydroaminomethylation by Beller and coworkers employed a bimetallic system to form primary amines from aliphatic aldehydes and ammonia (Figure 1c).[6] This method required temperatures of 130 °C and pressures of 78 bar, which contribute to overalkylation of the primary amine product to form 20% secondary amine. The groups of Xiao and Han developed methods with rhodium catalysts for hydroaminomethylation that produce linear secondary and tertiary arylamines but were unable to produce primary amines.[7-8] In 2019, our group developed a bimetallic, dual-catalytic hydroaminomethylation reaction that yielded linear secondary and tertiary amines, but no primary amine products were reported.[9] Despite these advances, the selective synthesis of linear primary amines by hydroaminomethylation catalyzed by transition metals remains a formidable challenge.

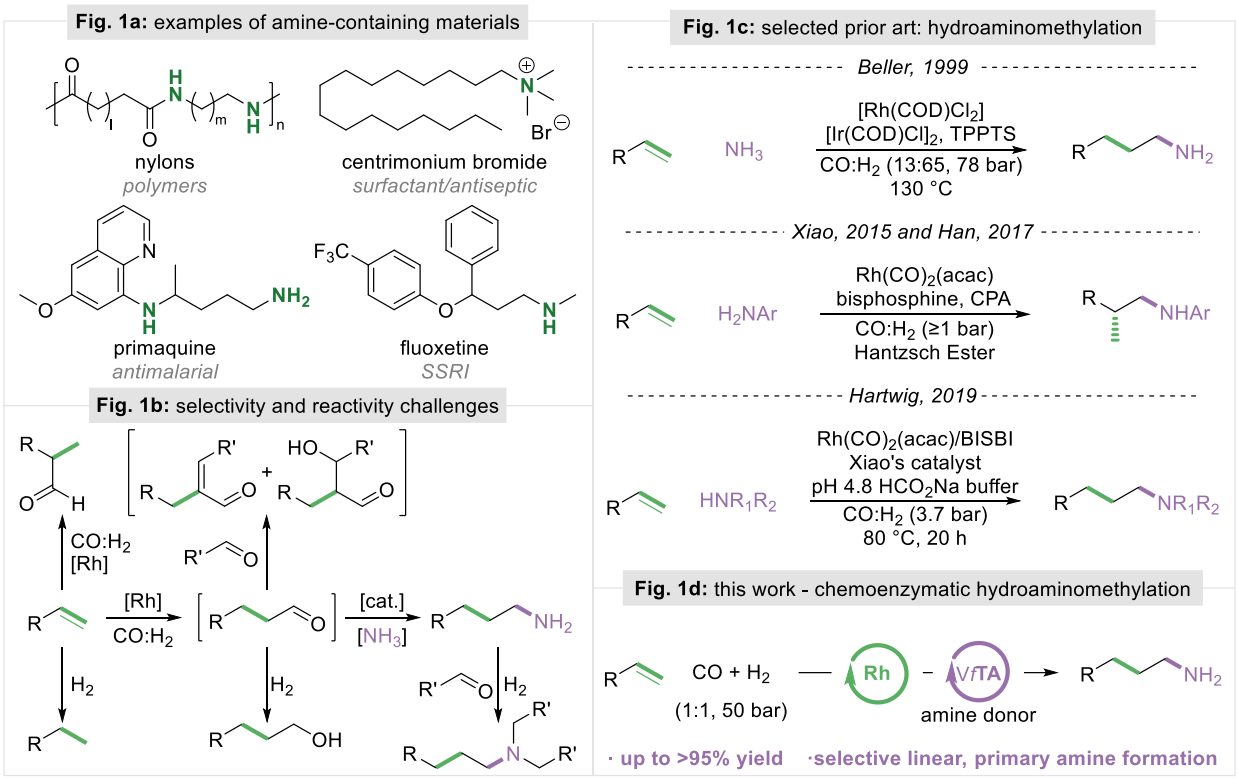

Figure 1. a) examples of amine-containing materials, b) selectivity and reactivity challenges, c) selected prior art, and d) this work. TPPTS = tris(3-sulfophenyl)phosphine trisodium salt, BISBI = 2,2'-bis(diphenylphosphinomethyl)-1,1'-biphenyl, CPA = chiral phosphoric acid, (*S*)-MBA = (*S*)-methyl benzylamine.

A hydroaminomethylation reaction that occurs with a high degree of control over the linear-to-branched (*l:b*) ratio and with a high degree of selectivity for the primary amine would enable the use of olefin feedstocks as direct precursors to valuable linear primary amines. The hydroformylation component of the hydroaminomethylation sequence is one of the most well-studied and widely-employed reactions used to produce millions of metric tons of aldehydes each year.[10] Reactions conducted with catalysts containing phosphorous-based ligands, in combination with rhodium, are known to selectively produce linear aldehydes from olefins.[11]

Although transition metal catalyzed reductive aminations of ketones and aldehydes can suffer from overalkylation, ω-transaminase enzymes are known to selectively form primary amines from aldehydes and ketones. Transaminases are a class of pyridoxal phosphate (PLP)-dependent enzymes that facilitate transamination by transfer of an amino group from a stoichiometric amine donor.[12] The application of enzymes to achieve high selectivity is a powerful strategy,[13] and enzymatic cascade reactions[14-18] and enzymatic reactions catalyzed by transaminase enzymes in particular[19] have been applied to the manufacture of various active pharmaceutical ingredients[20] and polymers.[21] Additionally, while preparing this manuscript, Gröger and coworkers disclosed a selective tandem chemoenzymatic system that produces alcohols from olefins.[22] We show that by careful selection of an organotransition metal catalyst for hydroformylation and an enzyme for reductive amination, we can avoid overalkylation and achieve site-selectivity for the conversion of a wide range of olefins to linear primary amines in both sequential and tandem processes.

2.3 Results & Discussion

2.3.1 Development of Reaction Conditions for Enzymatic Transamination in a Sequential Process.

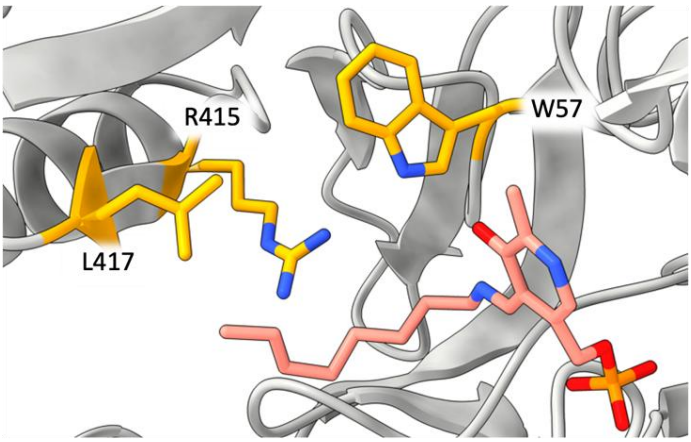

Figure 2. WT-*Vf*TA active site with docked octanal-PMP (pink) and sites of mutagenesis (gold). WT-*Vf*TA PDB: 4E3Q.[23]

Wild-type ω-transaminase enzymes from *Vibrio fluvialis* (WT-*Vf*TA) and *Chromobacterium violacium* (WT-*Cv*TA) are known to catalyze the transamination of hexanal and nonanal with (*S*)-methylbenzyl amine ((*S*)-MBA) as the amine donor.[24] With both (*S*)-MBA and L-alanine as amine donors, moderate yields of primary amine product (60-74%) were formed (Table 1, entries 1-2, 5-6) by purified WT-*Vf*TA and WT-*Cv*TA as catalysts. The conditions that form primary amine product in the highest yield with these purified enzymes were 100 mM sodium phosphate buffer (pH 7.5, 100 mM sodium chloride) and 0.5 mM PLP, with gentle stirring (140-150 rpm) at 30 °C (see supporting information for further details; Table S2). Minimal background reactivity was observed without the addition of enzyme (Table 1, entry 7).

Table 1. Evaluation of conditions for the enzymatic transamination reaction of octanal.[a]

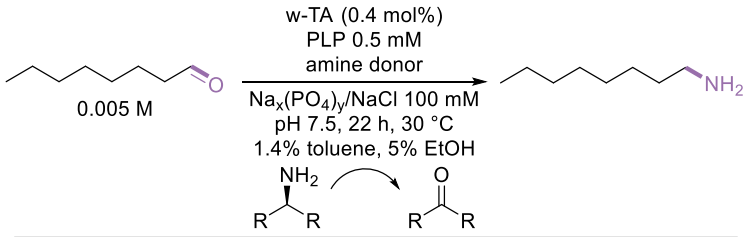

Entry	Enzyme	Amine Donor	Cosolvent	Yield (%)
1	WT-*Vf*TA	L-alanine (100 equiv)	—	63
2	WT-*Cv*TA	L-alanine (100 equiv)	—	60
3	*Vf*TA-3M	L-alanine (100 equiv)	—	< 5
4	*Vf*TA-3M/Q	L-alanine (100 equiv)	—	61
5	WT-*Vf*TA	(*S*)-MBA (7.5 equiv)	—	70
6	WT-*Cv*TA	(*S*)-MBA (7.5 equiv)	—	74
7	—	(*S*)-MBA (7.5 equiv)	—	trace
8	*Vf*TA-3M	(*S*)-MBA (7.5 equiv)	—	87
9	*Vf*TA-3M/Q	(*S*)-MBA (7.5 equiv)	—	82
10	*Vf*TA-3M	(*S*)-MBA (7.5 equiv)	PhMe	89
11	*Vf*TA-3M/Q	(*S*)-MBA (7.5 equiv)	PhMe	82
12	*Vf*TA-3M	(*S*)-MBA (7.5 equiv)	EtOH/PhMe	93
13	*Vf*TA-3M/Q	(*S*)-MBA (7.5 equiv)	EtOH/PhMe	87

[a]Reaction conducted on a 0.01 mmol scale. Yield was determined using a GC-FID calibration curve with dodecane as an internal standard.

To increase the activity of the WT-*Vf*TA enzyme for the formation of the primary amines from long-chain aldehydes, we conducted mutagenesis on WT-*Vf*TA. First, we computationally docked the aldimine intermediate formed from the condensation of pyridoxamine phosphate (PMP) and octanal[25] to identify which residues were proximal to the long- chain aldehyde (Figure 2). The docked PMP-imine aligns well with the docked native PMP (see supporting information, Figure S2 and Table S6). In the active site, residues W57, R415, and L417 are proximate to the docked substrate. Prior reports[26] also have identified these three positions as active site hotspots for mutagenesis.

Table 2. Evaluation of conditions for the hydroformylation of heptene.[a]

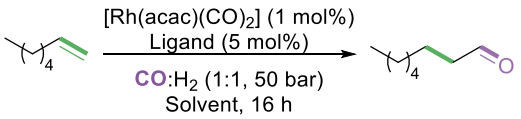

Entry	Ligand	Solvent (0.2 M)	T (°C)	Yield (%)
1	BISBI	toluene	80	99
2	BISBI	CPME	80	95
3	TPPTS	H_2O	120	6
4	SulfoXantphos	H_2O	120	7
5	BISBI	glycerol:H_2O (30:70)	80	11
6	BISBI	IPA:H_2O (10:90)	80	17
7	BISBI	IPA:H_2O (30:70)	80	64
8	BISBI	IPA:pH = 7.4 buffer (30:70)	80	0

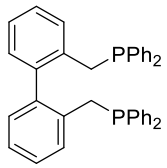

BISBI

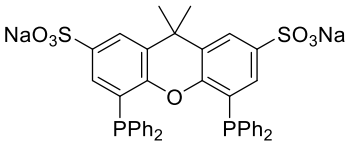

SulfoXantphos

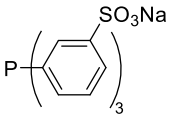

TPPTS

[a]Buffer = 100 mM sodium phosphate buffer, pH 7.5, 100 mM sodium chloride, and 0.5 mM PLP. Reaction was conducted on a 0.75 mmol scale. Yield was determined using a GC-FID calibration curve with dodecane as an internal standard. CPME = cyclopentyl methyl ether; BISBI = 2,2'-Bis(diphenylphosphinomethyl)-1,1'-biphenyl; TPPTS = 3,3',3''-phosphinidynetris(benzenesulfonic acid) trisodium salt.

Mutations at these residues (W57F, R415L, and L417V) increased the reactivity of WT-*Vf*TA variants toward long-chain aliphatic aldehydes over that of the wild-type enzyme, presumably by introducing small or hydrophobic residues to the active site. With this triple variant, *Vf*TA-3M, yields of up to 87% of octylamine were achieved (Table 1, entry 8). Site-saturation mutagenesis at the R415 position in the active site led to a W57F/R415Q/L417V *Vf*TA variant, *Vf*TA-3M/Q, that catalyzed the transamination of octanal in 82% yield (Table 1, entry 9).

We also investigated reductive amination of aldehydes with several homogenous[27-29] and heterogeneous[30-33] catalysts containing transition metals. We were unable to achieve selective formation of the primary amine with the homogenous catalysts we tested. The heterogenous catalysts we examined formed the desired primary amine product; however, these heterogeneous catalysts required moderate pressures of ammonia, leached metal into solution, and were poisoned by CO, which is required for an up-stream hydroformylation process (see Schemes S6-S8).

To realize a sequential hydroaminomethylation process, we proposed that the enzymatic reaction must tolerate the presence of organic solvents. Lyophilized whole cells with expressed protein and microaqueous conditions[34] with 99% organic solvents (CPME, THF, or toluene) and 1% sodium phosphate/sodium chloride buffer (pH 7.5) gave < 1% reaction product (See S4). Conversely, in buffered aqueous solutions with 1.4% toluene cosolvent, there was no decrease in activity for the *Vf*TA-3M or *Vf*TA-3M/Q variants (Table 1, entries 10-11), and the addition of 5% ethanol to the reaction mixture led to further increase in yields of octylamine (Table 1, entries 12-13). Secondary or tertiary amine products from these reactions were not detected by GC-FID.

L-alanine was found to be a less efficient amine donor for the *Vf*TA variants, as the *Vf*TA-3M/Q enzyme catalyst gave a moderate yield of primary amine product (Table 1, entry 5), and only trace primary amine product was observed from *Vf*TA-3M, with recovered aldehyde starting material (Table 1, entry 3).

2.3.2 Investigation of Reaction Conditions for the Hydroformylation Reaction in a Sequential Process.

To enable the enzymatic transamination step to be compatible with the hydroformylation step, we explored hydroformylation reactions under aqueous conditions.[35] The industrial hydroformylation of propene can be conducted under aqueous conditions (the Ruhrchemie/Rhône-Poulenc oxo process),[36] but aqueous hydroformylation is difficult to adapt to medium or long-chain olefins because of their insolubility in water.[37] Various techniques have been explored to increase the compatibility of heavier olefins with aqueous systems, including the use of cyclodextrins as phase-transfer agents and the incorporation of co-solvents to increase the solubility of the substrate.[38-40]

A benchmark hydroformylation of heptene in toluene with BISBI ligand and [Rh(acac)$(CO)_2$] pre-catalyst resulted in 99% yield of octanal (Table 2, entry 1). Our attempts to achieve the aqueous hydroformylation of heptene with water-soluble ligands in combination with rhodium resulted in poor yields, up to 7% (Table 2, entries 3-4). Biphasic systems with water gave yields up to 64%; however, the use of 100 mM sodium phosphate/sodium chloride, pH 7.5 buffer solution prevented the hydroformylation reaction from occurring (Table 2, entries 7-8). Thus, to conduct a sequential hydroaminomethylation process, we conducted the hydroformylation reactions in organic solvent

with BISBI ligand in an autoclave before adding the crude mixture of the hydroformylation reaction of heptene directly to the enzymatic transamination reaction in aqueous buffer. In this two-step, one-pot process, *Vf*TA-3M and *Vf*TA-3M/Q formed the primary amine in 59% and 60% yields, respectively, with no branched, secondary, or tertiary amine side products detected by GC-FID analysis.

2.3.3 Scope of the Sequential Chemoenzymatic Hydroaminomethylation Reaction.

We then investigated the scope of olefins amenable to the chemoenzymatic sequential hydroaminomethylation reaction (Table 3). For medium-chain to long-chain linear olefins, the highest yield for the transamination of heptanal (**2a**), octanal (**2c**), and nonanal (**2d**) was achieved with *Vf*TA-3M/Q, and the highest yield for the transamination of hexanal (**2b**) was achieved with WT-*Vf*TA. For long-chain olefins with pendant alcohols, the highest yields for the transamination of **2e** and **2f** were achieved with WT-*Vf*TA, and the highest yield for the transamination of **2g** was accomplished with *Vf*TA-3M/Q.

The sequential reaction tolerates a variety of common functional groups. An olefin bearing a primary bromide (**2h**) reacted to produce primary amine product in 74% yield with preservation of the halogen. Olefins bearing pendent methyl (**2i-k**) and ethyl (**2l**) esters reacted to produce primary amine products without cyclization to form lactams and without hydrolysis of the esters. The poorly soluble aldehyde formed from olefin **1m** provided primary amine **2m** in 30% yield. Primary amine **2n** formed in high yield with the 1,2-disubstituted olefin remaining intact and was

isolated in moderate yield from the enzymatic transamination at a 0.1 mmol scale. 1,1-Disubstituted olefins reacted to deliver primary amines with a pendant cyclohexane (**2o**), piperidine (**2p**), and azetidine (**2q**) moiety. Allylbenzene reacted to form primary amine **2r** in greater than 95% yield. A tertiary amine (**2s**) was also well-tolerated. An olefin containing a benzyl-protected alcohol (**2t**) reacted in the sequential process to form the primary amine in good yield, as did an olefin containing a pyridyl group (**2u**). The hydroformylation of olefins containing

Chart 1. Scope of the chemoenzymatic hydroaminomethylation reaction.[a]

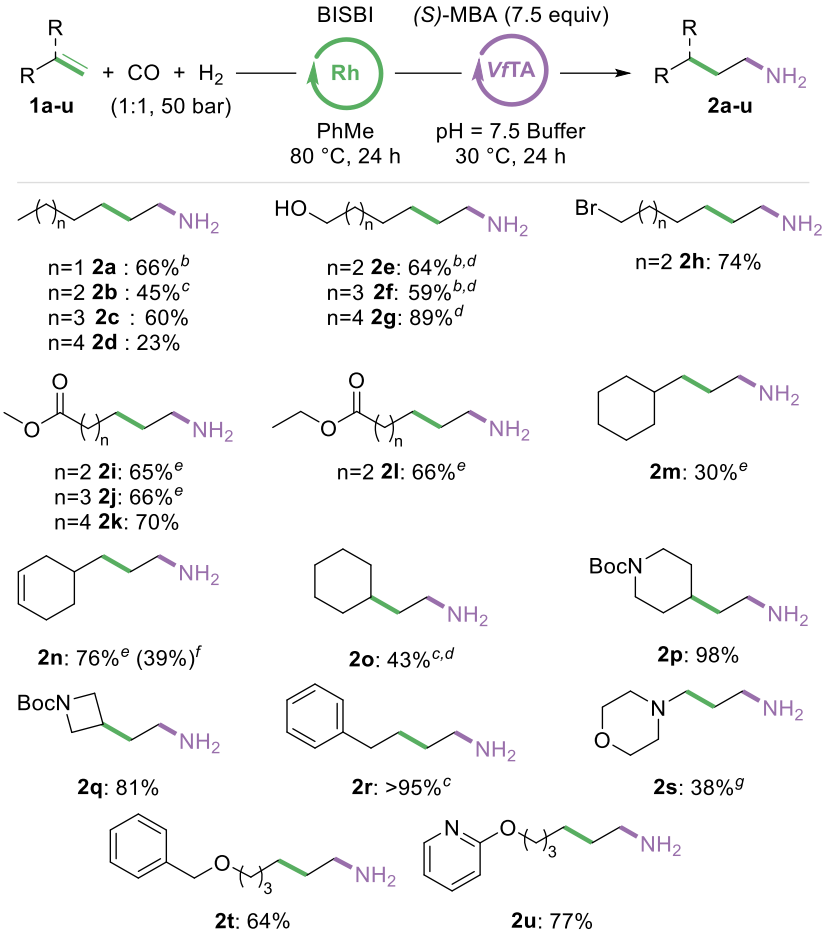

[a]Yield determined using GC-FID analysis with dodecane as internal standard or ^{1}H qNMR spectroscopy with dibromomethane as a standard. Rection conditions (unless otherwise specified): [Rh(acac)(CO)$_2$] (3 mol%), BISBI (5 mol%), PhMe (0.2 M), CO:H2 (1:1, 50 bar); [b]reaction conducted with WT-*Vf*TA; [c]transamination conducted with 10% DMSO and 22.5 equiv (*S*)-MBA; [d]hydroformylation conducted in DMF. [e]reaction conducted with *Vf*TA-3M. [f]isolated yield, 0.1 mmol scale. [g]hydroformylation conducted with BiPhePhos as ligand in THF solvent BiPhePhos = 6,6'-[(3,3′-Di-tert-butyl-5,5'-dimethoxy-[1,1'-biphenyl]-2,2'-diyl)bis(oxy)]bis(6H-dibenzo[d,f][1,3,2]dioxaphosphepine).

functional groups at the allylic or homoallylic position was accomplished in tetrahydrofuran (THF) solvent with BiPhePhos as the ligand, and the hydroformylations of substrates with poor solubility in toluene were conducted in dimethylformamide (DMF) solvent, which was well-tolerated by enzymatic reaction (See supporting information, Table S2).

2.3.4 Investigation of Conditions for a Tandem Chemoenzymatic Hydroaminomethylation Reaction.

Incorporation of a biocatalytic cascade capable of recycling the amine donor for this process would enable the direct transformation of olefin feedstocks to primary amines using ammonium salts,

carbon monoxide, hydrogen, and glucose as a terminal reductant.[41] We envisioned pairing the transaminase enzyme with an alanine dehydrogenase enzyme to turn over the amine donor and a glucose dehydrogenase enzyme to turn over the NADPH cofactor required by the alanine dehydrogenase enzyme. With WT-*Vf*TA, WT-*Bs*AlaDH, *Bs*GDH, 2.5 equivalents of pyruvate, and glucose in an ammonium formate buffer, amine **2k** is formed in 23% yield with this cascade approach (Scheme 1). Without the recycling mechanism, **2k** formed in 49% yield with 100 equivalents of L-alanine as the amine donor.

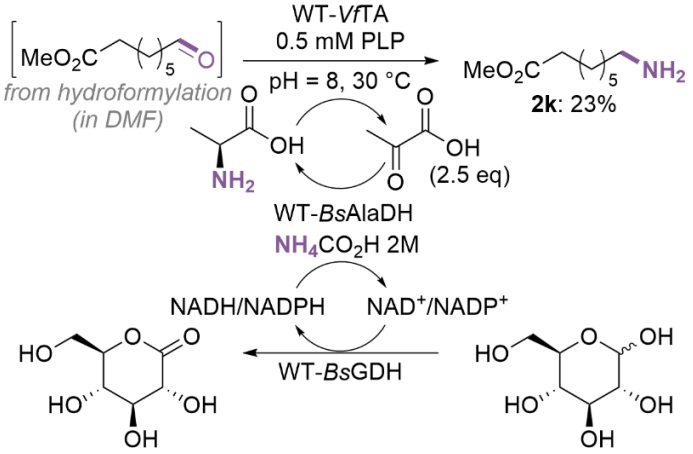

Scheme 1. Alanine recycling cascade for the transamination of linear aldehydes.

We sought to convert the sequential hydroaminomethylation approach into a one-pot tandem process. Gröger and coworkers,[22] recently reported the tandem one-pot hydroformylation and reduction of olefins to alcohols. By applying the reported conditions for hydroformylation with DPPon as a ligand for rhodium,[42] we were able to achieve 77% yield of octanal from heptene at 30 °C with 40 bar of syngas (Table 3, entry 1). When (*S*)-MBA was added to the hydroformylation reaction, the yield of octanal decreased to 45% in comparison to the control reaction. However, the addition of alanine, ammonium formate, or ammonium chloride did not significantly decrease the yield of octanal in comparison to the control reaction (see supporting information, Table S5). When the tandem hydroaminomethylation reaction was run with the addition of *Vf*TA-3M/Q and (*S*)-MBA as the amine donor, we achieved 20% of the desired linear primary amine from heptene; however, the tandem reaction formed dioctylamine in 5% yield and trace amounts of (*S*)-*N*-(1-phenylethyl)octan-1-amine. (Table 3, entry 2). To avoid formation of secondary amine side products, we aimed to use alanine and an ammonium salt as our amine sources. Application of the cofactor and amine donor recycling cascade composed of WT-*Bs*GDH and WT-*Bs*AlaDH in combination with WT-*Vf*TA, NH_4CO_2H, and alanine (Scheme 1) gave 2% yield of the desired linear primary amine from heptene with no formation of dioctylamine (Table 3, entry 4). Use of NH_4Cl and alanine as the amine sources at pH = 6.5 resulted in a 23% yield of the linear primary amine product from heptene with no branched amine products detected by GC-FID or by ^1H NMR spectroscopy (Table 3, entries 5-8). Lowering the concentration of heptene to 0.1 M while keeping the concentrations of rhodium and enzyme catalysts consistent gave 29% yield of desired primary amine product with no observed formation of dioctylamine (Table 3, entry 9). Therefore, we have demonstrated that one can selectively form linear primary amines in moderate yield with a cascade comprising metal-catalyzed hydroformylation and enzymatic transamination that operate

simultaneously. Future work will address improving yield while maintaining high selectivity in this tandem process.

Table 3. Evaluation of Conditions for a Tandem Chemoenzymatic Process.[a]

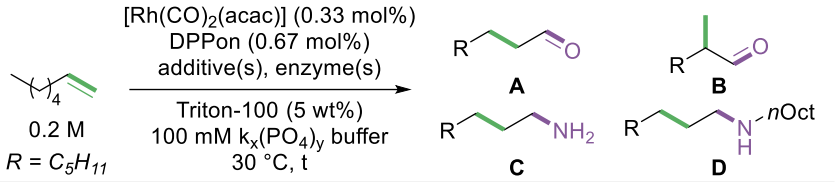

Entry	Additive(s)	Enzyme(s)	pH	t (h)	Yield A+B/**C**/D (%)
1	-	-	7.0	22	77 / **-** / -
2	(*S*)-MBA	*Vf*TA-3M/Q	7.0	22	3 / **20** / 5
3	(*S*)-MBA	*Vf*TA-3M/Q	6.5	6	5 / **14** / 3
4	NH_4CO_2H, Ala	WT-*Vf*TA, AlaDH, GDH	7.0	22	2 / **3** / 0
5	NH_4Cl, Ala	WT-*Vf*TA, AlaDH, GDH	7.0	22	3 / **21** / 0
6	NH_4Cl, Ala	WT-*Vf*TA, AlaDH, GDH	7.5	6	3 / **9** / 0
7	NH_4Cl, Ala	WT-*Vf*TA, AlaDH, GDH	6.5	6	5 / **23** / 0
8	NH_4Cl, Ala	WT-*Vf*TA, AlaDH, GDH	5.5	6	6 / **13** / 0
9[b]	NH_4Cl, Ala	WT-*Vf*TA, AlaDH, GDH	6.5	6	6 / **29** / 0

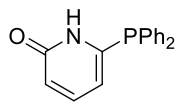

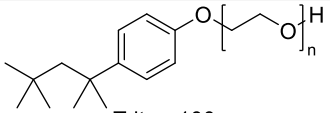

[a]Ala = 0.93 M alanine, 375 mM glucose, 0.2 mM NADPH/NADH; (*S*)-MBA = 0.41 M; NH_4CO_2H = 1 M; NH_4Cl = 200 mM; B1 = 100 mM potassium phosphate buffer pH 7.5, 100 mM sodium chloride, 10% glycerol; B2 = 50 mM tris HCl pH 7.5, 50 mM sodium chloride, 10% glycerol; B3 = 100 mM sodium phosphate pH 7.5, 100 mM sodium chloride, 0.5 mM PLP, 10% glycerol; 156 mM GDH = 100 uL of purified *Bs*GDH in B1; 58 mM AlaDH = 200 mL of WT-*Bs*AlaDH in B2; 65 mM *Vf*TA-3M/Q and WT-*Vf*TA = 700 uL in B3. [b]0.1 M heptene, 0.66 mol% [Rh], 1.4 mol% DPPon

2.4 Summary

In summary, we have developed a method for the highly linear- and primary-selective synthesis of amines by sequential transition-metal catalyzed hydroformylation and enzyme-catalyzed transamination reactions. The sequential method avoids the formation of secondary and tertiary amines, as well as branched alkylamines. We further demonstrated the broad substrate scope of this method and the feasibility of coupling this transformation with a biocatalytic cascade to enable the use of feedstock chemicals for the hydroaminomethylation of simple olefins. We additionally report progress on the development of a tandem process wherein metal-catalyzed hydroformylation and enzymatic transamination occur simultaneously. We report the development of conditions to avoid the formation of over-alkylated and branched products. These results show how a chemoenzymatic approach can lead to selective formation of a desired product, and we anticipate related approaches will enable additional classes of chemical transformations to occur with high selectivities.

2.5 References

(1) Lawrence, S. A., *Amines: synthesis, properties and applications*. Cambridge University Press: 2004.

(2) Hayes, K. S. Industrial processes for manufacturing amines *Appl. Catal. A: Gen.* **2001** *221*, 187-195.

(3) Philippe Kalck, M. U. Tandem Hydroaminomethylation Reaction to Synthesize Amines from Alkenes *Chem. Rev.* **2018**, *118*, 3833-3861.

(4) Irrgang, T.; Kempe, R. Transition-Metal-Catalyzed Reductive Amination Employing Hydrogen. *Chem. Rev.* **2020**, *120*, 9583-9674.

(5) Kumar, R.; Flodén, N. J.; Whitehurst, W. G.; Gaunt, M. J. A general carbonyl alkylative amination for tertiary amine synthesis. *Nature* **2020**, *581*, 415-420.

(6) Zimmermann, B.; Herwig, J.; Beller, M. The First Efficient Hydroaminomethylation with Ammonia: With Dual Metal Catalysts and Two-Phase Catalysis to Primary Amines. *Angew Chem Int Ed Engl* **1999**, *38*, 2372-2375.

(7) Chen, X.-C.; Lan, T.; Zhao, K.-C.; Guo, L.; Lu, Y.; Liu, Y. Efficient hydroaminomethylation of olefins catalyzed by Rh-complex ligated by P,O-hybrid ligand with chelating effect. *J. Catal.* **2022**, *411*, 158-166.

(8) J. M. Han, L. X.-H., Y. Zhi, Enantioselective Hydroaminomethylation of Olefins Enabled by Rh/Brønsted Acid Relay Catalysis. *Org. Lett.* **2017**, *19*, 1076.

(9) Hanna, S.; Holder, J. C.; Hartwig, J. F. A Multicatalytic Approach to the Hydroaminomethylation of alpha-Olefins. *Angew Chem Int Ed Engl* **2019**, *58*, 3368-3372.

(10) Franke, R., Selent, D.. Börner, A. Applied Hydroformylation *Chem. Rev.* **2012** *112* 5675-5732.

(11) Norrby, P. O., Organotransition Metal Chemistry: From Bonding to Catalysis. John Hartwig. Wiley Online Library: 2010.

(12) Kelly, S. A., Pohle, S. Wharry, S. Mix, S., Allen, C. C. R., Moody, T. S., Gilmore, B. F. Application of ω-Transaminases in the Pharmaceutical Industry *Chem. Rev.* **2018**, *118*, 349-367.

(13) Greg Hughes, J. L. Introduction: Biocatalysis in Industry. *Chem. Rev.* **2018**, *118*, 1-3.

(14) Huffman, M. A.; Fryszkowska, A.; Alvizo, O.; Borra-Garske, M.; Campos, K. R.; Canada, K. A.; Devine, P. N.; Duan, D.; Forstater, J. H.; Grosser, S. T.; Halsey, H. M.; Hughes, G. J.; Jo, J.; Joyce, L. A.; Kolev, J. N.; Liang, J.; Maloney, K. M.; Mann, B. F.; Marshall, N. M.; McLaughlin, M.; Moore, J. C.; Murphy, G. S.; Nawrat, C. C.; Nazor, J.; Novick, S.; Patel, N. R.; Rodriguez-Granillo, A.; Robaire, S. A.; Sherer, E. C.; Truppo, M. D.; Whittaker, A. M.; Verma, D.; Xiao, L.; Xu, Y.; Yang, H. Design of an in vitro biocatalytic cascade for the manufacture of islatravir. *Science* **2019**, *366*, 1255-1259.

(15) Mcintosh, J. A.; Benkovics, T.; Silverman, S. M.; Huffman, M. A.; Kong, J.; Maligres, P. E.; Itoh, T.; Yang, H.; Verma, D.; Pan, W.; Ho, H.-I.; Vroom, J.; Knight, A. M.; Hurtak, J. A.; Klapars, A.; Fryszkowska, A.; Morris, W. J.; Strotman, N. A.; Murphy, G. S.; Maloney, K. M.; Fier, P. S. Engineered Ribosyl-1-Kinase Enables Concise Synthesis of Molnupiravir, an Antiviral for COVID-19. *ACS Central Science* **2021**, *7*, 1980-1985.

(16) Winston, M. S.; Poirier, M.; Liu, Z.; Peng, F.; Humphrey, G. R.; Mcintosh, J. A.; Reibarkh, M.; Wang, F.; Guetschow, E. D.; Castro, S.; Hoyt, E.; Lamberto, D. J.; Sirk, K. pH-Switchable Phase-Transfer Agents for Host Cell Protein Rejection in the Cascaded Biocatalytic Synthesis of an Active Pharmaceutical Ingredient. *Org. Process Res. Dev.* **2023**, *27*, 179-188.

(17) Bell, E. L.; Finnigan, W.; France, S. P.; Green, A. P.; Hayes, M. A.; Hepworth, L. J.; Lovelock, S. L.; Niikura, H.; Osuna, S.; Romero, E.; Ryan, K. S.; Turner, N. J.; Flitsch, S. L. Biocatalysis. *Nat. Rev. Methods Primers* **2021**, *1*, 46.
(18) Siedentop, R.; Rosenthal, K. Industrially Relevant Enzyme Cascades for Drug Synthesis and Their Ecological Assessment. *Int. J. Mol. Sci.* **2022**, *23*, 3605.
(19) Savile, C. K.; Janey, J. M.; Mundorff, E. C.; Moore, J. C.; Tam, S.; Jarvis, W. R.; Colbeck, J. C.; Krebber, A.; Fleitz, F. J.; Brands, J.; Devine, P. N.; Huisman, G. W.; Hughes, G. J. Biocatalytic Asymmetric Synthesis of Chiral Amines from Ketones Applied to Sitagliptin Manufacture. *Science* **2010**, *329*, 305-309.
(20) Kleinbeck, F.; Mahut, M.; Schlama, T., Industrial Processes Using Biocatalysts. In *Biocatalysis for Practitioners*, 2021; pp 427-465.
(21) Ahmed, S. T.; Leferink, N. G. H.; Scrutton, N. S. Chemo-enzymatic routes towards the synthesis of bio-based monomers and polymers. *Mol. Catal.* **2019**, *467*, 95-110.
(22) Bork, H.; Naße, K. E.; Vorholt, A. J.; Gröger, H. Merging High-Pressure Syngas Metal Catalysis and Biocatalysis in Tandem One-Pot Processes for the Synthesis of Non-chiral and Chiral Alcohols from Alkenes in Water. *Angew. Chem. Int. Ed.* **2024**, *n/a*, e202401989.
(23) Midelfort, K. S.; Kumar, R.; Han, S.; Karmilowicz, M. J.; McConnell, K.; Gehlhaar, D. K.; Mistry, A.; Chang, J. S.; Anderson, M.; Villalobos, A.; Minshull, J.; Govindarajan, S.; Wong, J. W. Redesigning and characterizing the substrate specificity and activity of Vibrio fluvialis aminotransferase for the synthesis of imagabalin. *Protein Eng. Des. Sel.* **2013**, *26*, 25-33.
(24) Kaulmann, U., Smithies, K., Smith, M. E. B., Hailes, H. C., Ward, J. M. Substrate spectrum of ω-transaminase from Chromobacterium ciolaceum DSM30191 and its potential for biocatalysis *Enzyme Microb.* **2007**, *41*, 628-637.
(25) Ramírez-Palacios, C.; Wijma, H. J.; Thallmair, S.; Marrink, S. J.; Janssen, D. B. Computational Prediction of ω-Transaminase Specificity by a Combination of Docking and Molecular Dynamics Simulations. *J. Chem. Inf. Model.* **2021**, *61*, 5569-5580.
(26) Genz, M.; Vickers, C.; van den Bergh, T.; Joosten, H. J.; Dorr, M.; Hohne, M.; Bornscheuer, U. T. Alteration of the Donor/Acceptor Spectrum of the (S)-Amine Transaminase from Vibrio fluvialis. *Int. J. Mol. Sci.* **2015**, *16*, 26953-63.
(27) Murugesan, K.; Wei, Z.; Chandrashekhar, V. G.; Jiao, H.; Beller, M.; Jagadeesh, R. V. General and selective synthesis of primary amines using Ni-based homogeneous catalysts. *Chem. Sci.* **2020**, *11*, 4332-4339.
(28) Baumann, W.; Spannenberg, A.; Pfeffer, J.; Haas, T.; Köckritz, A.; Martin, A.; Deutsch, J. Utilization of Common Ligands for the Ruthenium-Catalyzed Amination of Alcohols. *Chem. Eur. J.* **2013**, *19*, 17702-17706.
(29) Senthamarai, T.; Murugesan, K.; Schneidewind, J.; Kalevaru, N. V.; Baumann, W.; Neumann, H.; Kamer, P. C. J.; Beller, M.; Jagadeesh, R. V. Simple ruthenium-catalyzed reductive amination enables the synthesis of a broad range of primary amines. *Nat. Commun.* **2018**, *9*.
(30) Murugesan, K.; Chandrashekhar, V. G.; Senthamarai, T.; Jagadeesh, R. V.; Beller, M. Reductive amination using cobalt-based nanoparticles for synthesis of amines. *Nat. Protoc.* **2020**, *15*, 1313-1337.
(31) Hahn, G.; Kunnas, P.; De Jonge, N.; Kempe, R. General synthesis of primary amines via reductive amination employing a reusable nickel catalyst. *Nat. Catal.* **2019**, *2*, 71-77.
(32) Senthamarai, T.; Chandrashekhar, V. G.; Gawande, M. B.; Kalevaru, N. V.; Zbořil, R.; Kamer, P. C. J.; Jagadeesh, R. V.; Beller, M. Ultra-small cobalt nanoparticles from molecularly-defined Co–salen complexes for catalytic synthesis of amines. *Chem. Sci.* **2020**, *11*, 2973-2981.

(33) Jagadeesh, R. V.; Murugesan, K.; Alshammari, A. S.; Neumann, H.; Pohl, M.-M.; Radnik, J.; Beller, M. MOF-derived cobalt nanoparticles catalyze a general synthesis of amines. *Science* **2017**, *358*, 326-332.
(34) Maugeri, Z.; Rother, D. Application of Imine Reductases (IREDs) in Micro-Aqueous Reaction Systems. *Adv. Synth. Catal.* **2016**, *358*, 2745-2750.
(35) Matsinha, L. C.; Siangwata, S.; Smith, G. S.; Makhubela, B. C. E. Aqueous biphasic hydroformylation of olefins: From classical phosphine-containing systems to emerging strategies based on water-soluble nonphosphine ligands. *Catal. Rev.* **2019**, *61*, 111-133.
(36) Kohlpaintner, C. W.; Fischer, R. W.; Cornils, B. Aqueous biphasic catalysis: Ruhrchemie/Rhône-Poulenc oxo process. *Appl. Catal. A: Gen.* **2001**, *221*, 219-225.
(37) Mcauliffe, C. Solubility in Water of Paraffin, Cycloparaffin, Olefin, Acetylene, Cycloolefin, and Aromatic Hydrocarbons. *J. Phys. Chem.* **1966**, *70*, 1267-1275.
(38) Cocq, A.; Bricout, H.; Djedaïni-Pilard, F.; Tilloy, S.; Monflier, E. Rhodium-Catalyzed Aqueous Biphasic Olefin Hydroformylation Promoted by Amphiphilic Cyclodextrins. *Catalysts* **2020**, *10*, 56.
(39) Leclercq, L.; Sauthier, M.; Castanet, Y.; Mortreux, A.; Bricout, H.; Monflier, E. Two-Phase Hydroformylation of Higher Olefins Using Randomly Methylated α-Cyclodextrin as Mass Transfer Promoter: A Smart Solution for Preserving the Intrinsic Properties of the Rhodium/Trisulfonated Triphenylphosphine Catalytic System. *Adv. Synth. Catal.* **2005**, *347*, 55-59.
(40) Monflier, E.; Fremy, G.; Castanet, Y.; Mortreux, A. Molecular Recognition between Chemically Modified β-Cyclodextrin and Dec-1-ene: New Prospects for Biphasic Hydroformylation of Water-Insoluble Olefins. *Angew. Chem. Int. Ed. Engl.* **1995**, *34*, 2269-2271.
(41) Guo, F.; Berglund, P. Transaminase biocatalysis: optimization and application. *Green Chem.* **2017**, *19*, 333-360.
(42) Straub, A. T.; Otto, M.; Usui, I.; Breit, B. Room Temperature Ambient Pressure (RTAP)-Hydroformylation in Water Using a Self-Assembling Ligand. *Adv. Synth. Catal.* **2013**, *355*, 2071-2075.
(43) Studier, F. W., Stable Expression Clones and Auto-Induction for Protein Production in E. coli. In *Structural Genomics: General Applications*, Chen, Y. W., Ed. Humana Press: Totowa, NJ, 2014; pp 17-32.
(44) Lu, C.; Wu, C.; Ghoreishi, D.; Chen, W.; Wang, L.; Damm, W.; Ross, G. A.; Dahlgren, M. K.; Russell, E.; Von Bargen, C. D.; Abel, R.; Friesner, R. A.; Harder, E. D. OPLS4: Improving Force Field Accuracy on Challenging Regimes of Chemical Space. *J. Chem. Theory Comput.* **2021**, *17*, 4291-4300.
(45) Mohamadi, F.; Richards, N. G. J.; Guida, W. C.; Liskamp, R.; Lipton, M.; Caufield, C.; Chang, G.; Hendrickson, T.; Still, W. C. Macromodel—an integrated software system for modeling organic and bioorganic molecules using molecular mechanics. *J. Comput. Chem.* **1990**, *11*, 440-467.
(46) Halgren, T. A.; Murphy, R. B.; Friesner, R. A.; Beard, H. S.; Frye, L. L.; Pollard, W. T.; Banks, J. L. Glide: A New Approach for Rapid, Accurate Docking and Scoring. 2. Enrichment Factors in Database Screening. *J. Med. Chem.* **2004**, *47*, 1750-1759.
(47) Friesner, R. A.; Murphy, R. B.; Repasky, M. P.; Frye, L. L.; Greenwood, J. R.; Halgren, T. A.; Sanschagrin, P. C.; Mainz, D. T. Extra Precision Glide: Docking and Scoring Incorporating a Model of Hydrophobic Enclosure for Protein−Ligand Complexes. *J. Med. Chem.* **2006**, *49*, 6177-6196.

(48) Amitai, G.; Adani, R.; Rabinovitz, I.; Sod-Moriah, G.; Haim, M. Compounds co-inducing cholinergic up-regulation and inflammation down-regulation and uses thereof. US2002160988, 2002.
(49) Schreuder Goedheijt, M.; Kamer, P. C. J.; van Leeuwen, P. W. N. M. A water-soluble diphosphine ligand with a large `natural' bite angle for two-phase hydroformylation of alkenes. *J. Mol. Catal. A: Chem.* **1998**, *134*, 243-249.

2.6 Experimental Information

2.6.1 General Information

All reactions were conducted under inert atmosphere in a nitrogen-filled glovebox or with standard Schlenk techniques, unless otherwise specified. All reagents and solvents were purchased from commercial sources and used as received, unless otherwise noted. All glassware was flame-dried or dried overnight at 120 °C, allowed to cool under vacuum, and stored in a N_2-atomsphere drybox until use unless otherwise noted. Tetrahydrofuran, toluene, and diethyl ether were purified by passing the degassed solvents (N_2) through a column of activated alumina (solvent purification system purchased from Innovative Technologies, Newburyport, MA). All other solvents were stored over 4 Å molecular sieves for at least 24 h prior to use. Compounds **1a-s**, **2a-g**, **2i-m**, and **2o-t** are commercially available. All reagents purchased from commercial suppliers were used as received. Deuterated solvents were purchased from Cambridge Isotope Laboratories and used as received.

Oligonucleotides were obtained from Integrated DNA Technologies. Enzymes and reagents used for cloning were obtained from New England BioLabs and Thermo Fisher Scientific. All expression media and buffers were prepared with ddH_2O (MilliQ A10 Advantage purification system, Millipore). All expression media were sterilized by either an autoclave (30 min, 121 °C) or a sterile syringe filter (0.22 μm). To maintain sterile conditions, sterile materials and *E. coli* cells were manipulated near a lit Bunsen burner. Cells were pelleted with centrifugation and lysed with a Qsonica Q125 equipped with a quarter-inch probe at 62% amplitude.

^{1}H, ^{13}C, and ^{19}F NMR spectra were recorded on Bruker AV-300, AVB-400, AV-500, AV-600, NEO-500, NEO-501, and AV-700 spectrometers at the University of California, Berkeley NMR facility. Chemical shifts are reported relative to residual solvent peaks ($CDCl_3$ = 7.26 ppm for ^{1}H NMR spectra and 77.16 ppm for ^{13}C NMR spectra, DMSO-*d6* = 2.50 ppm for ^{1}H NMR spectra and 39.52 ppm for ^{13}C NMR spectra). For ^{19}F NMR spectra, chemical shifts are reported relative to the δ –113.15 resonance of PhF used as an external reference or the δ –63.72 resonance of $PhCF_3$. The following abbreviations are used in reporting NMR data: s, singlet; d, doublet; t, triplet; q, quartet; p, pentet; hept, heptet; m, multiplet.

Gas Chromatography (GC) was performed on an HP 6890 GC system with an Agilent HP-5 column (25 m × 0.200 mm, 0.33 μm) for aldehyde quantification. Analysis of amine products was performed on an HP 6890 GC system with an Agilent CP-Sil 8 CB column for amines (30 m x 0.32 mm x 1.00 μm).

Powder X-ray diffraction data were collected at the Small Molecule X-Ray Crystallography Facility (CheXray) at the University of California, Berkeley. High-resolution mass spectra were recorded on a Perkin Elmer AxION 2 TOF mass spectrometer in ESI mode operated by the LBNL

Catalysis Laboratory at the University of California, Berkeley or were obtained from the QB3 Mass Spectrometry Facility at UC Berkeley. Analytical thin layer chromatography (TLC) was performed on Kieselgel 60 F254 glass plates precoated with a 0.25 mm thickness of silica gel. The TLC plates were visualized with UV light and by staining with $KMnO_4$. Preparatory TLC was performed on AnalTech preparatory TLC plates with a 1000 μm-thick silica coating and visualized by UV. Column chromatography was generally performed on a Teledyne Isco Combiflash® Rf system with RediSep GoldTM columns.

2.6.2 General Procedure for The Sequential Chemoenzymatic Hydroaminomethylation Reaction

Scheme S1. General procedure for the chemoenzymatic hydroaminomethylation reaction.

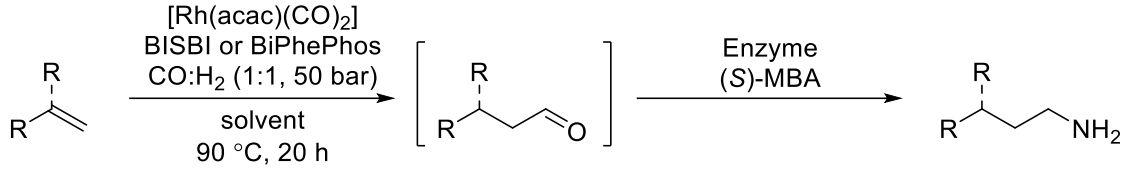

In a nitrogen-filled glovebox, $[Rh(acac)(CO)_2]$ (5.81 mg, 22.5 μmol) and BISBI (20.7 mg, 37.5 μmol) or BiPhePhos (29.5 mg, 37.5 μmol) were added to a 4 mL vial and dissolved in 1.50 mL of the desired solvent (toluene or DMF, see Table S1). The resulting solution was stirred for 5 minutes at 25 °C, after which time the olefin (0.750 mmol) was added. The vials were capped with a septum cap through which a needle had been placed, sealed into a Parr bomb, and the apparatus was removed from the glovebox. The Parr bomb was purged with 1:1 $CO:H_2$ (2 x 40 bar), then pressurized to 50 bar with 1:1 $CO:H_2$. The Parr bomb was placed into a heating block at 90 °C and the reaction solutions were stirred at 1000 rpm for 20 hours. The Parr bomb was then cooled to room temperature, and the gas was vented.

The hydroformylation solution was diluted to 0.375 M in the reaction solvent and stored at -20 °C as a stock solution. The enzymatic reaction was performed in a 4 mL vial with a Teflon cap and a flea stir bar. The reaction vial was loaded with 1.75 mL of buffer A (100 mM sodium phosphate pH 7.5, 100 mM sodium chloride buffer, and 0.5 mM pyridoxal phosphate (PLP)) and 7.5 equivalents (0.0750 mmol) of *(S)*-methylbenzyl amine (pH adjusted to 7.5 with 6 M HCl). 100 μL of ethanol was added and the reaction solution was swirled. Then, 150 μL of the transaminase at 15 mg/mL in buffer A with 10% glycerol was added to the vial. The reaction mixture was gently swirled prior to addition of the 26.7 μL of the crude hydroformylation reaction solution containing the aldehyde (0.0100 mmol). The reaction mixture stirred at 30 °C at 140-150 rpm for 22 h. Upon completion, 50-100 μL of 6 M NaOH was added to the reaction solution, followed by 1-1.5 mL of extraction solvent and internal standard (either dodecane for GC analysis or dibromomethane for NMR analysis) and the solution was vortexed until thoroughly mixed. The mixture was then centrifuged to separate the organic and aqueous layers and analyzed by gas chromatography or quantitative ^1H NMR to determine yield of product.

Table S1. List of olefins, solvents, and ligands for the hydroformylation reactions.

Entry	Olefin	n =	Ligand	Solvent	Entry	Olefin	n =	Ligand	Solvent
1	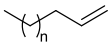	1	BISBI	Toluene	11	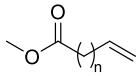	4	BISBI	DMF
2	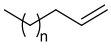	2	BISBI	Toluene	12	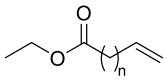	2	BISBI	DMF
3	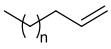	3	BISBI	Toluene	13	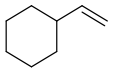	-	BISBI	Toluene
4	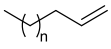	4	BISBI	Toluene	14	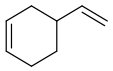	-	BISBI	Toluene
5	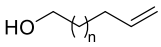	2	BISBI	DMF	15		-	BISBI	Toluene
6	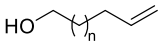	3	BISBI	DMF	16	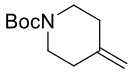	-	BISBI	DMF
7	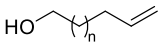	4	BISBI	DMF	17	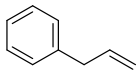	-	BISBI	Toluene
8	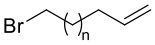	3	BISBI	Toluene	18	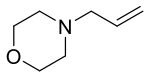	-	BiPhePhos	THF
9	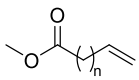	2	BISBI	DMF	19	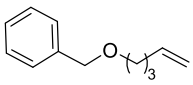	-	BISBI	Toluene
10	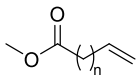	3	BISBI	DMF	20	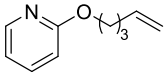	-	BISBI	Toluene
					21	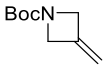	-	BISBI	DMF

2.6.3 Investigation of Hydroformylation Conditions with Complexes of Rhodium

Scheme S2: hydroformylation reaction

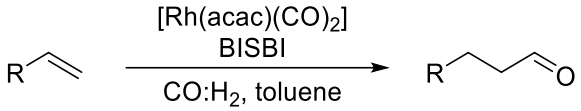

In a nitrogen-filled glovebox, olefin (0.750 mmol, 1.00 equiv.) was added to a dry 4 mL vial containing a stir bar, a pre-stirred solution of $[Rh(acac)(CO)_2]$ (5.81 mg, 0.0300 equiv., 22.5 μmol) and either BISBI (20.7 mg, 37.5 μmol) or BiPhePhos (29.5 mg, 37.5 μmol) dissolved in 1.50 mL of the desired degassed solvent or degassed solvent mixture. The vials were capped with a septum cap, through which a needle had been placed, sealed into a Parr bomb, and the apparatus was removed from the glovebox. The Parr bomb was then purged with $CO:H_2$ (1:1, 2x 40 bar), then pressurized to 50 bar. The Parr bomb was placed into a heating block pre-heated to the desired temperature (90 – 120 °C), and the reactions were stirred at 1000 rpm for 20 hours. The Parr bomb was then cooled to room temperature, and the syngas was vented. The vials were then removed, and an aliquot was subjected to GC-FID analysis with dodecane as internal standard (see Table 1)

2.6.4 General Methods for Protein Expression, Purification, and Characterization

Media Preparation: Autoinduction media[43] was prepared according to published procedures and 2 mL of the relevant 1000X antibiotics was added (0.05 mg/L of kanamycin and 0.1 mg/L of ampicillin).

***Protein Expression*:** Rosetta2 competent *E. coli* cells (QB3 Macrolab, UC Berkeley) were thawed on ice for 15 minutes. Then, 40 μL of Rosetta2 cells were transferred to sterile 14 mL Falcon tubes and transformed with the specified plasmid. Single colonies were picked to inoculate cultures (5-25 mL, LB media), which were grown for 18 hours at 37 °C while shaking at 275 rpm. Each overnight culture was used to inoculate 1-2 L of autoinduction media, which was further grown for 24 h at 37 °C, while shaking at 200-250 rpm. Cells were harvested by centrifugation (5000 rpm, 10 min, 4 °C), and the pellets were resuspended in 20 mL lysis buffer (50 mM $Na_xH_y(PO_4)_z$ 250 mM NaCl, 10 mM imidazole, pH 8.0).

***Protein Purification*:** Cell suspensions were thawed in a water bath at 25 °C, decanted to 50 mL glass beakers, and lysed on ice by sonication (10 x 12 s on, 10 x 12 s off, 62% amplitude with a quarter-inch probe). Crude lysates were transferred to sterile 50 mL Falcon tubes, and cell debris was removed by centrifugation (10,000 rpm, 45 min, 4 °C). The crude lysate was poured over Ni-NTA resin. The resin was washed with lysis buffer (15 mL), and protein was eluted with 15 mL elution buffer (50 mM sodium phosphate, 250 mM NaCl, 250 mM imidazole, pH 8.0). The protein was concentrated to 2.5 mL with an Amicon Ultra 15 spin concentrator (30,000 Da cut off) and desalted into the specified storage buffer with Sephadex G-25 desalting columns.

***Protein Storage*:** proteins were flash frozen in liquid nitrogen and stored at -80 °C for up to 2 months.

Protein Characterization Gel Electrophoresis: Protein purity was analyzed by sodium dodecyl sulfate-polyacrylamide (SDS-PAGE) gel electrophoresis with precast gels (polyacrylamide, 10-20% linear gradient, Biorad).

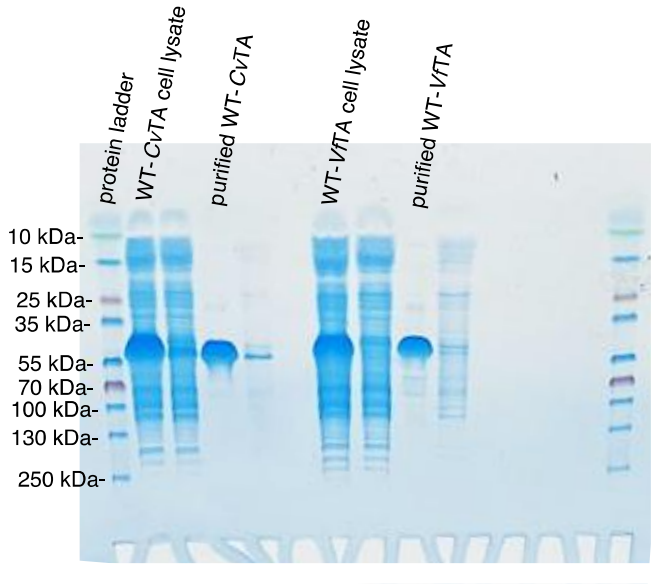

Figure S1. Representative SDS-Page gel for protein purification of WT-*Cv*TA and WT-*Vf*TA

***UV-Vis Spectroscopy*:** Protein concentration was determined by a NanoDrop 2000 UV-Vis Spectrophotometer (Thermo Scientific).

Protein Storage Buffers:

*Cv*TA, *Vf*TA, *Vf*TA 3M, and *Vf*TA 3M/Q: 100 mM sodium phosphate pH 7.5, 100 mM sodium chloride, 10% glycerol, 0.5 mM PLP.

*Bs*GDH: 100 mM potassium phosphate, 100 mM sodium phosphate, pH 7.5, 10% glycerol

*Bs*AlaDH: 50 mM trisHCl, 50 mM NaCl, pH 7.5, 10% glycerol

2.6.5 Investigation of Enzymatic Conditions for Transamination

To investigate reaction conditions, the enzymatic reaction was performed in a 4 mL vial with a Teflon cap and a flea stir bar. 1.75-1.85 mL of buffer A and the specified amine donor (0.0750-0.225 mmol, 7.50-22.5 equiv.) was added. The pH was adjusted with 6 M $HCl_{(aq.)}$ to pH 7.5 if necessary. Cosolvent 1 (0-100 µL) was added to bring the total volume of the reaction solution to 1.85 mL. 150 µL of the purified transaminase at 15 mg/mL in 100 mM sodium phosphate, 100 mM sodium chloride, 0.5 mM PLP buffer (pH 7.5) 10% glycerol was added to the reaction; the reaction mixture was gently swirled prior to addition of the second cosolvent. 26.7 µL of cosolvent 2 was added followed by the addition of octanal (1.56 µL, 1.00 equiv., 0.0100 mmol) directly to the reaction solution. The reaction mixture was stirred at 30 °C and 140-150 rpm for 22 h prior to workup. When the reaction was complete, 100 µL of 6 M NaOH was added, followed by 1-1.5 mL of ethyl acetate and internal standard, dodecane, for gas chromatography, and the reaction mixture was vortexed until thoroughly mixed. The mixture was then centrifuged to separate the organic and aqueous layers, and the organic phase was analyzed by gas chromatography to determine yield of product.

Table S2. Evaluation of buffer, amine donor, and cosolvent for identification of optimal conditions for the transamination of octanal.

Entry	enzyme	reaction buffer	amine donor (equiv.)	cosolvent 1 (100 μL)	cosolvent 2 (26.7 μL)	GC-FID yield (%)
1	WT-*Vf*TA	100 mM $Na_xH_y(PO_4)_z$, 100 mM NaCl, pH 7.5	(*S*)-MBA (7.5)	N/A	N/A	70
2	WT-*Cv*TA	100 mM $Na_xH_y(PO_4)_z$, 100 mM NaCl, pH 7.5	(*S*)-MBA (7.5)	N/A	N/A	74
3	WT-*Vf*TA	100 mM $Na_xH_y(PO_4)_z$, 100 mM NaCl, pH 7.5	(*S*)-MBA (7.5)	EtOH	toluene	38
4	WT-*Cv*TA	100 mM $Na_xH_y(PO_4)_z$, 100 mM NaCl, pH 7.5	(*S*)-MBA (7.5)	EtOH	toluene	70
5	WT-*Vf*TA	100 mM $Na_xH_y(PO_4)_z$, 100 mM NaCl, pH 7.5	(*S*)-MBA (22.5)	EtOH	toluene	22
6	WT-*Cv*TA	100 mM $Na_xH_y(PO_4)_z$, 100 mM NaCl, pH 7.5	(*S*)-MBA (22.5)	EtOH	toluene	30
7	WT-*Vf*TA	100 mM $Na_xH_y(PO_4)_z$, 100 mM NaCl, pH 7.5	(*S*)-MBA (7.5)	EtOH	N/A	82
8	WT-*Cv*TA	100 mM $Na_xH_y(PO_4)_z$, 100 mM NaCl, pH 7.5	(*S*)-MBA (7.5)	EtOH	N/A	78
9	WT-*Vf*TA	100 mM $Na_xH_y(PO_4)_z$, 100 mM NaCl, pH 7.5	(*S*)-MBA (7.5)	N/A	toluene	44
10	WT-*Cv*TA	100 mM $Na_xH_y(PO_4)_z$, 100 mM NaCl, pH 7.5	(*S*)-MBA (7.5)	N/A	toluene	63
11	WT-*Vf*TA	100 mM $Na_xH_y(PO_4)_z$, 100 mM NaCl, pH 7.5	(*S*)-MBA (7.5)	N/A	THF	66
12	WT-*Cv*TA	100 mM $Na_xH_y(PO_4)_z$, 100 mM NaCl, pH 7.5	(*S*)-MBA (7.5)	N/A	THF	67
13	WT-*Vf*TA	100 mM $Na_xH_y(PO_4)_z$, 100 mM NaCl, pH 7.5	(*S*)-MBA (7.5)	N/A	DMF	85
14	WT-*Cv*TA	100 mM $Na_xH_y(PO_4)_z$, 100 mM NaCl, pH 7.5	(*S*)-MBA (7.5)	N/A	DMF	79
15	WT-*Vf*TA	100 mM $Na_xH_y(PO_4)_z$, 100 mM NaCl, pH 7.5	IPA (7.5)	N/A	N/A	46
16	WT-*Cv*TA	100 mM $Na_xH_y(PO_4)_z$, 100 mM NaCl, pH 7.5	IPA (7.5)	N/A	N/A	68

MBA = methylbenzylamine; IPA = isopropylamine

2.6.6 General Procedure for the Biocatalytic Cascade Reaction

The enzymatic reaction was run in a 4 mL vial with a Teflon cap and a flea stir bar. To the reaction vessel was added 1.60 mL of buffer (0.5 mM PLP, 0.2 mM NADPH, 0.2 mM NADH, 1 M ammonium formate, pH 8.0) followed by 25.0-50.0 µL of solution of 1M glucose and 1M pyruvate. To the reaction mixture was added 150 µL of 15 mg/mL □-transaminase in buffer A with 10% glycerol followed by 50 µL *Bs*GDH (28 mg/mL) in 100 mM potassium phosphate, 100 mM sodium phosphate, pH 7.5, 10% glycerol and 200 µL of *Bs*AlaDH (7.4 mg/mL) in 50 mM Tris-HCl pH 7.5, 50 mM NaCl, 10% glycerol. The reaction mixture was gently swirled prior to addition of 26.7 µL of the crude hydroformylation reaction solution containing the aldehyde substrate directly to the reaction solution (0.0100 mmol, 1.00 equiv.). The reaction mixture was stirred at 30 °C and 140-150 rpm for 22 h prior to workup. When the reaction was complete, the pH was adjusted to 12-14 with 6 M NaOH, followed by 1.5 mL of $CDCl_3$ and 50.0 µL of dibromomethane as an internal standard for NMR, and the reaction mixture was vortexed until thoroughly mixed. The mixture was then centrifuged to separate the organic and aqueous layers, and the organic phase was analyzed by NMR to determine yield of product.

Table S3. Evaluation equivalence of glucose and pyruvate for optimal conditions for the transamination of octanal with a biocatalytic cascade.

entry	w-TA	equiv. pyruvate and glucose	% yield of amine
1	*Cv*TA	2.5	19
2	*Vf*TA	2.5	23
3	*Cv*TA	5	18
4	*Vf*TA	5	7
5	--	5	--

2.6.7 Evaluation of Micro-Aqueous Conditions for Transamination

Expression and Lyophilization: 8 mL starting cultures of *Vf*TA, *Vf*TA 3M, and *Cv*TA were grown for 16 h at 37 °C. 5 mL of the overnight cultures were used to inoculate 30 mL expression cultures in LB media. The cells were shaken at 250 rpm at 30 °C until they reached an OD of 1.1. The cells were induced with 35 µL of 1 M IPTG and shaken for 22 hours at 30 °C. SDS-Page gel electrophoresis confirmed the presence of overexpressed protein with a darkened band at 50 kD. The cell cultures were spun down and resuspended in 2 mL of MilliQ water and split into two portions of 1 mL. The 1 mL portions of cells were flash frozen in liquid nitrogen and lyophilized overnight. Lyophilized cell pellets were stored at -80 °C.

Investigation of Micro aqueous Reaction Conditions: lyophilized cell pellets were weighed (45 mg) into a 4 mL glass vial. 6.00 µL of 1 M sodium phosphate, 1 M sodium chloride, 10 mM PLP, pH 7 was added to rehydrate the lyophilized cells. To the rehydrated cells was added 0.600 mL of organic solvent followed by 9.70 µL of methyl benzylamine (7.50 equiv., 0.0750 mmol), 1.56 µL of octanal (1.00 equiv., 0.0100 mmol), and a small stir bar. The reactions were stirred rapidly at 30 °C overnight. Upon completion of the reaction, 40.0 µL of 0.5 M dodecane in ethyl acetate was added to the reaction vessel, and the reaction mixture was centrifuged to pellet the cell mass. The organic extract was analyzed by gas chromatography to determine the conversion of the octanal to octylamine product.

Table S4. Evaluation of micro aqueous conditions with a variety of organic solvents

Entry	Enzyme	Organic Solvent	% yield of octylamine
1	*Cv*TA	CPME	< 1%
2	*Vf*TA	CPME	< 1%
3	*Vf*TA 3M	CPME	< 1%
4	*Cv*TA	THF	< 1%
5	*Vf*TA	THF	< 1%
6	*Vf*TA 3M	THF	< 1%
7	*Cv*TA	toluene[a]	< 1%
8	*Vf*TA	toluene[a]	< 1%
9	*Vf*TA 3M	toluene[a]	< 1%

[a]reaction temperature was 25 °C and reaction mixture shaken at 250 rpm with no added stir bar

2.6.8 General Procedure for The Tandem Chemoenzymatic Hydroaminomethylation Reaction

Scheme S3. General procedure for the tandem chemoenzymatic hydroaminomethylation reaction.

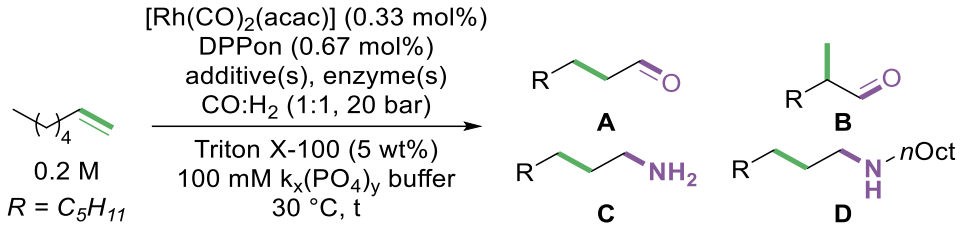

In a nitrogen-filled glovebox, [Rh(acac)(CO)$_2$] (1.41 mg, 5.46 µmol) and DPPon (7.50 mg, 26.9 µmol) were added to a 15 mL test tube, followed by the addition of Triton X-100 (24.0 mg, 5 wt%) to the bottom of the test tube. A stir bar was added, and to the solid was added degassed buffer and enzyme(s) to reach a final volume of 4 mL (see Table S5 for detailed amounts). The resulting suspension was stirred slowly for 2 – 5 minutes. Then, heptene (110 mL, 0.780 mmol, 1.00 equiv) was added. The test tubes were sealed into a Parr bomb, and the apparatus was removed from the glovebox. The Parr bomb was purged with 1:1 CO:H$_2$ (2 x 20 bar), then pressurized to 20 bar with 1:1 CO:H$_2$. The Parr bomb was placed into a heating block at 30 °C and the reaction solutions were stirred at 800 rpm for 6-22 hours. The Parr bomb was then cooled to room temperature, and the gas was vented. 600 µL of 6 M NaOH was then added to the reaction solution, followed by 8 mL of ethyl acetate solvent and internal standard (both dodecane for GC analysis and trimethoxybenzene for NMR analysis) and the solution was vortexed until thoroughly mixed. The mixture was then centrifuged to separate the organic and aqueous layers and analyzed by gas chromatography or quantitative ^{1}H NMR to determine yield of product.

Table S5. Evaluation of tandem hydroaminomethylation conditions.[a]

Entry	Enzymes	Additive/change from standard condition	amine donor (M)	pH	GC-FID % yield aldehyde (l and b)	GC-FID % yield 1° amine	NMR % yield 2° amine
1	--	PTS surfactant, 1 bar $CO:H_2$ (1:1), 25 °C	Excess (*S*)-MBA	7.0	1	--	--
2	--	--	(*S*)-MBA (0.41 M)	7.5	45	--	--
3	--	0.2 mM NADH/NADPH, 100 uL B1, 200 uL B2, 700 uL B3	NH_4CHOO (1 M), 0.70 M alanine	7.0	98	--	--
4	--	0.2 mM NADH/NADPH, 100 uL B1, 200 uL B2, 700 uL B3	NH_4Cl (200 mM), 0.70 M alanine	7.0	60	--	--
5	*Vf*TA-WT, GDH, AlaDH	0.2 mM NADH/NADPH,	--	6.5	30	--	--
6	*Vf*TA-WT, GDH, AlaDH	0.2 mM NADH/NADPH 0.78 mmol octanal	--	6.5	quant	--	--

[a]B1 = 100 mM potassium phosphate buffer pH 7.5, 100 mM sodium chloride, 10% glycerol; B2 = 50 mM tris HCl pH 7.5, 50 mM sodium chloride, 10% glycerol; B3 = 100 mM sodium phosphate pH 7.5, 100 mM sodium chloride, 0.5 mM PLP, 10% glycerol. Reaction temperature 30 °C, 800 RPM. PTS = polyoxyethanyl-a-tocopheryl sebacate

2.6.9 Investigation of Mass Balance for Tandem Hydroaminomethylation

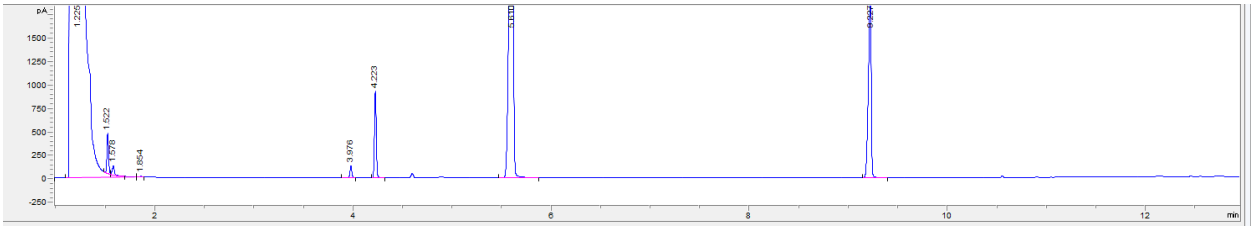

Figure S2. Crude GC-FID chromatogram of Table 3 Entry 9 tandem hydroaminomethylation. [octylamine: rt 4.223 min, octanal: rt 3.976 min, dodecane (standard): rt 5.610 min, trimethoxybenzene (standard): rt 9.227 min]

Table S6. Retention times of authentic standards evaluated for mass balance investigation

Entry	Authentic standard	Retention time (min)	Detected by GC-FID in Table 3, Entry 9 crude reaction mixture
1	Dioctylamine	11.149	No
2	Octanol	4.385	No
3	Octanoic acid	3.962	no
4	Heptene	1.327 (elutes with solvent peak)	Yes
5	Heptane	1.614	No

2.6.10 Molecular Docking with w-TA from Vibrio fluvialis

The ω-transaminase structure from *Vibrio fluvialis* (PDB: 4E3Q)[23] was used as the starting structure. Chains A and B were chosen for the docking simulation from the crystal structure tetramer. With Maestro release 2024-1, the protein structure was prepared by adding hydrogens, setting the protein preparation simulation pH at 7.4, converging heavy atoms to RMSD by 0.30, and optimizing protein hydrogen-bonding interactions with the OPLS4[44] force field. The receptor grid was generated with a box length of 30 Å centered on the PMP molecule. The structure of PMP and the aldimine generated from PMP (PMP-octanal) were prepared with the 3D Builder within Maestro and optimized with the OPLS4 force field with Minimization in MacroModel.[45] LigPrep generated structures in the correct protonation state for PMP and PMP-octanal[25]. Substrates were docked to the active site of *Vf*TA WT with Glide[46], with flexible ligand docking, XP (extra precision)[47] level performance, and the OPLS4 force field.

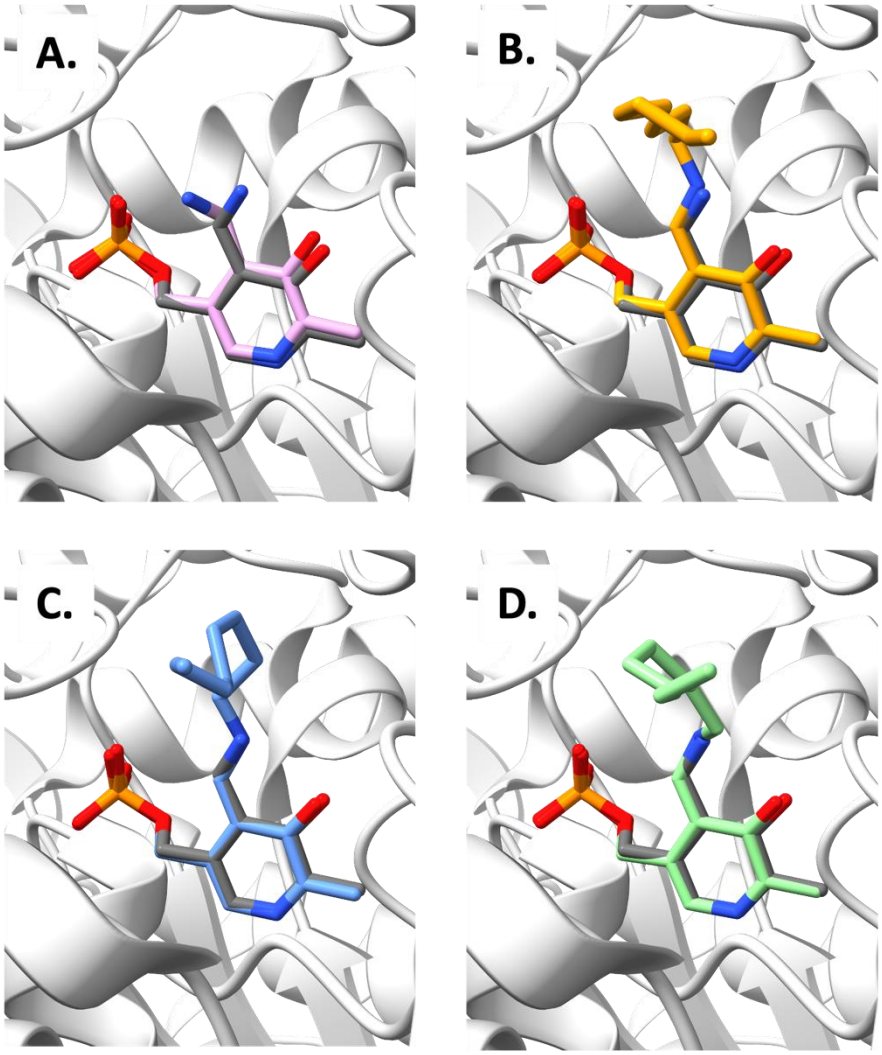

Figure S3. The results from docking PMP and the three conformers of PMP-octanal into *Vf*TA were overlayed with crystal structure of *Vf*TA (PDB: 4E3Q). **A.)** Docked PMP molecule (plum) has little deviation from the positioning of the PMP in the crystal structure (dim gray) within the active site of the *Vf*TA protein (light gray). Light gray (4E3Q *Vf*TA protein), dim gray (PMP from 4E3Q), plum (docked PMP). **B.)** PMP-octanal 1 (orange) overlayed with crystal structure. **C.)** PMP-octanal 2 (cornflower blue) overlayed with crystal structure. **D.)** PMP-octanal 3 (light green) overlayed with crystal structure.

The docking scores from the three best ligand conformations for PMP-octanal are shown below in comparison to the docking score for the native ligand PMP. The PMP-octanal conformation with the best docking score (PMP-octanal 1) was overlayed with the 4E3Q protein to determine residues that were near the hydrophobic octanal fragment.

Table S7. Docking scores for PMP and PMP-octanal conformers

Entry	Name	Docking Score
1	PMP	-9.635
2	PMP-octanal 1	-6.621
3	PMP-octanal 2	-5.910
4	PMP-octanal 3	-5.625

2.6.11 Enzyme Mutagenesis

The plasmids for WT-*Vf*TA, WT-*Cv*TA, and *Vf*TA variants used in this study were purchased from Twist Biosciences with codon optimization for *E. coli.* Protein genes were cloned into pET-28a+ vectors using NdeI/XhoI restriction sites.

Sequence of w-TA from *Vibrio fluvialis* (WT-*Vf*TA) (Uniprot ID: F2XBU9)

ATGAACAAACCTCAGTCGTGGGAGGCTCGCGCTGAGACTTATTCCTTGTACGGTTTCA
CTGATATGCCTAGTTTACACCAACGTGGCACCGTAGTGGTGACTCATGGAGAAGGCCC
GTATATTGTAGATGTGAATGGTCGCCGTTATTTAGACGCTAATTCTGGCTTGTGGAATAT
GGTTGCAGGCTTCGACCATAAGGGACTGATTGATGCCGCAAAAGCCCAGTACGAGCG
CTTCCCGGGATACCACGCATTTTTCGGTCGCATGTCAGACCAAACCGTCATGCTTTCC
GAAAAGCTGGTAGAAGTTAGCCCGTTTGACAGTGGTCGCGTGTTTTATACCAATTCCG
GTTCGGAAGCAAACGATACGATGGTTAAGATGTTGTGGTTTTTGCATGCTGCCGAAGG
AAAACCACAGAAACGCAAGATTCTGACGCGCTGGAATGCTTACCACGGGGTAACCG
CAGTCAGTGCAAGTATGACTGGCAAACCCTACAATTCTGTCTTCGGTTTGCCACTTCC
GGGTTTCGTGCATTTAACCTGCCCCCACTACTGGCGTTATGGAGAGGAGGGGGAGAC
CGAGGAGCAGTTCGTGGCCCGTTTGGCTCGTGAGTTAGAGGAGACTATCCAACGTGA
AGGCGCAGATACAATTGCAGGGTTCTTTGCTGAGCCTGTTATGGGAGCTGGTGGCGT
GATCCCGCCCGCCAAAGGGTATTTTCAGGCTATCCTTCCCATCTTGCGTAAGTACGATA
TCCCGGTTATTTCAGACGAGGTCATTTGTGGCTTCGGCCGTACTGGGAACACGTGGG
GGTGTGTGACGTACGACTTTACCCCCGATGCTATTATCTCATCAAAAAACTTGACAGC
CGGATTTTTTCCGATGGGGGCGGTCATTTTAGGCCCTGAATTATCCAAACGTTTGGAA
ACGGCGATCGAAGCCATTGAAGAATTCCCCCATGGTTTTACGGCGTCAGGTCACCCC
GTCGGGTGTGCTATCGCACTGAAAGCTATCGATGTGGTCATGAACGAAGGTCTTGCCG
AGAATGTTCGTCGCTTGGCTCCCCGTTTTGAAGAGCGTTTAAAGCACATCGCCGAAC
GTCCAAACATCGGTGAGTATCGTGGGATTGGCTTTATGTGGGCTTTGGAAGCCGTTAA
GGATAAAGCATCGAAAACTCCATTCGACGGGAACTTGTCCGTGAGCGAGCGTATCGC
TAATACCTGCACAGACCTTGGCTTGATTTGTCGTCCATTGGGTCAATCGGTAGTACTTT
GTCCACCGTTTATCCTGACTGAGGCGCAAATGGATGAGATGTTTGATAAACTTGAAAA
GGCCCTGGATAAAGTTTTCGCCTAA

Sequence of w-TA from *Chromobacterium violaceum* (WT-*Cv*TA) (UniProt ID: Q7NWG4)

ATGCAAAAACAACGCACTACTTCGCAATGGCGTGAGCTTGACGCCGCGCACCATCTG
CACCCATTCACCGACACGGCATCGTTGAACCAGGCCGGAGCGCGTGTTATGACGCGC
GGGGAAGGGGTTTACCTGTGGGACTCTGAGGGAAATAAAATCATCGATGGGATGGCA
GGTTTGTGGTGCGTAAATGTTGGATACGGACGCAAAGATTTCGCCGAAGCTGCTCGC
CGTCAGATGGAGGAGCTTCCGTTCTATAATACATTCTTCAAAACTACACACCCTGCGG
TAGTCGAATTAAGTTCGTTGTTAGCCGAGGTAACGCCCGCCGGATTTGATCGCGTATT

CTATACAAACTCAGGGAGCGAGTCGGTAGATACAATGATCCGTATGGTCCGCCGTTAC
TGGGATGTCCAAGGCAAACCTGAGAAAAAAACGTTAATCGGGCGTTGGAACGGTTAT
CACGGTAGTACGATTGGGGGAGCGTCACTGGGTGGCATGAAGTATATGCATGAGCAG
GGCGATTTACCGATTCCTGGAATGGCGCACATTGAACAACCTTGGTGGTATAAGCACG
GCAAGGATATGACCCCCGATGAATTCGGGGTAGTTGCCGCACGCTGGCTGGAAGAAA
AAATTCTTGAGATCGGCGCCGACAAGGTCGCGGCCTTCGTCGGAGAGCCTATCCAAG
GTGCCGGCGGCGTCATTGTTCCTCCAGCTACATACTGGCCGGAAATTGAGCGCATCTG
TCGCAAGTATGATGTTTTGTTGGTGGCTGACGAGGTCATCTGCGGATTCGGTCGTACC
GGAGAATGGTTCGGGCACCAACACTTTGGTTTTCAACCAGACTTGTTCACAGCCGCA
AAGGGGTTGTCGAGTGGGTATCTGCCGATTGGAGCCGTGTTCGTAGGCAAGCGCGTA
GCCGAGGGACTGATTGCAGGAGGGGACTTTAACCACGGGTTTACTTACTCAGGCCAC
CCGGTATGTGCTGCTGTCGCACATGCGAACGTCGCCGCGCTGCGTGATGAAGGTATCG
TTCAACGTGTGAAAGACGACATCGGACCCTACATGCAAAAGCGTTGGCGCGAGACAT
TCTCACGTTTCGAGCACGTTGACGATGTTCGCGGTGTTGGAATGGTACAGGCGTTCAC
GCTTGTAAAGAATAAAGCCAAACGCGAATTATTCCCAGATTTTGGAGAAATCGGCAC
GCTGTGCCGCGACATTTTCTTTCGCAACAACCTGATTATGCGCGCCTGTGGGGACCAC
ATCGTGTCTGCGCCGCCATTGGTTATGACCCGTGCGGAAGTTGACGAGATGTTGGCGG
TCGCGGAGCGCTGTCTTGAAGAATTTGAACAAACGCTTAAGGCTCGTGGCTTAGCTT
AG

Sequence of w-TA *Vf*TA-3M (W57F, R415L, L417V)

ATGAATAAACCACAGTCCTGGGAAGCTCGGGCGGAAACGTACTCACTGTACGGCTTT
ACGGACATGCCATCCCTCCATCAGCGGGGCACCGTTGTCGTAACCCACGGTGAGGGC
CCATACATTGTCGATGTTAATGGACGGAGATATTTAGACGCGAACTCAGGTTTATTTAA
TATGGTCGCGGGGTTCGATCATAAGGGCTTAATTGACGCGGCCAAAGCTCAGTATGAA
CGTTTTCCGGGTTATCACGCGTTCTTCGGGAGAATGAGCGATCAAACGGTTATGCTTT
CTGAAAAACTTGTTGAAGTGTCACCCTTTGATAGCGGCCGCGTGTTTTACACCAATAG
TGGTTCAGAGGCAAATGATACGATGGTTAAAATGCTTTGGTTTCTGCACGCAGCCGAA
GGGAAACCACAGAAACGTAAAATCCTGACTCGTTGGAATGCATATCATGGGGTCACT
GCCGTATCGGCGTCTATGACTGGAAAACCATATAATTCAGTGTTTGGTCTGCCTCTGCC
AGGTTTTGTACACCTTACTTGTCCACATTACTGGCGCTATGGTGAAGAAGGCGAAACT
GAAGAGCAGTTTGTTGCCCGTCTGGCTCGTGAACTCGAAGAAACTATTCAACGCGAA
GGAGCAGACACTATAGCCGGTTTTTTCGCAGAACCGGTTATGGGTGCTGGAGGCGTT
ATTCCACCAGCGAAAGGATATTTTCAGGCAATCTTACCTATTTTACGCAAATATGATATT
CCTGTTATCTCTGATGAAGTCATCTGCGGGTTCGGGCGAACCGGAAACACTTGGGGTT
GCGTAACGTACGACTTTACGCCTGATGCCATCATCTCGAGCAAAAACTTGACCGCTGG
GTTTTTTCCGATGGGAGCTGTGATTTTAGGGCCAGAGCTGTCGAAGCGCCTGGAGAC
AGCGATTGAAGCAATCGAAGAGTTTCCGCATGGCTTTACCGCATCTGGCCATCCTGTT
GGCTGTGCTATTGCTCTGAAGGCGATTGATGTGGTGATGAACGAAGGGCTCGCAGAG
AACGTCCGTCGCCTGGCCCCGCGTTTCGAAGAAAGACTGAAACATATAGCAGAGCGC
CCAAATATAGGTGAATATCGTGGCATTGGATTTATGTGGGCCTTAGAAGCCGTCAAGG
ATAAAGCGTCAAAAACCCCGTTTGATGGCAATCTGAGCGTTAGCGAACGTATTGCCA
ACACCTGTACAGATCTGGGTCTCATCTGTCTGCCAGTAGGTCAGTCTGTCGTGTTATG
CCCCCCATTCATTCTCACTGAAGCGCAGATGGATGAAATGTTTGACAAACTGGAGAA
AGCACTTGATAAAGTTTTCGCAGAAGTTGCATAA

Sequence of glucose dehydrogenase from *Bacillus subtilis* that was cloned into a pET-28a vector backbone (*Bs*GDH) (UniProt ID: P12310)

ATGTATCCGGATTTAAAAGGAAAAGTCGTCGCTATTACAGGAGCTGCTTCAGGGCTCG
GAAAGGCGATGGCCATTCGCTTCGGCAAGGAGCAGGCAAAAGTGGTTATCAACTATT
ATAGTAATAAACAAGATCCGAACGAGGTAAAAGAAGAGGTCATCAAGGCGGGCGGT
GAAGCTGTTGTCGTCCAAGGAGATGTCACGAAAGAGGAAGATGTAAAAAATATCGTG
CAAACGGCAATTAAGGAGTTCGGCACACTCGATATTATGATTAATAATGCCGGTCTTG
AAAATCCTGTGCCATCTCACGAAATGCCGCTCAAGGATTGGGATAAAGTCATCGGCAC
GAACTTAACGGGTGCCTTTTTAGGAAGCCGTGAAGCGATTAAATATTTCGTAGAAAAC
GATATCAAGGGAAATGTCATTAACATGTCCAGTGTGCACGAAGTGATTCCTTGGCCGT
TATTTGTCCACTATGCGGCAAGTAAAGGCGGGATAAAGCTGATGACAGAAACATTAGC
GTTGGAATACGCGCCGAAGGGCATTCGCGTCAATAATATTGGGCCAGGTGCGATCAAC
ACGCCAATCAATGCTGAAAAATTCGCTGACCCTAAACAGAAAGCTGATGTAGAAAGC
ATGATTCCAATGGGATATATCGGCGAACCGGAGGAGATCGCCGCAGTAGCAGCCTGGC
TTGCTTCGAAGGAAGCCAGCTACGTCACAGGCATCACGTTATTCGCGGACGGCGGTA
TGACACAATATCCTTCATTCCAGGCAGGCCGCGGTTA

Sequence of alanine dehydrogenase from *Bacillus subtilis* that was cloned into a pET-16hp vector backbone (*Bs*AlaDH) (UniProt ID: Q08352)

ATGATCATAGGGGTTCCTAAAGAGATAAAAAACAATGAAAACCGTGTCGCATTAACA
CCCGGGGGCGTTTCTCAGCTCATTTCAAACGGCCACCGGGTGCTGGTTGAAACAGGC
GCGGGCCTTGGAAGCGGATTTGAAAATGAAGCCTATGAGTCAGCAGGAGCGGAAATC
ATTGCTGATCCGAAGCAGGTCTGGGACGCCGAAATGGTCATGAAAGTAAAAGAACCG
CTGCCGGAAGAATATGTTTATTTTCGCAAAGGACTTGTGCTGTTTACGTACCTTCATTT
AGCAGCTGAGCCTGAGCTTGCACAGGCCTTGAAGGATAAAGGAGTAACTGCCATCGC
ATATGAAACGGTCAGTGAAGGCCGGACATTGCCTCTTCTGACGCCAATGTCAGAGGT
TGCGGGCAGAATGGCAGCGCAAATCGGCGCTCAATTCTTAGAAAAGCCTAAAGGCGG
AAAAGGCATTCTGCTTGCCGGGGTGCCTGGCGTTTCCCGCGGAAAAGTAACAATTAT
CGGAGGAGGCGTTGTCGGGACAAACGCGGCGAAAATGGCTGTCGGCCTCGGTGCAG
ATGTGACGATCATTGACTTAAACGCAGACCGCTTGCGCCAGCTTGATGACATCTTCGG
CCATCAGATTAAAACGTTAATTTCTAATCCGGTCAATATTGCTGATGCTGTGGCGGAAG
CGGATCTCCTCATTTGCGCGGTATTAATTCCGGGTGCTAAAGCTCCGACTCTTGTCACT
GAGGAAATGGTAAAACAAATGAAACCCGGTTCAGTTATTGTTGATGTAGCGATCGAC
CAAGGCGGCATCGTCGAAACTGTCGACCATATCACAACACATGATCAGCCAACATATG
AAAAACACGGGGTTGTGCATTATGCTGTAGCGAACATGCCAGGCGCAGTCCCTCGTA
CATCAACAATCGCCCTGACTAACGTTACTGTTCCATACGCGCTGCAAATCGCGAACAA
AGGGGCAGTAAAAGCGCTCGCAGACAATACGGCACTGAGAGCGGGTTTAAACACCG
CAAACGGACACGTGACCTATGAAGCTGTAGCAAGAGATCTAGGCTATGAGTATGTTCC
TGCCGAGAAAGCTTTACAGGATGAATCATCTGTGGCGGGTGCTTAA

Targeted screening: Q5 Site-directed mutagenesis kit from NEB was used for mutagenesis. The PCR product was purified, concentrated, and transformed into XL-1 blue cells from the Berkeley Macrolab. Primers were ordered from integrated DNA technologies (IDT) with standard desalting.

Table S8. Primers for targeted mutagenesis of position L415 in the *Vf*TA 3M variant

Mutation	Forward Primer	Reverse Primer
L415Q	TCT CAT CTG TCA GCC AGT AGG TC	CCC AGA TCT GTA CAG GTG
L415H	TCT CAT CTG TCA TCC AGT AGG TCA G	CCC AGA TCT GTA CAG GTG
L415R	TCT CAT CTG TCG TCC AGT AGG TCA G	CCC AGA TCT GTA CAG GTG

2.6.12 Evaluation of Conditions for the Formation of Primary Amine Products in the Sequential Hydroaminomethylation

We evaluated each substrate against our panel of enzymes to determine the substrate-enzyme pair that gave the highest yield. Based on our evaluation of substrates **1a, 1c** and **1d and 1e**, we hypothesized that the more polar substrates would react to form product in higher yield with WT-*Vf*TA; whereas, more nonpolar substrates would react to form product in higher yield with the variant enzymes *Vf*TA 3M and *Vf*TA 3M/Q.

Table S9. Evaluation of conditions for the formation of primary amine products in the sequential hydroaminomethylation

Substrate	Transaminase	Variation from Standard Conditions*	% yield linear primary amine product
1a	*Cv*TA WT	50 mM $Na_xH_y(PO_4)_z$, 50 mM NaCl, pH 7.5	64
1a	***Vf*TA WT**	**50 mM $Na_xH_y(PO_4)_z$, 50 mM NaCl, pH 7.5**	**66**
1a	*Vf*TA 3M	50 mM $Na_xH_y(PO_4)_z$, 50 mM NaCl, pH 7.5	50
1a	*Vf*TA 3M/Q	50 mM $Na_xH_y(PO_4)_z$, 50 mM NaCl, pH 7.5	62
1b	*Cv*TA WT	--	4
1b	*Vf*TA WT	--	23
1b	*Vf*TA 3M	--	24
1b	*Vf*TA 3M/Q	--	8
1b	***Vf*TA 3M/Q**	**15 equivalents of (*S*)-MBA, 10% DMSO**	**45**
1d	*Cv*TA WT	--	8
1d	*Vf*TA WT	--	6
1d	*Vf*TA 3M	--	22
1d	***Vf*TA 3M/Q**	**--**	**23**
1d	*Vf*TA 3M/Q	15 equivalents of (*S*)-MBA, 10% DMSO	18
1e	*Cv*TA WT	--	57
1e	***Vf*TA WT**	**--**	**64**
1f	*Cv*TA WT	--	58
1f	***Vf*TA WT**	**--**	**59**

1g	*Vf*TA 3M	--	84
1g	***Vf*TA 3M/Q**	**--**	**89**
1h	*Vf*TA WT	--	52
1h	*Vf*TA 3M	--	66
1h	***Vf*TA 3M/Q**	**--**	**74**
1i	***Vf*TA 3M**	**4 equivalents of (*S*)-MBA**	**65**
1i	*Vf*TA 3M/Q	4 equivalents of (*S*)-MBA	58
1j	***Vf*TA 3M**	**4 equivalents of (*S*)-MBA**	**66**
1j	*Vf*TA 3M/Q	4 equivalents of (*S*)-MBA	66
1k	*Cv*TA WT	--	50
1k	*Vf*TA WT	--	49
1k	***Vf*TA 3M/Q**	**4 equivalents of (*S*)-MBA**	**70**
1l	***Vf*TA 3M**	**4 equivalents of (*S*)-MBA**	**66**
1l	*Vf*TA 3M/Q	4 equivalents of (*S*)-MBA	65
1m	*Vf*TA 3M	--	27
1m	*Vf*TA 3M/Q	--	27
1m	***Vf*TA 3M**	**15 equivalents of (*S*)-MBA, 10% DMSO**	**30**
1n	***Vf*TA 3M**	**--**	**76**
1n	*Vf*TA 3M/Q	--	74
1o	*Cv*TA WT	--	32
1o	*Vf*TA WT	--	32
1o	*Vf*TA 3M	15 equivalents of (*S*)-MBA, 10% DMSO	32
1o	***Vf*TA 3M**	**--**	**43**
1p	*Vf*TA WT	--	78
1p	*Vf*TA 3M	--	91
1p	***Vf*TA 3M/Q**	**--**	**<95 %**
1q	*Vf*TA 3M	--	81
1q	***Vf*TA 3M/Q**	**--**	**81**
1r	*Cv*TA WT	--	58
1r	*Vf*TA WT	--	66
1r	***Vf*TA 3M**	**--**	**< 95%**
1r	*Vf*TA 3M/Q	--	94
1s	*Vf*TA 3M	--	32
1s	***Vf*TA 3M/Q**	**--**	**38**
1t	*Vf*TA 3M	--	56
1t	***Vf*TA 3M/Q**	**--**	**64**
1u	*Vf*TA 3M	--	76
1u	***Vf*TA 3M/Q**	**--**	**77**

*standard conditions: 100 mM $Na_xH_y(PO_4)_z$, 100 mM NaCl, pH 7.5, 0.5 mM PLP, 7.5 equivalents of (*S*)-MBA.

2.6.13 Quantification of Primary Amine Product of the Enzymatic Reaction

The reaction products were identified by comparison of retention times and mass spectrometry fragmentation with authentic standards on GC-FID and GC-Mass spectrometry and quantified with either a calibration curve with GC-FID or quantitative NMR, integrating the two protons at the α-position of the primary amine at 2.67-2.69 ppm with respect to dibromomethane standard (16 scans, D1 = 20 seconds).

GC-FID/MS Conditions: HP 7890B GC equipped with an Agilent 5977A MSD with an Agilent CP-Sil 8 CB column (CP7596) for amines (30 m x 0.32 mm x 1.00 micron). The method used was: 80 °C for 2.5 min, ramp 80 °C to 150 °C at 100 °C/min, hold 150 °C for 5 min, ramp 150 °C to 300 °C at 40 °C/min, hold 300 °C for 1 min, flow rate: 1.1 mL/min, average velocity: 36 cm/sec, carrier gas: helium. Amine products **2a-2v** are commercially available. Amine **2w** and **2x** were prepared according to literature methods.

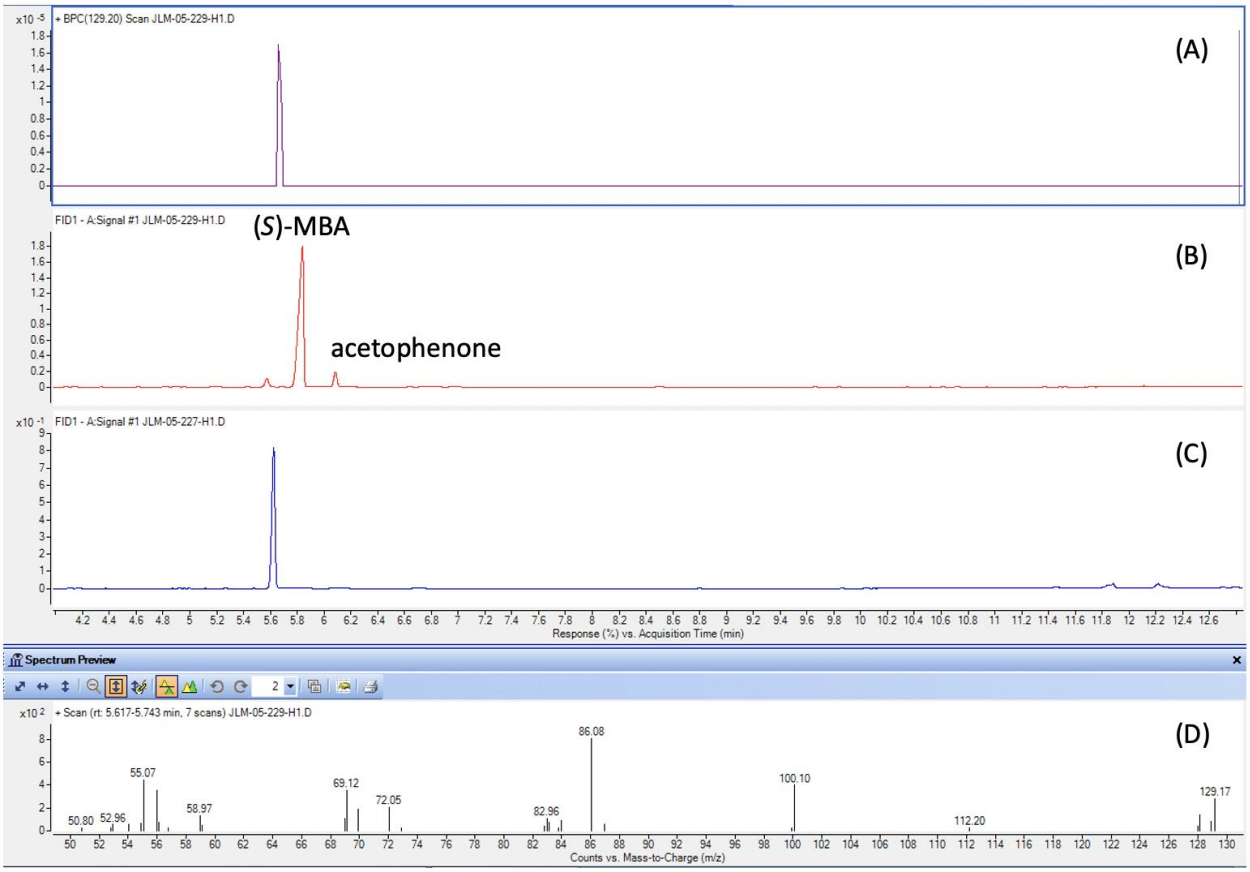

Figure S4. GC-FID/MS chromatogram of model substrate demonstrating the selectivity for the linear, primary amine. A) Extracted mass for octylamine from the crude reaction mixture, B) Crude reaction mixture, C) Authentic standard for octylamine, D) Mass spectra for octylamine in the reaction mixture.

hexan-1-amine (2a)

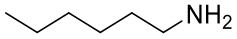

t_R (min) = 3.923

exact mass: 101.12

expected mass based on standard: [M] 101.1 m/z

mass detected: [M] 101.1 m/z

Yield: 66%

heptan-1-amine (2b)

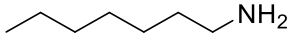

t_R (min) = 4.71

exact mass: 115.14

expected mass based on standard: [M] 115.2 m/z

mass detected: [M] 115.1 m/z

Yield: 45%

octan-1-amine (2c)

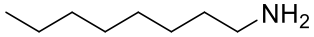

t_R (min) = 5.72

exact mass: 129.15

expected mass based on standard: [M] 129.17 m/z

mass detected: [M] 129.17 m/z

Yield: 60%

nonan-1-amine (2d)

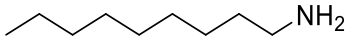

t_R (min)= 7.02

exact mass: 143.17

expected mass based on standard: [M] 143.2 m/z

mass detected: [M] 143.1

Yield: 23%

7-aminoheptan-1-ol (2e)

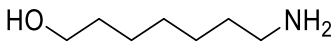

t_R (min) = 8.41

exact mass: 131.13

expected mass based on standard: [M-1] 130.1 m/z, [M-16] 114.0 m/z, **[M-30] 101.1 m/z**

mass detected: [M-30] 101.1 m/z

Yield: 64%

8-aminooctan-1-ol (2f)

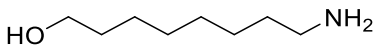

t_R (min) = 9.72

exact mass: 145.15

expected mass based on standard: [M-1] 144.2 m/z

mass detected: [M-1] 144.2 m/z

Yield: 59%

9-aminononan-1-ol (2g)

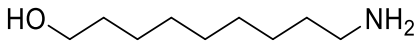

t_R (min) = 10.54

exact mass: 159.16

expected mass based on standard: [M-1] 158.1 m/z

mass detected: [M-1] 158.2 m/z

Yield: 89%

7-bromoheptan-1-amine (2h)

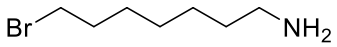

t_R (min) = 9.602

exact mass: 193.05

mass detected: 192.0 m/z

The spectral data agree well with the literature.[48] Yield: 74%

^{1}H NMR (500 MHz, $CDCl_3$) δ 3.41 (t, J = 6.8 Hz, 2H), 2.68 (t, J = 7.1 Hz, 2H), 1.90 – 1.81 (m, 2H), 1.44 (q, J = 4.2 Hz, 3H), 1.35 – 1.31 (m, 3H), 1.29 – 1.24 (m, 2H).

methyl 6-aminohexanoate (2i)

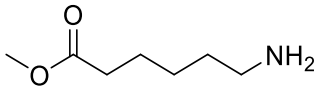

t_R (min) = 7.37

exact mass: 145.11

expected mass based on standard: [M] 145.1 m/z, [M-17] 128.1 m/z

mass detected: [M-17] 128.1 m/z

Yield: 65%

methyl 7-aminoheptanoate (2j)

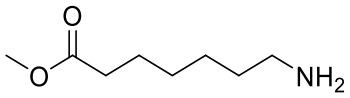

t_R (min) = 9.16

exact mass: 159.13

expected mass based on standard: [M] 159.1 m/z

mass detected: [M] 159.2 m/z

Yield: 66%

methyl 8-aminooctanoate (2k)

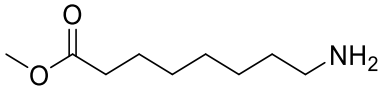

t_R (min) = 10.16

exact mass: 173.14

expected mass based on standard: [M] 173.1 m/z, [M-31] 142.1 m/z, [M-73] 100.1 m/z

mass detected: [M-31] 142.1 m/z, [M-73] 100.1 m/z

Yield: 70%

ethyl 6-aminohexanoate (2l)

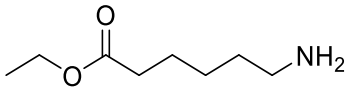

t_R (min) = 8.73

exact mass: 159.13

expected mass based on standard: [M] 159.1 m/z, [M-17] 142.1 m/z

mass detected: [M] 159.1 m/z, [M-17] 142.2 m/z

Yield: 66%

3-cyclohexylpropan-1-amine (2m)

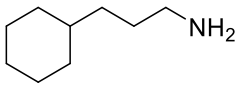

t_R (min) = 8.16

exact mass: 141.15

expected mass based on standard: 141.2 m/z

mass detected: 141.3 m/z

Yield: 30%

2-cyclohexylethan-1-amine (2o)

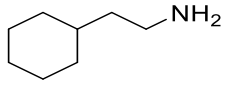

t_R (min) = 6.38

exact mass: 127.14

expected mass based on standard: [M] 127.1 m/z

mass detected: [M] 127.1 m/z

Yield: 43%

***tert*-butyl 4-(2-aminoethyl)piperidine-1-carboxylate (2p)**

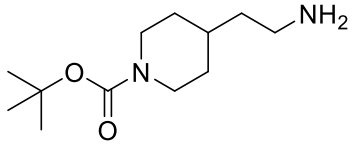

t_R (min) = 12.00

exact mass: 228.18

expected mass based on standard: [M] 228.3 m/z

mass detected: [M] 228.2 m/z

Yield: 98%

***tert*-butyl 3-(2-aminoethyl)azetidine-1-carboxylate (2q)**

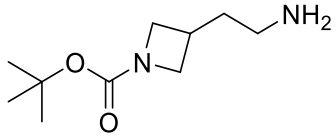

t_R (min) = 11.21

exact mass: 200.15

expected m/z based on standard: [M] 200.1 m/z, [M-42] 158.1 m/z, [M-57] 143.1 m/z

m/z detected: [M-42] 158.2 m/z , [M-57] 143.1 m/z

Yield: 81%

4-phenylbutan-1-amine (2r)

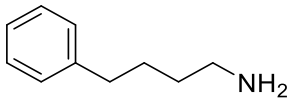

t_R (min) = 9.80

exact mass: 149.12

expected mass based on standard: [M] 149.1 m/z

mass detected: [M] 149.1 m/z

Yield: 95%

4-morpholinobutan-1-amine (2s)

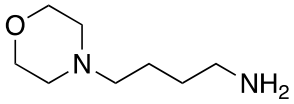

t_R (min) = 9.78

exact mass: 158.14

expected mass based on standard: [M] 158.1 m/z, [M-15], [M-18] 140.1 m/z, [M-31] 127.1 m/z, [M-58] 100.1 m/z

mass detected: [M-15], [M-18] 140.1 m/z, [M-31] 127.1 m/z, [M-58] 100.1 m/z

Yield: 38%

6-(benzyloxy)hexan-1-amine (2t)

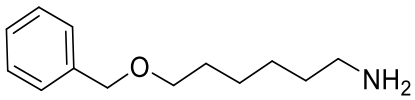

t_R (min) = 12.14;

exact mass: 207.16

expected mass based on standard: [M-1] 206.1 m/z

mass detected: [M] 207.0 m/z, [M-1] 206.1 m/z

Yield: 64%

6-(pyridin-2-yloxy)hexan-1-amine (2u)

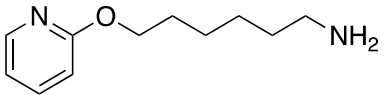

t_R (min) = 10.72

exact mass: 194.14

expected mass based on standard: [M] 194.2 m/z

mass detected: [M] 194.1 m/z

Yield: 77%

2.6.14 Synthesis of Heterogeneous Catalysts

Scheme S4. Synthesis of Co/GS@800C nanoparticle.

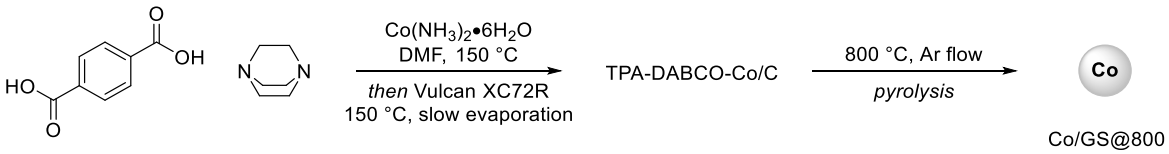

Step 1- TPA-DABCO-Co/C: This compound was prepared according to a literature procedure.[30] Open to air, in a 100 mL round-bottom flask, DMF (20.0 mL) was added to $Co(NH_3)_2•6H_2O$ (0.740 g, 2.54 mmol) and DABCO (0.860 g, 8.00 equiv. relative to Co, 7.62 mmol). The mixture was stirred for 3 minutes at room temperature at 750 rpm. During this time, the mixture turned dark blue. A solution of terephthalic acid (1.27 g, 8.40 equiv. relative to Co, 7.63 mmol) in hot DMF (15.0 mL) (*NOTE: TPA only dissolves in hot DMF*) was then added to the blue solution containing the cobalt. A light blue precipitate appeared. The flask containing the reaction slurry was attached to a condenser, then placed in an oil-bath pre-heated to 150 °C and refluxed for 30 min. (*NOTE: The stirring should be kept at 750 rpm and the solution should turn pale green, signifying the formation of TPA-DABCO-Co, after approximately 20 min*). Then, 2.50 g of Vulcan XC72R powder was added slowly followed by DMF (10.0 mL). The resulting suspension was again stirred at 150 °C and 750 rpm for 4 h attached to the reflux condenser. The reflux condenser was then removed, the stirring was stopped, and the flask temperature was maintained at 150 °C for 20 h open to air to allow the DMF solvent to evaporate. After the material was completely dry, it was cooled to room temperature and ground into a fine powder with a mortar and pestle for a total of 8.21 g of fine black powder. The powder XRD Data obtained agreed well with the literature.

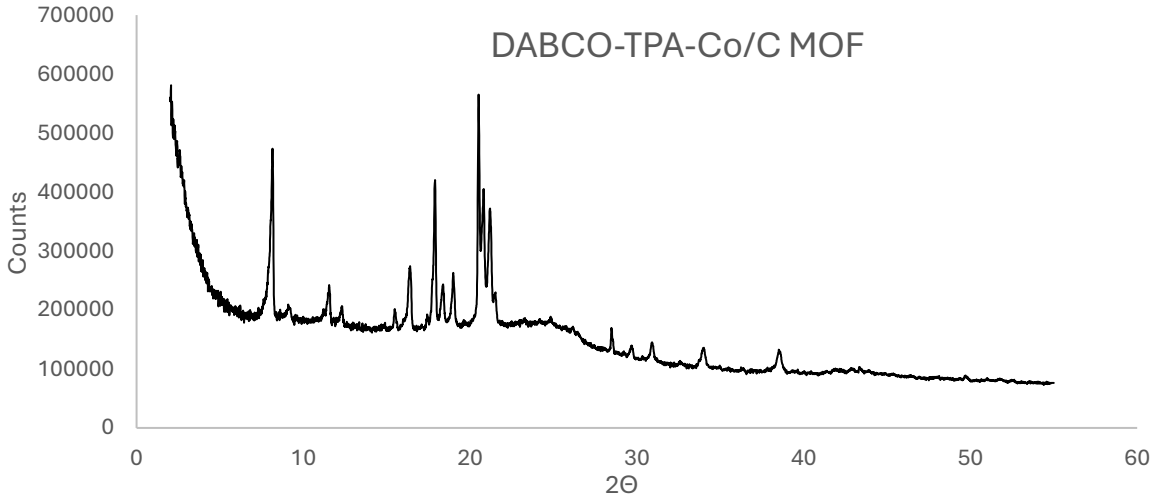

Figure S5. Powder XRD spectra of the DABCO-TPA-Co/C MOF.

Step 2- Co/GS@800C: 3.30 g of the TPA-DABCO-Co/C MOF was placed in a tube furnace. The material was pyrolyzed using the following program:

Scheme S5. Pyrolysis program for the synthesis of Co/GS@800C.

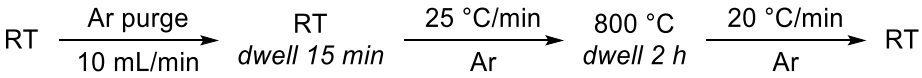

This procedure yielded 1.36 g of a fine black powder. The powder XRD matched the literature for the desired cobalt nanoparticle. This powder was used without further purification for the reductive amination reactions.

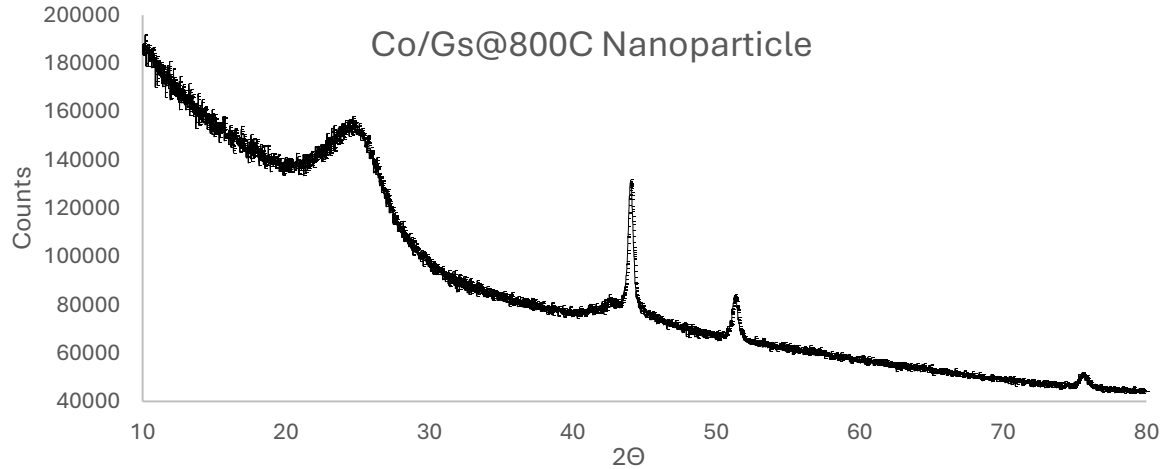

Figure S6. Powder XRD spectra of the Co/GS@800C Nanoparticle.

2.6.15 Investigation of Heterogenous Conditions for Reductive Amination

Scheme S6. Reaction Conducted with Co/GS@800C.

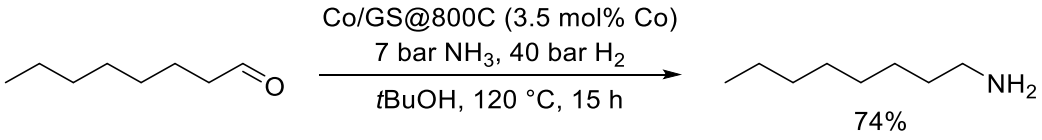

Under air, to a 4 mL vial was added Co/GS@800C nanoparticle (25 mg, 0.50 mmol, 0.035 equiv. Co), ^{t}BuOH (3.0 mL), and octanal (78.1 µL, 0.500 mmol). The vial was equipped with a stir bar and sealed with a septum cap into which a needle had been placed. The vial was placed into a 450 mL Parr bomb, the bomb was flushed with a stream of H_2 for 5 minutes, then charged with 7 bar of NH_3, and finally pressurized to 40 bar with H_2. The apparatus was then placed into a pre-heated heating block at 130 °C. After stirring at 1000 rpm for 15 h, the bomb was removed from the heating block and cooled to room temperature. Once cooled, the gas was vented, and the vial was removed. Internal standard (*n*-hexadecane, 147 µL, 0.500 mmol) was added, and the reaction mixture was passed through a syringe filter with EtOAc as eluent. The yield was determined by GC-FID.

Scheme S7. Carbon monoxide poisoning experiment with Co/GS@800C.

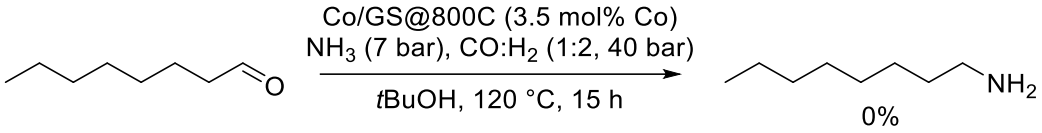

Under air, to a 4 mL vial was added Co/GS@800C nanoparticle (25 mg, 0.50 mmol), ^{t}BuOH (3.0 mL), and octanal (78.1, 0.500 mmol). The vial was equipped with a stir bar and sealed with a septum cap into which a needle had been placed. The vial was placed into a 450 mL Parr bomb, the bomb flushed under a stream of H_2 for 5 min, then charged with 7 bar of NH_3, and finally pressurized to 40 bar with 1:2 CO:H_2. The Parr bomb was then placed into a pre-heated heating block at 130 °C. After stirring at 1000 rpm for 15 h, the Parr bomb was removed from the heating block and cooled to room temperature. Once cooled, the gas was vented, and the vial removed. Internal standard (*n*-hexadecane, 147 µL, 0.500 mmol) was added as internal standard, the reaction mixture was passed through a syringe filter with EtOAc as eluent, and the yield was determined by GC-FID.

Scheme S8. Reaction conducted with hydroformylation catalyst and Co/GS@800C.

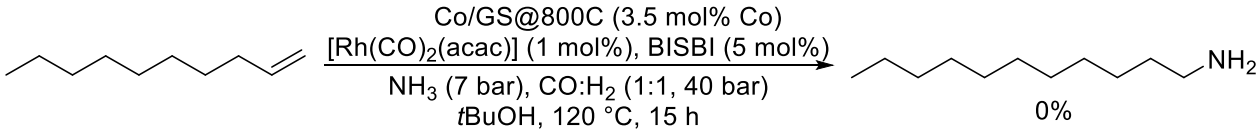

To a 4 mL vial was added Co/Gs@800C nanoparticle (25 mg, 1.0 equiv., 0.50 mmol), [$Rh(CO)_2$(acac)] (1.29 mg, 0.0100 equiv., 5.00 µmol), BISBI (13.8 mg, 0.0500 equiv., 25.0 µmol), *t*BuOH (2.5 mL), and 1-decene (94.6 , 1.00 equiv, 0.500 mmol). The vial was capped with a septum cap with a needle placed in it, then the vial was placed into a 450 mL Parr bomb, purged with H_2 (2x), then charged with 7 bar of NH_3, and finally pressurized to 40 bar with CO:H_2 (1:1). The apparatus was then placed into a pre-heated aluminum block at 130 °C and stirred at 1400 rpm for 15 h. The Parr bomb was then removed from the heating block and cooled to room temperature.

To the vial, *n*-hexadecane (147 μL, 0.500 mmol) was added as internal standard, and the reaction mixture was passed through a syringe filter with EtOAc. The filtrate was then analyzed by GC-FID.

2.6.16 Synthesis of Ligands

Scheme S9. Synthesis of SulfoXantphos (sodium 4,5-bis(diphenylphosphaneyl)-9,9-dimethyl-9H-xanthene-2,7-disulfonate)

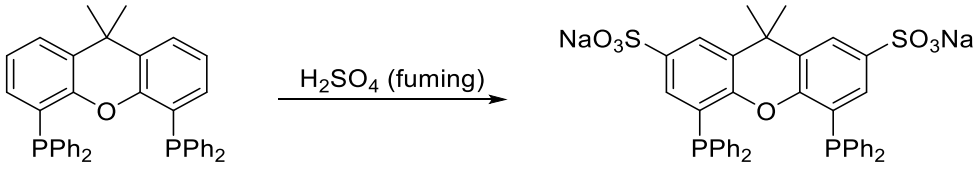

This compound was prepared according to a literature method.[49] To a bath of sulfuric acid (30% oleum, fuming) (1.92 g, 1.00 mL, 10.8 mmol) at 5 °C (benzene/dry ice bath) was added portion wise (9,9-dimethyl-9H-xanthene-4,5-diyl)bis(diphenylphosphane) (250 mg, 432 μmol). The resulting solution was then stirred at room temperature for 16 h. After this time, ice water was added (5 mL), forming a white suspension. Another 7 mL of room-temperature water was added, and the resulting slurry was poured into a vigorously stirred solution of *iso*-octylamine (1 mL) in toluene (5 mL). When poured into the toluene/amine solution, the aqueous layer of the reaction mixture was clear, and the toluene layer was slightly yellowed. When the biphasic solution was washed with H_2O, the water layer eventually ran clear. Upon adding NaOH (6M), the toluene layer turned clear, and the aqueous layer became slightly cloudy. The toluene layer was decanted, and the aqueous solution was neutralized to pH = 7 with conc. H_2SO_4 (and readjusted with 6M NaOH if necessary) to give a white suspension. This suspension was evaporated to dryness; then, the resulting solid was suspended in EtOH and refluxed for 1 h. After this time, the mixture was cooled to room temperature, filtered, and washed with EtOH. The solid was collected and dried to give sodium 4,5-bis(diphenylphosphaneyl)-9,9-dimethyl-9H-xanthene-2,7-disulfonate (199 mg, 254 μmol, 59%) as a free-flowing white powder after drying. The spectral data of this compound agreed with those in the literature.[49]

^{1}H NMR (500 MHz, D_2O) δ 7.98 (d, J = 2.1 Hz, 2H), 7.29 (t, J = 7.2 Hz, 4H), 7.23 (t, J = 7.5 Hz, 8H), 7.14 (s, 8H), 6.99 – 6.96 (m, 2H), 1.66 (s, 6H).

^{31}P NMR (202 MHz, D_2O) δ -19.0.

2.6.17 Synthesis of Olefins 1t and 1u

Scheme S10. Synthesis of ((pent-4-en-1-yloxy)methyl)benzene (**1t**).

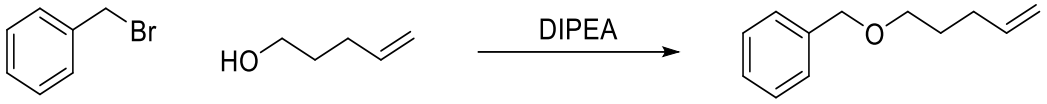

A 20 mL vial containing benzyl bromide (639 µL, 1.10 equiv., 5.37 mmol) and pent-4-en-1-ol (500 µL, 1.00 equiv., 4.88 mmol) in diisopropylethylamine (1.68 mL, 2.00 equiv., 9.76 mmol) was heated at 120 °C for 3 h. After this time, the crude mixture was concentrated *in vacuo* and purified by flash column chromatography (SiO_2, 5% EtOAc in hexanes) to afford ((pent-4-en-1-yloxy)methyl)benzene (601 mg, 70%) as a clear oil.

^{1}H NMR (500 MHz, $CDCl_3$) δ 7.38 – 7.27 (m, 5H), 5.83 (ddt, J = 16.9, 10.2, 6.6 Hz, 1H), 5.03 (dq, J = 17.2, 1.8 Hz, 1H), 4.97 (ddd, J = 10.2, 2.2, 1.1 Hz, 1H), 3.49 (t, J = 6.5 Hz, 2H), 2.20 – 2.12 (m, 2H), 1.73 (dq, J = 8.6, 6.7 Hz, 2H).

^{13}C{^{1}H} NMR (126 MHz, $CDCl_3$) δ 138.7, 138.3, 128.4, 127.6, 127.5, 114.7, 72.9, 69.8, 30.4, 29.0.

HRMS (ESI-TOF) Calc'd $[C_{12}H_{16}O+H]^+$ 177.1233, found 177.1235

Scheme S11. Synthesis of 2-(pent-4-en-1-yloxy)pyridine (**1u**).

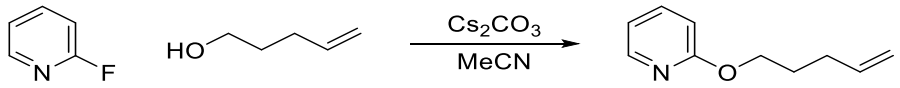

To a 20 mL vial was added 2-fluoropyridine (420 µL, 1.00 equiv., 4.88 mmol) and cesium carbonate (1.59 g, 1.00 equiv., 4.88 mmol) in acetonitrile (4.88 mL). Then, pent-4-en-1-ol (0.500 mL, 1.00 equiv., 4.88 mmol) was added to reaction mixture. The vial was capped and heated at 80 °C overnight. The suspension was then cooled and filtered; the solids were washed with DCM. The organic filtrate was concentrated *in vacuo*, and the resulting residue was subjected to flash column chromatography (SiO_2, 10% EtOAc in hexanes) to afford 2-(pent-4-en-1-yloxy)pyridine (300.9 mg, 38%) as a clear oil.

^{1}H NMR (500 MHz, $CDCl_3$) δ 8.14 (dd, J = 5.1, 2.0 Hz, 1H), 7.60 – 7.51 (m, 1H), 6.84 (ddd, J = 7.0, 5.0, 1.0 Hz, 1H), 6.72 (d, J = 8.4 Hz, 1H), 5.86 (ddt, J = 16.9, 10.2, 6.6 Hz, 1H), 5.06 (dp, J = 17.2, 1.9 Hz, 1H), 4.99 (dt, J = 10.2, 1.7 Hz, 1H), 4.30 (t, J = 6.6 Hz, 2H), 2.22 (dddd, J = 8.0, 6.4, 4.3, 1.5 Hz, 2H), 1.88 (dq, J = 9.8, 6.7 Hz, 2H).

^{13}C{^{1}H} NMR (126 MHz, $CDCl_3$) δ 164.0, 146.9, 138.4, 138.0, 116.5, 115.0, 111.0, 65.2, 30.2, 28.3.

HRMS (ESI-TOF) Calc'd $[C_{10}H_{13}NO+H]^+$ 164.1036, found 164.1031

2.6.18 Synthesis of Primary Amines 2n and 2x

3-(cyclohex-3-en-1-yl)propan-1-amine (2n)

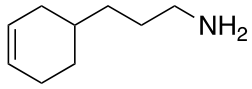

Scale-up of the sequential hydroaminomethylation: Under air, a solution of (*S*)-methylbenzyl amine (96.5 µL, 0.750 mmol, 7.50 equiv.) in 10 mL of buffer A (pH adjusted with 6 M HCl) was added to a 150 mL round bottom flask equipped with a small stir bar. To this solution was added 1 mL of EtOH, followed by 1.5 mL *Vf*TA-3M in buffer A with 10% glycerol. After the reaction vessel was gently swirled, 267 µL of hydroformylation crude (0.100 mmol) that was diluted to 0.375 M **1r** in DMF was added to the reaction mixture. The reaction was stirred at 150 rpm at 25 °C for 22 h, after which time the reaction was quenched with 1.5 mL of 6 M NaOH. The crude reaction mixture was extracted (25 mL $CHCl_3$ x 3). The organic layers were combined and dried over Na_2SO_4, filtered, and concentrated *in vacuo*. To remove the DMF, the crude solution was then diluted in 5 mL of ethyl acetate and washed 6 x with 10 mL of cold water adjusted to pH 12 with 6 M NaOH. The organic layer was concentrated to 1 mL and loaded onto silica, followed by purification by flash chromatography (0-15% MeOH/5% ammonium hydroxide in dichloromethane to afford the pure product **2r** (5.40 mg, 39% yield) as a light-yellow oil.

^{1}H NMR (500 MHz, $CDCl_3$) δ 5.70 – 5.58 (m, 2H), 2.69 (t, *J* = 7.1 Hz, 2H), 2.15 – 1.96 (m, 3H), 1.79 – 1.58 (m, 2H), 1.48 (dq, *J* = 8.8, 6.9 Hz, 3H), 1.41 (m, 2H), 1.31 – 1.16 (m, 3H).

^{13}C{^{1}H} NMR (126 MHz, $CDCl_3$) δ 127.19, 126.71, 77.36, 42.68, 34.02, 33.57, 32.06, 31.28, 29.09, 25.39

HRMS (ESI): calc'd [M+H]+ 140.1434, found 140.1434

Scheme S12: Synthesis of *tert*-butyl (6-(pyridin-2-yloxy)hexyl)carbamate.

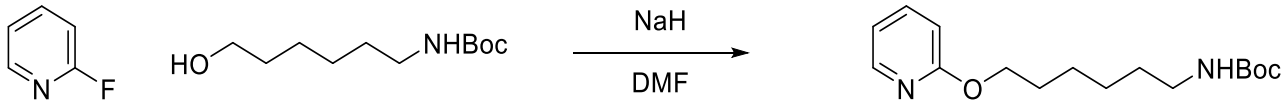

In a nitrogen-filled glovebox, solid sodium hydride (0.136 g, 1.10 equiv., 5.66 mmol) was added in portions at room temperature to a solution of *tert*-butyl (6-hydroxyhexyl)carbamate (1.23 g, 1.10 equiv., 5.66 mmol) in DMF (17.2 mL). The resulting mixture was stirred at 25 °C until H_2 evolution ceased. Then the reaction mixture was added dropwise *via* glass pipette to a vial containing 2-fluoropyridine (443 µL, 1.00 equiv., 5.15 mmol) in DMF (17.2 mL). This resulting solution was stirred for 12 h at 50 °C. After this time, the solvent was removed *in vacuo*, and the product was purified by flash column chromatography (SiO_2, 10% MeOH in DCM) to afford *tert*-butyl (6-(pyridin-2-yloxy)hexyl)carbamate (399.2 mg, 26%) as a clear oil.

^{1}H NMR (500 MHz, $CDCl_3$) δ 8.13 (dt, J = 5.0, 2.4 Hz, 1H), 7.57 – 7.50 (m, 1H), 6.83 (dt, J = 7.0, 3.8 Hz, 1H), 6.74 – 6.67 (m, 1H), 4.52 (s, 1H), 4.26 (td, J = 6.6, 2.1 Hz, 2H), 3.11 (d, J = 7.0 Hz, 2H), 1.82 – 1.71 (m, 2H), 1.55 – 1.33 (m, 15H).

$^{13}C\{^1H\}$ NMR (126 MHz, $CDCl_3$) δ 164.1, 156.1, 147.0, 138.6, 116.6, 111.2, 79.1, 65.9, 40.7, 30.2, 29.1, 28.6, 26.7, 25.9.

HRMS (ESI) $[C_{16}H_{26}N_2O_3+H]+$ calc'd: 295.2013; found: 295.2016

Scheme S13: Synthesis of 6-(pyridin-2-yloxy)hexan-1-amine (**2u**).

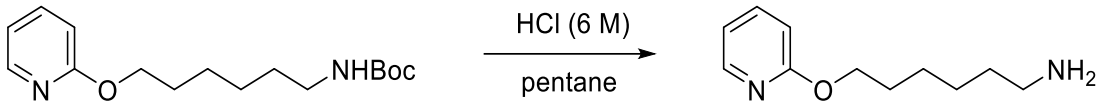

tert-Butyl (6-(pyridin-2-yloxy)hexyl)carbamate (0.200 g, 1.00 equiv., 0.340 mmol) was dissolved in 10 mL of pentane and added to a 20 mL vial with a Teflon stir bar. To this mixture was added 200 µL of 6 M HCl (aq.). The reaction vessel was loosely capped to allow H_2 evolution, then stirred at 800 rpm at room temperature for 16 h. Upon completion, 4 mL of water was added. The pH of the aqueous layer was adjusted to 14 with 6 M NaOH (aq.). The aqueous layer was extracted with ethyl acetate (2 x 5 mL). The organic layers were combined, dried with sodium sulfate, filtered, and concentrated *in vacuo* to afford 6-(pyridin-2-yloxy)hexan-1-amine (38.5 mg, 0.200 mmol, 58%) as a clear oil.

^1H NMR (500 MHz, $CDCl_3$) δ 8.13 (ddd, J = 5.0, 2.0, 0.8 Hz, 1H), 7.54 (ddd, J = 8.4, 7.1, 2.0 Hz, 1H), 6.83 (ddd, J = 7.0, 5.1, 1.0 Hz, 1H), 6.71 (dt, J = 8.4, 0.9 Hz, 1H), 4.27 (t, J = 6.7 Hz, 2H), 2.69 (t, J = 6.9 Hz, 2H), 1.78 (dq, J = 8.4, 6.7 Hz, 2H), 1.50 – 1.43 (m, 4H), 1.43 – 1.36 (m, 2H), 1.23 (s, 3H).

$^{13}C\{^1H\}$ NMR (126 MHz, $CDCl_3$) δ 164.2, 147.0, 138.6, 116.6, 111.2, 66.0, 42.3, 34.0, 29.2, 26.8, 26.1.

HRMS (ESI) $[C_{11}H_{19}N_2O+H]+$ calc'd: 195.1497; found: 195.1492

CHAPTER THREE

Tandem Chemoenzymatic Hydroaminomethylation of Olefins in Water Forms Linear Primary Amines

3.1 Abstract

Linear primary amines serve as crucial building blocks in pharmaceuticals, fine chemicals, polymers, and surfactants. Despite their importance, conventional methods for the synthesis of linear primary amines often suffer from overalkylation and the requirement for elevated temperatures and pressures. Herein, we report a tandem chemoenzymatic hydroaminomethylation strategy that converts terminal olefins into linear primary amines under mild conditions by integrating a Rh/DPPon-catalyzed hydroformylation performed in surfactant micelles with a wild-type ω-transaminase from wild-type *Vibrio fluvialis* (WT-*Vf*TA) and an amine donor recycling system composed of wild-type alanine dehydrogenase (WT-AlaDH) and wild-type glucose dehydrogenase (WT-GDH) enzymes. This cooperative cascade uses inexpensive feedstock reagents—including ammonium salts, alanine, carbon monoxide, hydrogen, and glucose—to achieve high selectivity for primary amines without the formation of secondary and tertiary amine byproducts. Moreover, the system's versatility is demonstrated by the synthesis of ^{15}N-labeled primary amines and biologically relevant compounds containing linear primary amines, underscoring the potential of this integrated tandem process and other chemoenzymatic methods for applications ranging from medicinal chemistry to industrial manufacturing.

3.2 Introduction

Linear primary amines are an increasingly important motif in pharmaceutical compounds[1] for fine and industrial chemicals, such as polymers and surfactants.[2] More recently, diamines of varying length and structure have been investigated as linkers in PROTACs (Figure 1a).[3-4] Despite their importance, common methods for the synthesis of linear primary amines, such as the amination of alcohols, the reduction of nitriles, and the reductive amination of carbonyl units, suffer from the production of undesired side products, including overalkylation to form secondary and tertiary amines.[5-8] These methods also require pre-functionalization of a hydrocarbon starting material to install the oxidized functional groups required for reactivity. Other common transformations, such as the Schmidt reaction or the Gabriel synthesis, typically require high temperatures, reactive intermediates, or harsh reagents, limiting the utility of these methods.[8-10] In addition, methods to synthesize amines from hydrocarbons, such as hydroamination of olefins or C–H amination of alkanes, are typically selective for the installation of the amine at a secondary carbon over the primary carbon.[11-14] Hydroaminomethylation, the conversion of an olefin to a primary amine by sequential hydroformylation and reductive amination, is an alternative method that can be harnessed for the synthesis of linear primary amines. However, previously disclosed hydroaminomethylation reactions have required high temperatures and pressures and suffered from overalkylation of the desired primary amine.[5-7, 15-18]

In 2024, Gröger and coworkers disclosed a chemoenzymatic strategy for the formation of alcohols from olefins using a hydroformylation, followed by enzymatic reduction (Figure 1b).[19] Contemporaneously, our group reported a linear- and primary-selective hydroaminomethylation by developing of a chemoenzymatic method[20-21] for the selective synthesis of linear primary amines by sequential Rh-catalyzed hydroformylation and enzymatic transamination.[22] Exquisite selectivity for linear primary amine products with no overalkylation was achieved by combining a linear-selective rhodium catalyst and an w-transaminase that selectively forms the desired primary amine. Gröger and coworkers disclosed a tandem chemoenzymatic method for the synthesis of branched 2-phenylpropan-1-amine from styrene.[23] While this report demonstrates a method for the

selective synthesis of primary amines under mild conditions, the reported methodology is limited to the synthesis of a single branched product and to the reactions of vinylarenes, albeit with high turnover numbers.

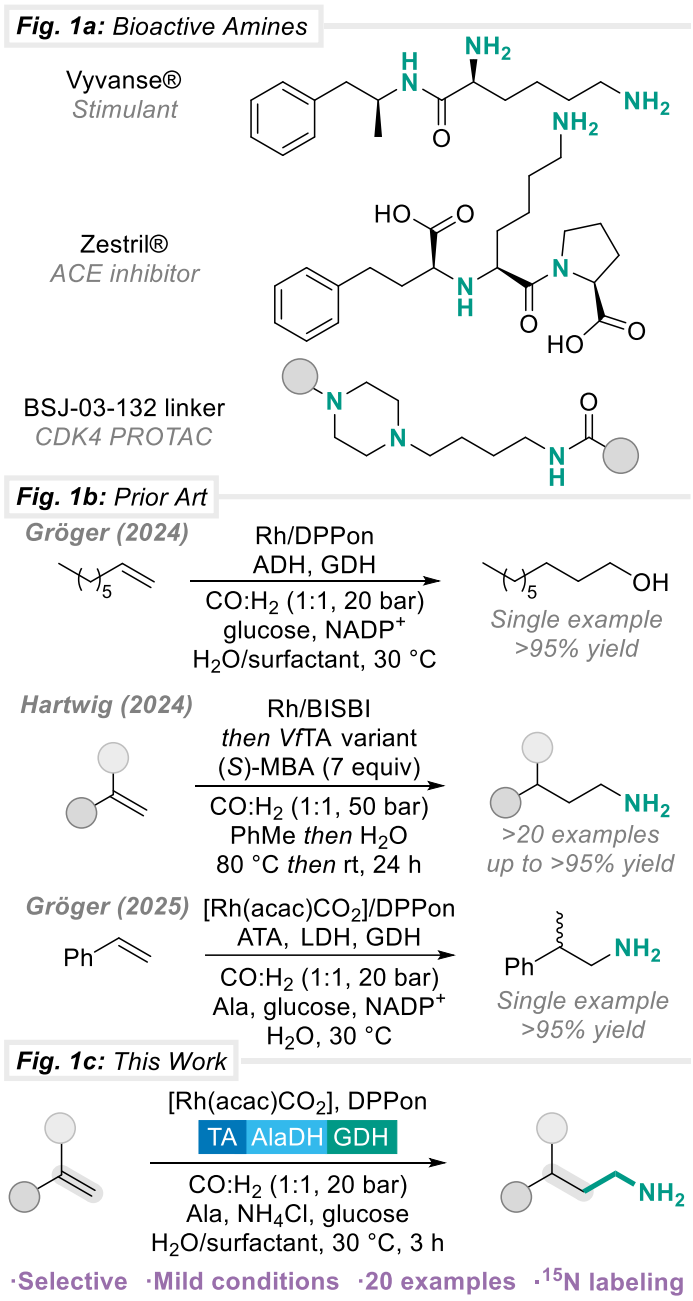

Figure 1. (a) Examples of bioactive molecules containing amines, (b) recent examples of chemoenzymatic hydrofunctionaliation reactions, and (c) this work.

In our iniital report of sequential hydroformylation and reductive amination, we reported one example of a rhodium-catalyzed hydroformylation with a catalyst that is encapsulated in a surfactant micelle and that operates simultaneously with an w-transaminase in aqueous media. We paired the Rh/DPPon hydroformylation catalyst developed by Breit and coworkers[24] with the wild-type transaminase enzyme from *Vibrio fluvialis* (WT-*Vf*TA). Coupling the transamination reaction with an amine donor recycling system enabled the direct and highly selective transformation of terminal olefins to primary amines using feedstock components (ammonium salts, alanine, carbon monoxide, hydrogen, and glucose).

The recycling system was composed of a biocatalytic cascade, wherein a wild-type alanine dehydrogenase enzyme (WT-AlaDH) converts the byproduct of the transamination reaction, oxalic acid, to the amine donor alanine in the presence of an ammonium salt. WT-AlaDH is NADH/NADPH-dependent; therefore a wild-type glucose dehydrogenase enzyme (WT-GDH) was employed to turn over NAD+/NADP+ using glucose as the terminal reductant.[25] We found that the combination of alanine and ammonium chloride as the nitrogen sources avoided the formation of secondary and tertiary amine side products. However, the disclosed tandem chemoenzymatic procedure suffered from low yield and poor mass balance.

Herein, we report a tandem, cooperative hydroaminomethylation strategy for the selective synthesis of linear primary amines in good yield from terminal olefins (Figure 1c). Our developed system converts alkenes of varied structures and is suitable for the installation of ^{15}N into primary amine products and for the synthesis of biologically relevant fine chemicals containing linear, primary amines.

3.3 Results & Discussion

3.3.1 Development of reaction conditions for tandem chemoenzymatic hydroaminomethylation of olefins in water.

We initiated our search for a chemoenzymatic system that would convert olefins to linear primary amines by studying the effect of conditions on the yield of linear primary amine from olefin **1a**. (Table 1). We found in initial experiments that lowering the concentration of substrate from 200 mM to 50 mM increased the yield of the linear primary amine (see the supporting information); therefore, we conducted further experiments on reactions at 50 mM concentration.

Table 1. Effect of the Deviation from Standard Conditions on Yield of Linear Primary Amine 2a from 1a.[a]

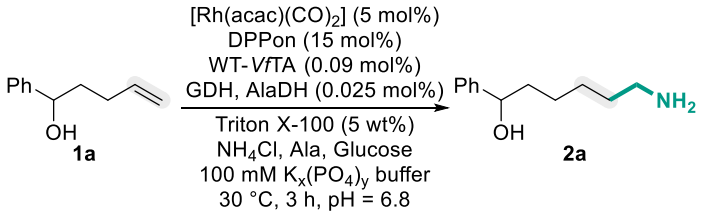

Entry	Deviation from above:	Conv. (%)	**1a** (%)	**2a** (%)
1	-	88	12	31
2	1/2 [VfTA, AlaDH, GDH]	54	46	20
3	1/2 [Ala, Glucose]	86	14	45
4	10 wt% Triton	82	18	66
5	10 wt% Triton, 40 bar syngas	54	46	48
6	10 wt% Triton, 10 mol% [Rh]	96	4	70
7	15 wt% Triton	80	20	71
8	15 wt% Triton, 2.5 mol% [Rh]	92	8	54
⇨9	15 wt% Triton, 2.5 mol% [Rh], 24 h	99	1	71

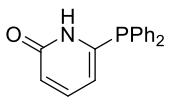

DPPon

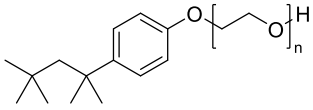

Triton X-100

[a]Yield and conversion determined by ^{1}H qNMR spectroscopy with 1,2-dibromoethane as internal standard. See supporting information for additional details. A *l:b* ratio of >20:1 was observed for each entry.

With olefin **1a** as substrate, we observed 29% yield of primary amine product at 1 h, with 54% remaining olefin and no observed aldehyde, alcohol, or alkane side products. However, after 3 h, we observed 46% of primary amine product, with 4% remaining olefin and 54% mass balance unaccounted for. Because we observed complete conversion of **1a** after 3 h and because we sought to avoid background reactions such as imine formation and reduction, we shortened the reaction time to 3 h for additional experiments.

We next evaluated the effect of catalyst concentration on the yield of primary amine and found that varying the concentrations of rhodium, DPPon, WT-*Vf*TA, WT-AlaDH, and WT-GDH, did not change the mass balance of the reaction appreciably. We hypothesized that the incomplete mass balance resulted from the reduction of imines formed *in situ* during the reaction between alanine and the intermediate aldehyde, or between the product amine and the intermediate aldehyde, or between the product amine and oxalate or gluconolactone formed from oxidation of glucose. Therefore, we sought to eliminate the presence of Rh nanoparticles, which could form during hydroformylation, by more effective encapsulation of the rhodium catalyst in the micelle.

Consistent with this hypothesis, decreasing the loading of the enzymes, which we had previously found to increase the rate of the transamination reaction, resulted in a lower yield of product with only a slight improvement to the mass balance. (Table 1, entry 2) and decreaseing the concentrations of glucose and alanine resulted in little to no change in yield or mass balance (Table 1, entry 3), but increasing the amount of surfactant, Triton X-100, from 5 to 10 wt% led to an increase in mass balance and a slight increase in the yield of primary amine (Table 2, entry 4). Further increasing the loading of Triton X-100 to 15 wt% and reduction of the rhodium loading to 2.5 mol% resulted in a yield of 71% after 24 h (Table 2, entry 9). The addition of up to 10% DMSO to the reaction did not adversely affect the yield or the mass balance (see SI for additional details).

3.4 Scope of the Tandem Chemoenzymatic Hydroaminomethylation Reaction

With conditions to conduct the tandem hydroaminomethylation, we evaluated the scope of the process with the combination of chemical and enzymatic catalysts. Under the conditions described, a range of olefins were transformed into the linear primary amines (Scheme 1). The chemoenzymatic reaction was often complete (full conversion of the olefin) within 3 h. Reactions of substrates that did not fully convert after 3 h were allowed to run for 24 h.

We first examined the range of monosubstituted terminal olefins that react under the described conditions. Electron neutral (**2b**), poor (**2c**), and rich (**2d**) homoallyl benzene derivatives react to produce linear primary amines in yields of 67-83% with *l:b* ratios that vary from 3:1 to 7:1. Additional pendant functional groups, such as the biologically relevant dihydroquionolone groups (**2e**), heteroaromatic groups (**2f**), and protected amines (**2g**) and azetidines (**2h**), were tolerated. Olefins bearing primary alkyl chlrodes (**2i**), cyclohexene (**2j**), and alcohols (**2k** and **2l**) formed the desired primary amines in good yield, with higher yields being observed for more soluble substrates. In addition, heptene was converted to octanamine (**2m**) in 52% yield. Under the reaction conditions, bioactive molecules also reacted: for example, unnatural amino acid **2n** was formed in 63% yield from olefin **1n**, and a precursor to vilanterol (**2o**), a β2-adrenergic agonist, was produced in 83% yield with a 17:1 *l:b* ratio. Primary amine **2p** formed from citronellene in 33% yield, and an analogue of probenecid (**2q**), an anti-gout medication, was formed in 31% yield.

In addition, we found that 1,1-disubstituted olefins bearing strained rings reacted. Primary amine **2r** was formed in 43% yield, while [3.3] and [3.5] azaspirocycles **2s** and **2t** were formed in 55% and 68% yields, respectively. A *l:b* ratio of >20:1 was observed for these 1,1-disubstituted olefins, likely due to a steric preference for the formation of the primary alkylrhodium intermediate during the hydroformylation step.

Finally, we found that the use of ^{15}N-labled alanine and ammonium chloride enables the formation of isotopically labeled linear primary amine products with high radioisotope incorporation. Due to the price of these isotopically labeled reagents, we performed the hydroaminomethylation reactions at a concentration of ^{15}N-Ala and $^{15}NH_4Cl$ reduced by 50%. Under these conditions, we produced ^{15}N-labeled amines **^{15}N-2o**, **^{15}N-2g**, and **^{15}N-2t** in 82%, 68%, and 73% yields, respectively, with *l:b* ratios comparable to the *l:b* ratios of their unlabeled counterparts. These examples demonstrate the value of this method for the isotopic labelling of compounds of biological interest.

Scheme 1. Scope of terminal olefins that undergo the tandem chemoenzymatic hydroaminomethylation reaction.[a]

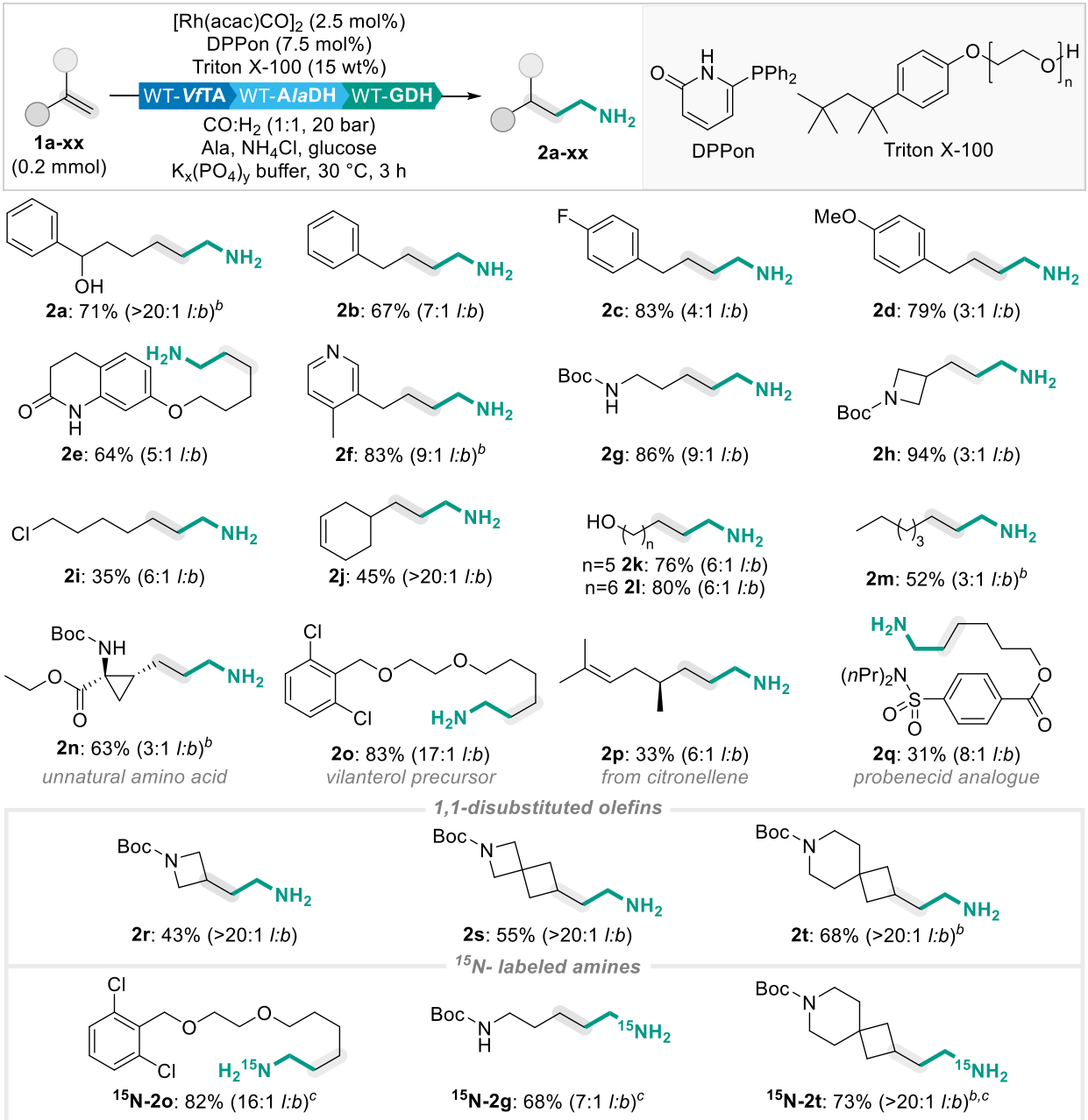

[a]Yield determined by ^{1}H qNMR spectroscopy with 1,2-dibromoethane as internal standard; *l:b* ratio determined by ^{1}H qNMR spectroscopy. [b]Reaction run for 24 h.[c]Reaction conducted using $^{15}NH_4Cl$ and ^{15}N-alanine, at half the normal concentration.

3.5 Summary

The tandem chemoenzymatic hydroaminomethylation strategy disclosed herein provides a robust and sustainable alternative to conventional synthetic routes for the synthesis of linear primary

amines. The cooperative integration of homogeneous catalysis with biocatalytic transformations in aqueous media led and the need for organic solvents and multistep procedures. The versatility of this chemoenzymatic method—evidenced by its broad substrate scope and the capability to incorporate isotopic labels—underscores its potential for application to the development and production of pharmaceuticals, agrochemicals, and beyond.

3.6 References

(1) Kerru, N.; Gummidi, L.; Maddila, S.; Gangu, K. K.; Jonnalagadda, S. B. A Review on Recent Advances in Nitrogen-Containing Molecules and Their Biological Applications. *Molecules* **2020**, *25*.

(2) Lawrence, S. A., *Amines: synthesis, properties and applications*. Cambridge University Press: 2004.

(3) Jiang, B.; Wang, E. S.; Donovan, K. A.; Liang, Y.; Fischer, E. S.; Zhang, T.; Gray, N. S. Development of Dual and Selective Degraders of Cyclin-Dependent Kinases 4 and 6. *Angew. Chem. Int. Ed.* **2019**, *58*, 6321-6326.

(4) Troup, R. I.; Fallan, C.; Baud, M. G. J. Current strategies for the design of PROTAC linkers: a critical review. *Explor. target. anti-tumor ther.* **2020**, *1*, 273-312.

(5) Philippe Kalck, M. U. Tandem Hydroaminomethylation Reaction to Synthesize Amines from Alkenes *Chem. Rev.* **2018**, *118*, 3833-3861.

(6) Irrgang, T.; Kempe, R. Transition-Metal-Catalyzed Reductive Amination Employing Hydrogen. *Chem. Rev.* **2020**, *120*, 9583-9674.

(7) Kumar, R.; Flodén, N. J.; Whitehurst, W. G.; Gaunt, M. J. A general carbonyl alkylative amination for tertiary amine synthesis. *Nature* **2020**, *581*, 415-420.

(8) Mitsunobu, O., 1.3 - Synthesis of Amines and Ammonium Salts. In *Comprehensive Organic Synthesis*, Trost, B. M.; Fleming, I., Eds. Pergamon: Oxford, 1991; pp 65-101.

(9) Gibson, M. S.; Bradshaw, R. W. The Gabriel Synthesis of Primary Amines. *Angew. Chem. Int. Ed. Engl.* **1968**, *7*, 919-930.

(10) Smith, P. A. S. The Schmidt Reaction: Experimental Conditions and Mechanism. *J. Am. Chem. Soc.* **1948**, *70*, 320-323.

(11) Streiff, S.; Jérôme, F. Hydroamination of non-activated alkenes with ammonia: a holy grail in catalysis. *Chem. Soc. Rev.* **2021**, *50*, 1512-1521.

(12) Müller, T. E.; Hultzsch, K. C.; Yus, M.; Foubelo, F.; Tada, M. Hydroamination: Direct Addition of Amines to Alkenes and Alkynes. *Chem. Rev.* **2008**, *108*, 3795-3892.

(13) Tran, B. L.; Li, B.; Driess, M.; Hartwig, J. F. Copper-Catalyzed Intermolecular Amidation and Imidation of Unactivated Alkanes. *J. Am. Chem. Soc.* **2014**, *136*, 2555-2563.

(14) Park, Y.; Kim, Y.; Chang, S. Transition Metal-Catalyzed C–H Amination: Scope, Mechanism, and Applications. *Chem. Rev.* **2017**, *117*, 9247-9301.

(15) Zimmermann, B.; Herwig, J.; Beller, M. The First Efficient Hydroaminomethylation with Ammonia: With Dual Metal Catalysts and Two-Phase Catalysis to Primary Amines. *Angew Chem Int Ed Engl* **1999**, *38*, 2372-2375.

(16) Chen, X.-C.; Lan, T.; Zhao, K.-C.; Guo, L.; Lu, Y.; Liu, Y. Efficient hydroaminomethylation of olefins catalyzed by Rh-complex ligated by P,O-hybrid ligand with chelating effect. *J. Catal.* **2022**, *411*, 158-166.

(17) J. M. Han, L. X.-H., Y. Zhi, Enantioselective Hydroaminomethylation of Olefins Enabled by Rh/Brønsted Acid Relay Catalysis. *Org. Lett.* **2017**, *19*, 1076.

(18) Hanna, S.; Holder, J. C.; Hartwig, J. F. A Multicatalytic Approach to the Hydroaminomethylation of alpha-Olefins. *Angew Chem Int Ed Engl* **2019**, *58*, 3368-3372.
(19) Bork, H.; Naße, K. E.; Vorholt, A. J.; Gröger, H. Merging High-Pressure Syngas Metal Catalysis and Biocatalysis in Tandem One-Pot Processes for the Synthesis of Non-chiral and Chiral Alcohols from Alkenes in Water. *Angew. Chem. Int. Ed.* **2024**, *n/a*, e202401989.
(20) Ahmed, S. T.; Leferink, N. G. H.; Scrutton, N. S. Chemo-enzymatic routes towards the synthesis of bio-based monomers and polymers. *Mol. Catal.* **2019**, *467*, 95-110.
(21) Gröger, H.; Gallou, F.; Lipshutz, B. H. Where Chemocatalysis Meets Biocatalysis: In Water. *Chem. Rev.* **2022**.
(22) Manske, J. L.; Nicolai, J.; Bloomer, B. J.; Clark, D. S.; Hartwig, J. F. A Chemoenzymatic Hydroaminomethylation Strategy for the Selective Synthesis of Linear Primary Amines from Olefins by Sequential and Tandem Processes. *ACS Catal.* **2024**, *14*, 14356-14362.
(23) Spang, J.; Bork, H.; Belov, F.; von Langermann, J.; Vorholt, A. J.; Gröger, H. One-pot hydroaminomethylation of an alkene under formation of primary amines by combining hydroformylation at elevated syngas pressure and biocatalytic transamination in water. *Org. Biomol. Chem.* **2025**, *23*, 688-692.
(24) Straub, A. T.; Otto, M.; Usui, I.; Breit, B. Room Temperature Ambient Pressure (RTAP)-Hydroformylation in Water Using a Self-Assembling Ligand. *Adv. Synth. Catal.* **2013**, *355*, 2071-2075.
(25) Guo, F.; Berglund, P. Transaminase biocatalysis: optimization and application. *Green Chem.* **2017**, *19*, 333-360.
(26) Erchinger, J. E.; Hoogesteger, R.; Laskar, R.; Dutta, S.; Hümpel, C.; Rana, D.; Daniliuc, C. G.; Glorius, F. EnT-Mediated N–S Bond Homolysis of a Bifunctional Reagent Leading to Aliphatic Sulfonyl Fluorides. *J. Am. Chem. Soc.* **2023**, *145*, 2364-2374.
(27) Studier, F. W. Stable expression clones and auto-induction for protein production in E. coli. *Methods Mol Biol* **2014**, *1091*, 17-32.
(28) Falk, E.; Makai, S.; Delcaillau, T.; Gürtler, L.; Morandi, B. Design and Scalable Synthesis of N-Alkylhydroxylamine Reagents for the Direct Iron-Catalyzed Installation of Medicinally Relevant Amines. *Angew. Chem. Int. Ed.* **2020**, *59*, 21064-21071.

3.7 Experimental Information

3.7.1 General Information

All reactions were conducted under inert atmosphere in a nitrogen-filled glovebox or with standard Schlenk techniques, unless otherwise specified. All reagents and solvents were purchased from commercial sources and used as received, unless otherwise noted. All glassware was flame-dried or dried overnight at 120 °C, allowed to cool under vacuum, and stored in a N_2-atomsphere drybox until use, unless otherwise noted. Tetrahydrofuran, toluene, and diethyl ether were purified by passing the degassed solvents (N_2) through a column of activated alumina (solvent purification system purchased from Innovative Technologies, Newburyport, MA). All other solvents were stored over 4 Å molecular sieves for at least 24 h prior to use. Compounds **1a-d**, **1f-n**, **1p**, and **1r-t** are commercially available. Olefin **1q** was synthesized according to a previously published method.[26] All reagents purchased from commercial suppliers were used as received. Deuterated solvents, ^{15}N-Alanine, and $^{15}NH_4Cl$ were purchased from Cambridge Isotope Laboratories and used as received. $CO:H_2$ (1:1) was purchased from Praxair in 99.99% purity.

Oligonucleotides were obtained from Integrated DNA Technologies. Enzymes and reagents used for cloning were obtained from New England BioLabs and Thermo Fisher Scientific. All expression media and buffers were prepared with ddH_2O (MilliQ A10 Advantage purification system, Millipore). All expression media were sterilized by either an autoclave (30 min, 121 °C) or a sterile syringe filter (0.22 µm). To maintain sterile conditions, sterile materials and *E. coli* cells were manipulated near a lit Bunsen burner. Cells were pelleted with centrifugation and lysed with a Qsonica Q125 equipped with a quarter-inch probe at 62% amplitude.

^{1}H, ^{13}C, ^{14}N, and ^{19}F NMR spectra were recorded on Bruker AV-300, AVB-400, AV-500, AV-600, NEO-500, NEO-501, and AV-700 spectrometers at the University of California, Berkeley NMR facility. Chemical shifts are reported relative to residual solvent peaks ($CDCl_3$ = 7.26 ppm for ^{1}H NMR spectra and 77.16 ppm for ^{13}C NMR spectra, DMSO-d_6 = 2.50 ppm for ^{1}H NMR spectra and 39.52 ppm for ^{13}C NMR spectra). For ^{19}F NMR spectra, chemical shifts are reported relative to the δ –113.15 resonance of PhF used as an external reference or the δ –63.72 resonance of $PhCF_3$. The following abbreviations are used in reporting NMR data: s, singlet; d, doublet; t, triplet; q, quartet; p, pentet; hept, heptet; m, multiplet.

Gas Chromatography (GC) was performed on an HP 6890 GC system with an Agilent HP-5 column (25 m × 0.200 mm, 0.33 µm) for aldehyde quantification. Analysis of amine products was performed on an HP 6890 GC system with an Agilent CP-Sil 8 CB column for amines (30 m x 0.32 mm x 1.00 µm).

High-resolution mass spectra were recorded on a Perkin Elmer AxION 2 TOF mass spectrometer in ESI mode operated by the LBNL Catalysis Laboratory at the University of California, Berkeley or were obtained from the QB3 Mass Spectrometry Facility at UC Berkeley. Analytical thin layer chromatography (TLC) was performed on Kieselgel 60 F254 glass plates precoated with a 0.25 mm thickness of silica gel. The TLC plates were visualized with UV light and by staining with $KMnO_4$. Preparatory TLC was performed on AnalTech preparatory TLC plates with a 1000 µm-thick silica coating and visualized by UV. Column chromatography was generally performed on a Teledyne Isco Combiflash® Rf system with RediSep Gold™ columns.

3.7.2 General Procedure for The Tandem Chemoenzymatic Hydroaminomethylation Reaction

Scheme S1. General procedure for the tandem chemoenzymatic hydroaminomethylation reaction.

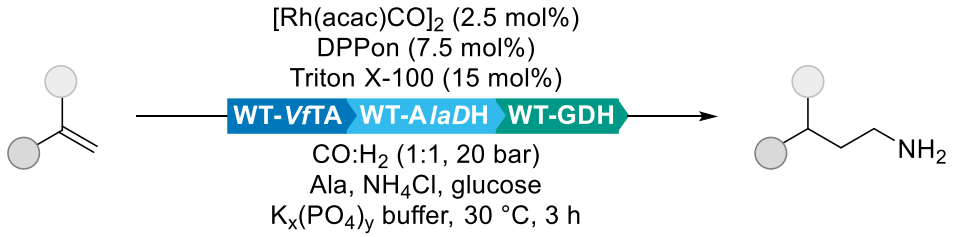

In a nitrogen-filled glovebox, [Rh(acac)$(CO)_2$] (1.3 mg, 2.5 mol%) and DPPon (4.2 mg, 7.5 mol%) were added to a flame-dried 18x150mm (25 mL) test tube. Degassed Triton X-100 (300 uL, 15 wt%) was added by glass pipette directly to the solid at the bottom of the test tube, and the test tube was tilted to ensure all the powder was covered. A flame-dried Teflon stir bar was then added, and the surfactant and catalyst were stirred for 10 seconds, forming a dark brown oil. To the test

tube was then added alanine buffer (100 mM potassium phosphate, pH = 7.0, 3.0 mL, 1 M alanine, 250 mM glucose, 0.5 mM pyridoxal phosphate, 2 mM NADPH, 0.27 mM NADPH) that had been degassed for 1 hour down the sides of the tube, washing any solid off of the walls of the test tube. The resulting solution was stirred for 15 seconds, forming a light green suspension that darkens over time. Solutions of WT-VfTA (700 uL), WT-AlaDH (200 uL), and WT-GDH (100 uL), that had been degassed by gentle vacuum for 30 minutes, were added carefully down the side of the test tube *via* micropipette, ensuring that bubbles are not formed *(**NOTE:** allowing the rhodium, ligand, and enzyme mixture to sit for greater than 15 minutes at this stage has been observed to result in a decrease in yield and mass balance).* After the addition of enzyme, the reaction mixture adopts a more yellow hue. Finally, the substrate (200 μmol) was added in one portion directly to the solution *via* Hamilton syringe and the final reaction mixture was then stirred for 5 seconds. The test tube was then placed into a 450 mL Parr bomb, the bomb was sealed, and the apparatus was removed from the glovebox. The Parr bomb was purged with 1:1 $CO:H_2$ (2 x 20 bar), then pressurized to 20 bar with 1:1 $CO:H_2$. The Parr bomb was then placed into a heating block pre-set to 30 °C and the reaction solutions were stirred at 800 rpm for 3 h. After this time, the Parr bomb was placed into an ice bath, and the pressure was vented once the bomb was cooled (***NOTE:*** *successful reactions are typically light green without precipitation of the enzyme*).

Upon completion, internal standard (either dodecane for GC analysis or dibromomethane for NMR analysis) and 1 mL of 6 M NaOH was added to the reaction solution, followed by 3 mL of extraction solvent. The solution was transferred to a 20 mL vial and the test tube was further washed with 3 mL of water followed by 3 mL of extraction solvent. The resulting solution was vortexed until thoroughly mixed. The mixture was then centrifuged to separate the organic and aqueous layers and analyzed by gas chromatography or quantitative ^1H NMR to determine yield of product. If isolated, the crude residue was purified by flash column chromatography (SiO_2, neutral Al_2O_3, or Amine-functionalized SiO_2) to afford pure product.

3.7.3 General Methods for Protein Expression, Purification, and Characterization

Media Preparation: Autoinduction media[27] was prepared according to published procedures and 2 mL of the relevant 1000X antibiotics was added (0.05 mg/L of kanamycin and 0.1 mg/L of ampicillin).

***Protein Expression*:** Rosetta2 competent *E. coli* cells (QB3 Macrolab, UC Berkeley) were thawed on ice for 15 minutes. Then, 40 μL of Rosetta2 cells were transferred to sterile 14 mL Falcon tubes and transformed with the specified plasmid. Single colonies were picked to inoculate cultures (5-8 mL, LB media), which were grown for 12-18 hours at 37 °C while shaking at 225 rpm. Each overnight culture was used to inoculate 1-2 L of autoinduction media, which was further grown for 24 h at 37 °C, while shaking at 200-225 rpm. Cells were harvested by centrifugation (5000 rpm, 10 min, 4 °C), and the pellets were resuspended in 20 mL suspension buffer (50 mM $Na_xH_y(PO_4)_z$ 250 mM NaCl, 10 mM imidazole, pH 8.0).

***Protein Purification*:** Cell suspensions were thawed in a water bath at 25 °C and lysed on ice by sonication (10 x 12 s on, 10 x 12 s off, 62% amplitude with a quarter-inch probe). Crude lysates were transferred to sterile 50 mL Falcon tubes, and cell debris was removed by centrifugation (10,000 rpm, 45 min, 4 °C). The crude lysate was poured over Ni-NTA resin. The resin was washed with lysis buffer (15 mL), and protein was eluted with 15 mL elution buffer (50 mM sodium

phosphate, 250 mM NaCl, 250 mM imidazole, pH 8.0). The protein was concentrated to 2.5 mL with an Amicon Ultra 15 spin concentrator (30,000 Da cut off for transaminase and 10,000 Da cut off for GDH and AlaDH) and desalted into the specified storage buffer with Sephadex G-25 desalting columns.

***Protein Storage*:** proteins were flash frozen in liquid nitrogen and stored at -80 °C for up to 2 months.

Protein Characterization Gel Electrophoresis: Protein purity was analyzed by sodium dodecyl sulfate-polyacrylamide (SDS-PAGE) gel electrophoresis with precast gels (polyacrylamide, 10-20% linear gradient, Biorad).

***UV-Vis Spectroscopy*:** Protein concentration was determined by a NanoDrop 2000 UV-Vis Spectrophotometer (Thermo Scientific).

Protein Storage Buffers:

WT-*Vf*TA: 100 mM sodium phosphate pH 7.5, 100 mM sodium chloride, 0.5 mM pyridoxal phosphate, 10% glycerol

WT-*Bs*GDH: 100 mM potassium phosphate, 100 mM sodium phosphate, pH 7.5, 10% glycerol

WT-*Bs*AlaDH: 50 mM trisHCl, 50 mM NaCl, pH 7.5, 10% glycerol

3.7.4 Evaluation of Conditions for the Formation of Primary Amine Products in the Tandem Hydroaminomethylation Reaction

Scheme S2. General procedure for the evaluation of conditions for the tandem chemoenzymatic hydroaminomethylation reaction.

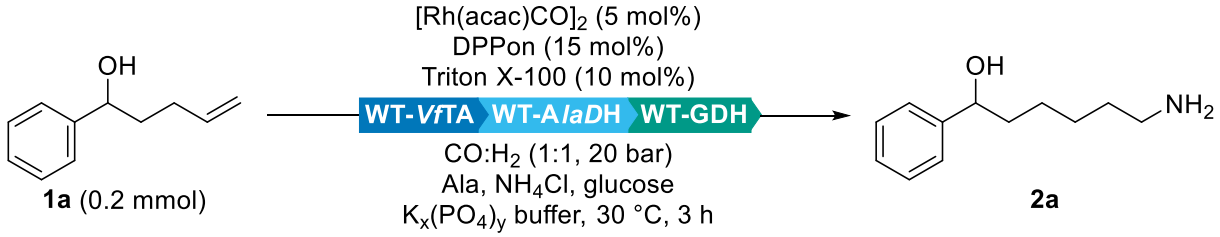

In a nitrogen-filled glovebox, [Rh(acac)(CO)$_2$] (2.6 mg, 5.0 mol%) and DPPon (8.4 mg, 15 mol%) were added to a flame-dried 18x150mm (25 mL) test tube. Degassed Triton X-100 (200 µL, 10 mol%) was added by glass pipette directly to the solid at the bottom of the test tube, and the test tube was tilted to ensure all the powder was covered. A flame-dried Teflon stir bar was then added, and the surfactant and catalyst were stirred for 10 seconds, forming a dark brown oil. To the test tube was then added alanine buffer (100 mM potassium phosphate, pH = 7.0, 3.0 mL, 1 M alanine, 250 mM glucose, 0.5 mM pyridoxal phosphate, 2 mM NADPH, 0.27 mM NADPH) that had been degassed for 1 hour (3.0 mL) down the sides of the tube, washing any solid off of the walls of the test tube. The resulting solution was stirred for 15 seconds, forming a light green suspension that darkens over time. Degassed solutions of WT-*Vf*TA (700 uL unless otherwise specified), WT-*Ala*DH (200 uL unless otherwise specified) and WT-*G*DH (100 uL unless otherwise specified) were added carefully down the side of the test tube *via* micropipette, ensuring that bubbles are not

formed. Finally, 1-phenylpent-4-en-1-ol **1a** (32.4 mg, 0.2 mmol) was added in one portion directly to the solution *via* Hamilton syringe, and the final reaction mixture was then stirred for 5 seconds. The test tube was then placed into a 450 mL Parr bomb, the bomb was sealed, and the apparatus was removed from the glovebox. The Parr bomb was purged with 1:1 $CO:H_2$ (2 x 20 bar), then pressurized to 20 bar with 1:1 $CO:H_2$. The Parr bomb was then placed into a heating block pre-set to 30°C and the reaction solutions were stirred at 800 rpm for 3 hours. After this time, the Parr bomb was placed into an ice bath, and the pressure was vented once the bomb was cooled. Upon completion, internal standard (either dodecane for GC analysis or dibromomethane for NMR analysis) and 1 mL of 6 M NaOH was added to the reaction solution, followed by 3 mL of extraction solvent. The solution was transferred to a 20 mL vial and the test tube was further washed with 3 mL of water followed by 3 mL of extraction solvent. The resulting solution was vortexed until thoroughly mixed. The mixture was then centrifuged to separate the organic and aqueous layers and analyzed by gas chromatography or quantitative ^{1}H NMR to determine yield of product.

3.7.5 Synthesis of Olefins

7-(pent-4-en-1-yloxy)-3,4-dihydroquinolin-2(1*H*)-one (1e)

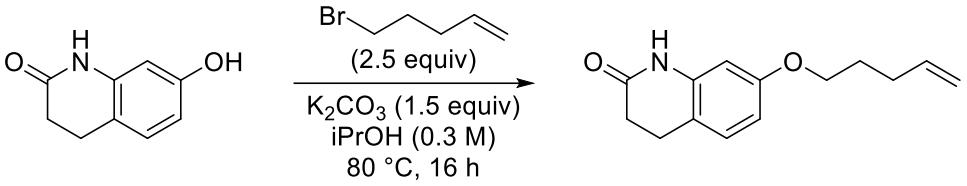

To a 20 mL vial equipped with a stir bar was added 7-hydroxy-3,4-dihydro-2(1*H*)quinolineone (456 mg, 1.00 equiv, 2.80 mmol) and K_2CO_3 (579 mg, 1.50 equiv, 4.19 mmol), followed by isopropanol (10.0 mL, 0.30 M) and 5-bromopent-1-ene (828 µL, 2.50 equiv, 6.99 mmol), sequentially. The headspace of the vial was flushed with N_2, the vial was sealed with a Teflon-lined cap, and the suspension was heated to 80 °C for 16 h. After this time, the suspension was cooled to 25 °C, diluted with EtOAc, and the phases were separated with water. The aqueous layer was extracted with EtOAc (3x). The organic layers were combined, dried with Na_2SO_4, filtered, and the resulting filtrate was concentrated *in vacuo*. The crude residue was subjected to flash column chromatography (SiO_2, 20% - 40% EtOAc in hexanes) to afford 7-(pent-4-en-1-yloxy)-3,4-dihydroquinolin-2(1H)-one (469 mg, 72%) as a white solid. The spectra agree with those reported in the literature.[28]

^{1}H NMR (500 MHz, $CDCl_3$) δ 8.06 (s, 1H), 7.04 (d, *J* = 8.3 Hz, 1H), 6.52 (dd, *J* = 8.3, 2.5 Hz, 1H), 6.32 (d, *J* = 2.4 Hz, 1H), 5.84 (ddt, *J* = 16.9, 10.2, 6.7 Hz, 1H), 5.06 (dq, *J* = 17.1, 1.7 Hz, 1H), 5.02 – 4.98 (m, 1H), 3.93 (t, *J* = 6.4 Hz, 2H), 2.93 – 2.86 (m, 2H), 2.62 (dd, *J* = 8.4, 6.6 Hz, 2H), 2.27 – 2.18 (m, 2H), 1.91 – 1.81 (m, 2H).

^{13}C{^{1}H} NMR (126 MHz, $CDCl_3$) δ 171.88, 158.84, 138.19, 137.88, 128.82, 115.85, 115.42, 108.86, 102.35, 67.50, 31.22, 30.22, 28.51, 24.72.

1,3-dichloro-2-((2-(pent-4-en-1-yloxy)ethoxy)methyl)benzene (1o)

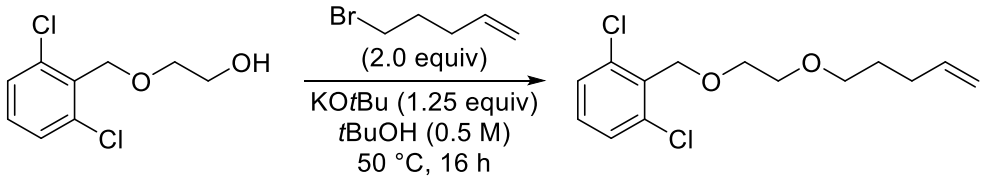

To a 40 mL vial equipped with a stir bar charged with 2-(2,6-dichlorobenzyloxy)ethanol (2.00 g, 1.00 equiv, 9.05 mmol) in *tert*-butanol (18.1 mL, 0.50 M) was added potassium *tert*-butoxide (1.27 g, 1.25 equiv, 11.3 mmol), and 5-bromo-1-pentene (2.17 mL, 2.00 equiv, 18.1 mmol) sequentially. The headspace of the vial was flushed with N_2, and the vial was subsequently sealed with a Teflon-lined cap and heated to 50 °C in a heating block for 16 h. After this time, the crude reaction mixture was cooled to rt, diluted with EtOAc, and poured into a separatory funnel containing H_2O. The aqueous layer was extracted with EtOAc (3x), the combined organics were dried with sodium sulfate, and the solid was filtered off. The filtrate was concentrated *in vacuo*, and the resulting crude oil was purified by flash column chromatography (SiO_2, 20 – 40% EtOAc in hexanes) to afford 1,3-dichloro-2-((2-(pent-4-en-1-yloxy)ethoxy)methyl)benzene (55%, 1.45g) as a clear oil.

^{1}H NMR (500 MHz, $CDCl_3$) δ 7.31 (d, *J* = 8.1 Hz,2H), 7.17 (ddd, *J* = 8.5, 7.5, 0.9 Hz, 1H), 5.81 (ddt, *J* = 16.9, 10.2, 6.6 Hz, 1H), 5.01 (dq, *J* = 17.1, 1.8 Hz, 1H), 4.94 (ddt, *J* = 10.2, 2.4, 1.3 Hz, 1H), 4.83 (s, 2H), 3.70 (dd, *J* = 5.9, 4.0 Hz, 2H), 3.61 (dd, *J* = 5.9, 4.0 Hz, 2H), 3.47 (t, *J* = 6.7 Hz, 2H), 2.11 (dtt, *J* = 8.0, 6.7, 1.5 Hz, 2H), 1.72 – 1.62 (m, 2H).

^{13}C{^{1}H} NMR (126 MHz, $CDCl_3$) δ 138.52, 137.10, 133.58, 129.99, 128.51, 114.78, 70.85, 70.21, 70.11, 67.69, 30.41, 29.02.

HRMS (ESI) $[C_{14}H_{18}Cl_2O_2+H]+$ calc;d.: 289.0758, found: 289.0757

3.7.6 ^{1}H and ^{19}F NMR spectra of Olefins

7-(pent-4-en-1-yloxy)-3,4-dihydroquinolin-2(1*H*)-one (2e)

^{1}H NMR spectrum ($CDCl_3$, 500 MHz)

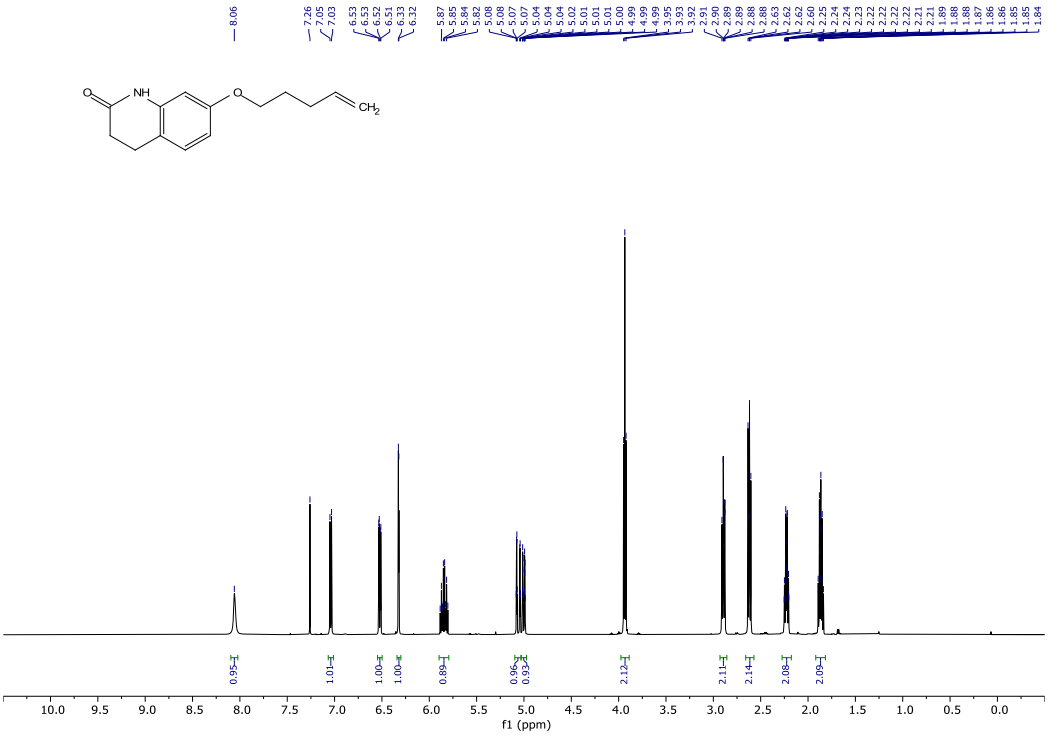

1,3-dichloro-2-((2-(pent-4-en-1-yloxy)ethoxy)methyl)benzene (1o)

^{1}H NMR spectrum ($CDCl_3$, 500 MHz)

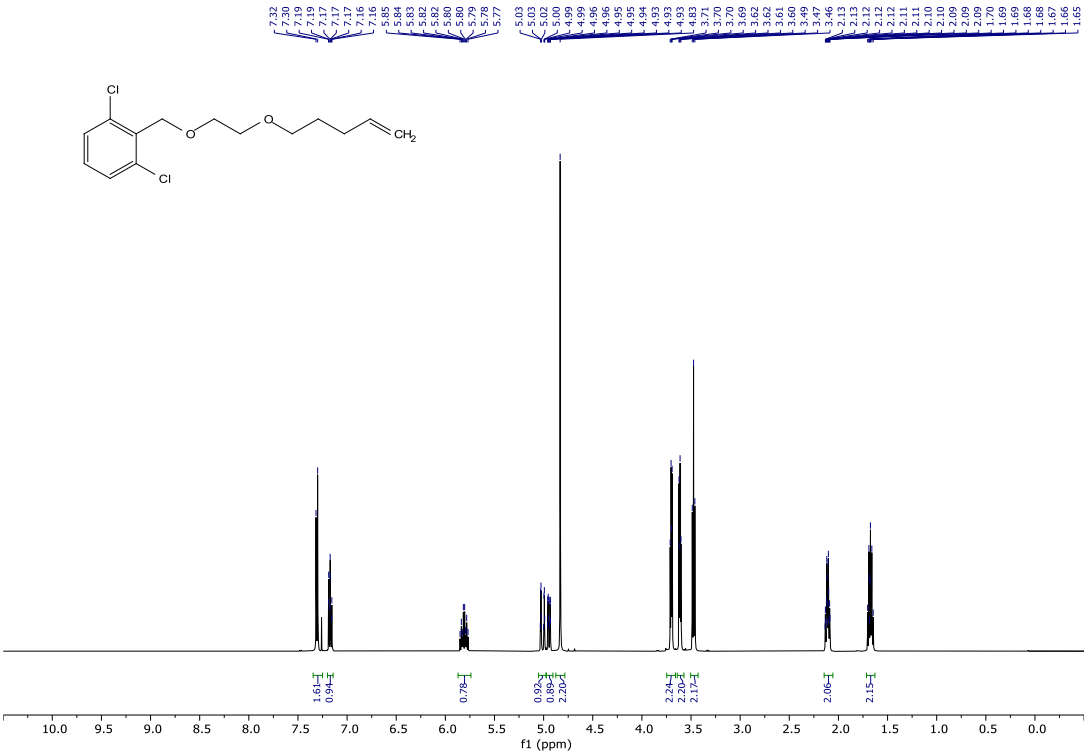

^{13}C{^{1}H} NMR spectrum ($CDCl_3$, 126 MHz)

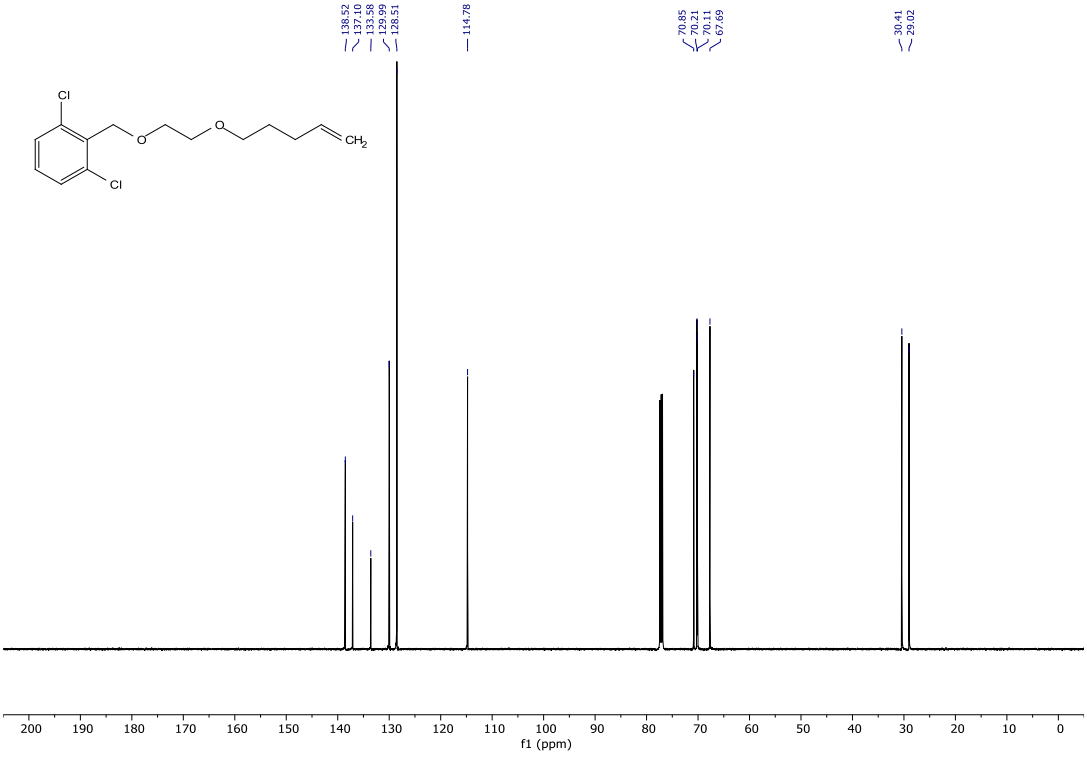

CHAPTER FOUR

Copper-Mediated Cyanodifluoromethylation of (Hetero)aryl Iodides and Activated (Hetero)aryl Bromides with $TMSCF_2CN$.

4.1 Abstract

The cyanodifluoromethyl group is unique because its size is closer than that of any other substituted difluoromethyl group to the size of the trifluoromethyl group, but its electronic properties are distinct from those of the trifluoromethyl group. In addition, the presence of the cyano group provides synthetic entry to a wide range of substituted difluoromethyl groups. However, the synthesis of cyanodifluoromethyl compounds requires multiple steps, highly reactive reagents (such as DAST, NSFI, or IF_5), or specialized starting materials (such as α,α-dichloroacetonitriles or α-mercaptoacetonitriles). Herein, we report a copper-mediated cyanodifluoromethylation of aryl and heteroaryl iodides and activated aryl and heteroaryl bromides with $TMSCF_2CN$. This cyanodifluoromethylation tolerates an array of functional groups, is applicable to late-stage functionalization of complex molecules, yields analogues of FDA-approved pharmaceuticals and fine chemicals, and enables the synthesis of a range of complex molecules bearing a difluoromethylene unit by transformations of the electron-poor CN unit. Calculations of selected steps of the reaction mechanism by Density Functional Theory indicate that the barriers for both the oxidative addition of iodobenzene to $[(DMF)CuCF_2CN]$ and the reductive elimination of the fluoroalkyl product from the fluoroalkyl copper intermediate lie in between those of $[(DMF)CuCF_3]$ and $[(DMF)CuCF_2C(O)NMe_2]$.

4.2 Introduction

Molecules containing alkyl or aryl fluorides are widespread in materials chemistry and are increasingly prevalent in approved pharmaceuticals[1] and agrochemicals,[2] constituting 20% and 50% of the market, respectively. Fluorine is prevalent because substitution of hydrogen atoms with fluorine can favorably impact the pKa, lipophilicity, molecular conformation, and metabolic stability of the parent compound.[3] To exert these effects, either an aryl fluoride or aryltrifluoromethyl group is often installed,[1, 4] in large part due to the commercial availability and synthetic accessibility of fluoro- and trifluoromethylarenes.[5-10] Other fluorinated groups, such as mono- and difluoromethyl groups, have beneficial properties,[3] but they are typically used less frequently because they are more difficult to introduce.

One such group is the cyanodifluoromethyl group. A comparison of the modified Swain-Lupton field parameter of a cyano group to that of a fluorine atom ($F_{CN} = 0.51$, $F_F = 0.45$)[11] suggests that the cyanodifluoromethyl group is more electron withdrawing than a trifluoromethyl group, and this electron-withdrawing property would deactivate an adjacent aryl group towards oxidative metabolism. The nitrile also provides opportunities for polar and hydrogen-bonding interactions with target substrates and serves as a bio-isostere for carbonyl groups, hydroxyl groups, and other hydrogen-bond acceptors.[2, 12] Arylacetonitriles are resistant to oxidation when the α-position lacks C–H bonds,[12] and the cyano group in these compounds typically undergoes hydrolysis, rather than releasing cyanide.[13-14] In addition to modulating the electronic properties of the adjacent nitrile and the electrophilicity of the nitrile carbon, the *gem*-difluoromethylene unit itself is commonly invoked as a bio-isostere of a carbonyl group, of ether oxygens, or of thioether sulfur atoms.

As a result of these properties, aryl-α,α-difluoroacetonitriles have garnered interest as herbicides,[15-16] pharmaceutical ingredients,[17-20] and liquid crystals (Figure 1a);[21] however, the investigation of aryl-α,α-difluoroacetonitriles has been limited because the cyanodifluoromethyl group is difficult to install. The most common route to cyanodifluoromethylarenes is a multi-step

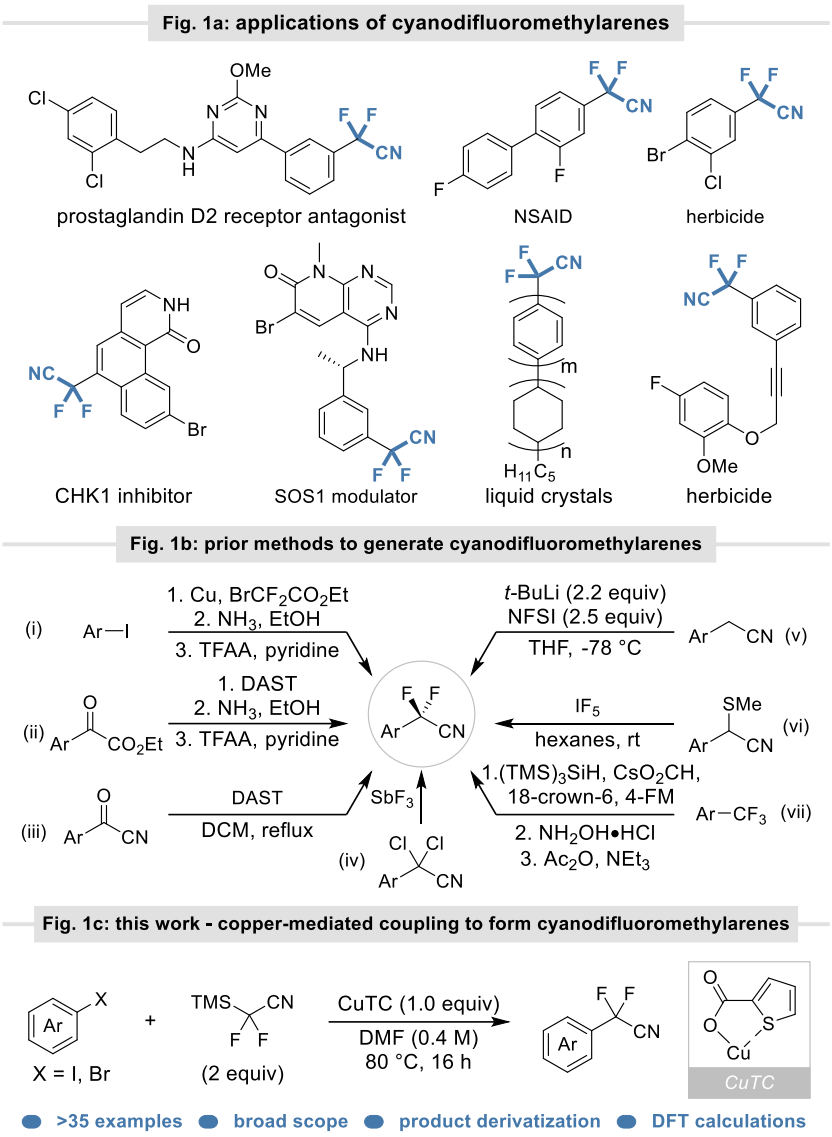

Figure 1. (a) Applications of cyanodifluoromethylarenes, (b) prior methods to generate cyanodifluoromethylarenes, and (c) this work: copper-mediated coupling to form cyanodifluoromethylarenes. TFAA = trifluoroacetic acid; 4-FM = 4-formylmorpholine.

sequence beginning with copper-mediated reductive coupling of an aryl iodide with a bromodifluoroester or with deoxofluorination of an aryl 2-oxoacetate to form an aryl-α,α-difluoroester (Figure 1b, i-ii). Subsequent addition of ammonia and dehydration of the resulting amide affords the aryl-α,α-difluoroacetonitrile.[22-23] These syntheses generally occur in low overall yields and require *de novo* construction of each cyanodifluoromethylarene. Introduction of the [-CF_2CN] group by alternative routes involving the formation of a C–F bond requires harsh conditions and highly reactive or toxic reagents, such as *N*,*N*-diethyl-1,1,1-trifluoro-λ^4-sulfanamine (DAST),[21] SbF_3,[24] *N*-fluorobenzene sulfonamide (NFSI),[25] or IF_5 (Figure 1b, iii-vi).[26] The functional group tolerance of such C–F bond-forming reactions, therefore, is limited, and these methods are not typically amenable to rapid diversification of the aryl substituent. Recently, Bandar and coworkers reported a base-promoted reductive coupling platform for the defluorofunctionalization of trifluoromethylarenes (Figure 1b, vii),[27] but this methodology, again, requires multiple steps to access the corresponding aryldifluoroacetonitrile.

Copper-mediated and copper-catalyzed fluoroalkylation reactions have been developed for the synthesis of trifluoromethylarenes,[28-33] aryldifluoromethylesters,[34-35] and aryldifluoromethylamides.[36] We sought to develop a coupling of aryl halides with a nucleophilic form of the cyanodifluoromethyl group to address the lack of suitable methods to synthesize aryl-α,α-difluoroacetonitriles rapidly, with broad scope, and in a fashion applicable to compounds of potential biological interest.

We report the copper-mediated coupling of aryl and heteroaryl iodides and electron-poor bromides with 2,2-difluoro-2-(trimethylsilyl)acetonitrile ($TMSCF_2CN$, **1**). This method (Figure 1c) delivers a diverse range of cyanodifluoromethylarenes in high yields with a simple, commercially available, inexpensive copper compound. The reaction tolerates a wide range of functional groups, making it suitable for the synthesis of complex, drug-like molecules, and DFT calculations show the barriers to oxidative addition and reductive elimination involving cyanodifluoromethyl copper complexes are lower in energy than those to oxidative addition and reductive elimination involving analogous trifluoromethylcopper complexes.

4.3 Results & Discussion

4.3.1. Development of reaction conditions for the coupling of aryl iodides with $TMSCF_2CN$.

Copper-mediated and copper-catalyzed fluoroalkylation reactions often require transmetallation of the fluoroalkyl group from a main group element to copper, and the rate of such transmetallation depends on the LX-type ligand on copper. We envisioned that a silicon-based reagent[37] containing the desired fluoroalkyl group,[38] TMS-CF_2CN (**1**) could transfer the cyanodifluoromethyl group to a copper compound containing the proper X-type ligand that would be replaced by the CF_2CN unit. The resulting fluoroalkylcopper species could then undergo oxidative addition of an aryl halide, followed by reductive elimination to deliver the desired product, but the effect of the nitrile in a fluoroalkyl group on these two steps is unknown. To investigate the potential of this scenario, we conducted a set of experiments with 1-*n*-butyl-4-iodobenzene, a series of Cu(I) complexes, and $TMSCF_2CN$ (Table 1).

Table 1. Evaluation of conditions for the copper-mediated coupling of aryl iodides and $TMSCF_2CN$ (1).

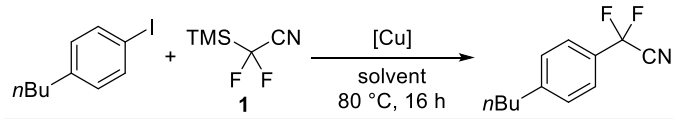

Entry	[Cu] (equiv)	Equiv **1**	solvent (M)	Yield (%)[a]
1	CuI (2.0)	5.0	DMSO (0.2)	16
2	CuDPP (2.0)	5.0	DMSO (0.2)	84
3	CuDPP (2.0)	5.0	DME (0.2)	91
4	CuDPP (1.0)	5.0	DME (0.2)	73
5	CuDPP (1.0)	2.0	DME (0.2)	76
6	CuDPP (1.0)	2.0	NMP (0.2)	96
7	CuDPP (1.0)	2.0	DMF (0.2)	96*
8	CuDPP (1.0)	2.0	DMF (0.4)	99*
9	CuDPP (0.5)	2.0	DMF (0.4)	48*
10[b]	CuDPP (1.0)	2.0	DMF (0.4)	99*
11	CuTC (1.0)	2.0	DMF (0.4)	99*

*Yield determined by Dr. Tomasso Fantoni; [a]determined by ^{19}F NMR spectroscopy with α,α,α-trifluorotoluene as internal standard. [b]Reaction time = 1 h. See Supporting Information for additional details.

After evaluating a variety of Cu(I) reagents, we found that Cu(I) diphenylphosphinate (CuDPP) mediated the cyanodifluoromethylation with excess **1** in DMSO and DME (entries 2-3). The reactions in DMF as solvent occurred with one, rather than two, equivalent of copper and with just 2 equivalents of **1** (entry 8). Reactions with 0.5 equivalents of Cu occurred in only 48% yield (entry 9). Ultimately, we found that the inexpensive Cu(I) thiophenecarboxylate (CuTC) complex mediated the reaction in DMF in high yield (entry 11). Reactions conducted with added ligands, such as 1,10-phenanthroholine or bipyridine, that

are common in copper-mediated transformations and reactions conducted with oxalamide- or oxalylhydrazide-bound copper species resulted in lower yields than those without added ligands in all cases (see Table S2 in the Supporting Information).

We hypothesize that $TMSCF_2CN$ undergoes transmetallation to copper by a cyclic transition state involving the carboxylate group of the thiophenecarboxylate ligand. No decomposition of **1** in the presence of the reaction partners and solvent in the absence of CuTC is observed. In principle, the reaction could be rendered catalytic by addition of NaTC or NaDPP to regenerate CuTC or CuDPP from the presumed CuI or CuBr product. However, NaDPP, NaTC, and other exogeneous activators of organosilanes, such as KF or CsF, lead to decomposition of silane **1** over the course of the reaction at 80 °C (see Tables S3 and S4 in the Supporting Information for these data**).**

Table 2. Yield of the cyanodifluoromethylation reaction under various conditions.[a]

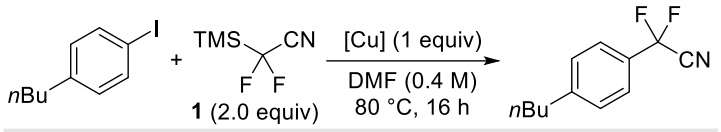

Entry	Conditions	Yield w/ CuTC	Yield w/ CuDPP
1	Standard conditions	99%	99%
2	under air	25%*	45%*
3	Schlenk technique	99%*	93%*
4	under air + N_2 purge	91%	36%
5	rt, 48 h	99%*	99%*
6	rt, 1 equiv **1**, 48 h	96%*	99%*

*Yield determined by Dr. Tomasso Fantoni; [a]determined using ^{19}F NMR spectroscopy with α,α,α-trifluorotoluene as internal standard.

CuTC is less expensive than CuDPP, and reactions conducted with CuTC generally delivered the products in similar yields to those of reactions conducted with CuDPP (see Figure S3 in the Supporting Information). When compared to the cost of common catalysts used in fluoroalkylation reactions such as (BrettPhos)Pd-G3,[39] at the appropriate stoichiometry, CuTC is among the lowest cost available ($0.25/mmol; see Supporting Information Table S5).

Although our studies were conducted in a nitrogen-filled glovebox, the reaction also proceeded smoothly when using Schlenk techniques or when assembling under air and flushing the reaction vessel with nitrogen before heating (Table 2, entries 3 and 4). The reaction proceeded at room temperature, albeit at a slower rate (entries 5-6), so further reactions were conducted at 80 °C to increase the rate of the cyanodifluoromethylation reaction.

The $TMSCF_2CN$ nucleophile **1** was synthesized on decagram-scale batches at Berkeley and was stable on the benchtop for over six months. This reagent is currently available in small-scale batches from Enamine while a process-scale synthesis is being developed.

4.3.2 Scope of the cyanodifluoromethylation reaction.

Having established conditions that deliver coupled product in high yield, we explored the scope of the copper-mediated cyanodifluoromethylation with an array of aryl and heteroaryl iodides and bromides (Chart 1). Products of the cyanodifluoromethylation reaction with low molecular weights were often too volatile to isolate in yields approaching those of the crude material. These products were converted in a one-pot procedure, as shown at the top of Chart 1, to more tractable derivatives for purification. Some products underwent decomposition to some degree upon purification by flash column chromatography,

although this did not prevent their isolation. A wide range of aryl iodides, including electron-poor (**3a-e**), electron-neutral (**3f-g**), and electron-rich arenes (**3h-i**) reacted under the developed conditions. Those containing common functional groups, including bromides and chlorides (**3a-b**, **3j**), esters (**3c**), nitro groups (**3d**), and carbamates (**3i**) reacted in high yield. An aryl iodides bearing an ortho-isopropyl (**3k**) substituent reacted, as did those with 2,6-dichloro (**3l**) and 2-methyl-6-

ethyl (**3m**) groups. Meta-substituted iodoarenes (**3n-p**) also reacted, as did heterocycles such as dibenzofuran (**3s**), pyridine (**3t**), and bipyrazole (**3u**). The yield of product **3r** on a 1 g scale was

Chart 1. Scope of (hetero)aryl iodides and activated (hetero)aryl bromides that undergo the cyanodifluoromethylation reaction with $TMSCF_2CN$ (1).

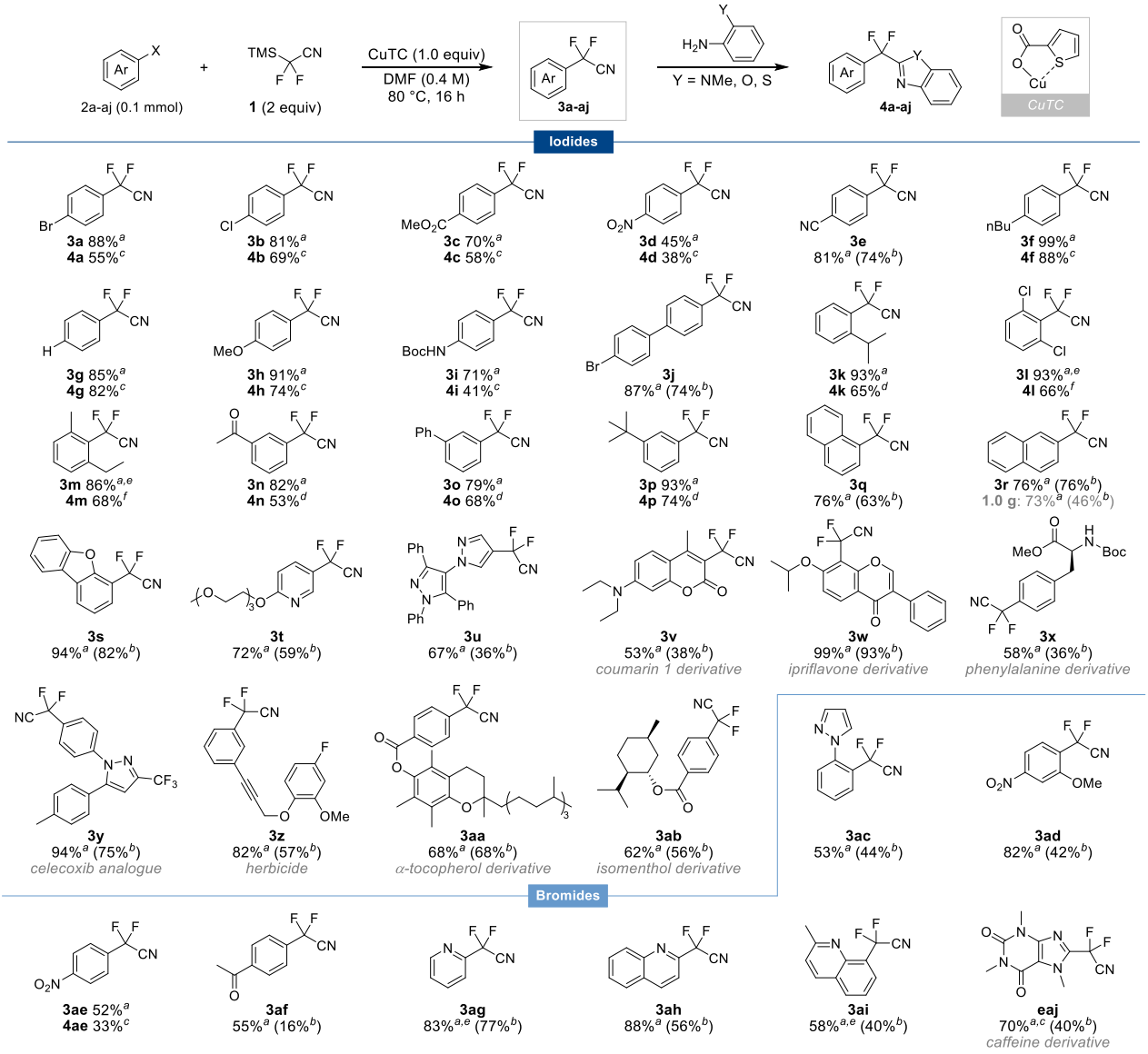

Reaction conducted with 0.1 mmol (hetero)aryl halide; [a]Yield of the cyanodifluoromethylarene determined by ^{19}F NMR spectroscopy with α,α,α-trifluorotoluene as internal standard. [b]Isolated yields of the cyanodifluoromethylarene. [c]Isolated yield of the benzimidazole (Y = NMe); [d]Isolated yield of the benzoxazole (Y = O); [e]1 equiv of CuDPP used instead of CuTC; [f]Isolated yield of the benzothiazole (Y = S).

similar to the yield of **3r** on a 0.1 mmol scale, although the product did decay by hydrolysis of the nitrile to a greater extent during chromatographic purification on large scale than on small scale.

The applicability of this method to the late-stage diversification of more structurally complex molecules was assessed. Derivatives of the laser dye coumarin 1 (**3v**), ipriflavone (**3w**), phenylalanine (**3x**), and an analogue of the NSAID celecoxib (**3y**) all formed in good to high yield

from the corresponding iodide. An herbicide bearing an alkyne (**3z**), and derivatives of vitamin E (**3aa**) and isomenthol (**3ab**), were also produced using this reaction.

Bromides of electron-poor arenes and of heteroarenes also underwent cyanodifluoromethylation. An aryl bromide with an ortho-pyrazole group (**3ac**) and aryl bromides bearing electron-withdrawing groups (**3ad-af**) reacted in good yields. 2-Bromopyridines (**3ag**) and quinolines bearing a bromide proximal to nitrogen (**3ah-ai**)

reacted. Biologically active heteroaryl bromides were also suitable for this transformation; an analogue of caffeine (**3ao**) was synthesized using this method. The yields of additional (hetero)aryl halides that were not isolated, and those that did not react, as determined by ^{19}F NMR spectroscopy, are provided in the Supporting Information.

4.3.3 Functionalization of the coupled products.

Chart 2. Functionalization reactions of aryl-α,α-difluoroacetonitriles.[a]

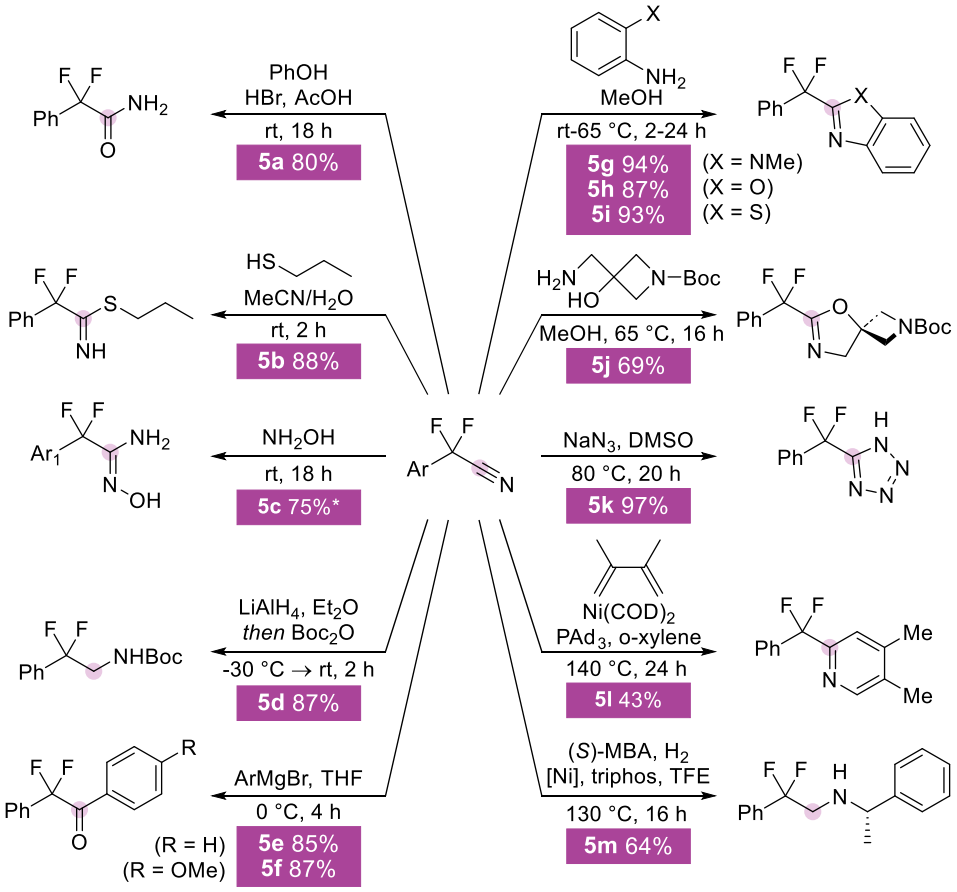

*Yield determined by Dr. Tomasso Fantoni; [a]See Supporting Information for detailed reaction conditions. Ar_1 = 4-*n*BuC_6H_4.

Because examples of aryl-α,α-difluoroacetonitriles are rare, we sought to explore the reactivity of the cyanodifluoromethyl group. The aryl-α,α-difluoroacetonitrile products undergo a wide range of reactions and enable the synthesis of molecules containing a benzylic difluoromethylene unit

(Chart 2). Several of these reactions highlight the increase in electrophilicity of the nitrile imparted by the vicinal fluorine atoms.

The nitrile carbon reacts with a range of nucleophiles. Acid-catalyzed addition of water gave α,α-difluoroamide **5a** in 80% yield. The addition of propylthiol and hydroxylamine formed imidothioate **5b** and hydroxyformamide **5c**. Hydroxyformamides, such as **5c**, can be used to synthesize α,α-difluorinated oxadiazoles[40] and other heterocycles. Reduction and protection of the cyanodifluoromethylarene afforded β,β-difluoroamide **5d** in 60% yield. Like the additions of hydrides, the addition of organomagnesium reagents formed aryl-α,α-difluoromethylketones **5e-f** in high yields. While one might be concerned about abstraction of the fluorine by electrophilic metals, this was not observed.

Condensations of ortho-substituted anilines also occurred to form benzimidazole **5g**, benzoxazole **5h**, and benzothiazole **5i**. Molecules containing the benzylic benzimidazole motif have been investigated as LRRK2 inhibitors[41] and as potent analgesics,[42] and this route provides access to difluorinated analogues of these compounds. Current methods to form such aryl-α,α-difluoroheterocycles require the use of a pre-formed heteroaryl-CF_2Br coupling partner, limiting opportunities for rapid diversification.[43] The novel α,α-difluorinated [3.4]-spirocycle **5j** also formed by the addition of a β-amino alcohol. We have demonstrated that these cycloaddition reactions can be conducted without isolation of the intermediate aryldifluoroacetonitrile (see Supporting Information).

The aryl cyanodifluoromethyl compounds also underwent cycloaddition and hydrogenative coupling reactions. Sodium azide reacted cleanly with the cyano group to give α,α-difluorinated tetrazole **5k**, which belongs to a class of compounds that has been investigated as URAT1 inhibitors.[44] A nickel-catalyzed dehydrogenative [4+2] reaction generated aryl-α,α-difluoropyridine **5l** in moderate yield when using PAd_3 as ligand.[45] Finally, a nickel-catalyzed hydrogenative C–N coupling with (*S*)-methylbenzylamine provided β,β-difluorinated secondary amine **5m**.[46] Thus, the elaboration of cyanodifluoromethylarenes prepared by our coupling reaction enables the construction of a wide range of structurally diverse α,α-difluoromethylarenes from aryl or heteroaryl halides, $TMSCF_2CN$, and common additional components.

To assess the differences in reactivity imparted by the fluorine atoms, we conducted a selection of control reactions with benzyl nitrile under analogous conditions (see Supporting Information for details). After 30 minutes, the fluorinated amide **5a** formed in 70% yield while the hydrolysis of benzyl nitrile converted only 34% of the nitrile to the amide. The addition of thiols or hydroxylamine to arylacetonitriles typically requires forcing conditions[47] or an acid catalyst,[48] and no product was observed from reactions of benzyl nitrile with these two reagents under conditions for reaction of **5b** and **5c**, respectively. The reduction of arylacetonitriles lacking fluorine substitution at the benzylic position also often requires high temperatures or catalysts to proceed; the addition of LAH to benzyl nitrile under analogous conditions for **5d** formed no reduced product.[49-50] Cyclization reactions to form products analogous to benzothiazole **5i** without fluorine atoms did not proceed under analogous conditions, even with the addition of $AlCl_3$ as Lewis acid.[51-53] We ascribe the demonstrated difference in reactivity between aryldifluoroacetonitriles and arylacetonitriles to the inductive effect of the fluorine atoms adjacent to the nitrile carbon.

4.4 Analysis of the cyanodifluoromethylation reaction by DFT calculations.

Having developed a method for the widely applicable conversion of aryl and heteroaryl iodides and bromides to cyanodifluoromethylarenes, we conducted calculations with density functional theory (DFT) to gain information on the barriers for reaction of aryl halides with the difluorocyanomethyl copper complex, relative to those for related fluoroalkylcopper complexes. To do so, we computed the barriers to oxidative addition of PhI to the [(DMF)CuCF$_2$R] intermediate and reductive elimination from the resulting [(DMF)Cu(Ph)(I)CF$_2$R] complex.[54-55] Unless otherwise noted, the energies we report are Gibbs free energies in kcal/mol for reactions computed with a DMF solvent continuum (see Supporting Information for complete computational details).

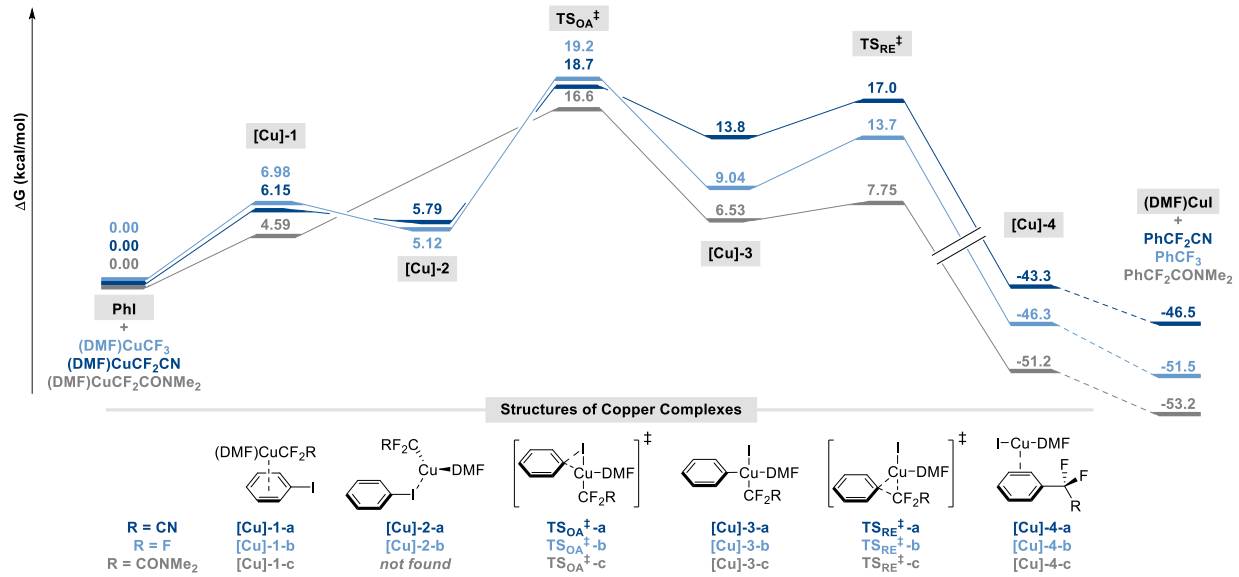

Figure 2. Computed free energy diagram for the reaction of PhI with [(DMF)CuCF$_2$R], in which R = CN, F, and C(O)NMe$_2$. Gibbs free energies calculated at the def2-TZVP level of theory for Cu and I with accompanying ECP; all other atoms were treated at the def2-SVPD level. Solvent = DMF, temperature = rt. Empirical dispersion is considered. See Supporting Information for additional details

The combined energy of [(DMF)CuCF$_2$R] and PhI was set to zero, and the copper complexes containing two DMF ligands, [(DMF)$_2$CuCF$_2$R], were computed to be higher in energy than the complexes [(DMF)CuCF$_2$R] by 7.34, 7.00, and 11.8 kcal/mol for R = CN, F, and CONMe$_2$, respectively. Computational[47] and experimental[55-56] studies of copper-mediated trifluoromethylation reactions imply that [(S)Cu(nucleophile)] (S = DMSO, DMF) complexes oxidatively add iodoarenes more rapidly than do [(L)Cu(nucleophile)]$^{n-}$ (L = phen, n= 0; L = halide, nucleophile, n = 1) complexes. We calculated the pathways in which one DMF remains bound to the copper because the computed free energies for oxidative additions occurring to [(DMF)CuCF$_3$] reported by Grushin and coworkers were lower than those for the combination of dissociation of DMF from [(DMF)$_2$CuCF$_3$] and oxidative addition.[54] The mechanism in which one DMF remains bound to Cu has been shown to reproduce the results of Hammett studies accurately and to capture the effects of ortho-substitution on reaction rate.

Figure 2 shows the computed reaction coordinates for the reaction of PhI with [(DMF)$CuCF_2R$] in which R = CN, F, and $C(O)NMe_2$. Complexes **[Cu]-1a–c** containing the cyanodifluoromethyl, trifluoromethyl and difluoro amide enolate groups are formed by coordination of the arene p system to the copper species prior to oxidative addition. The cyanodifluoromethyl- and trifluoromethylcopper species were computed to form a Lewis acid-base pair with the iodine atom of PhI (**[Cu]-2a** and **[Cu]-2b**), while no complex between PhI and the copper difluoroamide enolate was located along the pathway to oxidative addition. The barriers for the step that cleaves the C-I bond in iodobenzene were computed to be 12.9, 14.1, and 12.0 kcal/mol for R = CN, F, and $C(O)NMe_2$, respectively, while the overall barriers for reaction of PhI with the [(DMF)$CuCF_2R$] complexes were computed to be 18.7, 19.2, and 16.6 kcal/mol, respectively.

Due to the lower endothermicity of the oxidative addition of PhI to the cyanodifluoromethyl copper complex than to the trifluoromethyl copper complex, the transition state for the cyanodifluoromethylation should be earlier than that for the analogous trifluoromethylation reaction. This hypothesis is supported by our calculations: the Cu–C_{ipso} distance in **$TS_{OA}^{‡}$-a** for oxidative addition of PhI to the difluorocyanomethyl copper complex is longer (2.08 Å vs 2.05 Å), and the Ph–I bond is shorter (2.31 Å vs. 2.34 Å) than those in transition state **$TS_{OA}^{‡}$-b** for oxidative addition of PhI to the trifluoromethyl copper complex.

The arylcopper complexes **[Cu]-3-a–c** formed by oxidative addition all adopt a distorted square-planar geometry. Complex **[Cu]-3-a** is more destabilized, relative to the starting materials, than are complexes **[Cu]-3-b** and **[Cu]-3-c**. The difference in energy between transition state **$TS_{RE}^{‡}$-a** and complex **[Cu]-3-a** is smaller than the difference in energy between transition state **$TS_{RE}^{‡}$-b** and complex **[Cu]-3-b**. The calculated energy differences indicate that reductive elimination to form the cyanodifluoromethylarene product occurs with a lower barrier than formation of the analogous trifluoromethylarene product.

The reductive eliminations from copper complexes **[Cu]-3-a–c** proceed through transition states **$TS_{RE}^{‡}$-a–c** to form the fluoroalkylarene complexes **[Cu]-4-a–c** with barriers of just 3.2, 4.7, and 1.2 kcal/mol respectively. Oxidative addition is computed to be rate-determining because the differences in energies between **$TS_{RE}^{‡}$-a–c** and **[Cu]-3-a–c** respectively are smaller than the differences between **$TS_{OA}^{‡}$-a–c** and the respective starting materials for each of the fluoroalkyl groups investigated. Our group has previously identified by computation[57] a stabilizing interaction between the palladium center and the nitrile CN bond during reductive elimination from a phosphine-ligated fluoroalkyl-arylpalladium complex; however, we did not identify an analogous stabilizing interaction between the copper center and the nitrile CN bond using an independent gradient model based on Hirschfield partitions (IGMH analysis).[58]

4.5 Summary

We have developed a copper-mediated cyanodifluoromethylation of aryl and heteroaryl iodides and electron-poor aryl and heteroaryl bromides with $TMSCF_2CN$ that occurs with inexpensive, commercially available CuTC, requires no exogenous ligand, and occurs with broad functional group compatibility. We demonstrate that this method can be applied to the late-stage functionalization of complex molecules, and we show that the cyanodifluoromethyl group is a versatile synthon to generate a diverse range of products containing an aryl-α,α-difluoromethylene unit. DFT calculations suggest that the barriers to both oxidative addition and reductive elimination

are lower for the copper-mediated cyanodifluoromethylation than for the copper-mediated trifluoromethylation with the same DMF-ligated copper center, and that oxidative addition is rate-limiting.

4.6 References

(1) Inoue, M.; Sumii, Y.; Shibata, N. Contribution of Organofluorine Compounds to Pharmaceuticals. *ACS Omega* **2020**, *5*, 10633–10640.
(2) Wang, Q.; Song, H.; Wang, Q. Fluorine-containing agrochemicals in the last decade and approaches for fluorine incorporation. *Chin. Chem. Lett.* **2022**, *33*, 626–642.
(3) Meanwell, N. A. Fluorine and Fluorinated Motifs in the Design and Application of Bioisosteres for Drug Design. *J. Med. Chem.* **2018**, *61*, 5822–5880.
(4) Ogawa, Y.; Tokunaga, E.; Kobayashi, O.; Hirai, K.; Shibata, N. Current Contributions of Organofluorine Compounds to the Agrochemical Industry. *iScience* **2020**, *23*, 101467.
(5) Mandal, D.; Maji, S.; Pal, T.; Sinha, S. K.; Maiti, D. Recent advances in transition metal-mediated trifluoromethylation reactions. *Chem. Commun.* **2022**, *58*, 10442–10468.
(6) Szpera, R.; Moseley, D. F. J.; Smith, L. B.; Sterling, A. J.; Gouverneur, V. The Fluorination of C−H Bonds: Developments and Perspectives. *Angew. Chem. Int. Ed.* **2019**, *58*, 14824–14848.
(7) Liang, T.; Neumann, C. N.; Ritter, T. Introduction of Fluorine and Fluorine-Containing Functional Groups. *Angew. Chem. Int. Ed.* **2013**, *52*, 8214–8264.
(8) Campbell, M. G.; Ritter, T. Modern Carbon–Fluorine Bond Forming Reactions for Aryl Fluoride Synthesis. *Chem. Rev.* **2015**, *115*, 612–633.
(9) Arun, R.; Stiniya, S.; Saranya, P. V.; Anilkumar, G. An overview of palladium-catalyzed trifluoromethylation reactions. *J. Organomet. Chem.* **2022**, *979*, 122492.
(10) Evano, G.; Nitelet, A.; Thilmany, P.; Dewez, D. F. Metal-Mediated Halogen Exchange in Aryl and Vinyl Halides: A Review. *Front. Chem.* **2018**, *6*, 1–18.
(11) Hansch, C.; Leo, A.; Taft, R. W. A survey of Hammett substituent constants and resonance and field parameters. *Chem. Rev.* **1991**, *91*, 165–195.
(12) Fleming, F. F.; Yao, L.; Ravikumar, P. C.; Funk, L.; Shook, B. C. Nitrile-Containing Pharmaceuticals: Efficacious Roles of the Nitrile Pharmacophore. *J. Med. Chem.* **2010**, *53*, 7902–7917.
(13) Hutson, D. H.; Hoadley, E. C.; Griffiths, M. H.; Donninger, C. Mercapturic acid formation in the metabolism of 2-chloro-4-ethylamino-6-(1-methyl-1-cyanoethylamino)-s-triazine in the rat. *J. Agric. Food. Chem.* **1970**, *18*, 507–512.
(14) Wit, J.; Van Genderen, H. Metabolism of the herbicide 2,6-dichlorobenzonitrile in rabbits and rats. *Biochem. J.* **1966**, *101*, 698–706.
(15) Craig, G. W. E., M.; Zeller, M.; Bondy, S. S.; Comer, D. D.; Cheng, S.; Penzotti, J. E.;; Diederik, P. G., J.; Ehrler, J. 3-phenoxy-1-phenyl acetylene derivatives and their use as herbicides. WO2001055066, 2001.
(16) Bell, J.; Buysse, A. M. D., J. F.; Eckelbarger, J. D.; Epp, J. B.; Irving, N. M.; Kister, J.; Lo, W. C.; Loso, M. R.; Lowe, C. T.; Rohanna, J. C.; Satchivi, N. M.; Siddall, T. L.; Steward, K. M.; Yerkes, C. N. Pyridine and pyrimidine carboxylate herbicides and methods of use thereof. WO2019084353A1, 2018.
(17) Schiefer, I. T.; Abdul-Hay, S.; Wang, H.; Vanni, M.; Qin, Z.; Thatcher, G. R. J. Inhibition of Amyloidogenesis by Nonsteroidal Anti-inflammatory Drugs and Their Hybrid Nitrates. *J. Med. Chem.* **2011**, *54*, 2293–2306.

(18) Arrington, K. L.; Dudkin, V. Y. F., M. E.; Garbaccio, R. M.; Hartman, G. D.; Huang, S. Y.; Kreatsoulas, C.; Tasber, E. S. Inhibitors of Checkpoint Kinases. WO2007008502A2, 2007.
(19) Harris, K. J. A combination of niacin and a prostaglandin d2 receptor antagonist. WO2008039882A1, 2007.
(20) Gill, L. A.; Buckl, A. K., E. S.; Aay, N.; Tambo-ong, A. A.; Thompson, S.; Gliedt, M. J.; Knox, J. E.; Cregg, J.; Edwards, A. V.; Liu, Y. Burnett, G. L. Bicyclic heteroaryl compounds and uses thereof. US20210139517A1, 2021.
(21) Bartmann, E.; Krause, J. Synthesis of α,α-difluoronitriles from acyl cyanides. *J. Fluorine Chem.* **1993**, *61*, 117–122.
(22) Middleton, W. J.; Bingham, E. M. α,α-Difluoroarylacetic acids: preparation from (diethylamino)sulfur trifluoride and α-oxoarylacetates. *J. Org. Chem.* **1980**, *45*, 2883–2887.
(23) Hagele, G.; Haas, A. Fluorination of 2-oxo-ethane derivatives with diethylaminosulfur trifluoride (DAST). *J. Fluorine Chem.* **1996**, *76*, 15–19.
(24) Molloy, B. B. 2-Phenyl-2,2-difluoroethylamines. US3880927A, 1975.
(25) Kotoris, C. C.; Chen, M.-J.; Taylor, S. D. Preparation of Benzylic α,α-Difluoronitriles, -tetrazoles, and -sulfonates via Electrophilic Fluorination. *J. Org. Chem.* **1998**, *63*, 8052–8057.
(26) Hara, S.; Fukuhara, T. Desulfurizing Difluorination Reaction of Benzyl Sulfides Using IF_5. *Synlett* **2009**, *2009*, 198–200.
(27) Wright, S. E.; Bandar, J. S. A Base-Promoted Reductive Coupling Platform for the Divergent Defluorofunctionalization of Trifluoromethylarenes. *J. Am. Chem. Soc.* **2022**, *144*, 13032–13038.
(28) Morimoto, H.; Tsubogo, T.; Litvinas, N. D.; Hartwig, J. F. A Broadly Applicable Copper Reagent for Trifluoromethylations and Perfluoroalkylations of Aryl Iodides and Bromides. *Angew. Chem. Int. Ed.* **2011**, *50*, 3793–3798.
(29) Oishi, M.; Kondo, H.; Amii, H. Aromatic trifluoromethylation catalytic in copper. *Chem. Commun.* **2009**, 1909.
(30) Kondo, H.; Oishi, M.; Fujikawa, K.; Amii, H. Copper-Catalyzed Aromatic Trifluoromethylation via Group Transfer from Fluoral Derivatives. *Adv. Synth. Catal.* **2011**, *353*, 1247–1252.
(31) Knauber, T.; Arikan, F.; Röschenthaler, G.-V.; Gooßen, L. J. Copper-Catalyzed Trifluoromethylation of Aryl Iodides with Potassium (Trifluoromethyl)trimethoxyborate. *Chem. Eur. J.* **2011**, *17*, 2689–2697.
(32) Gonda, Z.; Kovács, S.; Wéber, C.; Gáti, T.; Mészáros, A.; Kotschy, A.; Novák, Z. Efficient Copper-Catalyzed Trifluoromethylation of Aromatic and Heteroaromatic Iodides: The Beneficial Anchoring Effect of Borates. *Org. Lett.* **2014**, *16*, 4268–4271.
(33) Urata, H.; Fuchikami, T. A novel and convenient method for trifluoromethylation of organic halides using $CF_3SiR'_3$/KF/Cu(I) system. *Tetrahedron Lett.* **1991**, *32*, 91–94.
(34) Levitre, G.; Granados, A.; Cabrera-Afonso, M. J.; Molander, G. A. Synthesis of α-Fluorinated Areneacetates through Photoredox/Copper Dual Catalysis. *Org. Lett.* **2022**, *24*, 3194–3198.
(35) Fujikawa, K.; Fujioka, Y.; Kobayashi, A.; Amii, H. A New Method for Aromatic Difluoromethylation: Copper-Catalyzed Cross-Coupling and Decarboxylation Sequence from Aryl Iodides. *Org. Lett.* **2011**, *13*, 5560–5563.
(36) Arlow, S. I.; Hartwig, J. F. Synthesis of Aryldifluoroamides by Copper-Catalyzed Cross-Coupling. *Angew. Chem.* **2016**, *128*, 4643–4648.

(37) Prakash, G. K. S.; Krishnamurti, R.; Olah, G. A. Fluoride-induced trifluoromethylation of carbonyl compounds with trifluoromethyltrimethylsilane (TMS-CF_3). A trifluoromethide equivalent. *J. Am. Chem. Soc.* **1989**, *111*, 393–395.
(38) Kosobokov, M. D.; Dilman, A. D.; Levin, V. V.; Struchkova, M. I. Difluoro(trimethylsilyl)acetonitrile: Synthesis and Fluoroalkylation Reactions. *J. Org. Chem.* **2012**, *77*, 5850–5855.
(39) Cho, E. J.; Senecal, T. D.; Kinzel, T.; Zhang, Y.; Watson, D. A.; Buchwald, S. L. The Palladium-Catalyzed Trifluoromethylation of Aryl Chlorides. *Science* **2010**, *328*, 1679–1681.
(40) Du, H.-C.; Bangs, M. C.; Simmons, N.; Matzuk, M. M. Multistep Synthesis of 1,2,4-Oxadiazoles via DNA-Conjugated Aryl Nitrile Substrates. *Bioconjugate Chem.* **2019**, *30*, 1304–1308.
(41) Galatsis, P.; Henderson, J. L. K., B. L.; Kurumbail, R. G.; Reese, M. R.; Stepan, A. F.; Verhoest, P. R.; Wager, T. T.; Pettersson, M. Y.; Garnsey, M. R. Novel imidazo [4,5-c] quinoline and imidazo [4,5-c][1,5] naphthyridine derivatives as lrrk2 inhibitors. WO2017046675A1, 2017.
(42) Moolten, M. S.; Fishman, J. B.; Chen, J.-C.; Carlson, K. R. Etonitazene: An opioid selective for the mu receptor types. *Life Sci.* **1993**, *52*, 199–203.
(43) Xiao, Y.-L.; Zhang, B.; Feng, Z.; Zhang, X. Heteroaryldifluoromethylation of Organoborons Catalyzed by Palladium: Facile Access to Aryl(Heteroaryl)difluoromethanes. *Org. Lett.* **2014**, *16*, 4822–4825.
(44) Nagai, K.; Baba, M. F., S.; Nagasawa, K.; Takahashi, H.; Kondoh, E.; Sogo, S.; Tanaka, K.; Itoh, Y. Difluoromethylene compound. US9650380B2, 2015.
(45) Ohashi, M.; Takeda, I.; Ikawa, M.; Ogoshi, S. Nickel-Catalyzed Dehydrogenative [4 + 2] Cycloaddition of 1,3-Dienes with Nitriles. *J. Am. Chem. Soc.* **2011**, *133*, 18018–18021.
(46) Chandrashekhar, V. G.; Baumann, W.; Beller, M.; Jagadeesh, R. V. Nickel-catalyzed hydrogenative coupling of nitriles and amines for general amine synthesis. *Science* **2022**, *376*, 1433–1441.
(47) Lin, C.-C.; Hsieh, T.-H.; Liao, P.-Y.; Liao, Z.-Y.; Chang, C.-W.; Shih, Y.-C.; Yeh, W.-H.; Chien, T.-C. Practical Synthesis of N-Substituted Cyanamides via Tiemann Rearrangement of Amidoximes. *Org. Lett.* **2014**, *16*, 892–895.
(48) Schultz, M.; Schiemann, K.; Bottom, G.; Blaukat, A.; Kober, I. Imidazole Derivatives. US2010249132, 2010.
(49) Shaber, S. H.; Nguyen, L. T. Fungicidal and herbicidal triazoles. US5264415, 1993.
(50) Vasil'eva, V. F.; Medvedev, B. A.; Galitsina, V. A.; Korsakova, I. Y.; Shvedov, V. I.; Mashkovskii, M. D. Synthesis and pharmacological properties of 4-guanidinomethyl- and 4-(N′-phenylamidino) quinolines. *Pharm. Chem. J.* **1981**, *15*, 349–353.
(51) Zhang, S.; Wang, S.; Leng, Y.; Wu, Y. One-pot synthesis of 2-acylbenzothiazoles from 2-aminobenzenethiols and arylacetonitriles via cyclization and sequential oxidation. *Tetrahedron Lett.* **2021**, *79*, 153300.
(52) Dhawale, K. D.; Ingale, A. P.; Shinde, S. V.; Thorat, N. M.; Patil, L. R. ZnO-NPs catalyzed condensation of 2-aminothiophenol and aryl/alkyl nitriles: Efficient green synthesis of 2-substituted benzothiazoles. *Synth. Commun.* **2021**, *51*, 1588–1601.
(53) Sun, Y.; Jiang, H.; Wu, W.; Zeng, W.; Wu, X. Copper-Catalyzed Synthesis of Substituted Benzothiazoles via Condensation of 2-Aminobenzenethiols with Nitriles. *Org. Lett.* **2013**, *15*, 1598–1601.
(54) Konovalov, A. I.; Lishchynskyi, A.; Grushin, V. V. Mechanism of Trifluoromethylation of Aryl Halides with $CuCF_3$ and the Ortho Effect. *J. Am. Chem. Soc.* **2014**, *136*, 13410–13425.

(55) Liu, H.; Wu, J.; Jin, Y.; Leng, X.; Shen, Q. Mechanistic Insight into Copper-Mediated Trifluoromethylation of Aryl Halides: The Role of CuI. *J. Am. Chem. Soc.* **2021**, *143*, 14367–14378.
(56) Giri, R.; Hartwig, J. F. Cu(I)−Amido Complexes in the Ullmann Reaction: Reactions of Cu(I)−Amido Complexes with Iodoarenes with and without Autocatalysis by CuI. *J. Am. Chem. Soc.* **2010**, *132*, 15860–15863.
(57) Kalkman, E. D.; Qiu, Y.; Hartwig, J. F. Transition-State Stabilization by Secondary Orbital Interactions between Fluoroalkyl Ligands and Palladium During Reductive Elimination from Palladium(aryl)(fluoroalkyl) Complexes. *ACS Catal.* **2023**, *13*, 12810–12825.
(58) Lu, T.; Chen, Q. Independent gradient model based on Hirshfeld partition: A new method for visual study of interactions in chemical systems. *J. Comput. Chem.* **2022**, *43*, 539–555.
(59) Mu, X.; Chen, S.; Zhen, X.; Liu, G. Palladium-Catalyzed Oxidative Trifluoromethylation of Indoles at Room Temperature. *Chem. Eur. J.* **2011**, *17*, 6039–6042.
(60) Wei, Y.; Yu, L.; Lin, J.; Zheng, X.; Xiao, J. DBU-Promoted Trifluoromethylation of Aryl Iodides with Difluoromethyltriphenylphosphonium Bromide. *Chin. J. Chem* . **2016**, *34*, 481484.
(61) Withbroe, G. J.; Singer, R. A.; Sieser, J. E. Streamlined Synthesis of the Bippyphos Family of Ligands and Cross-Coupling Applications. *Org. Process Res. Dev.* **2008**, *12*, 480–489.
(62) Tanwar, L.; Börgel, J.; Lehmann, J.; Ritter, T. Selective C–H Iodination of (Hetero)arenes. *Org. Lett.* **2021**, *23*, 5024–5027.
(63) Magné, V.; Ball, L. T. Synthesis of Air-stable, Odorless Thiophenol Surrogates via Ni-Catalyzed C−S Cross-Coupling. *Chem. Eur. J.* **2019**, *25*, 8903–8910.
(64) Chetty, S.; Armstrong, T.; Sharma Kharkwal, S.; Drewe, W. C.; De Matteis, C. I.; Evangelopoulos, D.; Bhakta, S.; Thomas, N. R. New InhA Inhibitors Based on Expanded Triclosan and Di-Triclosan Analogues to Develop a New Treatment for Tuberculosis. *Pharmaceuticals* **2021**, *14*, 361.
(65) Fang, J. D.; Yan, X. B.; Zhou, L.; Wang, Y. Z.; Liu, X. Y. Synthesis of 3-Organoselenyl-2*H*-Coumarins from Propargylic Aryl Ethers via Oxidative Radical Cyclization. *Adv. Synth. Catal.* **2019**, *361*, 1985–1990.
(66) Klapars, A.; Buchwald, S. L. Copper-Catalyzed Halogen Exchange in Aryl Halides: An Aromatic Finkelstein Reaction. *J. Am. Chem. Soc.* **2002**, *124*, 14844–14845.
(67) Mukhopadhyay, S.; Batra, S. Direct Transformation of Arylamines to Aryl Halides via Sodium Nitrite and *N*-Halosuccinimide. *Chem. Eur. J.* **2018**, *24*, 14622–14626.
(68) Gaussian 16, R. C., M. J. Frisch, G. W. Trucks, H. B. Schlegel, G. E. Scuseria, M. A. Robb, J. R. Cheeseman, G. Scalmani, V. Barone, G. A. Petersson, H. Nakatsuji, X. Li, M. Caricato, A. V. Marenich, J. Bloino, B. G. Janesko, R. Gomperts, B. Mennucci, H. P. Hratchian, J. V. Ortiz, A. F. Izmaylov, J. L. Sonnenberg, D. Williams-Young, F. Ding, F. Lipparini, F. Egidi, J. Goings, B. Peng, A. Petrone, T. Henderson, D. Ranasinghe, V. G. Zakrzewski, J. Gao, N. Rega, G. Zheng, W. Liang, M. Hada, M. Ehara, K. Toyota, R. Fukuda, J. Hasegawa, M. Ishida, T. Nakajima, Y. Honda, O. Kitao, H. Nakai, T. Vreven, K. Throssell, J. A. Montgomery, Jr., J. E. Peralta, F. Ogliaro, M. J. Bearpark, J. J. Heyd, E. N. Brothers, K. N. Kudin, V. N. Staroverov, T. A. Keith, R. Kobayashi, J. Normand, K. Raghavachari, A. P. Rendell, J. C. Burant, S. S. Iyengar, J. Tomasi, M. Cossi, J. M. Millam, M. Klene, C. Adamo, R. Cammi, J. W. Ochterski, R. L. Martin, K. Morokuma, O. Farkas, J. B. Foresman, and D. J. Fox, Gaussian, Inc., Wallingford CT, 2016.
(69) Marenich, A. V.; Cramer, C. J.; Truhlar, D. G. Universal Solvation Model Based on Solute Electron Density and on a Continuum Model of the Solvent Defined by the Bulk Dielectric Constant and Atomic Surface Tensions. *J. Phys. Chem. B.* **2009**, *113*, 6378–6396.

(70) R. Dennington, T. A. K., J. M. Millam, GaussView, Version 6.1; Semichem Inc., Shawnee Mission, KS (USA), 2016.
(71) Perdew, J. P.; Burke, K.; Ernzerhof, M. Generalized Gradient Approximation Made Simple. *Phys. Rev. Lett.* **1996**, *77*, 3865–3868.
(72) Adamo, C.; Barone, V. Toward reliable density functional methods without adjustable parameters: The PBE0 model. *J. Chem. Phys.* **1999**, *110*, 6158–6170.
(73) Grimme, S.; Ehrlich, S.; Goerigk, L. Effect of the damping function in dispersion corrected density functional theory. *J. Comput. Chem.* **2011**, *32*, 1456–1465.
(74) Lu, T.; Chen, F. Multiwfn: A multifunctional wavefunction analyzer. *J. Comput. Chem.* **2012**, *33*, 580–592.
(75) Humphrey, W.; Dalke, A.; Schulten, K. VMD: Visual molecular dynamics. *J. Mol. Graph.* **1996**, *14*, 33–38.

4.7 Experimental Information

4.7.1 General Information

All reactions were conducted under inert atmosphere in a nitrogen-filled glovebox or with standard Schlenk techniques, unless otherwise specified. All reagents and solvents were purchased from commercial sources and used as received, unless otherwise noted. All glassware was flame-dried or dried overnight at 120 °C, allowed to cool under vacuum, and stored in a N_2-atomsphere drybox until use unless otherwise noted. Tetrahydrofuran, toluene, and diethyl ether were purified by passing the degassed solvents (N_2) through a column of activated alumina (solvent purification system purchased from Innovative Technologies, Newburyport, MA). All other solvents were stored over 4 Å molecular sieves for at least 24 h prior to use. Compounds **2a-s**, **2x**, **2ac-aj** are commercially available. CuDPP was purchased from Ambeed. CuTC was purchased from either ChemScene or AA Blocks. All reagents purchased from commercial suppliers were stored in the glove box and used as received.

Deuterated solvents were purchased from Cambridge Isotope Laboratories and used as received.

^{1}H, ^{13}C, and ^{19}F NMR spectra were recorded on Bruker AV-300, AVQ-400, AV-500, AV-600, NEO-500, NEO-501 and AV-700 spectrometers at the University of California, Berkeley NMR facility. Chemical shifts are reported relative to residual solvent peaks ($CDCl_3$ = 7.26 ppm for ^{1}H NMR spectra and 77.16 ppm for $^{13}C\{^{1}H\}$ NMR spectra, DMSO-*d6* = 2.50 ppm for ^{1}H NMR spectra and 39.52 ppm for $^{13}C\{^{1}H\}$ NMR spectra). For ^{19}F NMR spectra, chemical shifts are reported relative to the δ –113.15 resonance of fluorobenzene used as an external reference or the δ –63.72 resonance of α,α,α-trifluorotoluene. The following abbreviations are used in reporting NMR data: s, singlet; d, doublet; t, triplet; q, quartet; p, pentet; hept, heptet; m, multiplet.

High-resolution mass spectra were recorded on an Agilent Time of Flight (Q-TOF) mass spectrometer in ESI mode operated by the Catalysis Center at the University of California, Berkeley or were obtained from the QB3 Mass Spectrometry Facility at UC Berkeley. Analytical thin layer chromatography (TLC) was performed on Kieselgel 60 F254 glass plates precoated with a 0.25 mm thickness of silica gel. The TLC plates were visualized with UV light. Preparatory TLC was performed on AnalTech preparatory TLC plates with a 1000 μm-thick silica coating and visualized by UV. Column chromatography was generally performed on a Teledyne Isco Combiflash® Rf system with RediSep Gold™ columns.

4.7.2 Initial Investigation of Reaction Conditions

In a nitrogen-filled glovebox, the copper salt (from 0.20 to 2.0 equiv) was added to a 4 mL vial equipped with a Teflon-coated stir bar. If applicable, the additive (from 0.00 to 1.20 equiv) and the ligand (0.110 mmol, 1.10 equiv) were added, if solid at rt. The solvent (from 0.10 to 1.00 mL) was added, followed by 1-butyl-4-iodobenzene (17.8 μL, 0.10 mmol, 1.00 equiv). When applicable, ligands that were liquid were then added at rt (0.110 mmol, 1.10 equiv). The reaction was sealed with a Teflon-lined cap and heated to 80 °C h for 16 h. After 16 h, the reaction was allowed to cool to rt. The internal standard, α,α,α-trifluorotoluene (12.27 μL, 0.10 mmol, 1.00 equiv), was added, and the yield of the reaction was determined by ^{19}F NMR spectroscopy.

Table S1. Effect of the copper complex, stoichiometry, and solvent on the copper-mediated coupling of aryl iodides and $TMSCF_2CN$ (**1**). Yield determined using ^{19}F NMR spectroscopy with α,α,α-trifluorotoluene as internal standard; [a]reaction conducted at rt; [b]reaction conducted at 65 °C; [c]reaction conducted at 100 °C.

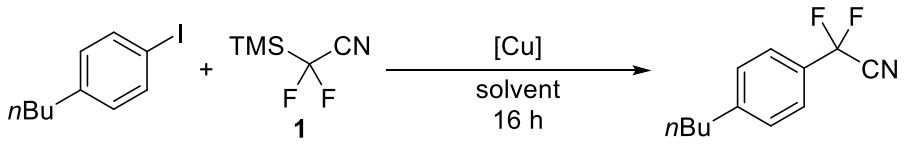

Entry	[Cu] (equiv)	**1** (equiv)	solvent (M)	T (°C)	Yield (%)
1	CuI (0.2)	5.0	DMSO (0.2)	80	0
2	CuI (0.5)	5.0	DMSO (0.2)	80	6
3	CuI (1.0)	5.0	DMSO (0.2)	80	19
4	CuI (2.0)	5.0	DMSO (0.2)	80	27
5	CuI (5.0)	5.0	DMSO (0.2)	80	48
6	CuCl (2.0)	5.0	DMSO (0.2)	80	65
7	CuBr (2.0)	5.0	DMSO (0.2)	80	41
8	CuBr•SMe_2 (2.0)	5.0	DMSO (0.2)	80	50
9	CuOAc (2.0)	5.0	DMSO (0.2)	80	65
10	CuTC (2.0)	5.0	DMSO (0.2)	80	72
11	CuDPP (2.0)	5.0	DMSO (0.2)	80	84
12	CuDPP (2.0)	5.0	DME (0.2)	80	91
13	CuDPP (1.0)	5.0	DME (0.2)	80	73
14	CuDPP (1.0)	2.5	DME (0.2)	80	79
15	CuDPP (1.0)	2.0	DME (0.2)	80	76
16	CuDPP (1.0)	1.2	DME (0.2)	80	64
17	CuDPP (1.0)	2.0	DCE (0.2)	80	67
18	CuDPP (1.0)	2.0	THF (0.2)	80	70
19	CuDPP (1.0)	2.0	NMP (0.2)	80	96
20	CuDPP (1.0)	2.0	DMF (0.2)	80	96
21	CuDPP (1.0)	2.0	DMF (0.1)	80	94
22	CuDPP (1.0)	2.0	DMF (1.0)	80	93
23	CuDPP (1.0)	2.0	DMF (0.4)	80	99
24	CuDPP (1.0)	2.0	DMF (0.4)	rt	86
25	CuDPP (1.0)	2.0	DMF (0.4)	65	95
26	CuDPP (1.0)	2.0	DMF (0.4)	100	99
27	CuTC (1.0)	2.0	DMF (0.4)	80	99

Table S2. Effect of ligands on the copper-mediated coupling of aryl iodides and TMSCF2CN (**1**). Yield determined by ^{19}F NMR spectroscopy with 3-nitrofluorobenzene as internal standard. [a]2 equiv CuDPP.

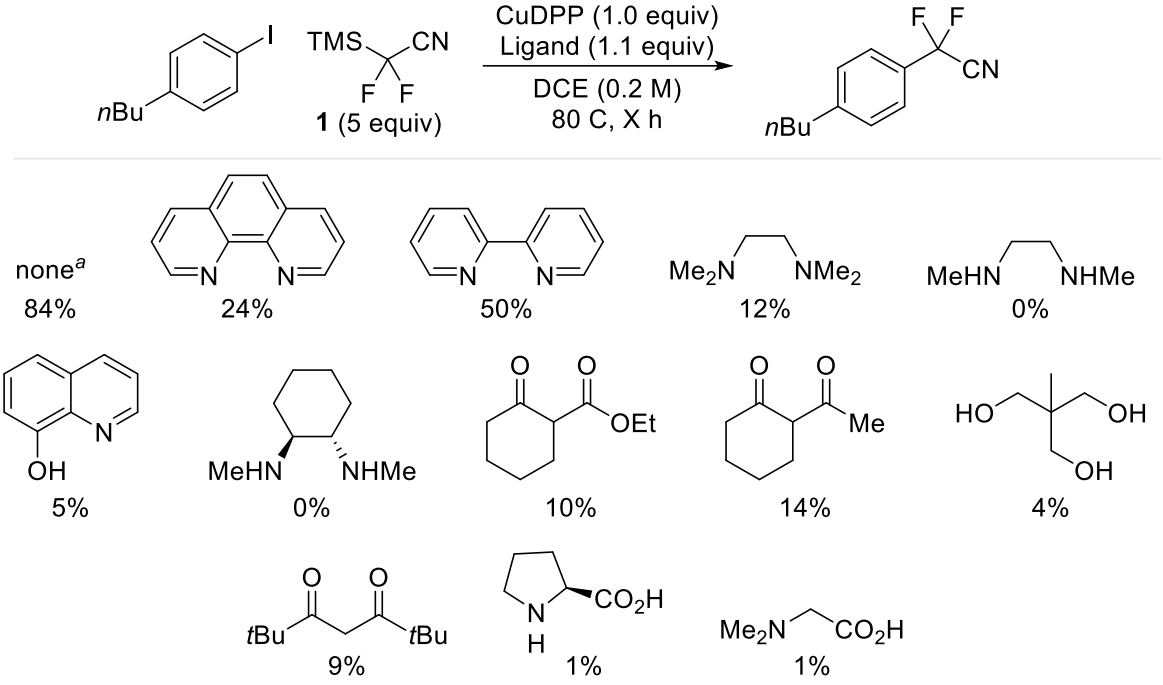

Table S3. Evaluation of additives in the copper-mediated cyanodifluoromethylation reaction. Yield determined using ^{19}F NMR spectroscopy with 3-nitrofluorobenzene as internal standard; [a]Reaction conducted at 100 °C.

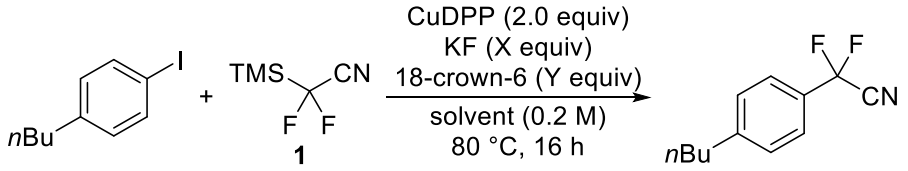

Entry	KF (equiv)	18-crown-6 (equiv)	solvent	Yield (%)
1	-	-	DCE	84
2	0.50	-	DCE	61
3	0.50	0.50	DCE	52
4	1.20	0.00	DCE	74
5	1.20	1.20	DCE	61
6	5.00	-	DCE	64
7	5.00	5.00	DCE	10
8[a]	1.20	1.20	toluene	56
9[a]	1.20	1.20	dioxane	41
10	1.20	1.20	DMSO	55

Table S4. Effect of the identity of the copper complex and the effect of additives on the cyanodifluoromethylation reaction. [a]Reaction conducted with 4-fluorobromobenzene as substrate. Yields determined using ^{19}F NMR spectroscopy with α,α,α-trifluorotoluene as internal standard.

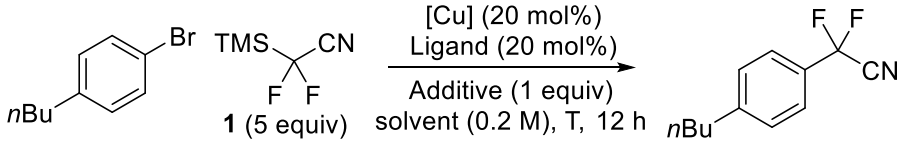

Entry	[Cu] / Ligand	Solvent, T (°C)	Additive	Yield
1[a]	[Cu-1]	DMSO, 100 °C	-	0
2[a]	[Cu-1]	DMSO, 100 °C	KF	0
3[a]	[Cu-1]	DMSO, 100 °C	CsF	0
4[a]	[Cu-2]	DMSO, 100 °C	-	0
5	CuDPP	DME, 80 °C	KF	12
6	CuDPP	DME, 80 °C	CsF	0
7	CuDPP	DME, 80 °C	RbF	0
8	CuDPP	DME, 80 °C	NaDPP	0
9	[Cu-3]	DME, 80 °C	-	0
10	[Cu-3]	DME, 80 °C	CsF	0
11	CuDPP + L1	DME, 80 °C	-	0
12	CuDPP + L2	DME, 80 °C	-	0
13	CuDPP + L3	DME, 80 °C	-	0
14	CuTC	DMF, 80 °C	NaTC	0

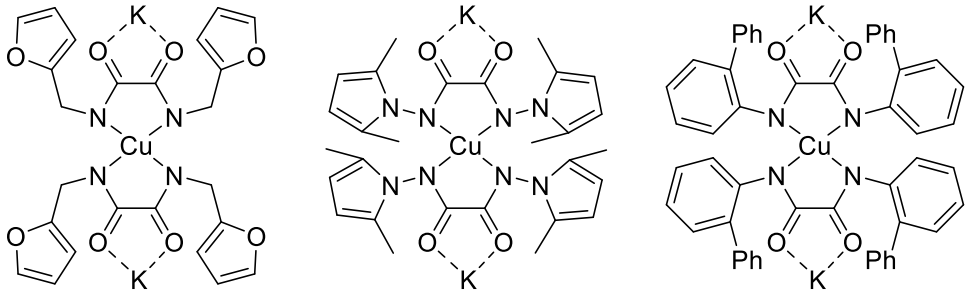

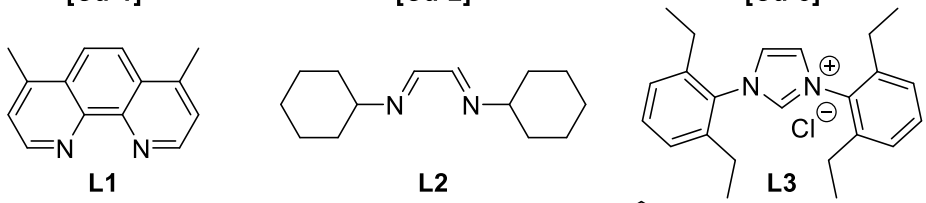

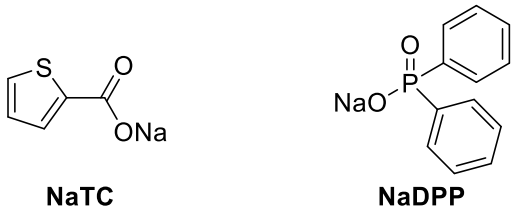

Table S5. Cost comparison of CuTC with other reagents and catalysts used in fluoroalkylation reactions at their required reagent or catalyst loadings. Prices retrieved from Ambeed, unless noted as retrieved from [a]Strem. Specific reagent stoichiometry was adapted from Buchwald and coworkers,[39] Liu and coworkers,[59] and Xiao and coworkers.[60]

Entry	Reagent	mol% used	cost/mol	cost/1.0 mmol rxn
1	CuI / phen	20 / 20	$97	$0.03
2	CuTC	100	$250	$0.25
3	$[Pd(allyl)Cl]_2$ / RuPhos	4 / 12	$29,213[a]	$1.18
4	$Pd(OAc)_2$ / Box-1	10 / 15	$21,880	$2.70
5	$(BrettPhos)PdG_3$	10	$27,376	$2.74
6	CuDPP	100	$3,300	$3.30
7	$Cu(MeCN_4)PF_6$	500	$663[a]	$3.32
8	$(phen)CuCF_3$	100	$44,124[a]	$44.12

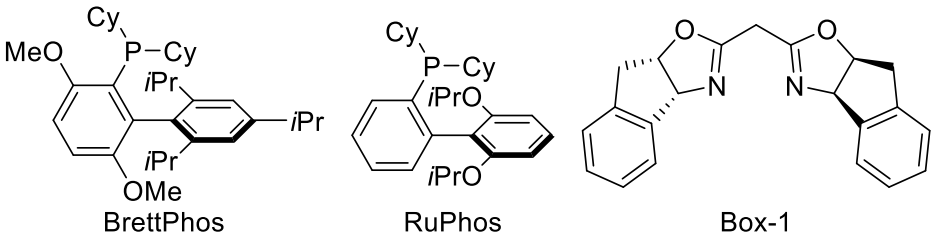

4.7.3 General Procedures

Scheme S1. General procedure 1: synthesis of aryl-α,α-difluoroacetonitriles.

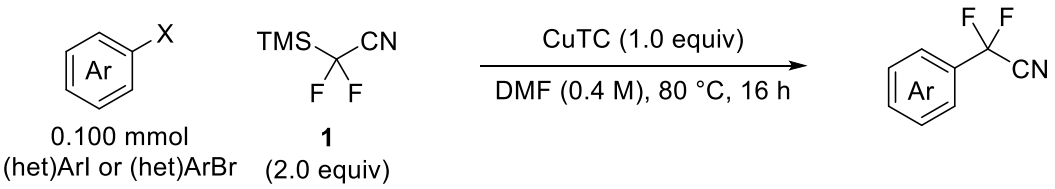

In a glovebox, a dry, 4 mL vial equipped with a Teflon stir bar was charged with the copper salt (1.00 equiv) and aryl halide (if solid) (0.100 mmol). Dry DMF was then added, followed by aryl halide (if liquid) and **1** (2.0 equiv). The vial was then capped, sealed with electrical tape, and stirred for 16 h at 80 °C. After this time, the crude reaction mixture was concentrated, then subjected to flash column chromatography (SiO_2, 20% EtOAc in Hexanes unless otherwise noted) to afford pure product. If derivatized, the crude reaction mixture was cooled, then subjected to general procedures 2-4 before concentration.

Scheme S2. General procedure 2: synthesis of aryl-α,α-difluoromethyl-1-*N*-methyl-1H-benzoimidazoles.

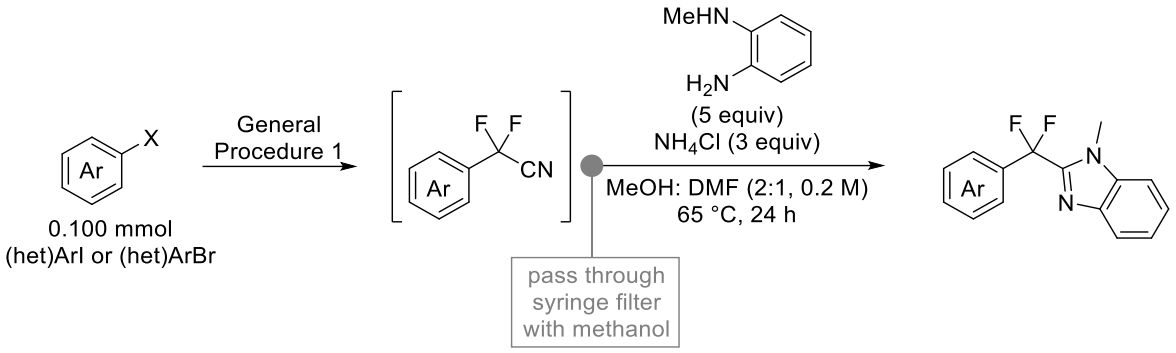

General procedure 1 was followed with 0.100 mmol of the aryl halide. Once cooled, the crude reaction mixture from general procedure 1 was passed through a syringe filter into a separate dry 4 mL vial charged with a stir bar and NH_4Cl (16.0 mg, 0.30 mmol, 3.0 equiv). Dry MeOH (500 µL) was passed through the syringe filter into the new vial to wash the material in the syringe filter. Freshly distilled 1-*N*-methylbenzene-1,2-diamine (56.7 µL, 0.50 mmol, 5.0 equiv) was then added to the vial, the headspace was flushed with nitrogen, and the vial sealed. The resulting mixture was stirred at 65 °C for 24 h. After this time, the reaction mixture was diluted with EtOAc and poured into a separatory funnel containing sat. aq. NH_4Cl. The aqueous solution was extracted with EtOAc (3x). The combined organic layers were dried over magnesium sulfate and filtered, and the filtrate was concentrated *in vacuo*. The crude residue was then purified by flash column chromatography (SiO_2, 20% EtOAc in Hexanes unless otherwise noted) to afford the pure product.

Scheme S3. General procedure 3: synthesis of aryl-α,α-difluoromethylbenzoxazoles.

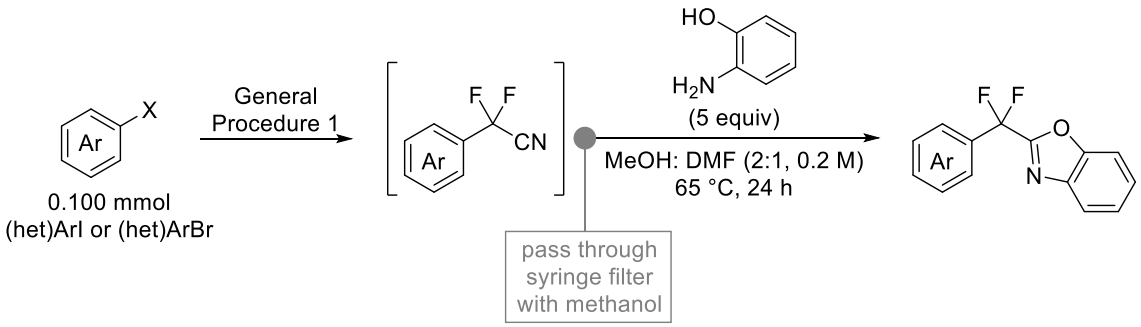

General procedure 1 was followed with 0.100 mmol of the aryl halide. Once cooled, the crude reaction mixture from general procedure 1 was passed through a syringe filter into a separate dry 4 mL vial charged with a stir bar. Dry MeOH (500 µL) was passed through the syringe filter into the new vial to wash the material. 2-aminophenol (54.6 mg, 0.50 mmol, 5.0 equiv) was then added, the headspace was flushed with nitrogen, and the resulting mixture was stirred at 65 °C for 24 h. After this time, the reaction mixture was diluted with EtOAc and poured into a separatory funnel containing sat. aq. NH_4Cl. The aqueous solution was extracted with EtOAc (3x). The combined organic layers were dried over magnesium sulfate, filtered, and the filtrate concentrated *in vacuo*. The crude residue was then purified by flash column chromatography (SiO_2, 20% EtOAc in Hexanes unless otherwise noted) to afford the pure product.

Scheme S4. General procedure 4: synthesis of aryl-α,α-difluoromethylbenzothiazoles.

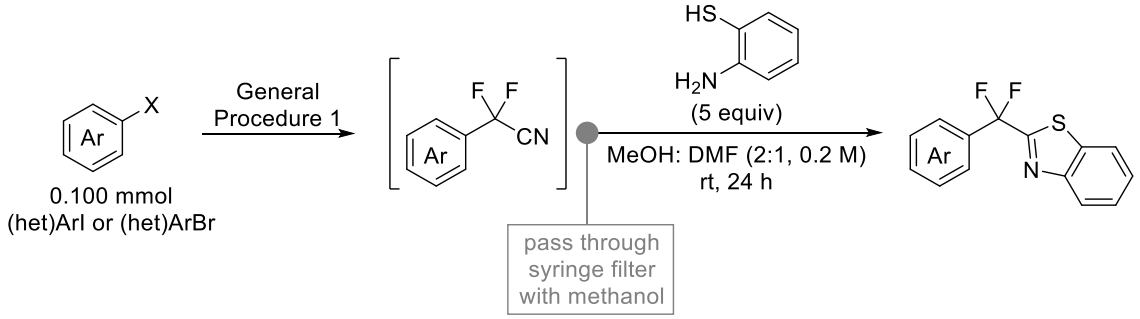

General procedure 1 was followed with 0.100 mmol of the aryl halide. Once cooled, the crude reaction mixture from general procedure 1 was passed through a syringe filter into a separate dry 4 mL vial charged with a stir bar. Dry MeOH (500 µL) was passed through the syringe filter into the new vial to wash the material. 2-aminobenzenethiol (53.5 µL, 0.50 mmol, 5.0 equiv) was then added, the headspace was flushed with nitrogen, and the resulting mixture was stirred at 65 °C for 24 h. After this time, the reaction mixture was diluted with EtOAc and poured into a separatory funnel containing sat. aq. NH_4Cl. The aqueous solution was extracted with EtOAc (3x). The combined organic layers were dried over magnesium sulfate and filtered, and the filtrate was concentrated *in vacuo*. The crude residue was then purified by flash column chromatography (SiO_2, 20% EtOAc in hexanes) to afford the pure product.

4.7.4 Procedure for Gram-Scale Reaction

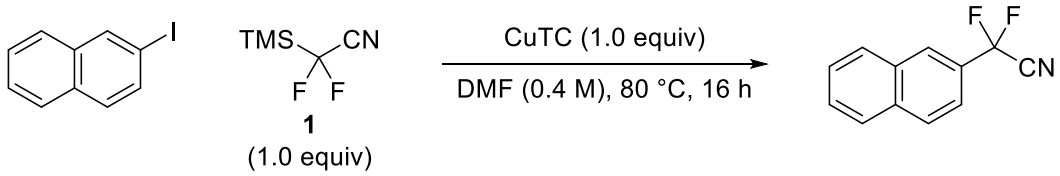

In a nitrogen-filled glovebox, a flame-dried 20 mL vial equipped with a stir bar was loaded with 2-iodonaphthalene (1.00 g, 3.94 mmol, 1.0 equiv) and CuTC (751 mg, 3.94 mmol, 1.0 equiv). DMF (0.40 M, 9.84 mL) was then added, followed by **1** (587 mg, 3.94 mmol, 2.00 equiv). The vial was capped, and the resulting suspension was stirred at 80 °C for 16 h. After this time, the DMF was removed *in vacuo,* and the crude residue was loaded directly onto a celite plug on top of a silica column. The crude residue was purified by flash column chromatography (SiO_2, 1% EtOAc, 1% DCM, 98% pentanes) to afford 2,2-difluoro-2-(naphthalen-2-yl)acetonitrile (370.6 mg, 46%, clear oil).

4.7.5 Evaluation of the Reactivity of Additional (hetero)Aryl Iodides and Bromides

Figure S1. ^{19}F NMR Yields of additional (hetero)aryl difluoroacetonitriles from their (hetero)aryl halides.

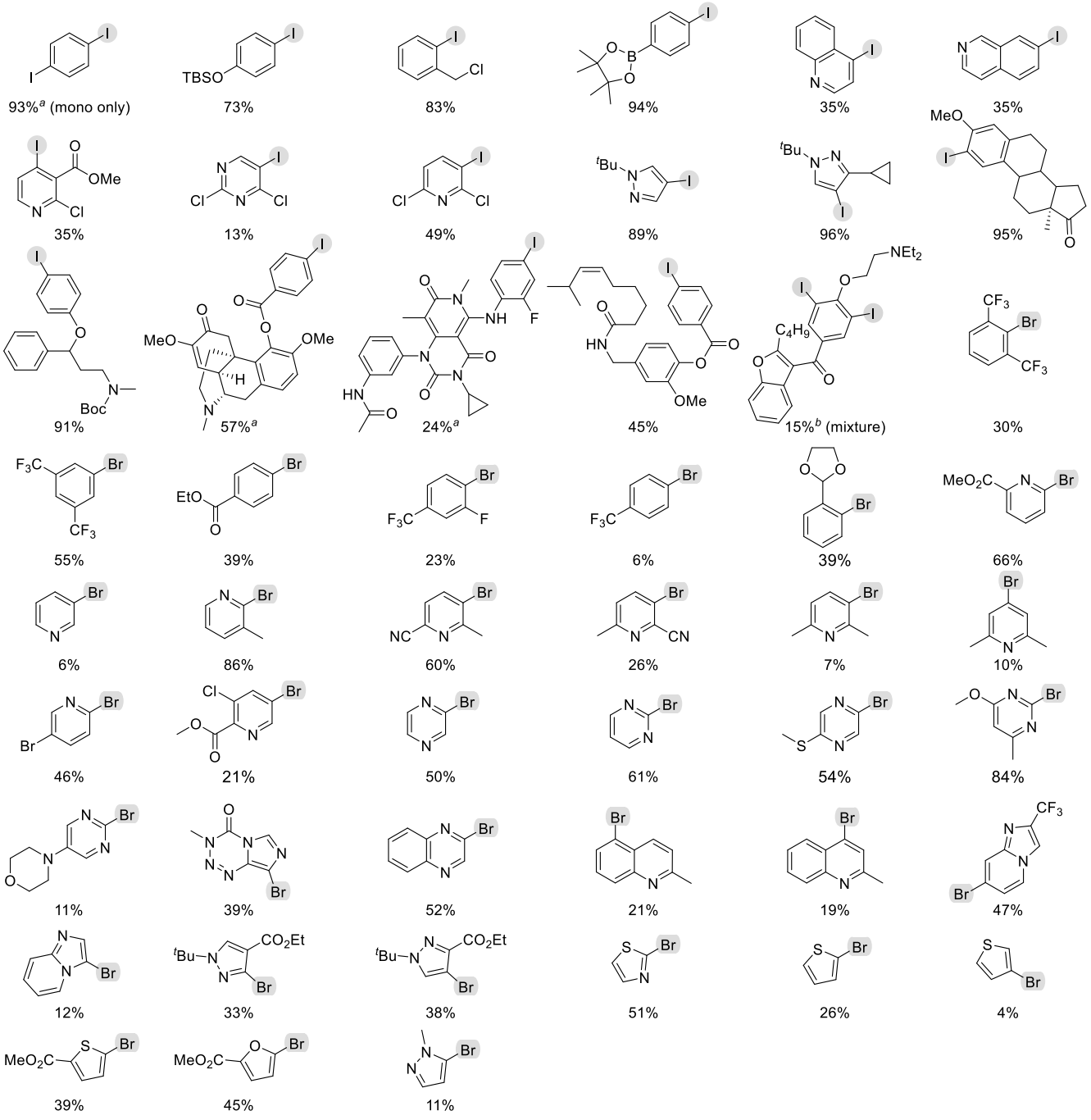

[a]2 equiv CuDPP, 4 equiv **1**; [b]3 equiv CuDPP, 6 equiv **1**.

Figure S2. (Hetero)aryl or vinyl iodides and (hetero)aryl bromides that did not undergo the cyanodifluoromethylation reaction.

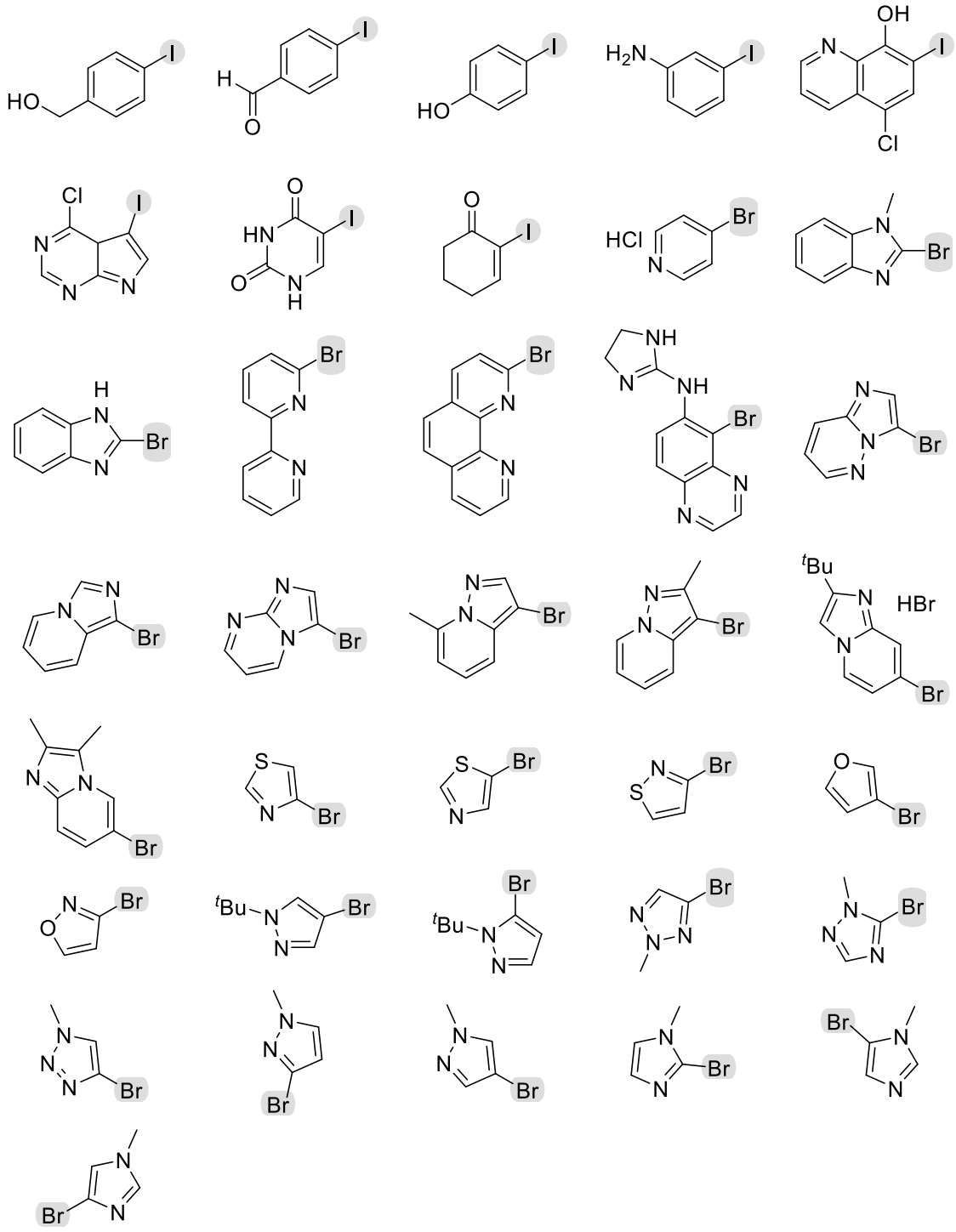

Figure S3. Comparison of yields from reactions with CuTC and CuDPP for selected (hetero)aryl iodides and bromides.

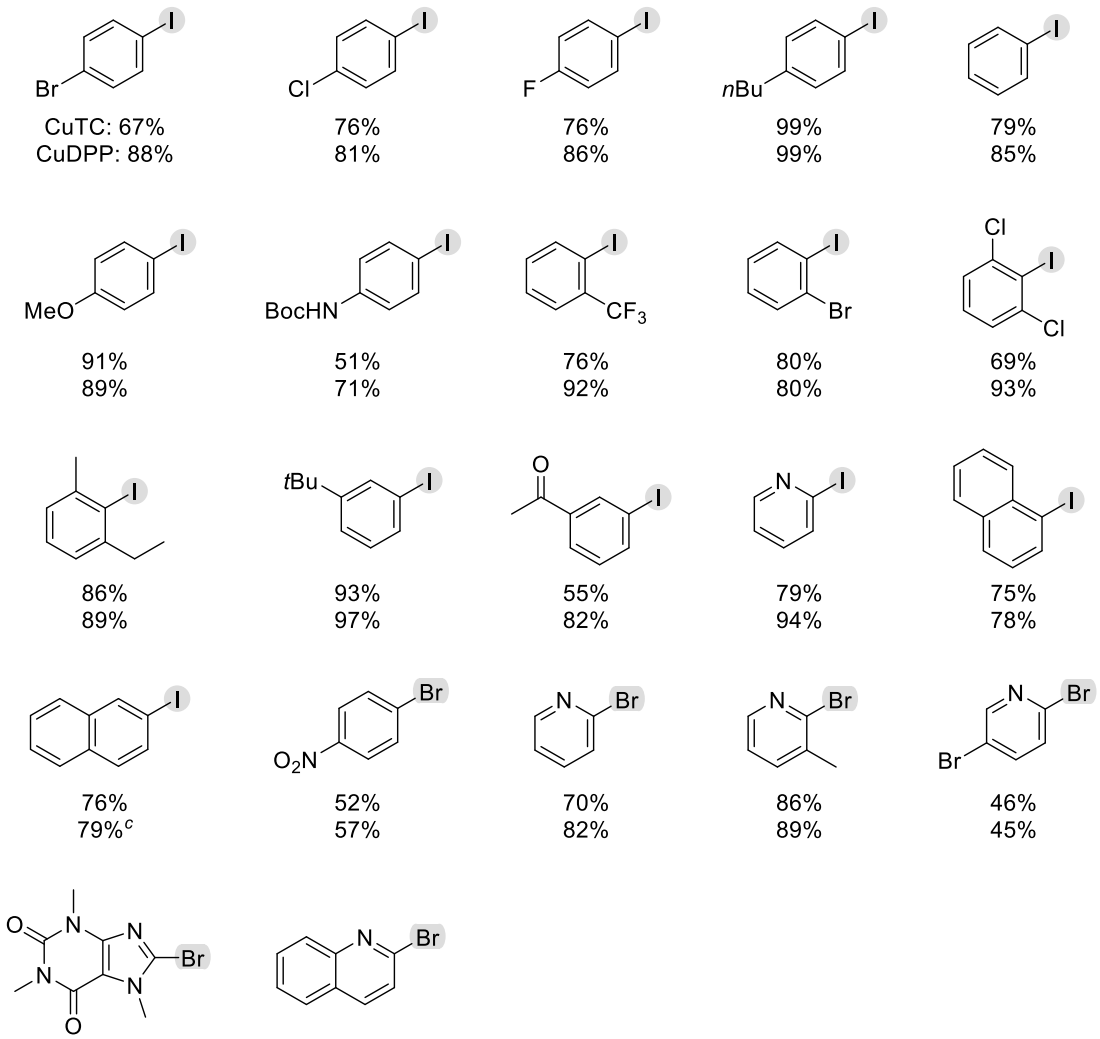

[a]Yields were determined using ^{19}F NMR spectroscopy with a,a,a-trifluorotoluene as internal standard; [b]2 equiv CuDPP, 4 equiv **1**.

4.7.6 Synthesis of $TMSCF_2CN$

2,2-difluoro-2-(trimethylsilyl)acetonitrile (1)

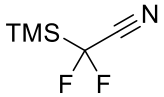

Compound **1** was prepared by a reported procedure.[38] A mixture of TMSCN (3.96 g, 40.0 mmol, 1.00 equiv), $TMSCF_2Br$ (8.12 g 40.0 mmol, 1.00 equiv), $BnNEt_3Cl$ (372 mg, 2.00 mmol, 5 mol%), and benzonitrile (15 mL) was heated to 110 °C for 80 min. The mixture was cooled to 0 °C, styrene oxide (5.5 mL, 48.0 mmol, 1.20 equiv) was added dropwise, and the mixture was stirred for 1 h at rt. Then, the reaction flask was immersed in a rt bath, and volatile components were removed by distillation under vacuum (1.00 Torr), collecting into a cold trap (−200 °C). The collected liquid was filtered through a glass wool plug and carefully fractionally distilled at atmospheric pressure at 110 °C using a Vigreux column to provide 2,2-difluoro-2-(trimethylsilyl)acetonitrile **1** as a colorless liquid (3.58 g, 24.0 mmol, 60% yield).

^{1}H NMR (500 MHz, $CDCl_3$) δ 0.36 (s, 9H).

^{19}F NMR (565 MHz, $CDCl_3$) δ -115.41

CAUTION: Extra care should be taken during the synthesis and distillation of this reagent due to the presence of TMSCN that hydrolyzes to form HCN.

4.7.7 Synthesis of (Hetero)Aryl Iodides

Scheme S5. Synthesis of 2-((2,5,8,11-tetraoxatridecan-13-yl)oxy)-5-iodopyridine (**2t**).

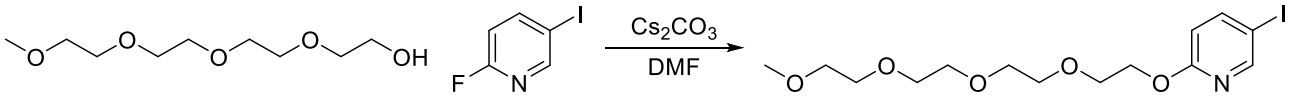

On the benchtop, tetraethyleneglycol monomethylether (1.13 mL, 2.0 equiv, 5.56 mmol) and 2-fluoro-5-iodopyridine (620.0 mg, 1.0 equiv, 2.78 mmol) were added to a suspension of cesium carbonate (2.26 g, 2.50 equiv, 6.95 mmol) in DMF (5.50 mL). The resulting suspension was heated to 150 °C for 72 h, then diluted with Ethyl acetate, extracted from NH_4Cl (sat. aq.) 4 times with EtOAc, the combined organics concentrated in vacuo, and the crude residue purified by flash column chromatography (SiO_2, 30% to 90% EtOAc in hexanes) to afford pure 2-((2,5,8,11-tetraoxatridecan-13-yl)oxy)-5-iodopyridine (442.2 mg, 39%) as a clear oil.

^{1}H NMR (500 MHz, $CDCl_3$) δ 8.28 (dd, J = 2.4, 0.7 Hz, 1H), 7.75 (dd, J = 8.7, 2.4 Hz, 1H), 6.61 (dd, J = 8.7, 0.7 Hz, 1H), 4.44 – 4.39 (m, 2H), 3.84 – 3.79 (m, 2H), 3.72 – 3.60 (m, 10H), 3.54 – 3.51 (m, 2H), 3.36 (s, 3H).

^{13}C{^{1}H} NMR (126 MHz, $CDCl_3$) δ 162.8, 152.3, 146.1, 113.5, 82.1, 71.7, 70.5, 70.4, 70.3, 69.3, 65.2, 58.8.

HRMS (ESI-TOF) $[C_{14}H_{22}INO_5+H]+$ calc'd: 412.0616, found: 412.0612

Scheme S6. Synthesis of 4-iodo-1',3',5'-triphenyl-1'H-1,4'-bipyrazole (**2u**).

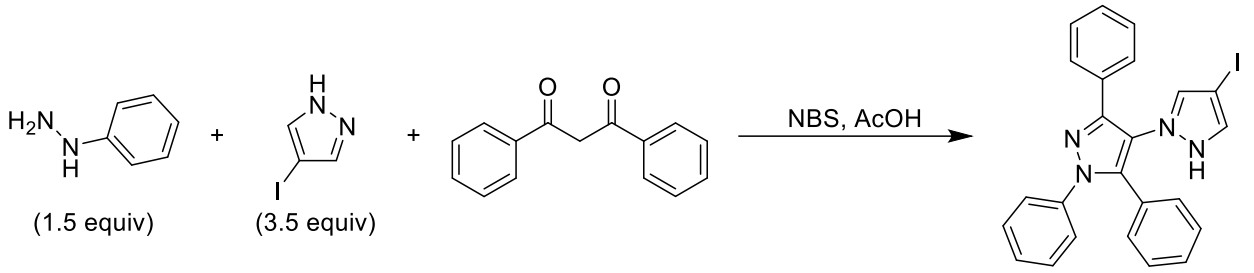

Compound **2v** was prepared by following a modified literature procedure.[61] To a solution of dibenzoylmethane (2.00 g, 1.00 equiv, 8.92 mmol) in NMP (7.93 mL) was added NBS (1.90 g, 1.20 equiv, 10.7 mmol). This reaction mixture was stirred for 12 h at rt, then 4-iodopyrazole (6.05 g, 3.50 equiv, 31.2 mmol) was added. The reaction was heated to 65 °C for 12 h, then diluted with acetic acid (5.00 mL). A solution of phenylhydrazine (1.33 mL, 1.50 equiv, 13.4 mmol) in MeOH (9.91 mL) was then added. The product began to precipitate from the solution as a yellow suspension upon addition of the hydrazine. After 12 h, the reaction was diluted with water (10.0 mL). The resulting crystals were stirred for 2 h, then filtered. The filter cake was washed sequentially with water, then with cold methanol, and then with hexane. This procedure provided 4-iodo-1',3',5'-triphenyl-1'H,2H-1l4-1,4'-bipyrazole (1.767 g, 3.61 mmol, 40.5 %) as a white, free-flowing powder.

^{1}H NMR (500 MHz, $CDCl_3$) δ 7.79 (s, 1H), 7.49 – 7.45 (m, 2H), 7.43 – 7.31 (m, 10H), 7.28 (d, J = 8.0 Hz, 2H), 7.16 (dt, J = 7.0, 1.4 Hz, 2H).

^{13}C{^{1}H} NMR (126 MHz, $CDCl_3$) δ 147.8, 146.1, 140.9, 139.6, 137.0, 130.6, 129.3, 129.2, 129.1, 128.7, 128.6, 128.6, 128.0, 127.2, 126.8, 125.3, 120.3, 57.5.

HRMS (ESI-TOF): Calc'd for $[C_{24}H_{18}IN_4]$+ (M+H)+ 489.0571, found 489.0550.

7-(diethylamino)-3-iodo-4-methyl-2H-chromen-2-one (2v)

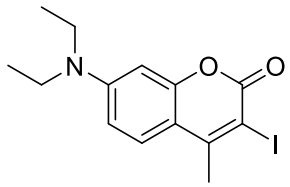

Compound **2x** was prepared using a known method.[62] Under an ambient atmosphere, 7-(diethylamino)-4-methyl-chromen-2-one (300.0 mg, 1.00 equiv, 1.29 mmol), silver mesylate (263.2 mg, 1.00 equiv, 1.29 mmol), lithium carbonate (95.8 mg, 1.00 equiv, 1.29 mmol), and iodine (329.2 mg, 1.00 equiv, 1.29 mmol) were dissolved in MeCN (5.0 mL). The reaction was capped and then stirred vigorously for 24 h at rt. After this time, the crude reaction mixture was passed through a silica plug with EtOAc as eluent. The filtrate was acidified with 2M HCl and extracted with EtOAc (3x). The combined organic layers were dried over magnesium sulfate and filtered, and the organic filtrate was concentrated *in vacuo*. The crude residue was purified by flash column chromatography (SiO_2, 10% EtOAc in hexanes) to afford 7-(diethylamino)-3-iodo-4-methyl-2H-

chromen-2-one (140.3 mg, 392.8 μmol, 30 %) as a light yellow solid. The spectral data match those reported in the literature.

^{1}H NMR (500 MHz, $CDCl_3$) δ 7.48 (d, J = 9.1 Hz, 1H), 6.60 (dd, J = 9.1, 2.6 Hz, 1H), 6.52 (d, J = 2.6 Hz, 1H), 3.44 (q, J = 7.1 Hz, 4H), 2.62 (s, 3H), 1.24 (t, J = 7.1 Hz, 6H).

5-iodo-6-isopropoxy-2-phenyl-4H-chromen-4-one (2w)

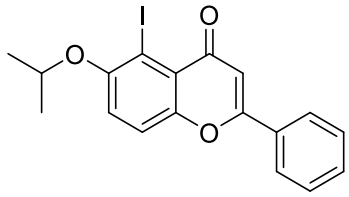

Compound **2x** was prepared using a known method.[62] Under ambient atmosphere, ipriflavone (264.4 mg, 1.00 equiv, 943.2 μmol), silver tosylate (394.8 mg, 1.50 equiv, 1.41 mmol), and iodine (359.0 mg, 1.5 equiv, 1.41 mmol) were dissolved in MeCN (5.0 mL) in a 20 mL vial. The vial was capped, and the reaction mixture was stirred vigorously for 24 h at rt. After this time, the mixture was passed through a silica plug with EtOAc as eluent; the filtrate was concentrated *in vacuo*, then purified by flash column chromatography (SiO_2, 40% EtOAc in hexanes) to afford 8-iodo-7-isopropoxy-3-phenyl-4H-chromen-4-one (122.4 mg, 301.3 μmol, 32%) as a white solid. The spectral data match those reported in the literature.

^{1}H NMR (500 MHz, $CDCl_3$) δ 8.20 (d, J = 8.9 Hz, 1H), 8.00 (s, 1H), 7.52 – 7.48 (m, 2H), 7.40 – 7.35 (m, 2H), 7.36 – 7.29 (m, 1H), 6.89 (d, J = 9.0 Hz, 1H), 4.73 (p, J = 6.1 Hz, 1H), 1.40 (d, J = 6.1 Hz, 6H).

1-(4-iodophenyl)-5-phenyl-3-(trifluoromethyl)-1H-pyrazole (2y)

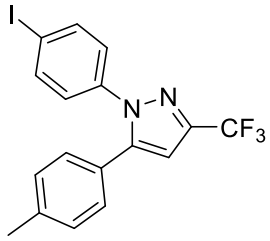

Compound **2y** was prepared using a reported method.[63] To a solution of 4,4,4-trifluoro-1-(p-tolyl)butane-1,3-dione (500.0 mg, 1.00 equiv, 2.17 mmol) in DMAc (7.24 mL) was added 1-(4-iodophenyl)hydrazine hydrochloride (587.6 mg, 1.00 equiv, 2.17 mmol) at rt, followed by 6M HCl (1.20 mL, 1.00 equiv, 2.17 mmol). The mixture was stirred at rt for 24 h, then cooled to 0 °C. Then, water (5.0 mL) was added slowly. After diluting with toluene (5 mL), the organic layer was washed with water (2x), dried over magnesium sulfate, and filtered; the filtrate was concentrated *in vacuo*. The crude residue was purified by flash column chromatography (SiO_2, 15% EtOAc in hexanes) to afford 1-(4-iodophenyl)-5-(p-tolyl)-3-(trifluoromethyl)-1H-pyrazole (842.8 mg, 1.97 mmol, 91%) as an off-white solid. The spectral data match those reported in the literature.

^{1}H NMR (500 MHz, $CDCl_3$) δ 7.63 – 7.57 (m, 2H), 7.08 (d, J = 7.8 Hz, 2H), 7.03 (d, J = 7.9 Hz, 2H), 7.01 – 6.97 (m, 2H), 6.63 (s, 1H), 2.29 (s, 3H).

^{19}F NMR (470 MHz, $CDCl_3$) δ -62.3.

Scheme S7. Synthesis of 4-fluoro-1-((3-(3-iodophenyl)prop-2-yn-1-yl)oxy)-2-methoxybenzene (**2z**).

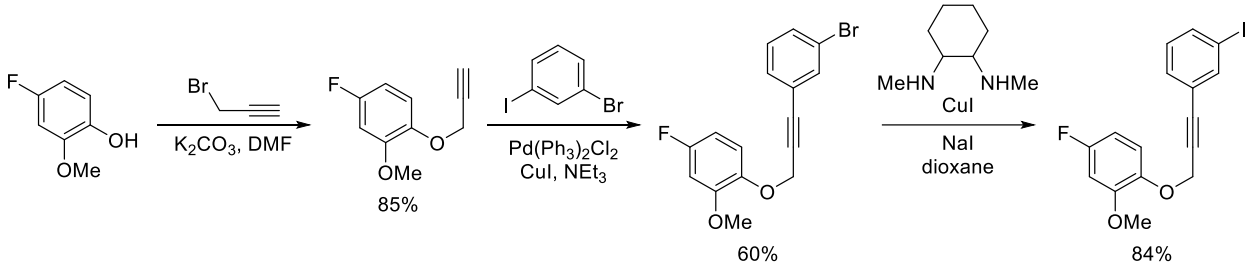

4-fluoro-2-methoxy-1-(prop-2-yn-1-yloxy)benzene

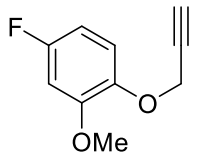

This compound was prepared using a reported method.[64] Under an inert atmosphere of nitrogen, 1,2-methoxy-4-fluorophenol (710 mg, 5.00 mmol, 1.00 equiv) was dissolved in anhydrous DMF (10 mL). K_2CO_3 (1.40 g, 10.0 mmol, 2.00 equiv) was added, and the resulting mixture was heated to 55 °C for 30 min. The reaction mixture was allowed to cool to rt, and propargyl bromide (650 µL, 6.00 mmol, 1.20 equiv) was added. The solution was stirred at rt for 6 h, monitoring for completion using TLC, then poured into ice-cold water. The aqueous layer was extracted with EtOAc (3 × 10 mL), and the combined organic phases were dried over $MgSO_4$ before removal of the solvent *in vacuo*. The crude residue was purified by flash column chromatography (SiO_2, 10% EtOAc in hexanes) to provide 4-fluoro-2-methoxy-1-(prop-2-yn-1-yloxy)benzene as a colorless liquid (765 mg, 4.25 mmol, 85% yield). The spectral data match those reported in the literature.

^{1}H NMR (500 MHz, $CDCl_3$) δ 7.00-6.97 (dd, J = 8.9, 5.5 Hz, 1H), 6.66 (dd, J = 10.1, 3.0 Hz, 1H), 6.62-6.58 (td, J = 8.4, 2.9 Hz, 1H), 4.72 (d, J = 2.4 Hz, 2H), 3.86 (s, 3H), 2.50 (t, J = 2.4 Hz, 1H).

^{13}C{^{1}H} NMR (151 MHz, $CDCl_3$) δ 158.52 (d, J = 240.4 Hz), 151.004 (d, J = 10.10 Hz), 143.06 (d, J = 3.2 Hz), 116.17 (d, J = 10.10 Hz), 106.01 (d, J = 22.5 Hz), 100.55 (d, J = 27.6 Hz), 78.70, 75.94, 57.76, 56.16.

^{19}F NMR (565 MHz, $CDCl_3$) δ -118.74

1-((3-(3-bromophenyl)prop-2-yn-1-yl)oxy)-4-fluoro-2-methoxybenzene

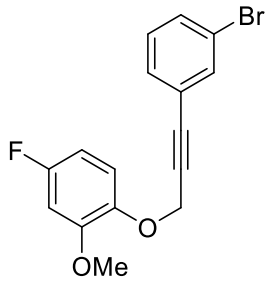

This compound was prepared using a modified literature procedure.[65] In a nitrogen-filled glovebox, a 20 mL vial equipped with a Teflon magnetic stir bar was charged with $Pd(PPh_3)_2Cl_2$ (0.10 mmol, 70.10 mg, 5 mol%), CuI (0.20 mmol, 38.0 mg, 10 mol%) and 4-fluoro-2-methoxy-1-(prop-2-yn-1-yloxy)benzene (360 mg, 2.00 mmol, 1.00 equiv). Triethylamine (10 mL) was added to the vial, and the reaction mixture was stirred for 10 min at 65°C. After stirring for 10 min, 1-bromo-3-iodobenzene (622 mg, 2.20 mmol, 1.10 equiv) was added, and the mixture was stirred overnight. The resulting mixture was then poured into an aqueous saturated solution of NH_4Cl (5 mL) and extracted twice with EtOAc (10 mL). The combined organic layers were washed with brine and dried over anhydrous Na_2SO_4. The crude residue was purified by flash column chromatography (SiO_2, 10% EtOAc in hexanes) to provide 1-((3-(3-bromophenyl)prop-2-yn-1-yl)oxy)-4-fluoro-2-methoxybenzene as a beige powder (402 mg, 1.20 mmol, 60% yield).

^1H NMR (500 MHz, $CDCl_3$) δ 7.56 (m, 1H), 7.46 (m, 1H), 7.34 (m, 1H), 7.17 (t, J = 7.9 Hz, 1H), 7.03 (dd, J = 8.9, 5.5 Hz, 1H), 6.68 (dd, J = 10.2, 2.9 Hz, 1H), 6.62 (td, J = 8.4, 2.9 Hz, 1H), 4.93 (s, 2H), 3.88 (s, 3H).

$^{13}C\{^1H\}$ NMR (151 MHz, $CDCl_3$) δ 158.53 (d, J = 240.4 Hz), 151.008 (d, J = 9.9 Hz), 143.18 (d, J = 3.2 Hz) 134.61, 131.98, 130.47, 129.88, 116.19 (d, J = 10.0 Hz), 106.06 (d, J = 22.5 Hz), 100.56 (d, J = 27.5 Hz), 86.04, 85.46, 58.46, 56.18.

^{19}F NMR (565 MHz, $CDCl_3$) δ -118.78

HRMS (ESI-TOF) $[C_{16}H_{12}BrFO_2]$+ calc'd: 334.00050, found: 334.00150

4-fluoro-1-((3-(3-iodophenyl)prop-2-yn-1-yl)oxy)-2-methoxybenzene (2z)

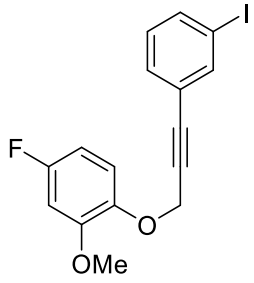

Compound **2ab** was prepared using a reported method.[66] In a nitrogen-filled glovebox, a 20 mL vial equipped with a Teflon magnetic stir bar was charged with CuI (8.0 mg, 0.04 mmol, 5.0 mol%), 1-((3-(3-bromophenyl)prop-2-yn-1-yl)oxy)-4-fluoro-2-methoxybenzene (285 mg, 0.85

mmol, 1.00 equiv) and NaI (255 mg, 1.70 mmol, 2.00 equiv). Racemic trans-N,N'-dimethyl-1,2-cyclohexanediamine (12.10 mg, 0.08 mmol, 10 mol%) and dioxane (1.00 mL) were added to the vial. The vial was sealed, and the reaction mixture was stirred at 110°C for 48 h. The resulting suspension was cooled to reach rt, diluted with 30% aq. ammonia (5 mL), poured into water (20 mL), and extracted with dichloromethane (3×10 mL). The combined organic layers were washed with brine and dried over anhydrous Na_2SO_4. The crude residue was purified by flash column chromatography (SiO_2, 10% EtOAc in hexanes) to provide 4-fluoro-1-((3-(3-iodophenyl)prop-2-yn-1-yl)oxy)-2-methoxybenzene as a yellow oil (273 mg, 0.710 mmol, 84% yield).

^{1}H NMR (500 MHz, $CDCl_3$) δ 7.77 (m, 1H), 7.66 (m, 1H), 7.37 (m, 1H), 7.05-7.01 (m, 2H), 6.68 (dd, J = 10.2, 2.9 Hz, 1H), 6.64-6.60 (td, J = 8.4, 2.9 Hz, 1H), 4.92 (s, 2H), 3.88 (s, 3H).

^{13}C{1H} NMR (151 MHz, $CDCl_3$) δ 158.49 (d, J = 240.4 Hz), 151.004 (d, J = 9.8 Hz), 143.17 (d, J = 3.10 Hz) 140.41, 137.81, 131.00, 129.92, 116.15 (d, J = 9.8 Hz), 106.04 (d, J = 22.6 Hz), 100.53 (d, J = 27.3 Hz), 93.67, 85.84, 85.47, 58.44, 56.16.

^{19}F NMR (565 MHz, $CDCl_3$) δ -118.71

HRMS (ESI-TOF) $[C_{16}H_{12}FIO_2+H]+$ calc'd: 382.9895, found: 382.9900

2,5,7,8-tetramethyl-2-(4,8,12-trimethyltridecyl)chroman-6-yl 4-iodobenzoate (2aa)

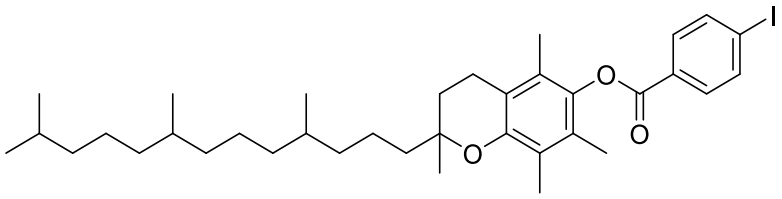

To a solution of (±)-α-tocopherol (250.0 mg, 580.4 µmol, 1.00 equiv) and triethylamine (81.00 µL, 580.4 µmol, 1.00 equiv) in DCM (2.90 mL) at 0 °C was added 4-iodobenzoyl chloride (154.7 mg, 580.4 µmol, 1.00 equiv) in one portion. The resulting suspension was then stirred for 2 h at rt. The reaction mixture was then diluted with DCM and washed with 2 M NaOH (3x), and the combined organic phases were concentrated *in vacuo*. The crude residue was purified by flash column chromatography (SiO_2, 20% EtOAc in hexanes) to provide 2,5,7,8-tetramethyl-2-(4,8,12-trimethyltridecyl)chroman-6-yl-4-iodobenzoate as a viscous clear oil (77.7 mg, 117.6 mmol, 20% yield). The spectral data match those reported in the literature.[67]

^{1}H NMR (500 MHz, $CDCl_3$) δ 7.95 (d, J = 8.4 Hz, 2H), 7.89 (d, J = 8.2 Hz, 2H), 2.61 (t, J = 6.8 Hz, 2H), 2.11 (s, 3H), 2.03 (s, 3H), 1.99 (s, 3H), 1.81 (td, J = 15.1, 6.9 Hz, 2H), 1.47 – 1.05 (m, 25H), 0.88 – 0.84 (m, 12H).

^{13}C{^{1}H} NMR (126 MHz, $CDCl_3$) δ 164.88, 155.27, 149.72, 140.61, 138.12, 131.69, 129.25, 126.92, 125.17, 123.36, 117.68, 101.47, 75.28, 40.63, 39.53, 37.69, 37.54, 37.44, 32.93, 31.38, 29.85, 28.13, 24.97, 24.60, 24.35, 23.83, 22.87, 22.78, 21.20, 20.78, 19.91, 19.84, 19.75, 13.18, 12.34, 12.01

(1*S*,2*R*,5*R*)-2-isopropyl-5-methylcyclohexyl 4-iodobenzoate (2ab)

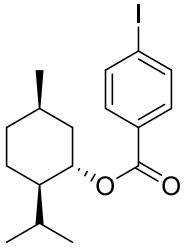

In a 20 mL vial equipped with a stir bar, 4-iodobenzoyl chloride (350.0 mg, 1.17 equiv 1.31 mmol) was added in one portion to a solution of (1*S*,2*R*,5*R*)-5-methyl-2-(propan-2-yl)cyclohexan-1-ol (175.0 mg, 1.00 equiv, 1.12 mmol) in pyridine (2.24 mL). The reaction mixture was stirred at 50 °C for 16 h. Then, the resulting suspension was diluted with DCM, filtered, and the filtrate concentrated *in vacuo*. This crude residue was purified by flash column chromatography (SiO_2, 2-10% MeOH in DCM) to afford (1*R*,2*S*,5*R*)-2-isopropyl-5-methylcyclohexyl-4-iodobenzoate (279.1 mg, 722.6 µmol, 65 % yield) as a clear oil.

^{1}H NMR (400 MHz, $CDCl_3$) δ 7.83 – 7.73 (m, 2H), 7.61 – 7.52 (m, 2H), 5.50 (td, J = 6.5, 3.3 Hz, 1H), 1.91 (tt, J = 7.7, 3.7 Hz, 1H), 1.74 (ddd, J = 13.4, 8.9, 4.5 Hz, 2H), 1.65 (td, J = 9.3, 3.6 Hz, 1H), 1.59 – 1.39 (m, 3H), 1.23 – 1.11 (m, 1H), 0.97 (dd, J = 13.9, 6.9 Hz, 6H), 0.90 (d, J = 6.8 Hz, 3H).

^{13}C{^{1}H} NMR (101 MHz, $CDCl_3$) δ 169.7, 142.6, 135.9, 105.2, 77.2, 50.7, 40.6, 34.8, 32.6, 31.3, 26.2, 25.7, 25.5, 24.1.

HRMS (EI) calc'd [$C_{17}H_{23}IO_2$+H]+ 386.0741, found 386.0743

4.7.8 Functionalization Reactions of Aryl-α,α-difluoromethylacetonitriles

2-(4-butylphenyl)-2,2-difluoroacetamide (5a)

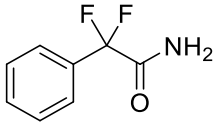

Compound **4a** was prepared using a literature procedure.[38] A 4 mL vial equipped with a Teflon magnetic stir bar was charged with 2,2-difluoro-2-phenylacetonitrile (21.00 mg, 0.10 mmol, 1.00 equiv) then with a solution of phenol (19.0 mg, 0.20 mmol, 2.00 equiv) in 33% HBr/AcOH (300 mg). The resulting solution was stirred for 18 h at rt. After this time, the reaction mixture was extracted with diethyl ether, dried over sodium sulfate, and concentrated *in vacuo* to provide 2,2-difluoro-2-phenylacetamide as a white solid (18.2 mg, 0.08 mmol, 80% yield).

^{1}H NMR (500 MHz, DMSO-d6) δ 8.37 (s, 1H), 8.02 (d, J = 9.6 Hz, 1H), 7.60 (td, J = 7.0, 3.5 Hz, 2H), 7.52 (d, J = 7.5 Hz, 3H).

^{13}C{^{1}H} NMR (126 MHz, DMSO-d6) δ 165.8 (td, J = 29.7, 8.6 Hz), 133.9 (t, J = 25.6 Hz), 131.3, 129.1 (d, J = 2.2 Hz), 125.6 (t, J = 6.0 Hz), 118.3 – 112.2 (m).

^{19}F NMR (471 MHz, DMSO-d6) δ -101.9.

HRMS (EI) $[C_8H_7F_2NO+H]+$ calc'd: 172.0553, found: 172.0547

propyl 2,2-difluoro-2-phenylethanimidothioate (5b)

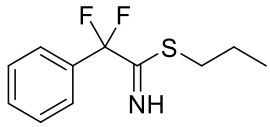

A 50 mL round bottomed flask equipped with a magnetic stir bar was charged with 2,2-difluoro-2-phenylacetonitrile (79.0 mg, 0.516 mmol, 1.00 equiv), acetonitrile (4.0 mL), and water (1.0 mL). The headspace was flushed with nitrogen and propanethiol (464 µL, 5.00 mmol, 10 equiv) was added dropwise. The resulting solution was stirred at rt for 2 h. After this time, the solvent was removed *in vacuo*. The resulting residue was dissolved in dichloromethane, dried over sodium sulfate, filtered, and the organic filtrate concentrated. Purification by column chromatography (SiO_2, 2% to 10% EtOAc in hexanes) provided propyl 2,2-difluoro-2-phenylethanimidothioate as a colorless liquid (101.4 mg, 0.4422 mmol, 86% yield).

^{1}H NMR (600 MHz, $CDCl_3$) δ 9.56 (br s, 1H), 7.57 (d, J = 7.4 Hz, 2H), 7.51– 7.43 (m, 3H), 2.91 (t, J = 7.3 Hz, 2H), 1.68 (h, J = 7.3 Hz, 2H), 1.00 (t, J = 7.4 Hz, 3H).

^{13}C{^{1}H} NMR (151 MHz, $CDCl_3$) δ 173.6 (t, J = 32.10 Hz), 133.9 (t, J = 26.6 Hz), 130.9, 128.7, 125.6 (t, J = 6.0 Hz), 116.7 (t, J = 249.10 Hz), 31.7, 21.8, 13.6.

^{19}F NMR (565 MHz, $CDCl_3$) δ -97.0.

HRMS (ESI-TOF) $[C_{11}H_{13}F_2NS+H]+$ calc'd.: 230.0808, found: 230.0810

(*Z*)-2-(4-butylphenyl)-2,2-difluoro-*N*'-hydroxyacetimidamide (5c)

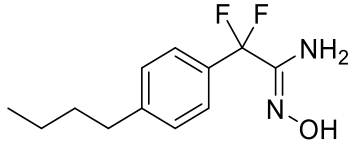

This compound was prepared using a literature procedure.[47] A 4 mL vial equipped with a Teflon magnetic stir bar was charged with 2,2-difluoro-2-phenylacetonitrile (21.00 mg, 0.10 mmol, 1.00 equiv) and a 50 wt% aqueous hydroxylamine solution (7.92 mg, 0.12 mmol, 1.20 equiv). EtOH (0.100 M) was added and the mixture was stirred at rt for 18 h. After this time, the reaction mixture was concentrated under reduced pressure and the residue was purified by flash column chromatography (10/90 EtOAc in hexanes) to provide (Z)-2-(4-butylphenyl)-2,2-difluoro-N'-hydroxyacetimidamide as a white powder (18.2 mg, 0.075 mmol, 75% yield)

^{1}H NMR (500 MHz, $CDCl_3$) δ 7.87 (s, 1H), 7.44 (d, J = 8.3 Hz, 2H), 7.24 (d, J = 8.3 Hz, 2H), 4.79 (s, 2H), 2.65 (t, J = 7.7 Hz, 2H), 1.61 (m, 2H), 1.36 (m, 2H), 0.93 (t, J = 7.4 Hz, 3H).

^{13}C{^{1}H} NMR (151 MHz, $CDCl_3$) δ 149.75 (t, J = 32.2 Hz), 145.85, 130.88 (t, J = 25.7 Hz), 128.51, 125.90 (t, J = 5.8 Hz), 116.94 (t, J = 242.2 Hz), 35.69, 33.48, 22.40, 14.05.

^{19}F NMR (565 MHz, $CDCl_3$) δ -97.3.

HRMS (EI) $[C_{12}H_{16}F_2N_2O+H]+$ calc'd: 243.1301, found: 243.1303

tert-butyl (2,2-difluoro-2-phenylethyl)carbamate (5d)

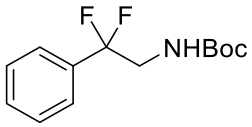

Step 1:

In a nitrogen-filled glovebox, a dry 4 mL vial equipped with a Teflon magnetic stir bar was charged with lithium aluminum hydride (94.9 mg, 2.50 mmol, 5.00 equiv) and dry and degassed diethyl ether (1.00 mL). The resulting suspension was cooled to –30 °C in the glovebox freezer. Then, a solution of 2,2-difluoro-2-phenylacetonitrile (76.6 mg, 0.500 mmol, 1.00 equiv) in dry, degassed diethyl ether (1.00 mL) was prepared and cooled to –30 °C in the glovebox freezer. The solution containing the nitrile was transferred cold, and dropwise, to the suspension of lithium aluminum hydride with stirring. Diethyl ether (0.5 mL) was used to complete the transfer, the reaction vial was sealed, allowed to warm to rt, and stirred vigorously for 2 h. After this time, the reaction mixture was cooled to 0 °C and carefully diluted with water, dropwise. The resulting mixture was extracted with EtOAc, dried over sodium sulfate, and concentrated *in vacuo* in a 20 mL vial.

Step 2:

In the 20 mL vial, the crude product was dissolved in dry DCM (2.0 mL) and treated with di-tert-butyl dicarbonate (105.0 mg, 0.481 mmol, 0.962 equiv). The reaction vial was sealed and the reaction mixture was stirred at rt for 24 h. After this time, the reaction mixture was concentrated *in vacuo* and the product was purified by column chromatography (2% to 10% EtOAc in hexanes) to provide tert-butyl (2,2-difluoro-2-phenylethyl)carbamate as a white powder (113.7 mg, 0.434 mmol, 87% yield). Note: The product exists as a 5.5:1 mixture of amide E/Z isomers that interconvert more slowly than the NMR timescale.

^{1}H NMR (600 MHz, $CDCl_3$) δ 7.53 – 7.47 (both isomers, m, 2H), 7.47 – 7.39 (both isomers, m, 3H), 4.87 (major isomer, broad t, J = 6.3 Hz, 1H), 4.58 (minor isomer, broad s, 1H), 3.76 (both isomers, td, J = 14.3, 6.4 Hz, 2H), 1.39 (major isomer, s, 9H), 1.30 (minor isomer, s, 9H).

^{13}C{^{1}H} NMR (151 MHz, $CDCl_3$) δ 155.6, 134.9 (t, J = 25.5 Hz), 130.3, 128.6, 125.4 (t, J = 6.10 Hz), 120.7 (t, J = 243.8 Hz), 80.1, 47.0 (t, J = 31.10 Hz), 28.4.

^{19}F NMR (565 MHz, $CDCl_3$) δ -102.8 (major isomer, t, J = 14.3 Hz), -103.0 (minor isomer, broad t, J = 13.3 Hz)

HRMS (EI) $[C_{13}H_{17}F_2NO_2+H]+$ calc'd.: 258.1301, found: 258.1300.

2,2-difluoro-1,2-diphenylethan-1-one (5e)

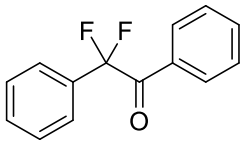

The title compound was prepared according to the following procedure: In a nitrogen-filled glovebox, a 25 mL Schlenk flask with a Teflon plug was charged with 2,2-difluoro-2-phenylacetonitrile (76.6 mg, 0.500 mmol, 1.00 equiv) and dry, degassed THF (1.5 mL). The Schlenk bomb was sealed and taken out of glovebox, where it was cooled in a dry ice/acetone bath (–78 °C) under nitrogen. Then, a solution of phenyl magnesium bromide (1.00 M, 0.525 mL, 0.525 mmol, 1.00 equiv) was added dropwise with a gas-tight syringe with stirring. After complete addition, the reaction mixture was transferred to a water ice bath (0 °C) and stirred on ice for 4 h. After this time, 3 M HCl was added on ice dropwise (2 mL). The resulting mixture was heated to 65 °C for 20 h. After this time, the reaction mixture was extracted with DCM, dried over sodium sulfate, and concentrated *in vacuo*. The resulting residue was purified by column chromatography (1% to 4% EtOAc in hexanes) to provide 2,2-difluoro-1,2-diphenylethan-1-one as a colorless liquid (99.7 mg, 0.429 mmol, 85% yield).

^{1}H NMR (600 MHz, $CDCl_3$) δ 8.04 (d, J = 7.5 Hz, 2H), 7.62 (d, J = 6.6 Hz, 2H), 7.59 (ddt, J = 8.7, 7.2, 1.3 Hz, 1H), 7.51.00– 7.42 (m, 5H).

^{13}C{^{1}H} NMR (151 MHz, $CDCl_3$) δ 189.1 (t, J = 31.00 Hz), 134.3, 133.3 (t, J = 25.10 Hz), 132.3, 131.1 (t, J = 1.5 Hz), 130.4 (t, J = 2.9 Hz), 129.0, 128.8, 125.8 (t, J = 6.0 Hz), 117.1 (t, J = 253.2 Hz).

^{19}F NMR (565 MHz, $CDCl_3$) δ -97.5.

HRMS (EI) $[C_{14}H_{10}F_2O+H]+$ calc'd.: 233.0774, found: 233.0772.

2,2-difluoro-1-(4-methoxyphenyl)-2-phenylethan-1-one (5f)

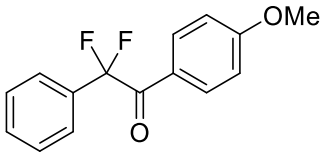

In a nitrogen-filled glovebox, a 25 mL Schlenk flask with a Teflon plug was charged with 2,2-difluoro-2-phenylacetonitrile (76.6 mg, 0.500 mmol, 1.00 equiv) and dry, degassed THF (1.5 mL). The Schlenk bomb was sealed and taken out of glovebox, where it was cooled in a dry ice/acetone bath (–78 °C) under nitrogen. Then, a solution of para-methoxy phenyl magnesium bromide (0.5 M, 1.00 mL, 0.525 mmol, 1.00 equiv) was added dropwise with stirring. After complete addition, the reaction mixture was transferred to a water ice bath (0 °C) and stirred on ice for 4 h. After this time, 3 M HCl was added on ice dropwise (2 mL). The resulting mixture was heated to 60 °C for 18 h. After this time, the reaction mixture was extracted with diethyl ether, dried over sodium sulfate, and concentrated *in vacuo*. The resulting residue was purified by column chromatography

(1% to 8% EtOAc in hexanes) to provide 2,2-difluoro-1-(4-methoxyphenyl)-2-phenylethan-1-one as a colorless solid (113.7 mg, 0.434 mmol, 87% yield).

^{1}H NMR (600 MHz, $CDCl_3$) δ 8.04 (d, J = 9.0 Hz, 2H), 7.64 – 7.59 (m, 2H), 7.50 – 7.42 (m, 3H), 6.91 (d, J = 9.10 Hz, 2H), 3.85 (s, 3H).

^{13}C{^{1}H} NMR (151 MHz, $CDCl_3$) δ 187.4 (t, J = 30.4 Hz), 164.5, 133.7 (t, J = 25.10 Hz), 133.0 (t, J = 3.10 Hz), 130.9, 128.9, 125.7 (t, J = 6.0 Hz), 125.1, 117.2 (t, J = 252.9 Hz), 114.1, 55.7.

^{19}F NMR (565 MHz, $CDCl_3$) δ -96.2.

HRMS (EI) [$C_{15}H_{12}F_2O_2$+H]+ calc'd.: 263.0877, found: 263.0878.

2-(difluoro(phenyl)methyl)-1-methyl-1H-benzo[d]imidazole (5g)

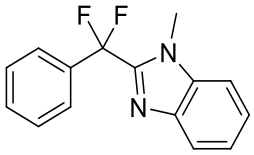

A 20 mL vial was charged with 2,2-difluoro-2-phenylacetonitrile (78.5 mg, 0.512 mmol, 1.00 equiv). Then, a solution of freshly vacuum distilled *N*-1-methylbenzene-1,2-diamine (183.3 mg, 1.50 mmol, 3.00 equiv) in dry methanol (5.0 mL) was added, followed by ammonium chloride (26.7 mg, 0.500 mmol, 1.00 equiv) and a Teflon stir bar. The headspace was flushed with nitrogen, and the vial was sealed with a Teflon cap and heated to 65 °C in a heating block for 24 h. After this time, the reaction was cooled to rt and concentrated *in vacuo*. The resulting residue was purified by flash column chromatography (SiO_2, 5% to 15% EtOAc in hexane) to provide 2-(difluoro(phenyl)methyl)-1-methyl-1H-benzo[d]imidazole as a white solid (124.2 mg, 0.481 mmol, 94% yield).

^{1}H NMR (600 MHz, $CDCl_3$) δ 7.91 (d, J = 8.0 Hz, 1H), 7.67 (d, J = 6.5 Hz, 2H), 7.53 – 7.42 (m, 3H), 7.40 (m, 2H), 7.32 (m, 1H), 3.91 (s, 3H).

^{19}F NMR (470 MHz, $CDCl_3$) δ -89.0.

^{13}C{^{1}H} NMR (126 MHz, $CDCl_3$) δ 147.2 (t, J = 33.0 Hz), 141.2, 136.4, 134.5 (t, J = 25.6 Hz), 130.7 (t, J = 1.9 Hz), 128.5, 125.9 (t, J = 5.6 Hz), 124.2, 122.7, 121.1, 117.1 (t, J = 240.0 Hz), 109.7, 30.9

HRMS (EI) [$C_{15}H_{12}F_2N_2$+H]+ calc'd.: 259.1039, found: 259.1041.

2-(difluoro(phenyl)methyl)benzo[d]oxazole (5h)

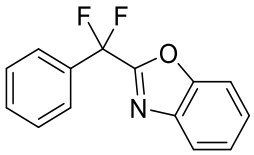

A 20 mL vial was charged with 2,2-difluoro-2-phenylacetonitrile (76.6 mg, 0.500 mmol, 1.00 equiv). Then, a solution of 2-aminophenol (81.8 mg, 0.750 mmol, 1.50 equiv) in dry methanol (5.0 mL) was added, and a Teflon stir bar was added. The headspace was flushed with nitrogen, the vial was sealed, and the reaction mixture was heated in a heating block at 65 °C for 24 h. After this time, the solvent was removed *in vacuo* and the resulting residue was purified by column chromatography (SiO_2, 1% to 10% EtOAc in hexanes) to provide 2-(difluoro(phenyl)methyl)benzo[d]oxazole as a colorless viscous liquid (107.1 mg, 0.437 mmol, 87% yield).

^{1}H NMR (600 MHz, $CDCl_3$) δ 8.04 (d, J = 9.0 Hz, 2H), 7.64 – 7.59 (m, 2H), 7.50 – 7.42 (m, 3H), 6.91 (d, J = 9.10 Hz, 2H), 3.85 (s, 3H).

^{13}C{^{1}H} NMR (151 MHz, $CDCl_3$) δ 187.4 (t, J = 30.4 Hz), 164.5, 133.7 (t, J = 25.10 Hz), 133.0 (t, J = 3.10 Hz), 130.9, 128.9, 125.7 (t, J = 6.0 Hz), 125.1, 117.2 (t, J = 252.9 Hz), 114.1, 55.7.

^{19}F NMR (565 MHz, $CDCl_3$) δ -97.0.

HRMS (EI) [$C_{14}H_9F_2NO$+H]+ calc'd.: 246.0724, found: 246.0725.

2-(difluoro(phenyl)methyl)benzo[d]thiazole (5i)

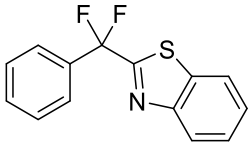

A 20 mL vial was charged with 2,2-difluoro-2-phenylacetonitrile (76.6 mg, 0.500 mmol, 1.00 equiv). Then, a solution of 2-aminobenzenethiol (93.9 mg, 0.750 mmol, 1.50 equiv) in dry methanol (5.0 mL) was added, followed by a Teflon stir bar. The headspace was flushed with nitrogen, the vial was sealed, and the reaction mixture was stirred at rt for 1 hr. After this time, the solvent was removed *in vacuo*, and the resulting residue was purified by column chromatography (SiO_2, 1% to 10% EtOAc in hexanes) to provide 2-(difluoro(phenyl)methyl)benzo[d]thiazole as a colorless viscous liquid (121.6 mg, 0.465 mmol, 93% yield).

^{1}H NMR (600 MHz, $CDCl_3$) δ 8.11 (d, J = 8.2 Hz, 1H), 7.95 (d, J = 8.0 Hz, 1H), 7.75 – 7.70 (m, 2H), 7.53 (ddd, J = 8.3, 7.1, 1.3 Hz, 1H), 7.50 – 7.45 (m, 4H).

^{13}C{^{1}H} NMR (151 MHz, $CDCl_3$) δ 165.2 (t, J = 36.5 Hz), 153.0, 135.2, 135.1 (t, J = 26.5 Hz), 130.9 (t, J = 1.5 Hz), 128.7, 126.8, 126.6, 126.0 (t, J = 5.8 Hz), 124.6, 122.0, 117.5 (t, J = 243.6 Hz).

^{19}F NMR (565 MHz, $CDCl_3$) δ -87.0.

HRMS (EI) $[C_{14}H_9F_2NS+H]+$ calc'd.: 262.0494, found: 262.0497.

tert-butyl 6-(difluoro(phenyl)methyl)-5-oxa-2,7-diazaspiro[3.4]oct-6-ene-2-carboxylate (5j)

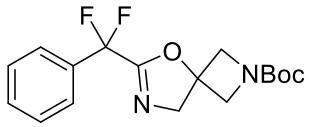

In a 20 mL vial, 2,2-difluoro-2-phenylacetonitrile (100.0 mg, 64.35 µL, 1.00equiv 653.0 µmol) was weighed, then dissolved in dry MeOH (3.265 mL). To this was added tert-butyl 3-(aminomethyl)-3-hydroxyazetidine-1-carboxylate (264.2 mg, 2.0 equiv 1.306 mmol), the headspace was flushed with N_2, and the vial was capped and stirred at 65 °C for 16 h. After this time, the reaction mixture was concentrated *in vacuo*. The crude solid was purified by flash column chromatography (SiO_2, 80% EtOAc in pentanes) to afford pure tert-butyl 6-(difluoro(phenyl)methyl)-5-oxa-2,7-diazaspiro[3.4]oct-6-ene-2-carboxylate (0.15 g, 0.45 mmol, 69%) as a clear glassy solid.

^{1}H NMR (500 MHz, $CDCl_3$) δ 7.62 – 7.58 (m, 2H), 7.53 – 7.44 (m, 3H), 4.25 (dd, J = 10.1, 1.3 Hz, 2H), 4.13 (t, J = 2.2 Hz, 2H), 3.98 (dd, J = 10.1, 1.3 Hz, 2H), 1.43 (s, 9H).

^{19}F NMR (470 MHz, $CDCl_3$) δ -100.2.

^{13}C{^{1}H} NMR (126 MHz, $CDCl_3$) δ 159.5 (t, J = 34.7 Hz), 155.0, 132.3 (t, J = 25.6 Hz), 130.2 (d, J = 2.0 Hz), 127.7, 124.6 (t, J = 6.10 Hz), 112.7 (t, J = 244.8 Hz), 80.4, 79.5, 63.2, 61.2 (s, brz), 27.4.

HRMS (EI) $[C_{17}H_{20}F_2N_2O_3+H]+$ calc'd: 339.1517, found 339.1515

5-(difluoro(phenyl)methyl)-1H-tetrazole (5k)

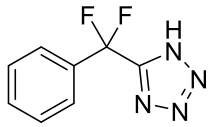

A 20 mL vial equipped with a Teflon magnetic stir bar was charged with 2,2-difluoro-2-phenylacetonitrile (78.5 mg, 0.512 mmol, 1.00 equiv) and DMSO (5.0 mL). Then, sodium azide (65.0 mg, 1.00 mmol, 1.95 equiv) was added. The headspace was flushed with nitrogen, and the vial was sealed with a Teflon cap and heated to 80 °C in a heating block for 20 h. After this time, the reaction was cooled to rt, transferred to a separatory funnel, and diluted with EtOAc (50 mL) and 1.5 M HCl (40 mL). The aqueous layer was extracted with EtOAc (4 x 50 mL), and the combined organic layers were concentrated in vacuo to provide the desired product as a mixture with DMSO. To remove residual DMSO, the product was taken up in EtOAc (20 mL) and washed with 1M HCl (8 x 5 mL). The organic layer was dried over sodium sulfate and concentrated *in vacuo* to provide a thick oil. This oil was stored at –10 °C for 24 h, after which time it solidified. The resulting solid was crushed to a powder and dried under high vacuum to provide 5-(difluoro(phenyl)methyl)-1H-tetrazole as a white powder. (97.5 mg, 0.497 mmol, 97% yield).

^{1}H NMR (600 MHz, $CDCl_3$) δ 15.42 (s, 1H), 7.66 (d, J = 7.8 Hz, 2H), 7.50 (m, 3H).

$^{13}C\{^{1}H\}$ NMR (151 MHz, $CDCl_3$) δ 166.4 (t, J = 32.2 Hz), 133.5 (t, J = 26.4 Hz), 131.5, 128.9, 125.6 (t, J = 6.0 Hz), 116.7 (t, J = 245.7 Hz).

^{19}F NMR (565 MHz, $CDCl_3$) δ -92.2.

HRMS (EI) $[C_{13}H_{12}F_2]$+ calc'd.: 197.0632, found: 197.0633.

2-(difluoro(phenyl)methyl)-4,5-dimethylpyridine (5l)

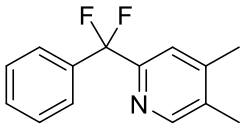

Compound **4l** was prepared by a modified literature procedure.[45] To a solution of $Ni(COD)_2$ (11.9 mg, 10 mol%, 43.3 μmol), tri(1-adamantanyl)phosphine (75.70 mg, 40.0 mol%, 173.4 μmol), and difluoro(phenyl)acetonitrile (42.7 μL, 1.00 equiv, 433 μmol) in o-xylene (1.00 mL) was added 2,3-dimethyl-1,3-butadiene (196 μL, 4.00 equiv, 1.73 mmol). The vial was then capped, sealed with electrical tape, and heated to 140 °C for 24 h. Once cooled, the crude reaction mixture was concentrated *in vacuo*, then subjected to flash column chromatography (SiO_2, 30% EtOAc in hexanes) to afford 2-(difluoro(phenyl)methyl)-4,5-dimethylpyridine (43.2 mg, 185 μmol, 43%) as a yellow oil.

^{1}H NMR (500 MHz, $CDCl_3$) δ 8.36 (s, 1H), 7.58 (ddd, J = 5.5, 3.2, 1.3 Hz, 2H), 7.48 (s, 1H), 7.43 – 7.37 (m, 3H), 2.32 (s, 3H), 2.26 (s, 3H).

^{19}F NMR (470 MHz, $CDCl_3$) δ -94.5.

$^{13}C\{^{1}H\}$ NMR (126 MHz, $CDCl_3$) δ 153.2 (t, J = 30.3 Hz), 150.1, 146.9, 137.0 (t, J = 27.6 Hz), 133.4 (d, J = 1.6 Hz), 129.9 (t, J = 2.0 Hz), 128.4, 125.9 (t, J = 5.8 Hz), 121.1 (t, J = 4.2 Hz), 119.0 (t, J = 243.0 Hz), 19.5, 16.3.

HRMS (EI) $[C_{14}H_{13}F_2N+H]$+ calc'd: 234.1087, found: 234.1089

(*S*)-2,2-difluoro-2-phenyl-N-(1-phenylethyl)ethan-1-amine (5m)

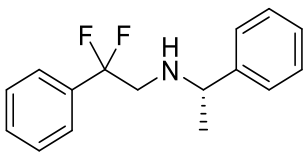

Compound **4m** was prepared using a literature procedure.[46] To a flame-dried glass vial in the glovebox was added nickel(II) triflate (4.63 mg, 5.0 mol%, 13.0 μmol), ((phenylphosphinediyl)bis(ethane-2,1-diyl))bis(diphenylphosphine) (8.32 mg, 6.0 mol%, 15.6 μmol), and degassed TFE (1.30 mL). The reaction mixture was stirred at rt in the box for 15 min; then, 2,2-difluoro-2-phenylacetonitrile (39.7 mg, 1.00 equiv 259 μmol) was added in one portion followed by (*S*)-(-)-1-phenylethylamine (167 μL, 5 equiv, 1.30 mmol). The vial was fitted with a

septum cap and needle, then placed into a parr bomb. The bomb was sealed, the assembly was removed from the glovebox, and the autoclave was flushed with 20 bar H_2 (2x) then pressurized to 40 bar H_2. The reaction mixture was stirred in a 130 °C heating block for 16 h. After this time, the reaction mixture was cooled, diluted with EtOAc, and extracted from aq. NaCl (sat.) with EtOAc (3x). The combined organic layers were dried over magnesium sulfate, filtered, and the filtrate concentrated *in vacuo*. The residue was purified by flash column chromatography (SiO_2, 20% EtOAc in hexanes) to afford pure (*S*)-2,2-difluoro-2-phenyl-N-(1-phenylethyl)ethan-1-amine (43.10 mg, 165 μmol, 64%) as a white solid.

^{1}H NMR (500 MHz, $CDCl_3$) δ 7.64 – 7.59 (m, 2H), 7.52 – 7.48 (m, 1H), 7.44 (t, J = 7.5 Hz, 2H), 7.40 – 7.33 (m, 2H), 7.30 – 7.27 (m, 3H), 6.64 (s, 1H), 5.10 (p, J = 7.2 Hz, 1H), 1.66 – 1.58 (m, 5H).

^{19}F NMR (470 MHz, $CDCl_3$) δ -102.3 (d, J = 43.7 Hz).

^{13}C{^{1}H} NMR (126 MHz, $CDCl_3$) δ 163.3 (t, J = 31.00 Hz), 141.9, 133.1 (t, J = 25.4 Hz), 131.00 (t, J = 2.0 Hz), 129.0, 128.7, 128.0, 126.3, 125.7 (t, J = 6.10 Hz), 115.0 (t, J = 252.9 Hz), 49.4, 21.5.

HRMS (EI) $[C_{16}H_{17}F_2N]$+ calc'd.: 276.1193, found: 276.1194.

4.7.9 Control Reactions with Benzyl Nitrile

Scheme S8. Control reaction with PhOH, HBr/AcOH, and the respective nitrile.

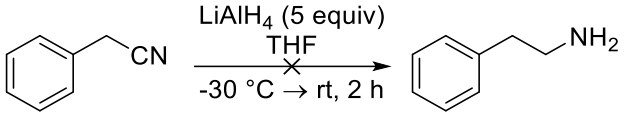

A 4 mL vial equipped with a stir bar was charged with 2,2-difluoro-2-phenylacetonitrile (76.6 mg, 1.0 equiv, 0.500 mmol) or benzyl nitrile (57.7 μL, 1.0 equiv, 0.500 mmol); to this vial was added a solution of phenol (94.1 mg, 2.0 equiv, 1.00 mmol) in 33% HBr in AcOH (1.50 g, 1.00 mL). The headspace was flushed with nitrogen, and the reslting solution was stirred for 30 minutes at room temperature. After this time the mixture was extracted with diethyl ether (3x), dried over Na_2SO4, and filtered. The organic was concentrated, and internal standard (mesitylene or α,α,α-trifluorotoluene) was added; the yield was determined by ^{1}H or ^{19}F qNMR spectroscopy.

Scheme S9. Control reaction with $LiAlH_4$ and benzyl nitrile.

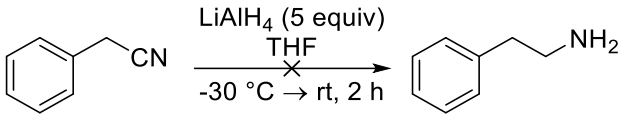

In a nitrogen-filled glovebox, solutions of $LiAlH_4$ (1.25 mL, 2.0 molar, 5.0 equiv, 2.50 mmol) and of benzyl nitrile (58.6 mg, 57.7 μL, 1 equiv, 0.500 mmol) in diethyl ether (1.00 mL) were prepared separately and cooled to -30 °C in the glovebox freezer. Once cool, the solution containing the nitrile was added dropwise via glass pipette to the solution containing the $LiAlH_4$ with stirring,

with an additional 0.50 mL diethyl ether used to complete the transfer. The vial was sealed and the reaction mixture was stirred vigorously at room temperature for 2 h. After this time, the rxn mixture was cooled to 0 °C, and water was added dropwise. The resulting solution was extracted with EtOAc (3x), then dried over magnesium sulfate. The resulting suspension was filtered, and the organics were concentrated *in vacuo*. There was no conversion as determined by ^{1}H qNMR spectroscopy with 1,3,5-trimethoxybenzene as internal standard. Analysis by GC-MS showed only starting material.

Scheme S10. Control reaction with 1-propanethiol and benzyl nitrile.

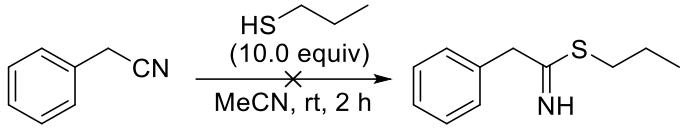

A 50 mL round bottom flask equipped with a stir bar was charged with Benzyl nitrile (58.6 mg, 57.7 µL, 1 Eq, 0.500 mmol) and MeCN (4.00 mL); the headspace was flushed with nitrogen, and 1-propanethiol (454 µL, 10.0 equiv, 5.00 mmol) was added dropwise. The resulting solution was stirred at rt for 2 h. After this time, the solvent was removed in vacuo. There was no conversion as determined by ^{1}H qNMR spectroscopy with 1,3,5-trimethoxybenzene as internal standard. Analysis by GC-MS showed only starting material.

Scheme S11. Control reaction with NH_2OH and benzyl nitrile.

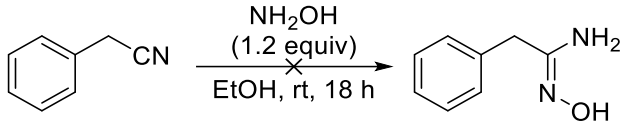

A 4 mL vial was equipped with a stir bar, benzyl nitrile (11.5 µL, 1.0 equiv, 0.10 mmol), and hydroxylamine (7.25 µL, 50% Wt in H_2O, 1.2 equiv, 120 µmol) followed by EtOH (1.00 mL). The resulting solution was stirred for 18h at rt. Then, the solvent was removed *in vacuo*. There was no conversion as determined by ^{1}H qNMR spectroscopy with 1,3,5-trimethoxybenzene as internal standard. Analysis by GC-MS showed only starting material.

Scheme S12. Control reaction with 2-aminothiophenol and benzyl nitrile.

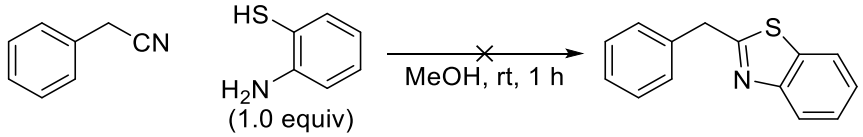

In a nitrogen-filled glovebox, a 20 mL vial was charged with benzyl nitrile (57.7 µL, 1.0 equiv, 0.50 mmol). A solution of 2-aminothiophenol (53.5 µL, 1.0 equiv, 0.50 mmol) in dry methanol (2.00 mL) was added, and the resulting mixture was stirred at rt for 1 h. After this time, the solvent was removed in vacuo. There was no conversion as determined by ^{1}H qNMR spectroscopy with 1,3,5-trimethoxybenzene as internal standard. Analysis by GC-MS showed only starting material.

Scheme S13. Control reaction with 2-aminothiophenol, $AlCl_3$, and benzyl nitrile.

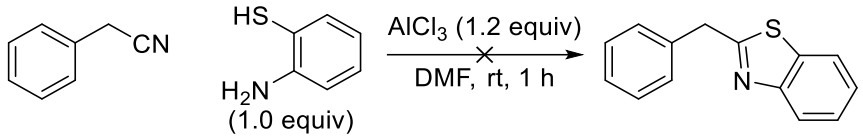

In a nitrogen-filled glovebox, a 20 mL vial was charged with benzyl nitrile (57.7 µL, 1.0 equiv, 0.50 mmol). A solution of 2-aminothiophenol (53.5 µL, 1.0 equiv, 0.50 mmol) in DMF (2.00 mL) was added. $AlCl_3$ (80.0 mg, 1.20 equiv, 0.60 mmol) in DMF (2.00 mL) was added dropwise to a solution of the thiol and benzyl nitrile at rt. The resulting solution was then stirred at rt for 1 h. After this time, the solvent was removed in vacuo. There was no conversion as determined by ^{1}H qNMR spectroscopy with 1,3,5-trimethoxybenzene as internal standard. Analysis by GC-MS showed only starting material.

4.7.10 Characterization Data of Isolated Products

2-((4-bromophenyl)difluoromethyl)-1-methyl-1H-benzo[d]imidazole (4a)

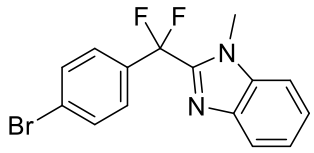

The title compound was prepared by performing general procedure 1 then general procedure 2 on 28.20 mg of the corresponding (hetero)aryl iodide: 18.40 mg, 55% yield (yellow oil).

^{1}H NMR (500 MHz, $CDCl_3$) δ 7.81 (d, J = 8.10 Hz, 1H), 7.64 (d, J = 8.3 Hz, 2H), 7.53 (d, J = 8.4 Hz, 2H), 7.43 – 7.38 (m, 2H), 7.31 (ddd, J = 8.3, 6.6, 1.6 Hz, 1H), 3.95 (t, J = 1.10 Hz, 3H).

^{19}F NMR (470 MHz, $CDCl_3$) δ -88.6.

^{13}C{^{1}H} NMR (126 MHz, $CDCl_3$) δ 146.8 (t, J = 33.2 Hz), 141.3, 136.5, 133.5 (t, J = 26.0 Hz), 131.8, 127.9 (t, J = 5.8 Hz), 125.5 (t, J = 2.5 Hz), 124.6, 122.9, 121.4, 117.1 (t, J = 239.7 Hz), 109.8, 31.1 (t, J = 3.9 Hz).

HRMS (ESI-TOF) $[C_{15}H_{11}BrF_2N_2+H]+$ calc'd.: 337.0146, found: 337.0145

2-((4-chlorophenyl)difluoromethyl)-1-methyl-1H-benzo[d]imidazole (4b)

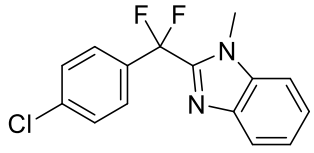

The title compound was prepared by performing general procedure 1 then general procedure 2 on 23.60 mg of the corresponding (hetero)aryl iodide: 20.10 mg, 69% yield (light yellow solid).

^{1}H NMR (500 MHz, $CDCl_3$) δ 7.82 (d, J = 8.2 Hz, 1H), 7.60 (d, J = 8.3 Hz, 2H), 7.48 (d, J = 8.3 Hz, 2H), 7.41 (q, J = 8.4 Hz, 2H), 7.31 (ddd, J = 8.2, 6.7, 1.5 Hz, 1H), 3.95 (s, 3H).

^{19}F NMR (470 MHz, $CDCl_3$) δ -88.4.

^{13}C{^{1}H} NMR (126 MHz, $CDCl_3$) δ 146.9 (t, J = 33.2 Hz), 141.3, 137.1 (t, J = 2.5 Hz), 136.4, 133.0 (t, J = 26.0 Hz), 128.9, 127.7 (t, J = 5.8 Hz), 124.6, 123.0, 121.4, 117.1 (t, J = 239.7 Hz), 109.8, 31.2 (t, J = 3.9 Hz).

HRMS (ESI-TOF) $[C_{15}H_{11}ClF_2N_2+H]+$ calc'd.: 293.0652, found: 293.0654

methyl 4-(difluoro(1-methyl-1H-benzo[d]imidazol-2-yl)methyl)benzoate (4c)

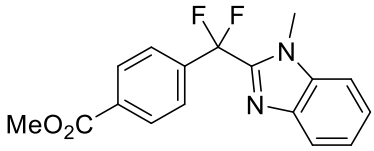

The title compound was prepared by performing general procedure 1 then general procedure 2 on 26.50 mg of the corresponding (hetero)aryl iodide: 18.50 mg, 58% yield (light brown solid).

^{1}H NMR (500 MHz, $CDCl_3$) δ 8.17 (d, J = 8.10 Hz, 2H), 7.80 (d, J = 8.2 Hz, 1H), 7.74 (d, J = 8.10 Hz, 2H), 7.43 – 7.38 (m, 2H), 7.31 (t, J = 7.4 Hz, 1H), 3.95 (s, 6H).

^{19}F NMR (470 MHz, $CDCl_3$) δ -89.4.

^{13}C{^{1}H} NMR (126 MHz, $CDCl_3$) δ 165.2, 145.7 (t, J = 27.7 Hz), 140.3, 137.7 (t, J = 21.4 Hz), 135.4, 131.4, 128.9, 125.3 (t, J = 5.0 Hz), 123.6, 121.9, 120.3, 116.0 (t, J = 200.10 Hz), 108.8, 51.4, 30.1 (t, J = 2.5 Hz).

HRMS (ESI-TOF) $[C_{17}H_{14}F_2N_2O_2+Na]+$ calc'd.: 339.0915, found: 339.0912

2-(difluoro(4-nitrophenyl)methyl)-1-methyl-1H-benzo[d]imidazole (4d, 4ae)

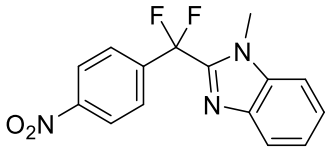

Compound **4d** was prepared by performing general procedure 1 then general procedure 2 on **24**.70 mg of the corresponding (hetero)aryl iodide: 11.30 mg, 38% yield (orange solid).

Compound **4ae** was prepared by performing general procedure 1 then general procedure 2 on **20**.1 mg of the corresponding (hetero)aryl bromide: 10.10 mg, 33% yield (orange solid).

^{1}H NMR (500 MHz, $CDCl_3$) δ 8.37 (d, J = 8.4 Hz, 2H), 7.88 (d, J = 8.4 Hz, 2H), 7.76 (d, J = 8.2 Hz, 1H), 7.46 – 7.40 (m, 2H), 7.31 (t, J = 7.6 Hz, 1H), 4.05 (s, 3H).

^{19}F NMR (470 MHz, $CDCl_3$) δ -89.1.

$^{13}C\{^{1}H\}$ NMR (126 MHz, $CDCl_3$) δ 149.4, 146.1 (t, J = 27.7 Hz), 141.2, 140.5 (t, J = 21.4 Hz), 136.5, 127.8 (t, J = 5.0 Hz), 124.9, 123.6, 123.1, 121.4, 118.4, 116.9 (t, J = 200.3 Hz), 109.9, 31.2 (t, J = 2.5 Hz).

HRMS (ESI-TOF) $[2(C_{15}H_{11}F_2N_3O_2)+H]+$ calc'd.: 607.1711, found: 607.1724

4-(cyanodifluoromethyl)benzonitrile (3e)

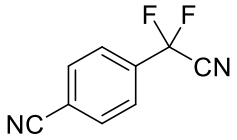

The title compound was prepared by performing general procedure 1 on 22.90 mg of the corresponding (hetero)aryl iodide: 13.10 mg, 74% yield (colorless oil). Flash column chromatography (SiO_2, 5% EtOAc in hexanes).

^{1}H NMR (400 MHz, $CDCl_3$) δ 7.88 (d, J = 8.8 Hz, 2H), 7.83 (d, J = 8.7 Hz, 2H).

$^{13}C\{^{1}H\}$ NMR (151 MHz, $CDCl_3$) δ 135.2 (t, J = 25.8 Hz), 133.1, 126.2 (t, J = 5.0 Hz), 117.0, 116.8, 111.6 (t, J = 47.9 Hz), 107.6 (t, J = 245.5 Hz).

^{19}F NMR (376 MHz, $CDCl_3$) δ -84.2.

HRMS (EI) $[C_9H_4F_2N_2]+$ calc'd.: 178.0343, found: 178.0340.

2-((4-butylphenyl)difluoromethyl)-1-methyl-1H-benzo[d]imidazole (4f)

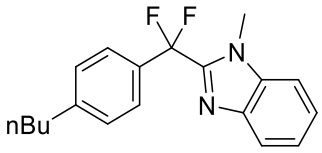

The title compound was prepared by performing general procedure 1 then general procedure 2 on 17.80 μL of the corresponding (hetero)aryl iodide: 27.60 mg, 88% yield (yellow oil).

^{1}H NMR (500 MHz, $CDCl_3$) δ 7.85 (d, J = 8.1 Hz, 1H), 7.53 (d, J = 8.0 Hz, 2H), 7.42 – 7.36 (m, 2H), 7.34 – 7.27 (m, 3H), 3.87 (d, J = 1.3 Hz, 3H), 2.66 (t, J = 7.8 Hz, 2H), 1.67 – 1.57 (m, 2H), 1.37 (h, J = 7.4 Hz, 2H), 0.93 (t, J = 7.4 Hz, 3H).

^{19}F NMR (470 MHz, $CDCl_3$) δ -88.3.

$^{13}C\{^{1}H\}$ NMR (126 MHz, $CDCl_3$) δ 146.1, 141.4. 136.5, 128.8, 126.1 (t, J = 6.3 Hz), 124.5, 123.0, 121.4, 109.9, 35.7, 33.4, 31.3, 22.5, 14.1

HRMS (ESI-TOF) $[2(C_{19}H_{20}F_2N_2)+H]+$ calc'd.: 629.3263, found 629.3246

2-(difluoro(phenyl)methyl)-1-methyl-1H-benzo[d]imidazole (4g)

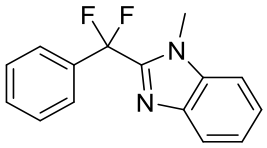

The title compound was prepared by performing general procedure 1 then general procedure 2 on 11.20 μL of the corresponding (hetero)aryl iodide: 21.00 mg, 82% yield (white solid).

^{1}H NMR (600 MHz, $CDCl_3$) δ 7.91 (d, J = 8.0 Hz, 1H), 7.67 (d, J = 6.5 Hz, 2H), 7.53 – 7.42 (m, 3H), 7.40 (m, 2H), 7.32 (m, 1H), 3.91 (s, 3H).

^{19}F NMR (470 MHz, $CDCl_3$) δ -89.0.

^{13}C{^{1}H} NMR (126 MHz, $CDCl_3$) δ 147.2 (t, J = 33.0 Hz), 141.2, 136.4, 134.5 (t, J = 25.6 Hz), 130.7 (t, J = 1.9 Hz), 128.5, 125.9 (t, J = 5.6 Hz), 124.2, 122.7, 121.1, 117.1 (t, J = 240.0 Hz), 109.7, 30.9

HRMS (EI) $[C_{13}H_{12}F_2]$+ calc'd.: 259.1039, found: 259.1041.

2-(difluoro(4-methoxyphenyl)methyl)-1-methyl-1H-benzo[d]imidazole (4h)

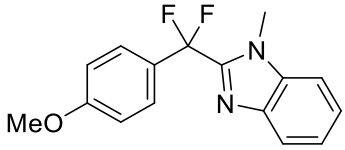

The title compound was prepared by performing general procedure 1 then general procedure 2 on 22.40 mg of the corresponding (hetero)aryl iodide: 22.50 mg, 74% yield (yellow oil).

^{1}H NMR (500 MHz, $CDCl_3$) δ 7.86 (d, J = 8.1 Hz, 1H), 7.55 (d, J = 8.4 Hz, 2H), 7.46 – 7.36 (m, 2H), 7.32 (ddd, J = 8.2, 6.4, 1.9 Hz, 1H), 6.98 (d, J = 8.5 Hz, 2H), 3.88 (s, 3H), 3.85 (s, 3H).

^{19}F NMR (470 MHz, $CDCl_3$) δ -87.2.

^{13}C{^{1}H} NMR (126 MHz, $CDCl_3$) δ 161.5 (t, J = 1.9 Hz), 147.7 (t, J = 33.6 Hz), 141.5, 136.5, 127.7 (t, J = 5.5 Hz), 126.8 (t, J = 26.2 Hz), 124.4, 122.9, 121.4, 117.4 (t, J = 239.3 Hz), 114.0, 109.8, 55.4, 31.2 (t, J = 3.4 Hz).

HRMS (ESI-TOF) $[2(C_{16}H_{14}F_2N_2O)+H]$+ calc'd.: 577.2221, found: 577.2194

tert-butyl (4-(difluoro(1-methyl-1H-benzo[d]imidazol-2-yl)methyl)phenyl)carbamate (4i)

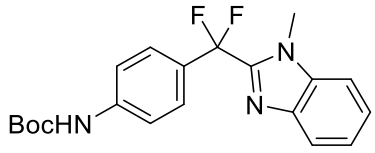

The title compound was prepared by performing general procedure 1 then general procedure 2 on 31.50 mg of the corresponding (hetero)aryl iodide: 15.10 mg, 41% yield (yellow oil).

^{1}H NMR: (500 MHz, CDCl3) δ 7.83 (d, J = 8.10 Hz, 1H), 7.53 (d, J = 8.9 Hz, 2H), 7.46 (d, J = 8.5 Hz, 2H), 7.41 – 7.36 (m, 2H), 7.31 (ddd, J = 8.2, 6.3, 1.8 Hz, 1H), 3.86 (s, 3H), 1.51 (s, 9H).

^{19}F NMR (470 MHz, $CDCl_3$) δ -88.0.

^{13}C{^{1}H} NMR (126 MHz, $CDCl_3$) δ 152.4, 147.5, 141.4, 140.8, 136.4, 128.7, 127.0 (t, J = 5.5 Hz), 124.3, 122.8, 121.3, 118.0, 109.7, 81.0, 31.1, 28.3, 14.2.

HRMS (ESI-TOF) [2($C_{20}H_{21}F_2N_3O_2$)+Na]+ calc'd.: 769.3096, found 769.3129

2-(4'-bromo-[1,1'-biphenyl]-4-yl)-2,2-difluoroacetonitrile (3j)

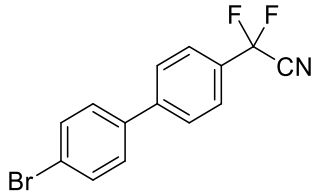

The title compound was prepared by performing general procedure 1 on 35.0 mg of the corresponding (hetero)aryl iodide: 22.6 mg, 75% yield (white solid).

^{1}H NMR (500 MHz, $CDCl_3$) δ 7.7 (d, J = 8.4 Hz, 2H), 7.7 (d, J = 8.4 Hz, 2H), 7.6 (d, J = 8.6 Hz, 1H), 7.5 (d, J = 8.5 Hz, 2H).

^{19}F NMR (470 MHz, $CDCl_3$) δ -82.9.

^{13}C{^{1}H} NMR (126 MHz, $CDCl_3$) δ 144.8 – 144.2 (m), 138.4, 138.1, 132.4, 130.5 (t, J = 25.3 Hz), 129.0, 127.9, 126.1 (t, J = 4.9 Hz), 123.1, 112.7 (t, J = 48.3 Hz), 108.9 (t, J = 243.0 Hz).

HRMS (ESI-TOF) [2($C_{14}H_8BrF_2N$)+ACN+H]+ calc'd.: 655.9954, found: 655.9933

2-(difluoro(2-isopropylphenyl)methyl)benzo[d]oxazole (4k)

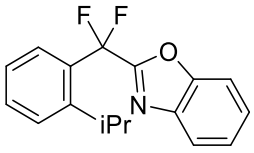

The title compound was prepared by performing general procedure 1 then general procedure 3 on 15.9 μL of the corresponding (hetero)aryl iodide: 18.80 mg, 65% yield (white solid).

^{1}H NMR (500 MHz, $CDCl_3$) δ 7.83 – 7.79 (m, 1H), 7.71 (dd, J = 8.0, 1.5 Hz, 1H), 7.60 (dd, J = 8.0, 1.3 Hz, 1H), 7.52 (t, J = 7.6 Hz, 1H), 7.49 – 7.43 (m, 2H), 7.41 (td, J = 7.7, 1.2 Hz, 1H), 7.36 – 7.31 (m, 1H), 3.15 (dq, J = 8.1, 6.6 Hz, 1H), 1.12 (d, J = 6.8 Hz, 6H).

^{19}F NMR (470 MHz, $CDCl_3$) δ -90.9.

^{13}C{^{1}H} NMR (126 MHz, $CDCl_3$) δ 159.0 (t, J = 29.6 Hz), 150.7, 148.3 (t, J = 2.4 Hz), 140.1, 131.5, 130.2 (t, J = 18.9 Hz), 127.3, 126.8, 125.9, 125.7 (t, J = 7.7 Hz), 125.3, 121.4, 114.9 (t, J = 202.9 Hz), 111.4, 29.8, 24.1.

HRMS (ESI-TOF) $[C_{17}H_{15}F_2NO+H]+$ calc'd.: 288.1194, found: 288.1196

2-((2,6-dichlorophenyl)difluoromethyl)benzo[d]thiazolecarboxylate (4l)

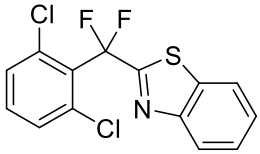

The title compound was prepared by performing general procedure 1 then general procedure 4 on 26.50 mg of the corresponding (hetero)aryl iodide: 21.30 mg, 66% yield (white solid).

^{1}H NMR (500 MHz, $CDCl_3$) δ 8.08 – 8.03 (m, 1H), 8.00 – 7.95 (m, 1H), 7.55 – 7.46 (m, 2H), 7.44 (q, J = 0.9 Hz, 1H), 7.43 (d, J = 1.1 Hz, 1H), 7.33 (ddt, J = 8.5, 7.4, 0.9 Hz, 1H).

^{19}F NMR (470 MHz, $CDCl_3$) δ -79.8.

^{13}C{^{1}H} NMR (126 MHz, $CDCl_3$) δ 164.3 (t, J = 34.7 Hz), 152.5, 135.6, 135.3 (t, J = 2.6 Hz), 131.7, 130.9, 130.1 (t, J = 23.4 Hz), 126.8 (d, J = 9.7 Hz), 124.9, 122.1, 117.4 (t, J = 246.0 Hz).

HRMS (ESI-TOF) $[C_{14}H_7Cl_2F_2NS+H]+$ calc'd.: 329.9717, found: 329.9720

2-((2-ethyl-6-methylphenyl)difluoromethyl)benzo[d]thiazole (4m)

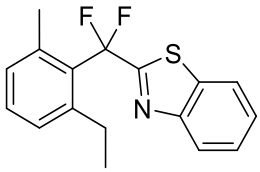

The title compound was prepared by performing general procedure 1 then general procedure 4 on 24.10 mg of the corresponding (hetero)aryl iodide: 20.20 mg, 68% yield (clear oil).

^{1}H NMR (500 MHz, $CDCl_3$) δ 8.09 (d, J = 8.1 Hz, 1H), 7.94 (d, J = 8.0 Hz, 1H), 7.55 – 7.44 (m, 2H), 7.32 (t, J = 7.6 Hz, 1H), 7.18 (d, J = 7.7 Hz, 1H), 7.12 (d, J = 7.6 Hz, 1H), 2.80 – 2.71 (m, 2H), 2.47 (t, J = 4.6 Hz, 4H), 1.23 (t, J = 7.5 Hz, 3H).

^{19}F NMR (470 MHz, $CDCl_3$) δ -76.8.

^{13}C{^{1}H} NMR (126 MHz, $CDCl_3$) δ 165.8 (t, J = 36.10 Hz), 152.8, 144.4 (t, J = 2.8 Hz), 137.8 (t, J = 3.10 Hz), 135.6, 131.3 (t, J = 22.7 Hz), 130.4 (d, J = 10.3 Hz), 129.2, 126.7 (d, J = 7.2 Hz), 124.9, 122.0, 119.9 (t, J = 243.7 Hz), 28.5 (t, J = 5.2 Hz), 22.8 (t, J = 6.3 Hz), 16.9 (d, J = 2.2 Hz).

HRMS (ESI-TOF) [$C_{17}H_{15}F_2NS$+H]+ calc'd.: 304.0966, found: 304.0969

1-(3-(benzo[d]oxazol-2-yldifluoromethyl)phenyl)ethan-1-one (4n)

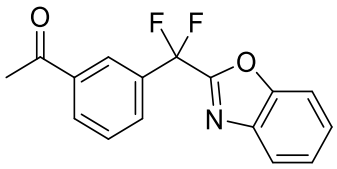

The title compound was prepared by performing general procedure 1 then general procedure 3 on 24.40 mg of the corresponding (hetero)aryl iodide: 15.30 mg, 53% yield (yellow solid). flash column chromatography (SiO_2, 30% EtOAc in hexanes).

^{1}H NMR (500 MHz, $CDCl_3$) δ 8.31 (t, J = 1.9 Hz, 1H), 8.12 (dt, J = 8.1, 1.3 Hz, 1H), 7.93 (dt, J = 8.1, 1.5 Hz, 1H), 7.83 – 7.78 (m, 1H), 7.66 – 7.58 (m, 2H), 7.49 – 7.38 (m, 2H), 2.65 (s, 3H).

^{19}F NMR (470 MHz, $CDCl_3$) δ -95.2.

^{13}C{^{1}H} NMR (126 MHz, $CDCl_3$) δ 196.9, 158.0 (t, J = 36.5 Hz), 150.8, 140.0, 137.6, 134.3, 130.9, 130.2 (t, J = 5.10 Hz), 129.3, 127.0, 125.7 (t, J = 6.3 Hz), 121.5, 114.0 (t, J = 244.5 Hz), 111.5, 26.7.

HRMS (ESI-TOF) [2($C_{16}H_{11}F_2NO_2$)+Na]+ calc'd.: 597.1408, found: 597.1383

2-([1,1'-biphenyl]-3-yldifluoromethyl)benzo[d]oxazole (4o)

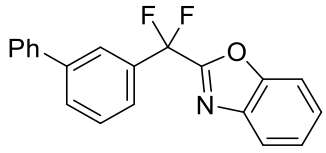

The title compound was prepared by performing general procedure 1 then general procedure 3 on 17.2 μL of the corresponding (hetero)aryl iodide: 21.70 mg, 68% yield (yellow oil).

^{1}H NMR (500 MHz, $CDCl_3$) δ 7.95 (d, J = 1.9 Hz, 1H), 7.85 – 7.81 (m, 1H), 7.77 – 7.73 (m, 1H), 7.71 (dt, J = 7.9, 1.4 Hz, 1H), 7.63 – 7.56 (m, 4H), 7.49 – 7.37 (m, 5H).

^{19}F NMR (470 MHz, $CDCl_3$) δ -95.2.

^{13}C{^{1}H} NMR (126 MHz, $CDCl_3$) δ 158.5 (t, J = 30.2 Hz), 158.8, 142.0, 140.1, 140.0, 134.2 (t, J = 21.4 Hz), 129.9, 129.2, 128.9, 127.9, 127.3, 126.8, 125.3, 124.4, 121.4, 116.3, 114.5 (t, J = 204.10 Hz), 111.4.

HRMS (ESI-TOF) $[C_{20}H_{13}F_2NO+H]+$ calc'd.: 322.1039, found: 322.1038

2-((3-(tert-butyl)phenyl)difluoromethyl)benzo[d]oxazole (4p)

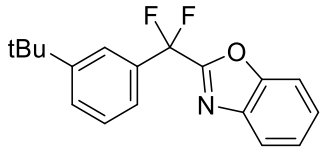

The title compound was prepared by performing general procedure 1 then general procedure 3 on 17.70 μL of the corresponding (hetero)aryl iodide: 22.20 mg, 74% yield (light yellow solid).

^{1}H NMR (500 MHz, $CDCl_3$) δ 7.83 (d, J = 7.8 Hz, 1H), 7.75 (s, 1H), 7.60 (d, J = 8.0 Hz, 1H), 7.54 (dd, J = 14.0, 7.8 Hz, 2H), 7.42 (dd, J = 11.7, 7.4 Hz, 3H), 1.35 (s, 9H).

^{19}F NMR (470 MHz, $CDCl_3$) δ -95.0.

^{13}C{1H} NMR (126 MHz, $CDCl_3$) δ 158.8 (t, *J* = 37.2 Hz), 152.1, 150.9, 140.3, 133.4 (t, J = 25.6 Hz), 128.6, 128.4, 126.8, 125.4, 123.1 (t, J = 5.8 Hz), 122.4 (t, J = 5.9 Hz), 121.5, 114.8 (t, J = 243.8 Hz), 111.5, 35.1, 31.4.

HRMS (ESI-TOF) $[C_{18}H_{17}F_2NO+H]+$ calc'd.: 302.1351, found: 302.1354

2,2-difluoro-2-(naphthalen-1-yl)acetonitrile (3q)

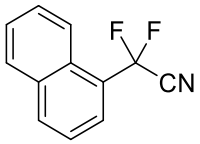

The title compound was prepared by performing general procedure 1 on 14.6 µL of the corresponding (hetero)aryl iodide: 19.70 mg, 63% yield (clear oil). The spectra correspond to those previously reported.[25]

^{1}H NMR (600 MHz, $CDCl_3$) δ 8.23 (dtd, J = 8.6, 2.2, 1.1 Hz, 1H), 8.08 (d, J = 8.3 Hz, 1H), 7.99 – 7.91 (m, 2H), 7.69 (ddd, J = 8.5, 6.9, 1.4 Hz, 1H), 7.63 (ddd, J = 8.0, 6.9, 1.1 Hz, 1H), 7.55 (t, J = 7.8 Hz, 1H).

^{19}F NMR (470 MHz, $CDCl_3$) δ -81.7.

^{13}C{^{1}H} NMR (151 MHz, $CDCl_3$) δ 134.2, 133.9, 129.3, 128.7, 128.3, 127.2, 126.3 (t, J = 23.3 Hz), 125.5 (t, J = 8.0 Hz), 124.4, 123.6 (t, J = 2.7 Hz), 112.9 (t, J = 47.8 Hz), 109.8 (t, J = 243.4 Hz).

2,2-difluoro-2-(naphthalen-2-yl)acetonitrile (3r)

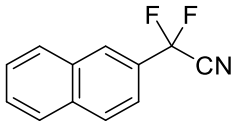

The title compound was prepared by performing general procedure 1 on 25.40 mg of the corresponding (hetero)aryl iodide: 15.40 mg, 76% yield (clear oil).

^{1}H NMR (500 MHz, $CDCl_3$) δ 8.21 (s, 1H), 8.01 – 7.92 (m, 3H), 7.68 – 7.61 (m, 3H)

^{19}F NMR (470 MHz, $CDCl_3$) δ -82.3

^{13}C{^{1}H} NMR (126 MHz, $CDCl_3$) δ 134.9, 132.2, 129.7, 129.0, 128.7, 128.3, 128.0, 127.6, 126.3 (t, J = 6.3 Hz), 120.7 (t, J = 3.8 Hz), 112.6 (t, J = 47.9 Hz), 109.2 (t, J = 243.2 Hz).

HRMS (ESI-TOF) $[C_{12}H_7F_2N+H]+$ calc'd.: 204.0571, found: 204.0580

2-(dibenzo[b,d]furan-4-yldifluoromethyl)benzo[d]thiazole (3s)

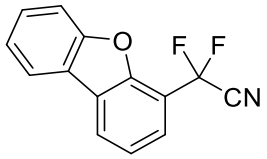

The title compound was prepared by performing general procedure 1 on 27.30 mg of the corresponding (hetero)aryl iodide: 18.50 mg, 82% yield (white solid).

^{1}H NMR (500 MHz, $CDCl_3$) δ 8.18 (dq, J = 7.8, 1.2 Hz, 1H), 8.00 (dt, J = 7.6, 0.9 Hz, 1H), 7.71 (ddt, J = 12.3, 8.3, 1.0 Hz, 2H), 7.56 (ddd, J = 8.5, 7.3, 1.4 Hz, 1H), 7.47 (t, J = 7.8 Hz, 1H), 7.43 (td, J = 7.6, 1.0 Hz, 1H).

^{19}F NMR (470 MHz, $CDCl_3$) δ -85.1

^{13}C{^{1}H} NMR (126 MHz, $CDCl_3$) δ 156.6, 152.1 (t, J = 2.5 Hz), 128.5, 126.4, 125.2 (t, J = 1.3 Hz), 123.7, 123.5 (t, J = 6.3 Hz), 122.8, 122.7, 120.9, 115.4 (t, J = 26.5 Hz), 112.3 (t, J = 244.5 Hz), 107.0.

HRMS (ESI-TOF) [$C_{14}H_7F_2NO$+H]+ calc'd.: 244.0529, found: 244.0529

2-(6-((2,5,8,11-tetraoxatridecan-13-yl)oxy)pyridin-3-yl)-2,2-difluoroacetonitrile (3t)

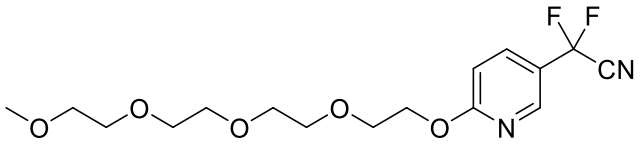

The title compound was prepared by performing general procedure 1 on 37.90 mg of the corresponding (hetero)aryl iodide: 18.50 mg, 59% yield (clear oil).

^{1}H NMR (500 MHz, $CDCl_3$) δ 8.47 (s, 1H), 7.79 (dd, *J* = 8.7, 2.7 Hz, 1H), 6.91 (d, *J* = 8.9 Hz, 1H), 4.54 (t, J = 5.0 Hz, 2H), 3.86 (t, J = 5.0 Hz, 2H), 3.72 – 3.63 (m, 10H), 3.55 – 3.53 (m, 2H), 3.37 (s, 3H).

^{19}F NMR (470 MHz, $CDCl_3$) δ -82.0.

^{13}C{^{1}H} NMR (126 MHz, $CDCl_3$) δ 166.2, 145.2 (t, J = 6.3 Hz), 135.4 (t, J = 3.8 Hz), 120.7 (t, J = 26.5 Hz), 112.1, 108.2 (t, J = 243.2 Hz), 71.9, 70.7 (t, J = 16.4 Hz), 69.3, 59.0.

HRMS (ESI-TOF) [$C_{14}H_{18}F_2N_2O_4$+H]+ calc'd.: 361.1567, found: 361.1570

2,2-difluoro-2-(1',3',5'-triphenyl-1'H-[1,4'-bipyrazol]-4-yl)acetonitrile (3u)

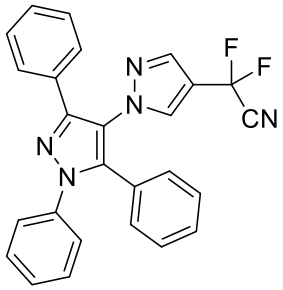

The title compound was prepared by performing general procedure 1 on 15.70 mg of the corresponding (hetero)aryl iodide: 5.00 mg, 36% yield (orange solid).

^{1}H NMR (500 MHz, $CDCl_3$) δ 8.01 (d, J = 0.9 Hz, 1H), 7.68 (q, J = 1.2 Hz, 1H), 7.47 – 7.43 (m, 2H), 7.40 – 7.31 (m, 10H), 7.30 – 7.24 (m, 2H), 7.16 – 7.12 (m, 2H).

^{19}F NMR (470 MHz, $CDCl_3$) δ -77.2.

^{13}C{^{1}H} NMR (126 MHz, $CDCl_3$) δ 147.7, 146.1, 141.1, 139.4, 138.2 (t, J = 3.8 Hz), 137.0, 132.9 (t, J = 5.0 Hz), 130.3, 129.5, 129.3, 129.2, 129.1, 128.9, 128.8, 128.7, 128.6, 128.2

HRMS (ESI-TOF) [$C_{26}H_{17}F_2N_5$+H]+ calc'd.: 438.1527, found: 438.1537

2-(7-(diethylamino)-4-methyl-2-oxo-2H-chromen-3-yl)-2,2-difluoroacetonitrile (3v)

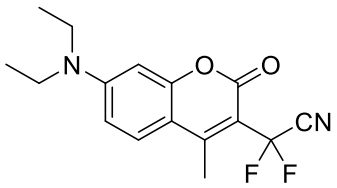

The title compound was prepared by performing general procedure 1 on 34.50 mg of the corresponding (hetero)aryl iodide: 11.30 mg, 38% yield (yellow solid). flash column chromatography (SiO_2, 20 – 40% EtOAc in hexanes).

^{1}H NMR (500 MHz, $CDCl_3$) δ 7.57 (d, J = 9.3 Hz, 1H), 6.65 (dd, J = 9.3, 2.7 Hz, 1H), 6.47 (d, J = 2.6 Hz, 1H), 3.45 (q, J = 7.1 Hz, 4H), 2.58 (t, J = 3.3 Hz, 3H), 1.23 (t, J = 7.2 Hz, 6H).

^{19}F NMR (470 MHz, $CDCl_3$) δ -78.3.

^{13}C{^{1}H} NMR (126 MHz, $CDCl_3$) δ 158.7, 156.1, 155.7, 152.4, 127.4, 112.6, 110.1, 109.7, 108.2, 108.1, 97.0, 45.0, 14.9, 12.4.

HRMS (ESI-TOF) [$C_{16}H_{16}F_2N_2O_2$+H]+ calc'd.: 307.1253, found: 307.1258

2,2-difluoro-2-(7-isopropoxy-4-oxo-3-phenyl-4H-chromen-8-yl)acetonitrile (3w)

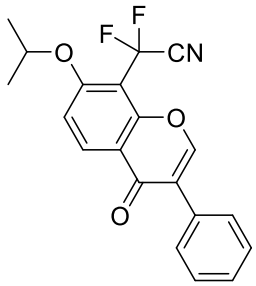

The title compound was prepared by performing general procedure 1 on 40.60 mg of the corresponding (hetero)aryl iodide: 33.10 mg, 93% yield (white solid).

^{1}H NMR (500 MHz, $CDCl_3$) δ 8.49 (dt, J = 9.0, 1.0 Hz, 1H), 8.01 (s, 1H), 7.58 – 7.53 (m, 2H), 7.48 – 7.38 (m, 3H), 7.15 – 7.10 (m, 1H), 4.93 (p, J = 6.1 Hz, 1H), 1.51 (d, J = 6.1 Hz, 6H).

^{19}F NMR (470 MHz, $CDCl_3$) δ -81.3.

^{13}C{^{1}H} NMR (126 MHz, $CDCl_3$) δ 174.6, 160.9 (t, J = 3.8 Hz), 154.9, 152.4, 132.6, 131.0, 128.9, 128.6, 128.5, 125.6, 118.6, 112.9 (t, J = 46.6 Hz), 111.2, 106.9, 106.6, 73.7, 21.6.

HRMS (ESI-TOF) [$C_{20}H_{15}F_2NO_3$+H]+ calc'd.: 356.1093, found: 356.1100

Methyl-(S)-2-((tert-butoxycarbonyl)amino)-3-(4-(cyanodifluoromethyl)phenyl)propanoate (3x)

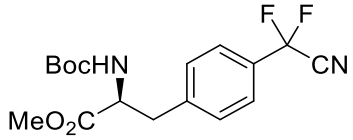

The title compound was prepared by performing general procedure 1 on 39.70 mg of the corresponding (hetero)aryl iodide: 12.60 mg, 36% yield (light orange solid).

^{1}H NMR (500 MHz, $CDCl_3$) δ 7.61 (dd, J = 8.5, 6.8 Hz, 2H), 7.31 (d, J = 7.9 Hz, 2H), 6.87 (d, J = 7.9 Hz, 1H), 5.10 – 4.90 (m, 1H), 4.68 – 4.54 (m, 1H), 3.73 (d, J = 11.4 Hz, 3H), 3.29 – 3.03 (m, 1H), 1.41 (d, J = 4.0 Hz, 9H).

^{19}F NMR (470 MHz, $CDCl_3$) δ -82.7.

^{13}C{^{1}H} NMR (126 MHz, $CDCl_3$) δ 172.0, 171.8, 154.9, 141.5, 137.6, 135.7, 131.f3, 130.3, 125.4, 80.3, 54.1, 52.4, 38.3, 28.2.

HRMS (ESI-TOF) [$C_{17}H_{20}F_2N_2O_4$+H]+ calc'd.: 627.1125, found: 627.1153

2,2-difluoro-2-(4-(5-(p-tolyl)-3-(trifluoromethyl)-1H-pyrazol-1-yl)phenyl)acetonitrile (3y)

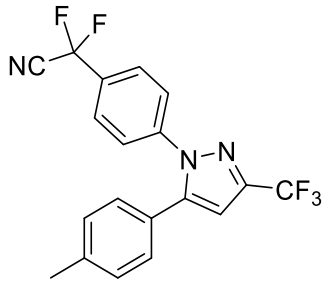

The title compound was prepared by performing general procedure 1 on 46.70 mg of the corresponding (hetero)aryl iodide: 30.8 mg, 75% yield (white solid).

^{1}H NMR (500 MHz, $CDCl_3$) δ 7.67 (d, J = 8.4 Hz, 2H), 7.52 (d, J = 8.5 Hz, 2H), 7.20 (d, J = 7.9 Hz, 2H), 7.13 (d, J = 8.2 Hz, 2H), 2.39 (s, 3H).

^{19}F NMR (470 MHz, $CDCl_3$) δ -62.3, -83.1.

^{13}C{^{1}H} NMR (126 MHz, $CDCl_3$) δ 145.3, 144.3 (q, J = 38.6 Hz), 142.8 (t, J = 2.0 Hz), 140.0, 130.8 (t, J = 25.6 Hz), 129.9, 128.9, 126.4 (t, J = 5.0 Hz), 125.9, 125.8, 121.2 (q, J = 269.10 Hz), 112.3 (t, J = 48.0 Hz), 108.4, 106.5 (q, J = 2.0 Hz), 21.5.

HRMS (ESI-TOF) $[C_{19}H_{12}F_5N_3+H]+$ calc'd.: 378.1024, found: 378.1028

2,2-difluoro-2-(3-(3-(4-fluoro-2-methoxyphenoxy)prop-1-yn-1-yl)phenyl)acetonitrile (3z)

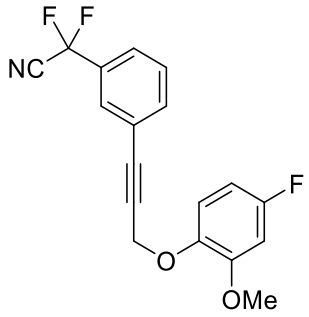

The title compound was prepared by performing general procedure 1 on 37.0 mg of the corresponding (hetero)aryl iodide: 18.0 mg, 57% yield (white solid).

^{1}H NMR (500 MHz, $CDCl_3$) δ 7.7 – 7.7 (m, 1H), 7.6 – 7.6 (m, 2H), 7.5 (t, J = 7.8 Hz, 1H), 7.0 (dd, J = 8.9, 5.4 Hz, 1H), 6.7 (dd, J = 10.1, 2.9 Hz, 1H), 6.6 (ddd, J = 8.8, 8.0, 2.9 Hz, 1H), 4.9 (s, 2H), 3.9 (s, 3H).

^{19}F NMR (470 MHz, $CDCl_3$) δ -83.7, -118.3 (td, J = 9.0, 5.6 Hz).

^{13}C{^{1}H} NMR (126 MHz, $CDCl_3$) δ 159.3, 157.7, 151.1 (d, J = 8.8 Hz), 143.0, 135.6, 131.7 (t, J = 21.4 Hz), 129.4, 128.5(t, J = 3.8 Hz), 125.1(t, J = 3.8 Hz), 123.9, 116.3 (d, J = 8.8 Hz), 112.2 (t, J = 40.3 Hz), 108.2 (t, J = 204.10 Hz), 106.0 (d, J = 12.6 Hz), 100.5 (d, J = 22.7 Hz), 86.3, 85.5, 58.3, 56.0.

HRMS (ESI-TOF) $[C_{18}H_{12}F_3NO_2+H]+$ calc'd.: 332.0893, found: 332.0893

2,5,7,8-tetramethyl-2-(4,8,12-trimethyltridecyl)chroman-6-yl-4-(cyanodifluoromethyl) benzoate (3aa)

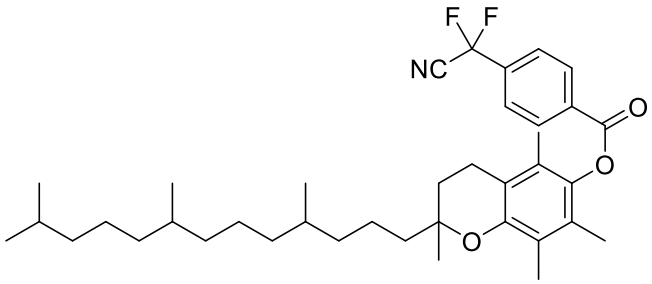

The title compound was prepared by performing general procedure 1 on 62.10 mg of the corresponding (hetero)aryl iodide: 39.20 mg, 68% yield (clear oil). Prep TLC (5% EtOAc in Pentanes).

^{1}H NMR (500 MHz, $CDCl_3$) δ 8.42 (d, J = 8.2 Hz, 2H), 7.85 (d, J = 8.2 Hz, 2H), 2.63 (t, J = 6.8 Hz, 2H), 2.14 (s, 3H), 2.06 (s, 3H), 2.02 (s, 3H), 1.90 – 1.75 (m, 2H), 1.67 – 1.02 (m, 24H), 0.87 (dd, J = 8.6, 6.5 Hz, 12H).

^{19}F NMR (470 MHz, $CDCl_3$) δ -84.4

^{13}C{^{1}H} NMR (126 MHz, $CDCl_3$) δ 163.7, 149.8, 140.4, 135.5 (t, J = 25.2 Hz), 133.7, 131.0, 126.6, 125.7 (t, J = 5.0 Hz), 124.9, 123.4, 117.7, 112.1 (t, J = 47.9 Hz), 108.3 (t, J = 244.4 Hz), 75.2, 39.4, 37.4, 37.3, 32.8, 28.0, 24.8, 24.5, 22.7, 22.6, 21.1, 20.7, 19.7, 13.1, 12.2, 11.9.

HRMS (ESI-TOF) $[C_{38}H_{53}F_2NO_3+H]+$ calc'd.: 610.4066, found: 610.4075

(1S,2R,5R)-2-isopropyl-5-methylcyclohexyl 4-(cyanodifluoromethyl)benzoate (3ab)

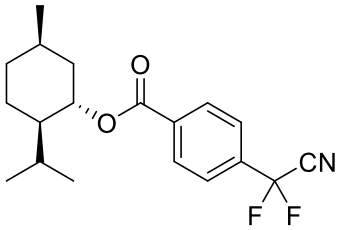

The title compound was prepared by performing general procedure 1 on 41.70 mg of the corresponding (hetero)aryl iodide: 20.40 mg, 56% yield (white solid). Flash column chromatography (SiO_2, 2 – 10% EtOAc in hexanes).

^{1}H NMR (500 MHz, CDCl3) δ 8.21 (dq, J = 7.8, 0.9 Hz, 2H), 7.76 (dq, J = 7.7, 0.9 Hz, 2H), 5.34 (td, J = 6.4, 3.3 Hz, 1H), 2.01 – 1.91 (m, 1H), 1.86 – 1.46 (m, 7H), 1.34 – 1.24 (m, 1H), 0.99 (dd, J = 9.5, 6.8 Hz, 6H), 0.90 (d, J = 6.8 Hz, 3H).

^{19}F NMR (470 MHz, CDCl3) δ -84.2.

$^{13}C\{^{1}H\}$ NMR (126 MHz, CDCl3) δ 164.4, 135.0 (d, J = 2.4 Hz), 134.8, 134.6, 130.4, 125.4 (t, J = 5.0 Hz), 112.2 (t, J = 47.9 Hz), 108.3 (t, J = 244.0 Hz), 73.6, 45.7, 35.7, 29.9, 27.7, 26.5, 21.3, 20.9, 20.7, 19.3.

HRMS (EI) $[C_{19}H_{23}F_2NO_2]$+ calc'd.: 335.1652, found: 335.1661

2-(2-(1H-pyrazol-1-yl)phenyl)-2,2-difluoroacetonitrile (3ac)

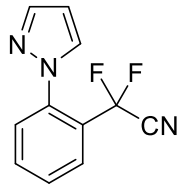

The title compound was prepared by performing general procedure 1 on 34.50 mg of the corresponding (hetero)aryl bromide: 14.90 mg, 44% (viscous clear oil).

^{1}H NMR (500 MHz, $CDCl_3$) δ 7.74 (d, J = 1.9 Hz, 1H), 7.35 (dd, J = 8.0, 1.5 Hz, 1H), 7.15 (d, J = 2.4 Hz, 1H), 6.87 (t, J = 7.6 Hz, 1H), 6.83 – 6.74 (m, 2H), 6.19 (t, J = 2.2 Hz, 1H).

^{19}F NMR (470 MHz, $CDCl_3$) δ -81.3.

$^{13}C\{^{1}H\}$ NMR (126 MHz, $CDCl_3$) δ 141.8, 139.0, 131.4 (d, J = 286.8 Hz), 126.8 (t, J = 7.8 Hz), 126.4, 112.4 (t, J = 46.4 Hz), 109.0, 108.0, 107.1, 105.2, 29.9.

HRMS (ESI-TOF) $[C_{11}H_7F_2N_3+H]$+ calc'd.: 220.0681, found: 220.0681

2,2-difluoro-2-(2-methoxy-4-nitrophenyl)acetonitrile (3ad)

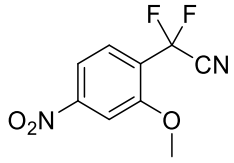

The title compound was prepared by performing general procedure 1 on 24.20 mg of the corresponding (hetero)aryl bromide: 9.50 mg, 42% yield (white solid).

^{1}H NMR (500 MHz, $CDCl_3$) δ 7.94 (dd, J = 8.6, 2.1 Hz, 1H), 7.89 (d, J = 2.0 Hz, 1H), 7.77 (d, J = 8.5 Hz, 1H), 4.10 (s, 3H).

^{19}F NMR (470 MHz, $CDCl_3$) δ -89.1.

$^{13}C\{^{1}H\}$ NMR (126 MHz, $CDCl_3$) δ 158.1, 151.7, 127.3 (t, J = 7.6 Hz), 124.9 (t, J = 25.2 Hz), 115.5, 111.8 (t, J = 46.6 Hz), 107.2, 105.5 (t, J = 244.4 Hz), 56.9

HRMS (ESI-TOF) $[C_9H_6F_2N_2O_3+H]$+ calc'd.: 229.0376, found: 229.0375

2-(4-acetylphenyl)-2,2-difluoroacetonitrile (3af)

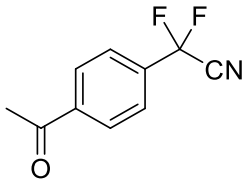

The title compound was prepared by performing General Procedure 1 on 24.60 mg of the corresponding (hetero)Aryl bromide: 3.10 mg, 16% yield (5.90 mg, clear oil)

^{1}H NMR (500 MHz, $CDCl_3$) δ 8.11 (dt, *J* = 8.9, 0.9 Hz, 1H), 7.79 (dt, *J* = 7.9, 0.9 Hz, 1H), 2.66 (s, 2H).

^{19}F NMR (470 MHz, $CDCl_3$) δ -84.3.

^{13}C NMR{^{1}H} (126 MHz, $CDCl_3$) δ 196.6, 140.5 – 139.9 (m), 135.1 (t, J = 25.2 Hz), 129.1, 125.7 (t, J = 5.0 Hz), 112.1 (t, J = 47.7 Hz), 108.2 (t, J = 244.1 Hz), 26.8.

HRMS (ESI-TOF) [$C_{10}H_7F_2NO$+H]+ calc'd.: 196.0527, found 196.0527

2,2-difluoro-2-(pyridin-2-yl)acetonitrile (3ag)

The title compound was prepared by performing general procedure 1 on 9.60 μL of the corresponding (hetero)aryl bromide: 24.0 mg, 77% yield (clear oil).

^{1}H NMR (600 MHz, $CDCl_3$) δ 8.75 (d, J = 4.6 Hz, 1H), 7.93 (t, J = 7.8 Hz, 1H), 7.71 (d, J = 7.9

Hz, 1H), 7.54 (dd, J = 7.6, 4.9 Hz, 1H)

^{19}F NMR (376 MHz, $CDCl_3$) δ -86.6.

^{13}C{^{1}H} NMR (151 MHz, $CDCl_3$) δ 150.2, 149.4 (t, J = 28.1

Hz), 138.1 (d, J = 2.9 Hz), 127.1, 120.1 (t, J = 2.6 Hz), 112.1 (t, J = 45.4 Hz), 108.3 (t, J = 244.5 Hz)

HRMS (ESI-TOF) [$C_7H_4F_2N_2$+H]+ calc'd.: 155.0415, found: 155.0414

2,2-difluoro-2-(quinolin-2-yl)acetonitrile (3ah)

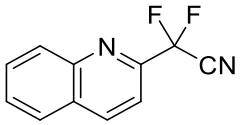

The title compound was prepared by performing general procedure 1 on 20.0 mg of the corresponding (hetero)aryl bromide: 11.0 mg, 56% yield (yellow solid).

^{1}H NMR (500 MHz, $CDCl_3$) δ 8.33 (d, J = 8.5 Hz, 1H), 8.19 (dd, J = 8.5, 1.2 Hz, 1H), 7.86 (dd, J = 8.2, 1.4 Hz, 1H), 7.79 (ddd, J = 8.4, 6.9, 1.5 Hz, 1H), 7.68 (d, J = 8.6 Hz, 1H), 7.64 (ddd, J = 8.1, 6.8, 1.2 Hz, 1H).

^{19}F NMR (470 MHz, $CDCl_3$) δ -85.5.

^{13}C{^{1}H} NMR (126 MHz, $CDCl_3$) δ 148.8 (t, J = 28.7 Hz), 147.1, 138.6, 131.1, 130.3, 129.1, 127.7, 115.7 (t, J = 2.0 Hz), 111.9 (t, J = 44.8 Hz), 109.0 (t, J = 244.8 Hz).

HRMS (ESI-TOF) $[C_{11}H_6F_2N_2+H]+$ calc'd.: 205.0572, found: 205.0573

2,2-difluoro-2-(2-methylquinolin-8-yl)acetonitrile (3ai)

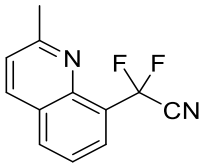

The title compound was prepared by performing general procedure 1 on 24.50 mg of the corresponding (hetero)aryl bromide:9.70 mg, 40% yield (light yellow solid).

^{1}H NMR (500 MHz, $CDCl_3$) δ 8.11 (d, J = 8.5 Hz, 1H), 8.00 (dd, J = 7.7, 4.0 Hz, 2H), 7.56 (t, J = 7.8 Hz, 1H), 7.41 (d, J = 8.5 Hz, 1H), 2.81 (s, 3H).

^{19}F NMR (470 MHz, $CDCl_3$) δ -87.2

^{13}C{^{1}H} NMR (126 MHz, $CDCl_3$) δ 160.5, 144.5 (d, *J* = 3.6 Hz), 136.1, 132.4, 127.5 (t, *J* = 23.3 Hz), 127.1– 126.3 (m), 124.7, 123.5, 113.7 (t, *J* = 46.5 Hz), 107.4 (t, *J* = 242.0 Hz), 29.9, 25.5.

HRMS (ESI-TOF) $[C_{12}H_8F_2N_2+H]+$ calc'd.: 219.0728, found: 219.0731

2,2-difluoro-2-(1,3,7-trimethyl-2,6-dioxo-2,3,6,7-tetrahydro-1H-purin-8-yl)acetonitrile (3aj)

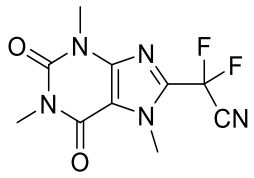

The title compound was prepared by performing general procedure 1 on 27.60 mg of the corresponding (hetero)aryl bromide: 10.90 mg, 40% yield (white solid). Purified by flash column chromatography (SiO_2, 50% EtOAc in hexanes).

^{1}H NMR (500 MHz, $CDCl_3$) δ 4.18 (t, J = 1.5 Hz, 3H), 3.60 (s, 3H), 3.42 (s, 3H).

^{19}F NMR (470 MHz, $CDCl_3$) δ -82.9

$^{13}C\{^{1}H\}$ NMR (126 MHz, $CDCl_3$) δ 155.4, 151.2, 146.6, 138.8 (t, J = 30.2 Hz), 110.6, 109.9 (t, J = 44.10 Hz), 104.3 (t, J = 243.2 Hz), 33.3, 30.0, 28.3

HRMS (ESI-TOF) $[C_{10}H_9F_2N_5O_2+H]+$ calc'd.: 270.0803, found: 270.0797

4.7.11 Computational Details

Computational Details - DFT

DFT calculations were conducted at the Molecular Graphics and Computational Facility (MGCF) at the University of California, Berkeley, using the Gaussian 16[68] software package. All calculations, including geometry optimizations, were performed in DMF solvent using the SMD solvent continuum model reported by Truhlar and co-workers according to the Solvent-Accessible Surface (scrf=smd, sufrace=sas, SC=Qconv=VeryTight).[69] Initial geometries were constructed in GaussView[70] and optimized to stationary points (either minima or first-order saddle points) using the PBE0 functional (the hybrid functional based on the Perdew-Burke-Ernzerhof functional [PBE][71] as described by Adamo[72]) with Grimme's D3 dispersion correction with Becke-Johnson damping (GD3BJ)[73] and the basis sets def2-TZVP (with effective core potential) for Cu and I, and def2-SVPD for all other atoms. The nature of each stationary point was evaluated by accompanying frequency calculations (all positive eigenvalues for minima and exactly one negative eigenvalue for transition states). Several isomers were considered, but only those representing the minimum-energy paths are presented here. Transition states were connected to ground states by following the intrinsic reaction coordinate (IRC) downhill from the transition state. IGMH analysis[58] was conducted with Multiwfn 3.8(dev)[74] using the default parameters and a grid resolution of 0.1 Bohr. Grid data were visualized with VMD.[75] All other parameters were left as their defaults.

Figure S14. Full-Color Visualization of NCI in **TS$_{OA}^{‡}$-a** .[a]

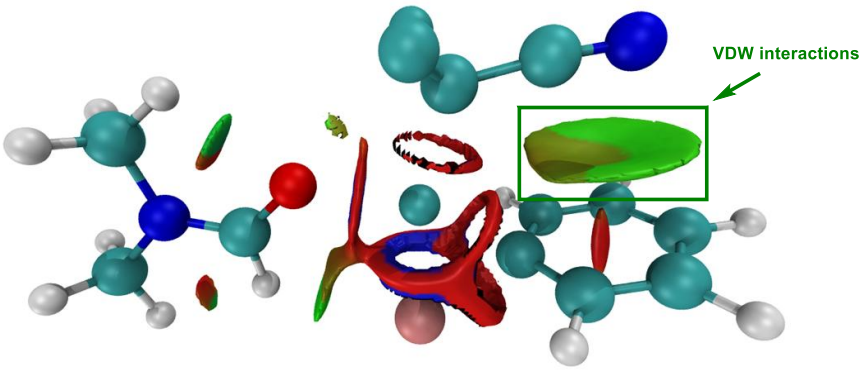

[a]Blue: attractive and stabilizing interactions; [b]red: repulsive and destabilizing interactions; [c]green: van der Waals interactions.

Figure S15. Full-Color Visualization of NCIs in **$TS_{RE}^{‡}$-a**. [a]

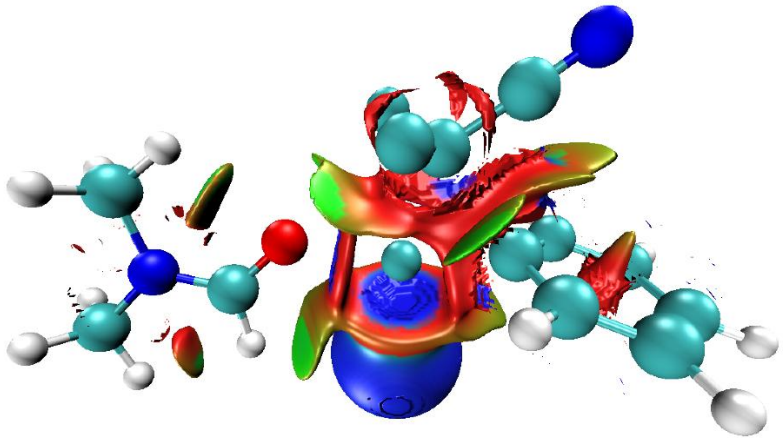

[a]Blue: attractive and stabilizing interactions; [b]red: repulsive and destabilizing interactions; [c]green: van der Waals interactions.

Figure S16. Visualization of NCIs in **[Cu]-3a**. [a]

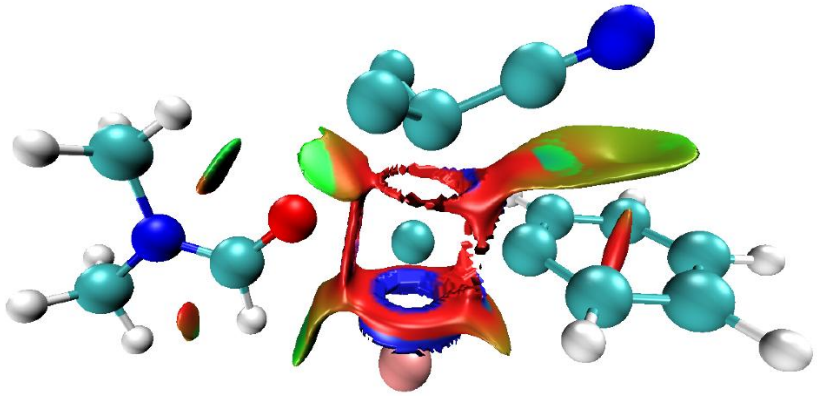

[a]Blue: attractive and stabilizing interactions; [b]red: repulsive and destabilizing interactions; [c]green: van der Waals interactions.

Table S6. Computed Energies of Reaction Components and of Fluroalkylcopper Complexes

Structure	E (Hartree)	Thermal Correction to Free Energy (Hartree)	G (Hartree)
PhI	-528.951267	0.059372	-528.891895
(DMF)$CuCF_2CN$	-2218.461359	0.080141	-2218.381218
$(DMF)_2CuCF_2CN$	-2466.54901	0.171767	-2466.377240
(DMF)$CuCF_3$	-2225.492122	0.076056	-2225.416066
$(DMF)_2CuCF_3$	-2473.576103	0.164799	-2473.411304
(DMF)$CuCF_2CONMe_2$	-2373.286721	0.161644	-2373.125077
$(DMF)_2CuCF_2CONMe_2$	-2621.362385	0.249738	-2621.112647
(DMF)CuI	-2186.200629	0.066200	-2186.134429
$PhCF_2CN$	-561.288323	0.075566	-561.212757
α,α,α-trifluorotoluene	-568.327251	0.071722	-568.255529
$PhCF_2CONMe_2$	-716.122090	0.154746	-715.967344
[Cu]-1a	-2747.421279	0.157965	-2747.263314
[Cu]-1b	-2754.448954	0.152117	-2754.296837
[Cu]-1c	-2902.247624	0.237961	-2902.009663
[Cu]-2a	-2747.421341	0.157454	-2747.263887
[Cu]-2b	-2754.450905	0.151112	-2754.299793
$TS_{OA}^{‡}$-a	-2747.401965	0.158603	-2747.243362
$TS_{OA}^{‡}$-b	-2754.431447	0.154080	-2754.277367
$TS_{OA}^{‡}$-c	-2902.231771	0.241279	-2901.990492
[Cu]-3a	-2747.416185	0.165096	-2747.251089
[Cu]-3b	-2754.448676	0.155121	-2754.293555
[Cu]-3c	-2902.24998	0.243417	-2902.00656
$TS_{RE}^{‡}$-a	-2747.407616	0.161669	-2747.245947
$TS_{RE}^{‡}$-b	-2754.442177	0.156111	-2754.286066
$TS_{RE}^{‡}$-c	-2902.24742	0.24281	-2902.00461
[Cu]-4a	-2747.504194	0.162041	-2747.342153
[Cu]-4b	-2754.538516	0.156706	-2754.381810
[Cu]-4c	-2902.34006	0.241534	-2902.09852

4.7.12 XYZ Coordinates of Optimized Geometries

PhI

C	0.00000	0.00000	-3.33070
C	0.00000	1.20630	-2.63060
C	-0.00000	-1.20630	-2.63060
H	0.00000	2.15550	-3.17080
H	-0.00000	-2.15550	-3.17080
C	0.00000	1.21470	-1.23550
C	-0.00000	-1.21470	-1.23550
H	0.00000	2.16020	-0.69130
H	-0.00000	-2.16020	-0.69130
C	0.00000	0.00000	-0.54740
H	0.00000	0.00000	-4.42240
I	-0.00000	-0.00000	1.54360

(DMF)CuCF$_2$CN

C	-2.51500	-1.06500	0.00270
N	-3.07570	0.13240	-0.00220
H	-3.23730	-1.89720	0.00350
C	-4.51700	0.26660	-0.00680
H	-4.98620	-0.72330	-0.00630
H	-4.84300	0.82200	0.88400
H	-4.83750	0.81840	-0.90180
C	-2.32980	1.36880	-0.00340
H	-1.25090	1.17060	0.00160
H	-2.58220	1.95220	-0.90010
H	-2.58930	1.95800	0.88740
O	-1.29790	-1.33010	0.00640
Cu	0.38620	-0.41340	0.00410
C	2.10060	0.48320	0.00150
F	2.31360	1.30810	1.10470
F	2.30310	1.32140	-1.09360
C	3.19710	-0.49300	-0.00960

N	3.98190	-1.34660	-0.01840

$(DMF)_2CuCF_2CN$

C	-1.89170	1.61330	-1.11890
N	-2.28410	1.95010	0.11610
H	-2.73500	1.54540	-1.83400
C	-3.67170	2.18650	0.42830
H	-4.28750	2.02530	-0.46460
H	-4.00700	1.50010	1.22010
H	-3.81690	3.21920	0.78080
C	-1.33320	2.12930	1.18560
H	-0.33740	1.83540	0.83850
H	-1.31030	3.18330	1.50360
H	-1.61750	1.51160	2.04880
O	-0.73090	1.39260	-1.46400
Cu	0.12790	-0.64120	-0.31750
C	-1.49610	-1.70350	-0.16040
F	-2.40970	-1.52480	-1.20020
F	-1.29150	-3.08530	-0.13110
C	2.94600	-0.36940	0.19260
N	4.11820	0.24250	0.20580
H	2.95400	-1.38390	0.62240
C	5.29310	-0.39950	0.74910
H	5.03710	-1.40130	1.11160
H	6.06840	-0.48270	-0.02630
H	5.69460	0.19490	1.58250
C	4.28450	1.57860	-0.31870
H	3.32520	1.94930	-0.69010
H	4.65590	2.24410	0.47360
H	5.01760	1.56720	-1.13800
O	1.90440	0.14230	-0.26380
C	-2.20840	-1.36370	1.07710
N	-2.68600	-1.01140	2.07440

(DMF)$CuCF_3$

C	-2.41180	-0.97500	0.00220
N	-2.86700	0.26680	0.00200
H	-3.20470	-1.74030	-0.00200
C	-4.29200	0.52250	-0.00910
H	-4.84380	-0.42370	-0.01460
H	-4.57390	1.10120	0.88200
H	-4.55960	1.10290	-0.90350
C	-2.02490	1.44040	0.00820
H	-0.96380	1.16290	0.03630
H	-2.21370	2.03590	-0.89630
H	-2.25570	2.05400	0.89040
O	-1.22260	-1.34810	0.00720
Cu	0.51160	-0.54520	-0.00270
C	2.27970	0.21400	-0.00200
F	2.80640	0.48740	1.24680
F	2.40620	1.42490	-0.65710
F	3.26780	-0.55400	-0.58780

$(DMF)_2CuCF_3$

C	2.33350	-0.97930	0.09840
N	3.23710	-1.95890	0.03010
H	2.77930	0.00830	0.32090
C	4.64160	-1.69940	0.23300
H	4.79660	-0.63430	0.44170
H	5.02110	-2.28840	1.08160
H	5.21590	-1.97540	-0.66430
C	2.85340	-3.32080	-0.24940
H	1.76930	-3.37060	-0.38910
H	3.35710	-3.67590	-1.16090
H	3.14580	-3.97560	0.58520
O	1.11830	-1.12230	-0.06170
Cu	-0.23660	0.71980	-0.02300

C	0.86620	2.31210	-0.02650
F	1.63550	2.50400	1.11240
F	1.81430	2.37210	-1.03780
F	0.22460	3.53520	-0.15530
C	-3.00670	-0.09190	0.01840
N	-4.03000	-0.93250	0.03390
H	-3.29120	0.97330	0.02370
C	-5.39410	-0.45730	0.05320
H	-5.40970	0.63850	0.05260
H	-5.93360	-0.82560	-0.83150
H	-5.90840	-0.82450	0.95320
C	-3.83610	-2.36400	0.03030
H	-2.76610	-2.58920	0.01740
H	-4.29470	-2.80370	0.92770
H	-4.31560	-2.80230	-0.85690
O	-1.81480	-0.45070	-0.00070

(DMF)CuCF$_2$CONMe$_2$

C	-3.05370	0.85930	0.04470
N	-3.11730	-0.44680	-0.15900
H	-4.03970	1.34460	0.12300
C	-4.40110	-1.11250	-0.22580
H	-5.20920	-0.38490	-0.09350
H	-4.51530	-1.60790	-1.20020
H	-4.46810	-1.87380	0.56470
C	-1.96150	-1.30370	-0.29600
H	-1.04310	-0.71010	-0.37790
H	-1.88310	-1.97090	0.57400
H	-2.06810	-1.91500	-1.20230
O	-2.03160	1.56370	0.15120
Cu	-0.13230	1.27930	0.10770
C	1.75950	0.87590	-0.04350
F	2.51160	1.02240	1.13910

F	2.43140	1.70410	-0.93360
C	1.93410	-0.54900	-0.54850
O	2.26920	-0.75810	-1.71430
N	1.62470	-1.55190	0.31080
C	1.12940	-1.37000	1.65590
H	0.67860	-0.37890	1.77850
H	0.35500	-2.12430	1.85200
H	1.92690	-1.49180	2.40510
C	1.73750	-2.92220	-0.12680
H	2.27140	-2.95920	-1.08070
H	2.28770	-3.50950	0.62300
H	0.74070	-3.37530	-0.25550

$(DMF)_2CuCF_2CONMe_2$

C	3.05810	-1.51730	-1.06580
N	3.64580	-1.28860	0.10040
H	3.75050	-1.47570	-1.92400
C	5.04120	-0.91840	0.16170
H	5.47340	-0.92240	-0.84530
H	5.14370	0.08900	0.59170
H	5.59340	-1.62670	0.79590
C	2.94360	-1.33630	1.35990
H	1.93150	-1.73200	1.21710
H	3.48880	-1.99090	2.05380
H	2.87600	-0.33020	1.79590
O	1.86080	-1.78690	-1.25610
Cu	0.23160	-1.11140	-0.37030
C	-1.53930	-0.97690	0.41310
F	-2.14360	-2.21470	0.72370
F	-1.50910	-0.32370	1.67480
C	0.64010	1.94160	-0.21770
N	1.01860	3.18310	0.10110
H	-0.41960	1.86160	-0.52280

C	0.09060	4.28550	0.04510
H	-0.89140	3.92810	-0.28650
H	-0.01540	4.75010	1.03710
H	0.44690	5.05270	-0.65900
C	2.36780	3.47710	0.51580
H	2.95780	2.55550	0.50680
H	2.82390	4.20990	-0.16680
H	2.36980	3.90240	1.53070
O	1.37500	0.95130	-0.19460
C	-2.54840	-0.17390	-0.43230
O	-2.11680	0.43190	-1.41610
N	-3.85750	-0.15050	-0.10380
C	-4.78210	0.54310	-0.97220
H	-4.98380	1.56300	-0.60560
H	-4.36660	0.60890	-1.98200
H	-5.73200	-0.00820	-0.99980
C	-4.44530	-0.65750	1.11730
H	-5.11620	-1.50370	0.90250
H	-3.68640	-0.97700	1.83020
H	-5.04310	0.14040	1.58340

(DMF)CuI

C	-2.93120	-0.93450	0.01150
N	-3.28550	0.33950	0.02580
H	-3.77690	-1.64060	-0.01090
C	-4.67970	0.71760	-0.07240
H	-5.30510	-0.18010	-0.12910
H	-4.97160	1.30950	0.80620
H	-4.84050	1.32420	-0.97520
C	-2.31340	1.41130	0.06420
H	-1.93230	1.63690	-0.94300
H	-2.79510	2.30760	0.47020
H	-1.46800	1.14710	0.71560

O -1.76880 -1.38350 0.02450

Cu -0.00700 -0.57770 0.00200

I 2.30160 0.23350 -0.00730

$PhCF_2CN$

C -2.28210 -1.19940 0.18960

C -0.90520 -1.21640 -0.01710

C -2.96610 0.01470 0.25460

H -0.36670 -2.16320 -0.06840

H -4.04550 0.02350 0.41650

C -0.22090 -0.00790 -0.16380

C -2.27320 1.21790 0.11750

H -2.80820 2.16770 0.16820

C -0.89640 1.21260 -0.08970

H -0.35090 2.15080 -0.19750

H -2.82370 -2.14080 0.29680

C 1.27050 -0.01940 -0.36910

F 1.66940 -1.14220 -1.01370

F 1.67060 1.03410 -1.12180

C 2.01570 0.04410 0.91840

N 2.55450 0.09400 1.93730

α,α,α-trifluorotoluene

C -2.11930 -1.21620 0.00030

C -0.72820 -1.20200 -0.00390

C -2.83140 -0.01520 0.00270

H -0.16770 -2.13860 -0.00590

H -3.92290 -0.02960 0.00590

C -0.05230 0.02220 -0.00620

C -2.15130 1.20150 0.00050

H -2.70710 2.14070 0.00180

C -0.75750 1.22520 -0.00410

H -0.22280 2.17500 -0.00670

H	-2.65130	-2.16910	0.00130
C	1.44700	0.01100	-0.00110
F	1.95000	-0.70160	-1.02700
F	1.97710	1.23670	-0.08410
F	1.94290	-0.55040	1.11950

$PhCF_2CONMe_2$

C	-3.13640	0.47230	1.20110
C	-1.79200	0.10860	1.21310
C	-3.85180	0.47190	0.00330
H	-1.23240	0.10960	2.14910
H	-4.90580	0.75580	-0.00380
C	-1.16110	-0.25590	0.02190
C	-3.21810	0.10910	-1.18480
H	-3.77440	0.10570	-2.12390
C	-1.87320	-0.25550	-1.17840
H	-1.37800	-0.53930	-2.10740
H	-3.62880	0.75390	2.13380
C	0.29290	-0.63910	0.03700
C	1.25120	0.57750	-0.10210
O	0.75190	1.68250	-0.27510
N	2.57260	0.34950	-0.02200
C	3.23160	-0.92980	0.14130
H	2.54040	-1.76920	0.07850
H	3.98620	-1.04560	-0.65010
H	3.74520	-0.96490	1.11370
C	3.47940	1.47350	-0.11680
H	4.05650	1.41850	-1.05230
H	2.91440	2.40880	-0.09440
H	4.18310	1.44660	0.72730
F	0.57690	-1.30300	1.19870
F	0.54920	-1.51720	-0.97990

[Cu]-1a

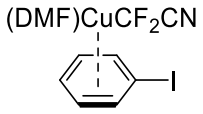

C	-0.64480	-1.66130	-0.04030
C	0.11030	-1.42180	-1.21190
C	1.44430	-1.89010	-1.26070
C	1.98370	-2.61230	-0.17570
C	1.22060	-2.82610	0.95900
C	-0.09590	-2.33920	1.03870
Cu	1.39720	0.20170	-0.65630
H	2.00520	-1.81260	-2.19500
H	1.63700	-3.37350	1.80640
H	-0.68730	-2.51440	1.93790
H	-0.36550	-1.0890	-2.10280
O	-0.09920	1.66050	-0.82930
H	3.00410	-2.99240	-0.23700
C	-0.64710	2.02120	0.22500
N	-1.76710	2.73000	0.28870
H	-0.22200	1.76920	1.21250
C	-2.36510	3.06840	1.55770
H	-1.72800	2.71470	2.37620
H	-2.48780	4.15790	1.64200
H	-3.35580	2.59750	1.64570
C	-2.48770	3.11280	-0.90130
H	-1.92230	2.80520	-1.78560
H	-3.47610	2.62950	-0.91190
H	-2.63200	4.20250	-0.91680
C	3.10520	0.98810	0.03100
F	2.99560	2.31710	0.44000
F	4.14700	1.0330	-0.89630
I	-2.62790	-1.01710	0.04300
C	3.57050	0.22180	1.18730

N	3.81480	-0.48080	2.07900

[Cu]-1b

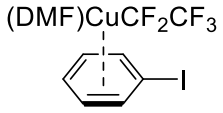

C	-0.63680	-1.62480	0.01340
C	0.20430	-1.39240	-1.09920
C	1.52640	-1.89150	-1.06160
C	1.97270	-2.63250	0.05360
C	1.13030	-2.82980	1.13300
C	-0.17900	-2.31570	1.12530
Cu	1.53200	0.20440	-0.48030
H	2.14870	-1.82930	-1.95730
H	1.47460	-3.39110	2.00370
H	-0.83600	-2.48490	1.97900
H	-0.20010	-0.96320	-2.01730
O	0.07560	1.70100	-0.67550
H	2.98510	-3.03890	0.05840
C	-0.62150	1.98560	0.31130
N	-1.72310	2.72490	0.26800
H	-0.35690	1.63690	1.32500
C	-2.51220	2.95870	1.45340
H	-2.01790	2.51440	2.32490
H	-2.63540	4.03850	1.62110
H	-3.50930	2.50730	1.33910
C	-2.24730	3.22420	-0.98000
H	-1.52560	3.03850	-1.78080
H	-3.19590	2.71950	-1.21890
H	-2.43720	4.30360	-0.89800
C	3.31000	0.78660	0.19220
F	3.44120	2.12520	0.52810
F	4.37360	0.59450	-0.67650

I	-2.61520	-0.96420	-0.05520
F	3.74730	0.15060	1.34360

[Cu]-1c

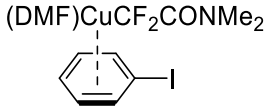

C	-1.49410	-1.56130	0.21020
C	-0.84880	-1.83390	-1.01870
C	0.24160	-2.73580	-1.02130
C	0.63050	-3.38110	0.17290
C	-0.02570	-3.09670	1.35690
C	-1.08520	-2.17150	1.38580
Cu	0.95800	-0.69410	-0.97930
H	0.67390	-3.05160	-1.97350
H	0.27510	-3.58790	2.28400
H	-1.59110	-1.95210	2.32650
H	-1.26980	-1.46880	-1.95680
O	-0.05500	1.12560	-1.35780
H	1.44960	-4.10120	0.15230
C	-0.20080	1.90860	-0.40680
N	-1.0230	2.96710	-0.41560
H	0.34400	1.77260	0.54230
C	-1.11560	3.82530	0.73930
H	-0.41520	3.49780	1.51610
H	-0.88220	4.86390	0.46370
H	-2.13930	3.79170	1.14060
C	-1.83010	3.27960	-1.55500
H	-1.68800	2.51900	-2.32810
H	-2.88670	3.30120	-1.25120
H	-1.56250	4.26740	-1.95780
C	2.89200	-0.40470	-0.55280
F	3.70040	-0.36760	-1.68420

F	3.49480	-1.42070	0.22230
I	-3.11720	-0.24940	0.23690
C	3.09760	0.90980	0.17830
O	3.62130	1.87160	-0.38290
N	2.59950	0.98990	1.44080
C	1.86660	-0.06050	2.10800
H	1.0480	0.38030	2.63060
H	1.48620	-0.79370	1.39080
H	2.48650	-0.58450	2.85160
C	2.75430	2.21060	2.19350
H	3.16180	1.98670	3.19050
H	3.43510	2.88240	1.66330
H	1.78330	2.71580	2.32570

[Cu]-2a

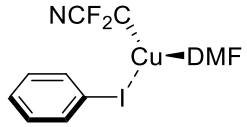

C	-2.85620	-0.00960	-0.02320
C	-3.18450	1.33710	0.14210
C	-4.52400	1.69260	0.30420
C	-5.52120	0.71750	0.30160
C	-5.17730	-0.62410	0.13570
C	-3.84280	-0.99690	-0.02820
Cu	2.37000	0.69400	-0.12170
I	-0.84890	-0.54930	-0.26720
H	-4.78410	2.74520	0.43360
H	-5.95200	-1.39400	0.13270
H	-3.57680	-2.04690	-0.15830
H	-2.40490	2.10080	0.14670
O	2.39030	-1.21400	-0.39050
H	-6.56710	1.0300	0.42910
C	2.30260	-2.08670	0.50390

N	1.93700	-3.33250	0.27460
H	2.53280	-1.85940	1.55640
C	1.85760	-4.29780	1.34780
H	2.15080	-3.82910	2.29350
H	0.82880	-4.67560	1.43320
H	2.52660	-5.14470	1.13940
C	1.56980	-3.79060	-1.04640
H	1.67790	-2.97370	-1.76470
H	2.21790	-4.62860	-1.33910
H	0.52740	-4.13880	-1.03750
C	2.31180	2.61870	0.10270
F	2.92210	3.07910	1.26790
F	2.94050	3.33270	-0.91570
C	0.92030	3.08410	0.14500
N	-0.21360	3.32790	0.16400

[Cu]-2b

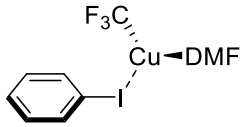

C	-2.60490	0.44110	-0.00510
C	-3.92930	0.88020	-0.02400
C	-4.95600	-0.06350	-0.08380
C	-4.66360	-1.42680	-0.12350
C	-3.33510	-1.85060	-0.10310
C	-2.29830	-0.91950	-0.04420
Cu	1.90350	0.03260	-0.01030
I	-1.03830	1.82170	0.08250
H	-5.99340	0.27710	-0.09910
H	-3.09560	-2.91570	-0.13320
H	-1.25780	-1.24680	-0.02900
H	-4.16240	1.94540	0.00700
O	1.12550	-1.73750	0.02130

H	-5.47170	-2.15910	-0.17020
C	1.81560	-2.78220	0.03290
N	1.31170	-4.00190	0.03830
H	2.91590	-2.74180	0.03980
C	2.17050	-5.16540	0.05190
H	3.22170	-4.85740	0.05790
H	1.96510	-5.77000	0.94680
H	1.97850	-5.78100	-0.83850
C	-0.11210	-4.24900	0.03000
H	-0.65310	-3.30180	0.01790
H	-0.38070	-4.83560	-0.85970
H	-0.39440	-4.82040	0.92530
C	2.81490	1.73080	-0.06720
F	4.19800	1.68170	-0.05010
F	2.55480	2.50380	-1.18510
F	2.53210	2.59850	0.97260

$TS_{OA}^{‡}$-a

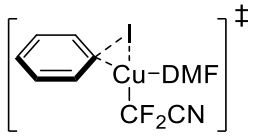

C	1.78940	-0.61850	0.00870
C	2.45060	-0.51330	1.24010
C	3.81910	-0.25100	1.25440
C	4.53200	-0.12040	0.06170
C	3.86170	-0.22940	-1.15770
C	2.49390	-0.49240	-1.19650
Cu	-0.04350	0.36990	-0.01840
I	0.03620	-2.12640	-0.03080
C	0.33520	2.37190	-0.02710
F	-0.19320	2.96860	-1.16840
F	-0.30800	3.00950	1.02890
H	4.33200	-0.16060	2.21440

H	4.40810	-0.12180	-2.09720
H	1.98170	-0.60680	-2.15240
H	1.90510	-0.64450	2.17520
O	-2.12980	0.72460	-0.02690
H	5.60600	0.07170	0.08240
C	-3.03370	-0.12270	0.02720
N	-4.32780	0.16590	0.03840
H	-2.81070	-1.20400	0.07020
C	-5.32720	-0.87390	0.11130
H	-4.84040	-1.85500	0.15050
H	-5.94520	-0.74240	1.01160
H	-5.98320	-0.83180	-0.77050
C	-4.80050	1.52950	-0.01570
H	-3.94630	2.20990	-0.07690
H	-5.44450	1.66650	-0.89650
H	-5.38880	1.75800	0.88490
C	1.73970	2.77830	0.04010
N	2.87810	2.98870	0.09940

$TS_{OA}^{‡}$-b

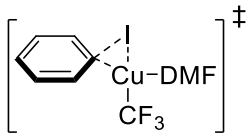

C	1.80390	-0.50080	0.06380
C	2.28570	-0.30520	1.36490
C	3.61360	0.07780	1.54220
C	4.46720	0.22000	0.44630
C	3.98360	-0.02660	-0.84000
C	2.65680	-0.39930	-1.04210
Cu	-0.02200	0.40880	-0.16950
I	0.09330	-2.08890	-0.15920
C	0.56360	2.33340	-0.12300
F	-0.21320	3.21560	-0.84410

F	0.54470	2.87230	1.15120
H	3.98350	0.25890	2.55390
H	4.64550	0.07140	-1.70340
H	2.28570	-0.59150	-2.04910
H	1.62730	-0.42620	2.22560
O	-2.08930	0.75110	-0.17320
H	5.50870	0.50990	0.59540
C	-2.96130	-0.07030	0.15530
N	-4.25870	0.19560	0.19800
H	-2.70140	-1.10580	0.43780
C	-5.21670	-0.80730	0.60160
H	-4.70000	-1.74660	0.82930
H	-5.76290	-0.47070	1.49490
H	-5.94290	-0.98220	-0.20550
C	-4.77830	1.49840	-0.14670
H	-3.95540	2.15120	-0.45150
H	-5.49940	1.40460	-0.97140
H	-5.29440	1.93720	0.71950
F	1.83660	2.61710	-0.55780

$TS_{OA}^{‡}$-c

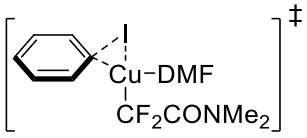

C	2.31770	0.10660	0.05680
C	2.79670	0.50270	1.31510
C	3.63910	1.60830	1.40150
C	4.03880	2.29310	0.25190
C	3.59130	1.85930	-0.99820
C	2.74630	0.75890	-1.10940
Cu	0.25760	-0.16960	0.12390
I	1.84040	-2.12720	-0.17300
C	-0.32740	1.77270	0.18910

F	0.16680	2.40010	1.31790
F	0.20400	2.53750	-0.85900
H	3.99010	1.93250	2.38370
H	3.90460	2.38160	-1.90490
H	2.40610	0.42100	-2.08860
H	2.49790	-0.03480	2.21550
O	-1.52940	-1.29110	0.17970
H	4.70570	3.15350	0.32860
C	-2.54150	-0.96470	0.82190
N	-3.77110	-1.38010	0.54650
H	-2.48160	-0.29080	1.69280
C	-4.89530	-0.98430	1.36170
H	-4.55780	-0.31940	2.16450
H	-5.64140	-0.45920	0.74810
H	-5.37170	-1.87060	1.80590
C	-4.04420	-2.24500	-0.57640
H	-4.45220	-3.20390	-0.22440
H	-4.78580	-1.77310	-1.23640
H	-3.11920	-2.42450	-1.13160
C	-1.83250	1.96840	0.19410
O	-2.41140	2.34400	1.21420
N	-2.49830	1.61970	-0.93430
C	-3.93130	1.77520	-0.99770
H	-4.30090	2.13720	-0.03470
H	-4.20540	2.49300	-1.78660
H	-4.40650	0.81160	-1.23420
C	-1.88110	1.10050	-2.13200
H	-0.88460	0.69790	-1.92570
H	-2.50370	0.28520	-2.52610
H	-1.79120	1.87460	-2.91010

[Cu]-3a

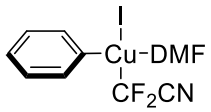

C	1.90320	-0.02150	-0.00950
C	2.58170	-0.13630	1.19870
C	3.96980	-0.29140	1.17290
C	4.65420	-0.32600	-0.04250
C	3.95030	-0.21080	-1.24120
C	2.56170	-0.05460	-1.23360
Cu	0.01710	0.22480	0.00390
I	-0.24140	-2.29950	-0.00290
C	0.38790	2.18420	0.02060
F	-0.18900	2.68690	-1.10530
F	-0.29640	2.69040	1.08350
H	4.51600	-0.38300	2.11450
H	4.48110	-0.23780	-2.19560
H	2.01500	0.04290	-2.17290
H	2.05000	-0.10410	2.15080
O	-1.88670	0.72170	-0.04300
H	5.73960	-0.44090	-0.05510
C	-2.91410	0.01440	0.04000
N	-4.13400	0.50980	0.00080
H	-2.85030	-1.07870	0.15070
C	-5.29430	-0.34880	0.09350
H	-4.98110	-1.39370	0.19480
H	-5.89890	-0.06510	0.96660
H	-5.91080	-0.24130	-0.81010
C	-4.38000	1.92790	-0.14100
H	-3.42930	2.46660	-0.17690
H	-4.94560	2.11400	-1.06490
H	-4.97510	2.28370	0.71150
C	1.75610	2.71710	0.09150

N	2.83300	3.13250	0.15220

[Cu]-3b

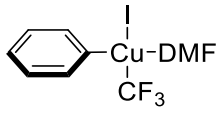

C	1.94160	0.31840	0.07850
C	2.48270	0.23840	1.35670
C	3.87290	0.19910	1.49420
C	4.69660	0.24850	0.36890
C	4.13030	0.34120	-0.90240
C	2.74140	0.38090	-1.05680
Cu	0.06290	0.28510	-0.14220
I	0.08000	-2.26620	-0.16360
C	0.18210	2.24710	-0.05350
F	-0.22650	2.72710	-1.24850
F	-0.72510	2.66040	0.86150
H	4.31020	0.12720	2.49270
H	4.76920	0.38350	-1.78760
H	2.30310	0.45380	-2.05350
H	1.84310	0.19680	2.23970
O	-1.87070	0.44770	-0.45000
H	5.78170	0.21790	0.48370
C	-2.71670	0.04550	0.38060
N	-4.01150	0.25310	0.25670
H	-2.41860	-0.51670	1.27850
C	-4.94810	-0.25580	1.23380
H	-4.41140	-0.80160	2.01750
H	-5.50540	0.57670	1.68600
H	-5.66310	-0.93360	0.74630
C	-4.56380	0.98820	-0.85910
H	-3.75540	1.35340	-1.49810
H	-5.22820	0.33470	-1.44170

H	-5.14970	1.83790	-0.48200
F	1.30650	2.91760	0.23950

[Cu]-3c

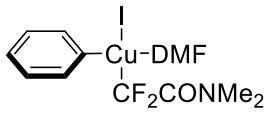

C	1.56630	-0.69890	0.19620
C	2.27060	-1.21210	1.28040
C	3.59580	-1.61710	1.09830
C	4.20350	-1.49750	-0.15180
C	3.48300	-0.97650	-1.22670
C	2.15610	-0.57230	-1.05780
Cu	-0.26990	-0.25470	0.40230
I	-0.93100	-2.64060	-0.39800
C	0.47810	1.52270	0.94550
F	-0.58560	2.21200	1.45000
F	1.35140	1.47510	1.97570
H	4.15400	-2.02210	1.94530
H	3.95210	-0.87820	-2.20790
H	1.60040	-0.16560	-1.90420
H	1.80620	-1.29590	2.26400
O	-2.15830	0.24150	0.55990
H	5.24180	-1.80620	-0.28700
C	-2.67760	1.15680	-0.11880
N	-3.97380	1.40060	-0.13270
H	-2.06000	1.81810	-0.74490
C	-4.52040	2.46510	-0.94360
H	-3.71540	2.96480	-1.49380
H	-5.24630	2.05410	-1.65960
H	-5.03390	3.19870	-0.30590
C	-4.90930	0.62310	0.64750
H	-5.44780	1.28220	1.34300

H	-5.64050	0.14580	-0.02010
H	-4.37180	-0.14480	1.21050
C	0.93850	2.28490	-0.30010
O	0.03060	2.60210	-1.07130
N	2.23330	2.54980	-0.52860
C	2.58170	3.26890	-1.73690
H	3.16190	4.16600	-1.47780
H	3.19930	2.63010	-2.38580
H	1.67480	3.56250	-2.27030
C	3.36370	2.22260	0.32270
H	3.23030	1.26990	0.83550
H	4.24820	2.13830	-0.31840
H	3.54830	3.01610	1.06180

$TS_{RE}^{‡}$-a

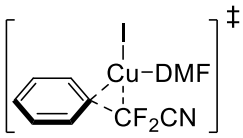

C	1.88640	0.26650	0.18890
C	2.27500	0.34160	1.52440
C	3.51690	-0.18710	1.88400
C	4.35400	-0.73330	0.91280
C	3.95630	-0.75990	-0.42760
C	2.72170	-0.24150	-0.80640
Cu	0.00240	0.19170	-0.07120
I	-0.44720	-2.38960	-0.30810
C	0.86300	2.04950	-0.30900
F	0.07150	2.36520	-1.37310
F	0.38050	2.68330	0.78160
H	3.83030	-0.15660	2.92920
H	4.61540	-1.18560	-1.18680
H	2.40920	-0.24960	-1.85130
H	1.62470	0.79130	2.27660

O	-1.86460	0.91450	0.02260
H	5.32940	-1.13130	1.19780
C	-2.89670	0.30190	0.36170
N	-4.10030	0.84520	0.36560
H	-2.86040	-0.75210	0.67980
C	-5.26240	0.09010	0.77570
H	-4.96620	-0.92450	1.06350
H	-5.74590	0.58230	1.63170
H	-5.98540	0.03600	-0.05080
C	-4.32000	2.21400	-0.04300
H	-3.36910	2.66860	-0.33420
H	-5.01630	2.23810	-0.89340
H	-4.76230	2.78300	0.78700
C	2.18440	2.63420	-0.60880
N	3.20140	3.12340	-0.85530

$TS_{RE}^{‡}$-b

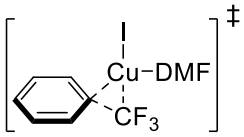

C	1.80390	-0.50080	0.06380
C	2.28570	-0.30520	1.36490
C	3.61360	0.07780	1.54220
C	4.46720	0.22000	0.44630
C	3.98360	-0.02660	-0.84000
C	2.65680	-0.39930	-1.04210
Cu	-0.02200	0.40880	-0.16950
I	0.09330	-2.08890	-0.15920
C	0.56360	2.33340	-0.12300
F	-0.21320	3.21560	-0.84410
F	0.54470	2.87230	1.15120
H	3.98350	0.25890	2.55390
H	4.64550	0.07140	-1.70340

H	2.28570	-0.59150	-2.04910
H	1.62730	-0.42620	2.22560
O	-2.08930	0.75110	-0.17320
H	5.50870	0.50990	0.59540
C	-2.96130	-0.07030	0.15530
N	-4.25870	0.19560	0.19800
H	-2.70140	-1.10580	0.43780
C	-5.21670	-0.80730	0.60160
H	-4.70000	-1.74660	0.82930
H	-5.76290	-0.47070	1.49490
H	-5.94290	-0.98220	-0.20550
C	-4.77830	1.49840	-0.14670
H	-3.95540	2.15120	-0.45150
H	-5.49940	1.40460	-0.97140
H	-5.29440	1.93720	0.71950
F	1.83660	2.61710	-0.55780

$TS_{RE}^{‡}$-c

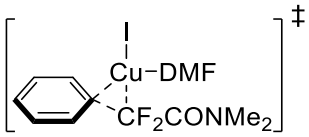

C	-1.40620	0.29540	0.95840
C	-1.37410	0.10940	2.33930
C	-2.23780	0.85430	3.14580
C	-3.14450	1.74020	2.56820
C	-3.17960	1.89930	1.18040
C	-2.31570	1.17300	0.36460
Cu	0.28780	-0.02920	0.13970
I	1.25510	2.23920	-0.80760
C	-1.07570	-1.58790	0.04740
F	-0.31350	-2.16380	-0.94520
F	-0.88970	-2.35190	1.12700
H	-2.20700	0.72280	4.22920

H	-3.88270	2.59920	0.72500
H	-2.34130	1.31790	-0.71410
H	-0.68750	-0.60750	2.79100
O	1.98080	-1.16630	0.14740
H	-3.83230	2.30590	3.19920
C	3.10860	-0.72210	0.43420
N	4.20660	-1.45840	0.47020
H	3.26240	0.34180	0.67750
C	5.48430	-0.87860	0.81510
H	5.36600	0.19210	1.01640
H	5.89260	-1.37150	1.70930
H	6.19480	-1.01350	-0.01310
C	4.18630	-2.87100	0.16800
H	3.16720	-3.17740	-0.08390
H	4.85400	-3.07860	-0.68030
H	4.53880	-3.44320	1.03820
C	-2.54970	-1.68240	-0.39640
O	-3.34620	-2.20300	0.37110
N	-2.85640	-1.20700	-1.61450
C	-4.22130	-1.31280	-2.08050
H	-4.78810	-1.97350	-1.41940
H	-4.69650	-0.31970	-2.09660
H	-4.22890	-1.72000	-3.10100
C	-1.94550	-0.55650	-2.53380
H	-1.61490	-1.24900	-3.32110
H	-2.47190	0.28130	-3.00920
H	-1.06340	-0.14730	-2.03240

[Cu]-4a

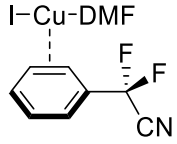

C	-1.84290	1.12920	0.50570

C	-2.84630	0.60290	1.32420
C	-2.52040	0.14960	2.59820
C	-1.20140	0.22220	3.05090
C	-0.20810	0.75830	2.23230
C	-0.52640	1.22240	0.95690
Cu	1.46120	-0.81170	-0.33810
I	3.62070	0.31250	-0.04780
C	-2.20290	1.58470	-0.88290
F	-1.10290	1.79670	-1.63830
F	-2.94450	0.64070	-1.52100
H	-3.29810	-0.27060	3.23780
H	0.82350	0.81610	2.58280
H	0.24890	1.64200	0.31630
H	-3.87420	0.54210	0.96310
O	-0.19560	-1.72250	-0.77490
H	-0.94800	-0.14010	4.04860
C	-1.10230	-2.03520	0.02430
N	-2.28410	-2.48990	-0.35300
H	-0.96510	-1.95630	1.11390
C	-3.28220	-2.87560	0.61750
H	-2.88210	-2.76240	1.63040
H	-4.17800	-2.24820	0.50730
H	-3.56830	-3.92530	0.45910
C	-2.63490	-2.63230	-1.74750
H	-1.85850	-2.18110	-2.37110
H	-2.73810	-3.69690	-2.00320
H	-3.59560	-2.13390	-1.93390
C	-2.99820	2.84320	-0.88200
N	-3.60870	3.82130	-0.84180

[Cu]-4b

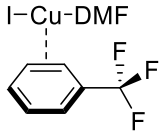

C	-2.26630	-1.24540	0.04230
C	-1.31830	-1.53900	-0.96030
C	-0.31090	-2.48930	-0.69570
C	-0.25700	-3.11190	0.56830
C	-1.19570	-2.80370	1.54200
C	-2.20730	-1.87070	1.28010
Cu	0.51880	-0.53500	-0.31440
I	3.07120	-0.45570	-0.01940
C	-3.36880	-0.26310	-0.22280
F	-3.51550	0.61740	0.78050
F	-3.17970	0.44160	-1.34220
H	0.34890	-2.82200	-1.49900
H	-1.15070	-3.28940	2.51780
H	-2.94420	-1.63430	2.04900
H	-1.43150	-1.12000	-1.96100
O	-0.27440	1.35430	-0.11560
H	0.52520	-3.84470	0.77080
C	0.40710	2.37250	0.09420
N	-0.09880	3.58910	0.23400
H	1.50630	2.32000	0.17840
C	0.75120	4.73210	0.47260
H	1.79890	4.41470	0.52070
H	0.63400	5.46630	-0.33780
H	0.47750	5.21460	1.42220
C	-1.52000	3.83300	0.14980
H	-2.04390	2.88860	-0.02080
H	-1.87600	4.28770	1.08550
H	-1.73180	4.52620	-0.67720
F	-4.56340	-0.87950	-0.35400

[Cu]-4c

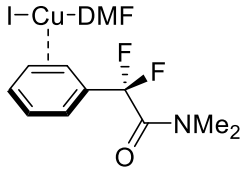

C	-1.60530	0.04590	0.49250
C	-1.71400	-1.01770	1.40240
C	-1.22270	-0.87970	2.69360
C	-0.61180	0.31450	3.09220
C	-0.51050	1.37980	2.20200
C	-1.01140	1.26200	0.89100
Cu	0.82360	0.37570	0.18580
I	2.63150	2.10430	-0.43780
C	-2.21690	-0.10980	-0.88050
F	-2.23160	1.07820	-1.55020
F	-1.44260	-0.93610	-1.62960
H	-1.30860	-1.71000	3.39600
H	-0.05940	2.32230	2.51450
H	-1.04210	2.13260	0.23520
H	-2.18320	-1.95180	1.09100
O	1.40780	-1.58000	0.03520
H	-0.22370	0.41770	4.10660
C	2.57260	-1.95690	-0.17630
N	2.95800	-3.22480	-0.14470
H	3.37800	-1.23950	-0.41140
C	4.32770	-3.60210	-0.40480
H	4.92640	-2.70950	-0.61890
H	4.75000	-4.11830	0.46970
H	4.37420	-4.28290	-1.26730
C	2.02970	-4.29000	0.15580
H	1.03540	-3.86960	0.33160
H	1.98710	-4.99690	-0.68530
H	2.36340	-4.83360	1.05160

C	-3.64880	-0.72320	-0.86830
O	-3.78260	-1.86560	-1.28370
N	-4.64770	0.03230	-0.38510
C	-5.99200	-0.50310	-0.38270
H	-6.01330	-1.45650	-0.91640
H	-6.33550	-0.65550	0.65150
H	-6.67100	0.20900	-0.87300
C	-4.53950	1.37460	0.14470
H	-4.99110	2.09920	-0.54900
H	-5.08240	1.42230	1.09860
H	-3.50720	1.66850	0.33210

CHAPTER FIVE

Palladium-Catalyzed Desymmetrization of Benzylic Difluoromethylene Units for the Synthesis of Congested Stereocenters Bearing Fluorine

5.1 Abstract

Molecules containing fluorine are widespread in modern materials, agrochemicals, and pharmaceuticals because the inclusion of fluorine in a molecule can beneficially modulate the physiochemical properties of the parent molecule. Stereocenters bearing fluorine are particularly valuable as bio-isosteres of alcohols and of C(sp^3)-H bonds. Preparing different isomers of secondary and tertiary benzylic fluorides can affect molecular conformation and modulate biological activity; however, synthesizing these chiral alkyl fluorides from non-chiral starting materials is challenging. We report a palladium-catalyzed desymmetrization strategy for the alkylation of (hetero)aryl-α,α-difluoromethylene units that enables the synthesis of enantioenriched 2° and 3° C(sp^3) stereocenters bearing fluorine. The use of $Ba(OTf)_2$ as Lewis acid, Li*O*t*Bu as base, and the novel germanium-containing bisphosphine ligand (*R*)-DTMGM-BINAP (DTMGM = 3,5-(trimethylgermanyl)-4-methoxyphenyl), enables the desymmetrization of (hetero)aryl-α,α-difluorides in high yields and in high enantioselectivities under mild conditions. We demonstrate that a wide range of carbon nucleophiles and a wide range of benzylic difluorides react under the developed conditions. Additionally, the use of a masked acyl cyanide nucleophile enables rapid functionalization of the fluorinated products to form stereo-defined α-fluorinated carbonyl compounds.

5.2 Introduction

Over the last 50 years, fluorine has played an increasingly prevalent role in the pharmaceutical, agrochemical, and materials industries.[1] In 2020, 35% of newly-approved small-molecule pharmaceuticals[2] and 88% of agrochemicals[3] newly assigned common names contained fluorine; an approximately three times increase compared to twenty years ago.[4] The fluorine atom is valuable for the discovery of novel bioactive molecules as its inclusion modulates a variety of important molecular properties; such as solubility, conformation, p*K*a, Log*P*, and others.[5-7] Chiral molecules are significant in numerous life processes because biological systems depend on chiral environments for recognition events. As such, the effect produced by one enantiomer of a compound can be entirely distinct from the other enantiomer of the same compound.[8-13] When placed at the benzylic position, the unique electronic, physiochemical, and conformational effects exerted by a fluorine atom compared to a hydrogen atom enable the fluorine atom to serve as a non-metabolizable bio-isostere of a benzylic proton or a more lipophilic bio-isostere of a hydroxyl group.[14-15] Fluorination at the benzylic position can also prevent racemization of enantioenriched molecules.[16-18] Computational studies of morphine derivatives[19] by Harrison and coworkers and synthetic studies of fentanyl derivatives[20] by Dockendorff and coworkers demonstrate that fluorination at the benzylic position suppresses negative side effects by modulation of *p*Ka. Similarly, an α-fluorinated analogue of scopolamine has been identified by Zhu and coworkers as a promising antidepressant (Figure 1a).[21] Therefore, the inclusion of a fluorine atom at the benzylic position, particularly in an enantioselective manner, is of great interest for the synthesis of pharmaceuticals and fine chemicals.

Although secondary and tertiary stereocenters bearing fluorine are desirable, enantioselective methods for the syntheses of benzylic stereocenters bearing a C(sp^3)–F bond from racemic starting materials remain underexplored. Strategies that involve reactions that form C–F bonds with a chiral phase-transfer reagent,[22] such as derivatives of Cinchona alkaloids, chiral phosphoric acids, or others frequently suffer from low to moderate enantioselectivities.[22-25] Additionally, these

strategies for enantioselective C–F bond-forming reactions routinely rely upon hydrogen bonding with the substrate, adjacent directing groups, or conformational bias to impart enantioselectivity (*i.e.* substrate control).[26] In addition, due to the reactive sources of nucleophilic fluoride employed, poor yields and functional group tolerance are frequently reported.[27] The synthesis of fluorinated stereocenters by C–C bond-forming reactions between partner(s) containing fluorine has been reported with palladium[28] or copper[29] as single-metal catalysts, and with iridium and copper dual-catalyst systems.[30] However, these methods also leverage cyclic or chelating substrates to achieve high enantioselectivities.

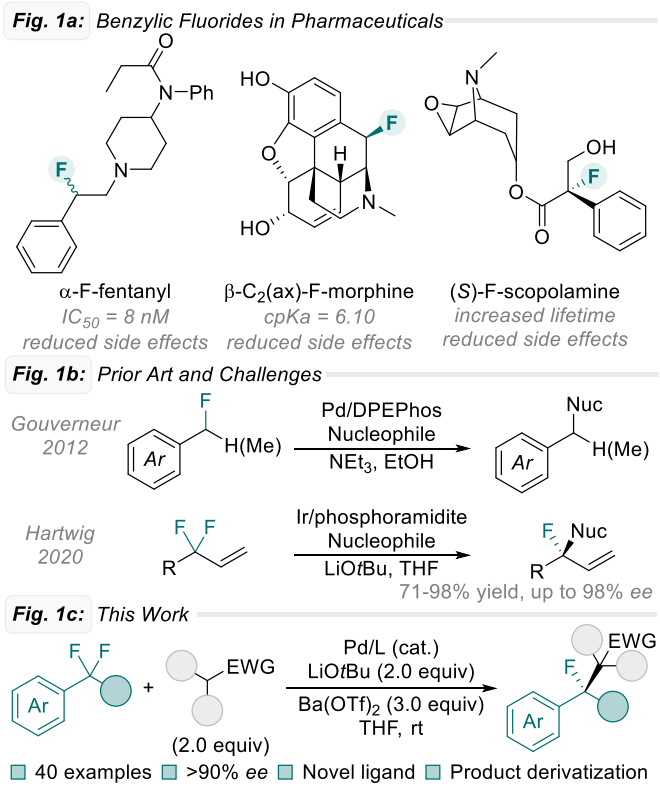

Figure 1. (a) biologically active molecules containing a benzylic fluoride, (b) prior art for defluorinative benzylic/allylic substitution, and (c) this work.

In contrast, the desymmetrization of a prochiral difluorinated electrophile by C(sp^3)–F bond activation would enable the synthesis of stereocenters containing both secondary and tertiary fluorides from difluoromethylarenes and alkyl-difluoromethylarenes, respectively, and would eliminate the need for an exogenous reactive fluoride source. In addition, the installation of difluoromethylene units has been extensively studied due to the utility of the -CF_2- unit in the pharmaceuticals industry, and numerous methods have been developed to form α,α-difluoromethylarenes, rendering the prochiral starting material readily accessible. [31-40] Although attractive, a desymmetrization approach poses several challenges: first, the C(sp^3)–F bond is often considered inert due to is high strength, low polarizability, and highly ionic character;[41] second, exhaustive defluorination is typically observed after removal of one fluorine atom from a di- or trifluoromethyl group because the strength of the C–F bond decreases with the number of fluorine atoms bonded to the carbon;[42] and third, with an *A* value of 0.25, the fluorine atom is smaller than a methyl (*A* = 1.74) or methoxy (*A* = 0.55) group,[43] rendering high levels of enantioinduction based on the steric environment of the substrate challenging.

In 2012, Gouverneur and coworkers demonstrated the palladium-catalyzed defluorinative alkylation of benzylic-α-fluoromethyl gruops;[28] however, α,α-difluoromethylarenes were inert under the reported conditions due to the increased strength of the germinal C(sp^3)–F bonds. In 2020, our group reported the asymmetric allylic alkylation (AAA) of allylic *gem*-difluorides using an iridium phosphoramidite catalyst (Figure 1b).[44] For this transformation, we employed a "push-pull" strategy, wherein LiOTf acted as a fluorophilic Lewis acid (pull) to aid in C–F bond activation by the electron-rich (push) iridium catalyst.[41] Encouraged by this precedent, we aimed

to extend our "push-pull" approach to *gem*-difluorides at positions less activated and less coordinating than the allylic position. We envisioned that this could be achieved by developing conditions for the asymmetric alkylation of benzylic α,α-difluoromethylene units catalyzed by low-valent palladium(0) (Figure 1c). While many studies have been conducted on palladium-catalyzed AAA, there are significantly fewer metal-catalyzed benzylic substitution reported in the literature when compared to allylic substitution reactions.[45]

Benzylic alkylation is inherently more challenging than allylic alkylation because of the lower rate of formation of η^3-benzyl species than η^3-allyl species.[46] Transition-metal catalyzed benzylic alkylation reactions are also more challenging to achieve with non-naphthylic substrates versus naphthylic substrates[47-51] because of the stronger coordination of the naphthalene π system to the metal, enabling greater preorganization of the intermediate leading to oxidative addition,[52] and a higher energetic penalty paid for dearomatization of benzene than for one ring of napthhalene,[53] resulting in a larger activation energy for the formation of a Pd-η^3-fluorobenzyl oxidative addition complex than of a Pd-η^3-fluoronaphthyl species formed through oxidative addition.[48, 54]

5.3 RESULTS & DISCUSSION

5.3.1 Development of Conditions for the Desymmetrization of Benzylic Difluoromethylene Units

Table 1. Evaluation of conditions for the desymmetrization of 1a.[a]

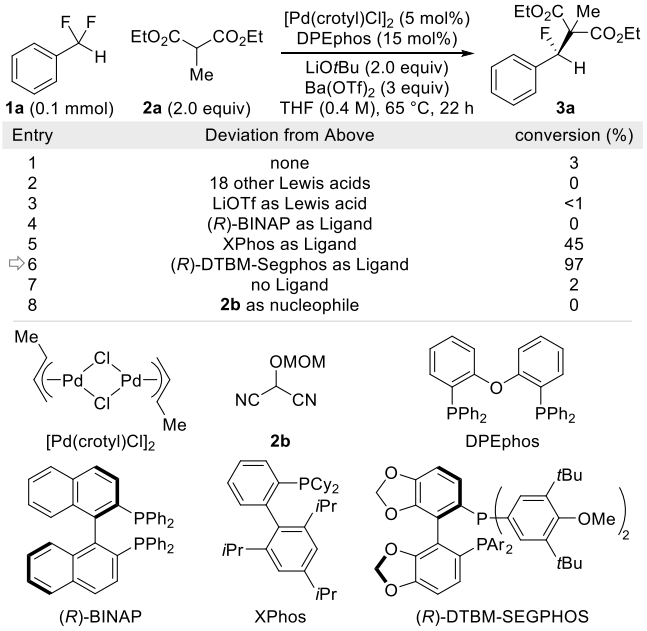

Entry	Deviation from Above	conversion (%)
1	none	3
2	18 other Lewis acids	0
3	LiOTf as Lewis acid	<1
4	(*R*)-BINAP as Ligand	0
5	XPhos as Ligand	45
⇨6	(*R*)-DTBM-Segphos as Ligand	97
7	no Ligand	2
8	**2b** as nucleophile	0

[a]Conversion determined using ^{19}F qNMR spectroscopy with 1-fluoronaphthalene as internal standard.

Initial studies to test the potential to extend our "push-pull" strategy for the desymmetrization of difluoroalkylarenes beyond the one example with diflulromethyl naphthalene in modest enantiomeric excess were conducted with 2-difluoromethylbenzene and diethyl-2-methylmalonate catalyzed by $[Pd(crotyl)Cl]_2$, a series of bisphosphine ligands, LiO*t*Bu, and LiOTf.[44]

Initial studies to test the potential to extend our "push-pull" strategy for the desymmetrization of difluoroalkylarenes beyond the one example with diflulromethyl naphthalene in modest ee were conducted with 2-difluoromethylbenzene and diethyl-2-methylmalonate catalyzed by $[Pd(crotyl)Cl]_2$, a series of bisphosphine, LiO*t*Bu, and LiOTf.[44]

Under the conditions we used for the reaction of difluoromethyl naphthalene with BINAP as ligand, less than 1% conversion was detected by ^{19}F NMR spectroscopy of the unpurified reaction mixture (see SI for additional information). We hypothesized that oxidative addition of the C(sp^3)–F bond was, most likely, rate-limiting, due to the high strength of this bond[55] and the dearomatization of the aryl ring to form

the intermediate Pd-η^3-fluorobenzyl species.;[49, 56] Therefore, we sought to accelerate the oxidative addition step.

We hypothesized that a stronger, more fluorophilic Lewis acid than LiOTf would be required to cleave the less reactive C–F bond in difluoromethylbenzene compared to the C–F bond in 2-difluoromethylnapthalene. The reaction of difluoromethylbenzene (**1a**) with malonate nucleophile **2a** proceeded in 3% yield, as determined by quantitative ^{19}F NMR spectroscopy, with barium(II) triflate ($Ba(OTf)_2$), lithium tert-butoxide (Li*O*t*Bu*), $[Pd(crotyl)Cl]_2$, and DPEphos in THF at 65 °C for 48 h. (Table 1, entry 1). Reactions with a variety of additional Lewis acids led to no conversion, and the reaction with LiOTf as the Lewis acid resulted in <1% conversion of the difluoride (Table 1, entries 2-3). In addition, we observed that the reaction was effective only in the presence of both lithium and barium salts (see supporting information).

To further accelerate oxidative addition, we examined the steric and electronic effects of the ligand on the reaction. Mono- and bis-phosphine ligands that bear sterically encumbered and/or electron-rich aryl groups on phosphorous are known to accelerate oxidative addition in palladium-catalyzed reactions.[57] The evaluation of a variety of commercially available monophosphine and bisphosphine ligands with these properties showed that (*R*)-DTBM-SEGPHOS generated a catalyst that led to the desymmetrization of difluoromethylbenzene **1a** with nucleophile **2a** in 99% yield at 65 °C after 24 h as determined by ^{19}F NMR spectroscopy (Table 1, entry 6. See supporting information for additional details). Ligands that were strongly electron-donating but not sterically bulky, and ligands that were sterically bulky but less electron-donating, generated less active catalysts. Variation of the biaryl backbone had a minimal effect on the reaction yield or enantioselectivity. A complete evaluation of reaction parameters can be found in the supporting information.

Table 2. Evaluation of conditions for the conversion of 1q to 3aj.[a]

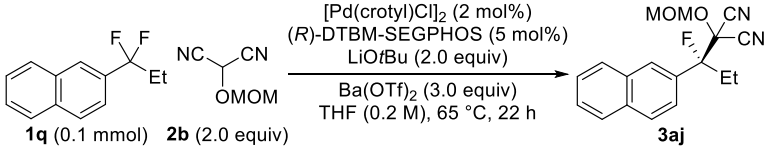

1q (0.1 mmol) **2b** (2.0 equiv) **3aj**

Entry	Deviation from Above	Conv. **1q** (%)	Yield **3aj** (%)
⇨ 1	none	>99	97
2	XPhos as ligand	0	0
3	2.0 equiv $Ba(OTf)_2$	>99	53
4	0.05 M concentration	90	33
5	0.40 M concentration	>99	68
6	5 mol% palladium, 15 mol% ligand	>99	86
7	1 mol% palladium, 3 mol% ligand	60	40

[a]Yield and conversion determined using ^{19}F qNMR spectroscopy with 1-fluoronaphthalene as internal standard.

Next, we sought to understand the effect of the barium salt on the reaction. If the metal-fluoride lattice energy ($\Delta U_{lattice}$) drives the increase in reactivity due to the inclusion of a barium salt, we hypothesized that magnesium salts would be more active Lewis acids ($\Delta U_{lattice}$(Ba) = -2357 and $\Delta U_{lattice}$(Mg) = -2961 kJ/mol, respectively);[58] however, the reaction of difluoromethylbenzene with malonate **2a** and $Mg(OTf)_2$ as Lewis acid resulted in no conversion of starting material. Solid-state ^{19}F NMR spectra of the solid byproducts generated upon completion of the reaction contained resonances for LiF[59] (δ = -201 ppm) and $Ba(OTf)_2$[60] (δ = -75 ppm), but they did not contain signals corresponding to BaF_2[61] or $BaLiF_3$[62] (δ = -12 and -98 ppm, respectively). Therefore, we hypothesize that the barium cation binds to the arene by a cation-π interaction and that this interaction stabilizes the transition state for the oxidative addition and the resulting palladium π-(fluoro)allyl species in a manner similar to the complexation of chromium to an arene.[63-65] It is known that α-chlorotoluene undergoes more rapid solvolysis when complexed with $Cr(CO)_3$ than when uncomplexed due to stabilization of the

benzylic cation by coordination to the metal.[66-67] Alkaline earth (Ae) metals engage extensively in M-π interactions,[68-70] and these interactions have been found to increase the rate of substrate activation in reactions catalyzed by Ae Lewis acids.[68, 71] However, we cannot rule out the possibility that barium is also involved in the S_N2-type reductive elimination,[72] and the precipitation of LiF should serve as a thermodynamic driving force for the oxidative addition.

We next investigated the formation of 3° stereocenters bearing fluorine at the electrophilic carbon by employing α,α-difluoropropylnaphthalene **1q**. We also evaluated the soft carbon nucleophile 2-(methoxymethoxy)-malononitrile (MAC, **2b**) for the defluorination to provide an additional avenue for further functionalization of the product.[73-76] Even though the catalyst containing XPhos led to product from the reaction of malonate nucleophile **2a** with electrophile **1a** (see Table 1, entry 5), the same catalyst did not lead to product when MAC nucleophile **2b** was reacted with difluoropropyl electrophile **2j** (Table 2, entry 2). However, a systematic modification of reaction concentration, catalyst loading, solvent, and reagent stoichiometry led to the conditions in Table 3 entry 1, which gave a high yield of the coupled product **3aj**. The product of the reaction of **2b** with 2-difluoroethylnaphthalene **1q** was isolated in 76% yield and 74% *ee*. With the ability to forge both secondary and tertiary stereocenters bearing fluorine established, we focused on increasing the enantioselectivity of the reaction.

5.3.2 Increased Reactivity and Selectivity Enabled by Ligand Development

Table 3. Evaluation of the effect of germanium-containing ligands on the yield and enantioselectivity of the conversion of 1q to 3q.[a]

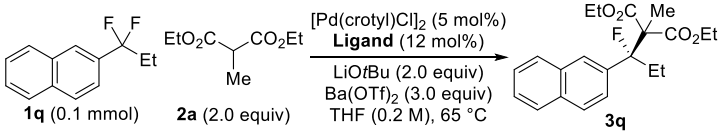

Entry	Ligand	Conv. **1q** (%)	Yield **3q** (%)	*ee* **3q** (%)
1	(R)-DTBM-SEGPHOS	>99	76	74
2	(R)-DTBM-BINAP	>99	56	73
3	(R)-DTMGM-BINAP	>99	86	76
4[b]	(R)-DTMGM-BINAP	>99	87	84
⇨ 5[c,d]	(R)-DTMGM-BINAP	78	68	94

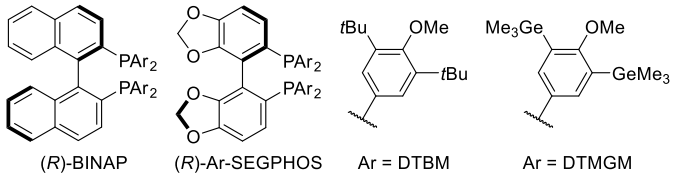

[a]Isolated yields; conversion determined using ^{19}F qNMR specteroscopy with 1-fluoronaphthalene as internal standard; *%ee* determined using chiral HPLC analysis; [b]Reaction conducted at rt; [c]Reaction conducted at 0 °C; [d]Reaction time = 96 h.

While the desymmetrization reaction proceeded in good yield, we sought to increase the enantioselectivity of the reaction. We hypothesized that oxidative addition is the rate-limiting and enantioselectivity-determining step; therefore, a further increase in the rate of oxidative addition to allow reactions at lower temperatures could increase enantioselectivity. To do so, we developed new ligands that would improve the rate of the reaction, the enantioselectivity of the reaction, or both.

We hypothesized that polarizable substituents on the aryl groups bound to phosphorous could engage in attractive dispersive interactions with the fluorinated substrate to increase the reaction rate. Other aryl substituents could improve the enantioselectivity by stabilizing and favoring the transition state for one enantiomer over the other. It has previously been demonstrated by Buchwald and Liu,[77] and by our group,[78] that bisphosphine ligands containing silicon and germanium atoms in place of carbon in the *tert*-butyl functionality of the DTBM substituent increase the rate and enantioselectivity of the copper-catalyzed hydroboration of disubstituted

alkenes by stabilizing the transition state for one enantiomer from hydrocupration by attractive London dispersion interactions. To this end, we synthesized BINAP-type ligands containing Ge in place of the central C atom in the *tert*-butyl group (Table 2).

The reaction of difluoropropyl electrophile **1q** and malonate nucleophile **2a**; catalyzed by the combination of $[Pd(crotyl)Cl]_2$, $Ba(OTf)_2$, Li*O*t*Bu*, and the germanium-containing ligand (*R*)-DTMGM-BINAP (DTMGM = di-(trimethylgermanyl)-methoxyphenyl); occurred at a faster rate than when the ligand containing the *tert*-butyl group, but the enantioselectivity was only slightly higher when the reaction was conducted at 65 °C (Table 3, entries 1-3). With DTMGM-BINAP, the reaction occurred at room temperature, resulting in a yield of **3q** of 86% in 84% *ee* after 24 h (Table 3, entry 4). By reducing the temperature further to 0 °C, the enantioselectivity increased to 94% *ee* with a yield of 68% after 96 h (Table 3, entry 5). With the germanium-containing ligands, the conversion of reactions with 10 mol% $Ba(OTf)_2$ were similar to those with excess $Ba(OTf)_2$, albeit with slightly reduced reaction yields.

5.3.3 Scope of α,α-Difluoroalkyl(hetero)arenes and Carbon Nucleophiles that Undergo the Desymmetrization Reaction

With conditions and a new ligand identified that increase yield and enantioselectivity, the range of (hetero)aryl-α,α-difluoride electrophiles and of carbon nucleophiles that undergo the desymmetrization reaction were evaluated in collaboration with Abigail Soliven. Because racemic samples of each product are required, we began by synthesizing a variety of products with (*rac*)-DTBM-SEGPHOS as the ligand on palladium (Chart 1). The evaluation of the yield and enantioselectivity of these transformations with (*R*)-DTMGM-BINAP is currently ongoing.

When subjected to the reaction conditions, a variety of α,α-difluoro(hetero)arenes reacted with malonate nucleophile **2a** to form 2° fluorine bearing stereocenters. Unactivated difluoromethylbenzene **3a** reacted to form the product in 71% isolated yield. Arenes substituted at the 4-position with electron-withdrawing trifluoromethyl (**3b**), cyano (**3c**), difluoromethyl (**3d**), or ethyl ester (**3e**) groups reacted with **2a** in yields of 24% – 72%. Substitution at the 3-position was also tolerated in the reaction, affording **3f** and **3g** in 55% and 81% yield respectively. Reactions containing $Ba(OtBu)_2$ (1.0 equiv) without an additional Lewis acid led to defluorination at difluoromethyl groups that are both benzylic and allylic (**3h**). In addition, naphthyl electrophiles **3i**, **3j**, and **3k** reacted in 83%, 45%, and 41% yields, respectively. Heteroaryl-substituted difluoromethyl electrophiles also underwent the title reaction. For example, 2-difluoromethylpyridine **1l** reacted with **2a** to form product **3l** in 78% yield. However, the reactions of electrophiles attached to the pyridyl ring at the 2- and 3-positions occurred in lower 13% (**3m**) and 21% (**3n**) yields, respectively.

Electrophiles containing alkyl substituents on the difluoromethylene unit were also tolerated under the reaction conditions, enabling the formation of stereocenters containing 3° fluorides. The methyl-substituted benzylic electrophiles **1o** and **1p** formed **3o** and **3p** in 24% and 75% yield respectively. Ethyl-substituted **3q** formed in 86% yield, and the methyl-substituted quinoline product **3r** formed in nearly quantitative yield. Finally, products containing a protected amine (**3s**) and heteroaryl units (**3t**) on the benzylic carbon were formed in 26% and 13% yields, respectively.

We also evaluated the scope of carbon nucleophiles that reacted under the described conditions. Malonate nucleophiles containing phenyl (**3u**), cyanoalkyl (**3v**), allyl (**3w**), protected

Chart 1. Scope of Benzylic Difluoride Electrophiles and of Carbon Nucleophiles that Undergo the Desymmetrization Reaction using (*rac*)-DTBM-SEGPHOS.[a]

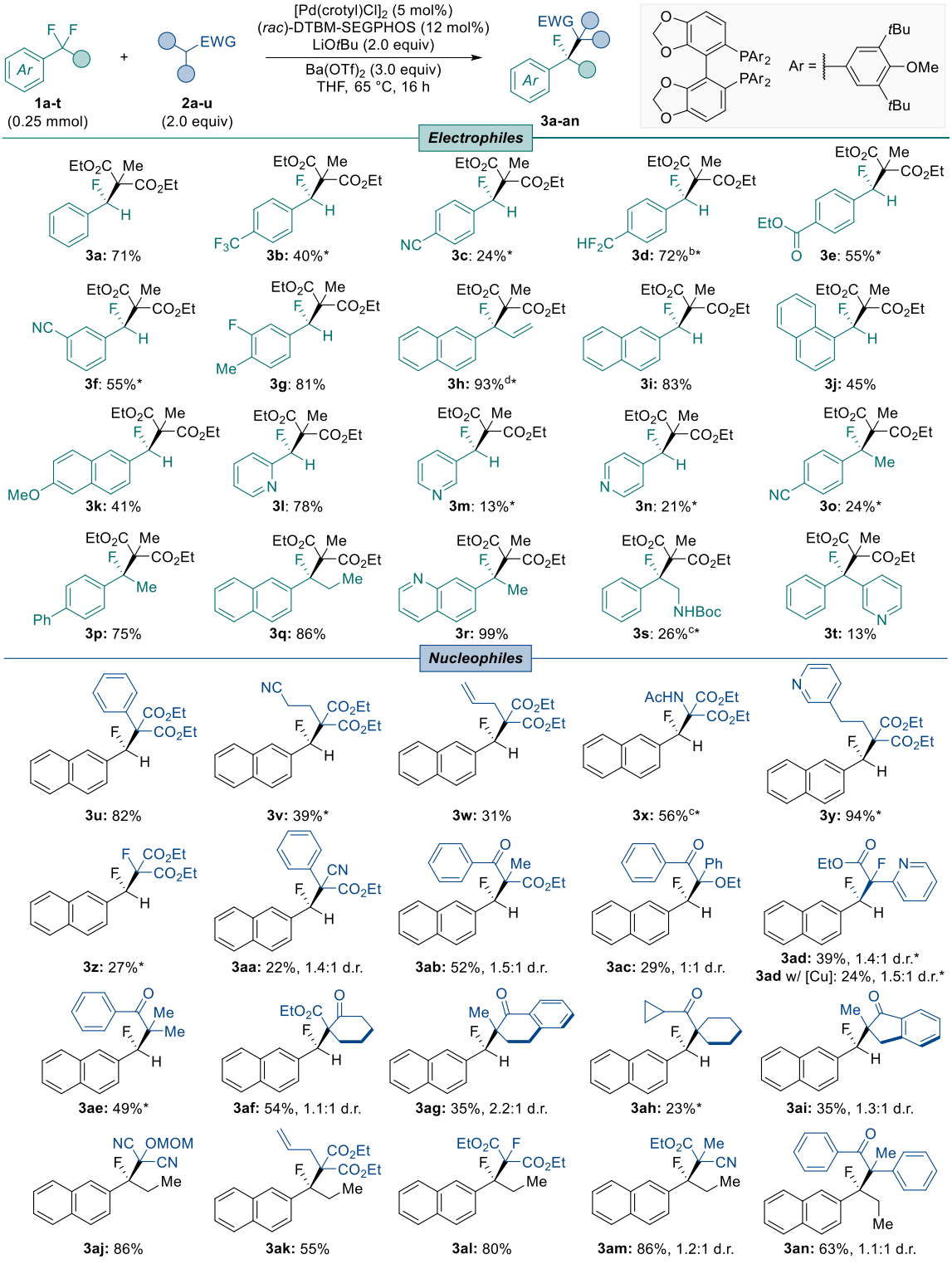

*Yields determined by Abigail Soliven; [a]Isolated yields; d.r. determined using ^{19}F NMR spectroscopy; [b]bis-alkylation product not detected; [c]reaction time = 96 h; [d]reaction time = 48 h, no lewis acid, $Ba(OtBu)_2$ (1.0 equiv); [Cu] = $Cu(MeCN)_4PF_6$ (5.0 mol%), (*R*,*R*)-Ph-BPE (5.5 mol%), pre-stirred with nucleophile.

amino (**3x**), 3-pyridyl (**3y**), and fluoro (**3z**) substituents on the nucleophilic carbon all reacted, with yields ranging from 27% for **3z** to 94% for **3y**. Additional acyclic nucleophiles, such as those containing electron-withdrawing groups in place of one (**3aa**, **3ab**) or both (**3ac-3ae**) of the malonate esters, reacted in yields of 22% - 52%. 2-Pyridyl-substituted nucleophile **2l** reacted to form **3ad** in 39% yield under the described conditions. We also found that six-membered β-keto esters and ketones react as nucleophiles to form the substitution products **3af-3ah** in moderate yields, as do five-membered ring ketones (**3af**). Finally, masked acyl cyanide nucleophile **2b** reacts cleanly to form 3° fluoride product **3aj** in 86% yield; this product can be further functionalized to access α-fluoro esters, amides, and thioesters (*vida infra*). Other carbon nucleophiles, such as malonate nucleophiles bearing allyl (**3ak**) or fluoro (**3al**) substituents, reacted in 50% and 80% yield, respectively. Finally, less-stabilized nucleophiles formed products **3am** and **3an** in 86% and 63% yields, respectively.

For all nucleophiles forming a stereocenter at the nucleophilic carbon, low diastereomeric ratios of 1:1 to 2.2:1 were obtained. As such, in preliminary experiments, we developed conditions with a copper bisphosphine complex known in diastereo-divergent fluoroalkylation reactions. Preliminary results for the formation of **3ad** suggest that ligating the nucleophile (**2l**) in the presence of 5 mol% $Cu(MeCN)_4PF_6$ and (*R*,*R*)-Ph-BPE as the ligand,[79] influences the diastereomeric ratio to a minimal extent (Chart 1).

During the evaluation of the scope, the presence of 2-naphthaldehyde was observed when conducting the reaction of nucleophile **2a** with electrophile **1i** to form product **3i**. We hypothesized that trace amounts of water were present in the commercial bottle of $Ba(OTf)_2$. To minimize the possibility of water contamination, and because we had noticed previously that some commercial bottles of $Ba(OTf)_2$ contained trace water, we sought to use $Ba(O\textit{t}Bu)_2$ in its place. To maintain the presence of both lithium and barium, LiOTf (3.0 equiv) was added as the Lewis acid. Previous experiments using nucleophile **2b** and electrophile **1i** had shown that the desymmetrization reaction occurs with this combination of base and Lewis acid, albeit in slightly lower yield than with the combination of Li*O*t*Bu and $Ba(OTf)_2$ (see Table S6 in the supporting information).

The reaction of **2a** with electrophile **1i** conducted with 1.0 equiv of $Ba(O\textit{t}Bu)_2$ and 3.0 equiv of LiOTf formed the coupled product **3i** in 55% yield without formation of 2-naphthaldehyde. In addition, the yield of the reaction with the combination of $Ba(OtBu)_2$ and LiOTf was higher (55%) than that with $Ba(OTf)_2$ and LiOtBu (39%). Further evaluation of the effect of this combination on the enantioselectivity and the yield of the reactions of other substrate combinations is currently under investigation.

5.4 Functionalization of Masked Acyl Cyanide-Coupled Products

The coupled products formed from the reaction of MAC nucleophile **2b** with difluoro electrophiles offer opportunities for further downstream functionalization.[73-76] The MAC group is an acyl cyanide equivalent, and can be unmasked with camphor sulphonic acid (CSA) to afford a highly reactive cyanohydrin. This cyanohydrin can be intercepted in a two-step, one-pot sequence by various nucleophiles to form products containing an α-fluoro carbonyl unit (Scheme 1).

By adapting procedures in the literature, MAC substituted naphthyl **3aj** was converted to α-fluoro carboxylic acid **4a** and ester **4b** in 85% and 65% yields, respectively. Formation of morpholino

amide **4c** proceeded in 87% yield, and formation of Weinreb amide **4d** proceeded in 40% yield. In addition, thioester **4e** was formed in 24% yield. Functional handles, such as a carboxylic acid (**4a**) or a Weinreb amide (**4d**), can themselves be leveraged for further functionalization of the fluorine-containing material. We envision that the described desymmetrization and functionalization sequence will be valuable for the construction of fluorochemicals in an enantioselective manner.

Scheme 1. Functionalization Reactions of the Coupled Product Containing the MAC Nucleophile.[a]

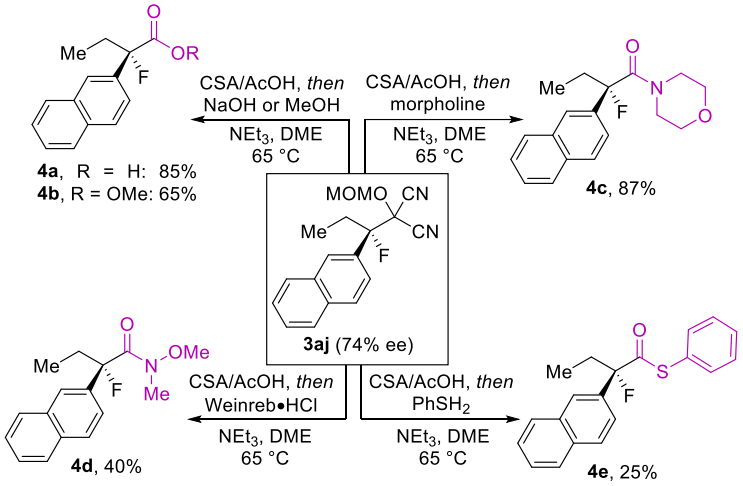

[a]Isolated yields. Weinreb•HCl = *N,O*-dimethylhydroxylamine hydrochloride. See supporting information for detailed reaction conditions.

5.5 Summary

In summary, we have developed a palladium-catalyzed desymmetrization strategy that converts benzylic difluoromethylene units into congested stereocenters bearing fluorine with high yield and enantioselectivity. The incorporation of a novel germanium-containing bisphosphine ligand in concert with $Ba(OTf)_2$ and Li*O*t*Bu* enables the efficient activation and selective transformation of (hetero)aryl-α,α-difluorides with a broad range of carbon nucleophiles. Moreover, the transformation tolerates various functional groups, such as pyridyl, di- and trifluoromethyl, ester, cyano, amino, fluoro, and allyl units. In addition, coupled products formed from reaction with a masked acyl cyanide nucleophile undergo downstream functionalization reactions that generate α-fluorinated carbonyl compounds. This work seeks to address critical challenges in the enantioselective synthesis of fluorinated stereocenters from racemic starting materials, thereby providing a robust platform for the preparation of valuable fluorinated building blocks with potential applications in pharmaceuticals, agrochemicals, and advanced materials.

5.6 References

(1) Inoue, M.; Sumii, Y.; Shibata, N. Contribution of Organofluorine Compounds to Pharmaceuticals. *ACS Omega* **2020**, *5*, 10633-10640.

(2) Novel Drug Approvals for 2020. https://www.fda.gov/drugs/new-drugs-fda-cders-new-molecular-entities-and-new-therapeutic-biological-products/novel-drug-approvals-2020 (accessed August 22, 2023).

(3) Ogawa, Y.; Tokunaga, E.; Kobayashi, O.; Hirai, K.; Shibata, N. Current Contributions of Organofluorine Compounds to the Agrochemical Industry. *iScience* **2020**, *23*, 101467.
(4) Kirsch, P., *Modern fluoroorganic chemistry: synthesis, reactivity, applications*. Wiley-VCH: Weinheim, Great Britain, 2004.
(5) Gillis, E. P.; Eastman, K. J.; Hill, M. D.; Donnelly, D. J.; Meanwell, N. A. Applications of Fluorine in Medicinal Chemistry. *J. Med. Chem.* **2015**, *58*, 8315-8359.
(6) Purser, S.; Moore, P. R.; Swallow, S.; Gouverneur, V. Fluorine in medicinal chemistry. *Chem. Soc. Rev.* **2008**, *37*, 320-330.
(7) Meanwell, N. A.; Eastman, K. J.; Gillis, E. P., Tactical Applications of Fluorine in Drug Design and Development. In *Fluorine in Heterocyclic Chemistry Volume 1*, Springer International Publishing: 2014; pp 1-54.
(8) McVicker, R. U.; O'Boyle, N. M. Chirality of New Drug Approvals (2013–2022): Trends and Perspectives. *J. Med. Chem.* **2024**, *67*, 2305-2320.
(9) Bacheley, L.; Guillamot, G.; Phansavath, P.; Ratovelomanana-Vidal, V. Asymmetric transfer hydrogenation of fluorinated ketone and imine derivatives: An efficient access to valuable building blocks. *Tetrahedron* **2024**, *152*, 133781.
(10) Tokunaga, E.; Akiyama, H.; Soloshonok, V. A.; Inoue, Y.; Hara, H.; Shibata, N. Biological evaluation of both enantiomers of fluoro-thalidomide using human myeloma cell line H929 and others. *PLOS ONE* **2017**, *12*, e0182152.
(11) Tredwell, M.; Gouverneur, V., 1.5 Fluorine in Medicinal Chemistry: Importance of Chirality. In *Comprehensive Chirality*, Elsevier: 2012; pp 70-85.
(12) Senkuttuvan, N.; Komarasamy, B.; Krishnamoorthy, R.; Sarkar, S.; Dhanasekaran, S.; Anaikutti, P. The significance of chirality in contemporary drug discovery-a mini review. *RSC Adv.* **2024**, *14*, 33429-33448.
(13) Brooks, W. H.; Guida, W. C.; Daniel, K. G. The Significance of Chirality in Drug Design and Development. *Curr. Top. Med. Chem.* **2011**, *11*, 760-770.
(14) Meanwell, N. A. Fluorine and Fluorinated Motifs in the Design and Application of Bioisosteres for Drug Design. *J. Med. Chem.* **2018**, *61*, 5822-5880.
(15) Richardson, P. Applications of fluorine to the construction of bioisosteric elements for the purposes of novel drug discovery. *Expert Opin. Drug Discov.* **2021**, *16*, 1261-1286.
(16) Spahn, V.; Del Vecchio, G.; Rodriguez-Gaztelumendi, A.; Temp, J.; Labuz, D.; Kloner, M.; Reidelbach, M.; Machelska, H.; Weber, M.; Stein, C. Opioid receptor signaling, analgesic and side effects induced by a computationally designed pH-dependent agonist. *Sci. Rep.* **2018**, *8*, 8965.
(17) Sheikhi, N.; Bahraminejad, M.; Saeedi, M.; Mirfazli, S. S. A review: FDA-approved fluorine-containing small molecules from 2015 to 2022. *Eur. J. Med. Chem.* **2023**, *260*, 115758.
(18) Melnykov, K. P.; Liashuk, O. S.; Holovach, S.; Shatnia, V.; Horbenko, A.; Lesyk, D.; Melnyk, V.; Skrypnik, D.; Beshtynarska, A.; Borysko, P.; Viniichuk, O.; Grygorenko, O. O. Physicochemical and Biological Evaluation of gem-Difluorinated Saturated Oxygen Heterocycles as Bioisosteres for Drug Discovery. *Chem. Eur. J.* **2024**, *n/a*, e202404390.
(19) Alexander, N.; Augenstein, M.; Sorensen, A. M.; Garcia, C.; Greene, A.; Harrison, A. W. Computational design of β-fluorinated morphine derivatives for pH-specific binding. *Chem. Phys. Lett.* **2021**, *777*, 138723.
(20) Rosas, R., Jr.; Huang, X.-P.; Roth, B. L.; Dockendorff, C. β-Fluorofentanyls Are pH-Sensitive Mu Opioid Receptor Agonists. *ACS Med. Chem. Lett.* **2019**, *10*, 1353-1356.

(21) Wang, L.; Zhu, X.; Wang, B.; Wang, Y.; Wang, M.; Yang, S.; Su, C.; Chang, J.; Zhu, B. Design, Synthesis, and Activity Evaluation of Fluorine-Containing Scopolamine Analogues as Potential Antidepressants. *J. Med. Chem.* **2024**.
(22) Zhu, Y.; Han, J.; Wang, J.; Shibata, N.; Sodeoka, M.; Soloshonok, V. A.; Coelho, J. A. S.; Toste, F. D. Modern Approaches for Asymmetric Construction of Carbon-Fluorine Quaternary Stereogenic Centers: Synthetic Challenges and Pharmaceutical Needs. *Chem Rev* **2018**, *118*, 3887-3964.
(23) Butcher, T. W.; Amberg, W. M.; Hartwig, J. F. Transition-Metal-Catalyzed Monofluoroalkylation: Strategies for the Synthesis of Alkyl Fluorides by C−C Bond Formation. *Angew. Chem. Int. Ed.* **2021**.
(24) Xu, P.; Guo, S.; Wang, L.; Tang, P. Silver-Catalyzed Oxidative Activation of Benzylic C□H Bonds for the Synthesis of Difluoromethylated Arenes. *Angew. Chem. Int. Ed.* **2014**, *53*, 5955-5958.
(25) Yang, X.; Wu, T.; Phipps, R. J.; Toste, F. D. Advances in Catalytic Enantioselective Fluorination, Mono-, Di-, and Trifluoromethylation, and Trifluoromethylthiolation Reactions. *Chem. Rev.* **2015**, *115*, 826-870.
(26) González-Esguevillas, M.; Miró, J.; Jeffrey, J. L.; MacMillan, D. W. C. Photoredox-catalyzed deoxyfluorination of activated alcohols with Selectfluor®. *Tetrahedron* **2019**, *75*, 4222-4227.
(27) Zhu, Y.; Han, J.; Wang, J.; Shibata, N.; Sodeoka, M.; Soloshonok, V. A.; Coelho, J. A. S.; Toste, F. D. Modern Approaches for Asymmetric Construction of Carbon–Fluorine Quaternary Stereogenic Centers: Synthetic Challenges and Pharmaceutical Needs. *Chem. Rev.* **2018**, *118*, 3887-3964.
(28) Blessley, G.; Holden, P.; Walker, M.; Brown, J. M.; Gouverneur, V. Palladium-Catalyzed Substitution and Cross-Coupling of Benzylic Fluorides. *Org. Lett.* **2012**, *14*, 2754-2757.
(29) Lin, H.; Huang, X.; Jiao, W.; Fang, D.; Wang, M.; Liao, J. Enantioselective Cu-Catalyzed Nucleophilic Substitutions of Polyfluoroarenes: Synthesis of Chiral Polyfluoroaryl Diarylmethanes. *Org. Lett.* **2023**, *25*, 3239-3244.
(30) He, Z.-T.; Jiang, X.; Hartwig, J. F. Stereodivergent Construction of Tertiary Fluorides in Vicinal Stereogenic Pairs by Allylic Substitution with Iridium and Copper Catalysts. *J. Am. Chem. Soc.* **2019**, *141*, 13066-13073.
(31) Sap, J. B. I.; Meyer, C. F.; Straathof, N. J. W.; Iwumene, N.; am Ende, C. W.; Trabanco, A. A.; Gouverneur, V. Late-stage difluoromethylation: concepts, developments and perspective. *Chem. Soc. Rev.* **2021**, *50*, 8214-8247.
(32) Purushotam; Bera, A.; Banerjee, D. Recent advances on non-precious metal-catalysed fluorination, difluoromethylation, trifluoromethylation, and perfluoroalkylation of N-heteroarenes. *Org. Biomol. Chem.* **2023**, *21*, 9298-9315.
(33) Li, X.; Song, Q. Introduction of Difluoromethyl Through Radical Pathways. *Eur. J. Org. Chem.* **2024**, *27*, e202400423.
(34) Ferguson, D. M.; Malapit, C. A.; Bour, J. R.; Sanford, M. S. Palladium-Catalyzed Difluoromethylation of Aryl Chlorides and Bromides with TMSCF2H. *J. Org. Chem.* **2019**, *84*, 3735-3740.
(35) Jelen, J.; Tavčar, G. Deoxyfluorination: A Detailed Overview of Recent Developments. *Synthesis* **2024**, *57*, 1517-1541.
(36) Geri, J. B.; Wade Wolfe, M. M.; Szymczak, N. K. The Difluoromethyl Group as a Masked Nucleophile: A Lewis Acid/Base Approach. *J. Am. Chem. Soc.* **2018**, *140*, 9404-9408.

(37) Trofymchuk, S.; Bugera, M.; Klipkov, A. A.; Ahunovych, V.; Razhyk, B.; Semenov, S.; Boretskyi, A.; Tarasenko, K.; Mykhailiuk, P. K. Scalable Approach to Fluorinated Heterocycles with Sulfur Tetrafluoride (SF4). *J. Org. Chem.* **2021**.
(38) Nicolai, J.; Fantoni, T.; Butcher, T. W.; Arlow, S.; Ryabukhin, S. V.; Volochnyuk, D. M.; Hartwig, J. F. Copper-Mediated Cyanodifluoromethylation of (Hetero)aryl Iodides and Activated (Hetero)aryl Bromides with TMSCF2CN. *J. Am. Chem. Soc.* **2024**, *146*, 15464-15472.
(39) Polterauer, D.; Wagschal, S.; Bersier, M.; Bovino, C.; Roberge, D. M.; Hone, C. A.; Kappe, C. O. Deoxyfluorination of Ketones with Sulfur Tetrafluoride (SF4) and Dialkylamines in Continuous Flow Mode. *Org. Process Res. Dev.* **2024**, *28*, 2919-2927.
(40) Choi, K.; Mormino, M. G.; Kalkman, E. D.; Park, J.; Hartwig, J. F. Palladium-Catalyzed Aryldifluoromethylation of Aryl Halides with Aryldifluoromethyl Trimethylsilanes. *Angew. Chem. Int. Ed.* **2022**, *61*, e202208204.
(41) Stahl, T.; Klare, H. F. T.; Oestreich, M. Main-Group Lewis Acids for C–F Bond Activation. *ACS Catal.* **2013**, *3*, 1578-1587.
(42) Lemal, D. M. Perspective on Fluorocarbon Chemistry. *J. Org. Chem.* **2004**, *69*, 1-11.
(43) Anslyn, E. V.; Dougherty, D. A., *Modern Physical Organic Chemistry*. University Science Books: 2006.
(44) Butcher, T. W.; Yang, J. L.; Amberg, W. M.; Watkins, N. B.; Wilkinson, N. D.; Hartwig, J. F. Desymmetrization of difluoromethylene groups by C-F bond activation. *Nature* **2020**, *583*, 548-553.
(45) Zhang, S.; Yamamoto, Y.; Bao, M. Benzyl Palladium Intermediates: Unique and Versatile Reactive Intermediates for Aromatic Functionalization. *Adv. Synth. Catal.* **2021**, *363*, 587-601.
(46) Le Bras, J.; Muzart, J. Production of Csp3–Csp3 Bonds through Palladium-Catalyzed Tsuji–Trost-Type Reactions of (Hetero)Benzylic Substrates. *Eur. J. Org. Chem.* **2016**, *2016*, 2565-2593.
(47) Liégault, B.; Renaud, J.-L.; Bruneau, C. Activation and functionalization of benzylic derivatives by palladium catalysts. *Chem. Soc. Rev.* **2008**, *37*, 290-299.
(48) Liu, J.-H.; Wen, W.; Liao, J.; Shen, Q.-W.; Lin, Y.; Wu, Z.-L.; Cai, T.; Guo, Q.-X. Catalytic asymmetric Tsuji–Trost α−benzylation reaction of N-unprotected amino acids and benzyl alcohol derivatives. *Nat. Commun.* **2022**, *13*, 2509.
(49) Kuwano, R.; Kondo, Y.; Matsuyama, Y. Palladium-Catalyzed Nucleophilic Benzylic Substitutions of Benzylic Esters. *J. Am. Chem. Soc.* **2003**, *125*, 12104-12105.
(50) Schwarz, K. J.; Yang, C.; Fyfe, J. W. B.; Snaddon, T. N. Enantioselective α-Benzylation of Acyclic Esters Using π-Extended Electrophiles. *Angew. Chem. Int. Ed.* **2018**, *57*, 12102-12105.
(51) Kuwano, R. Catalytic Transformations of Benzylic Carboxylates and Carbonates. *Synthesis* **2009**, *2009*, 1049-1061.
(52) Chen, P.-P.; Lucas, E. L.; Greene, M. A.; Zhang, S.-Q.; Tollefson, E. J.; Erickson, L. W.; Taylor, B. L. H.; Jarvo, E. R.; Hong, X. A Unified Explanation for Chemoselectivity and Stereospecificity of Ni-Catalyzed Kumada and Cross-Electrophile Coupling Reactions of Benzylic Ethers: A Combined Computational and Experimental Study. *J. Am. Chem. Soc.* **2019**, *141*, 5835-5855.
(53) Primault, G.; Legros, J.-Y.; Fiaud, J.-C. Palladium-catalyzed benzylic-like nucleophilic substitution of benzofuran-, benzothiophene- and indole-based substrates by dimethyl malonate anion. *J. Organomet. Chem.* **2003**, *687*, 353-364.
(54) Xu, J.; Bercher, O. P.; Watson, M. P. Overcoming the Naphthyl Requirement in Stereospecific Cross-Couplings to Form Quaternary Stereocenters. *J. Am. Chem. Soc.* **2021**.

(55) O'Hagan, D. Understanding organofluorine chemistry. An introduction to the C-F bond. *Chem Soc Rev* **2008**, *37*, 308-19.
(56) Johns, A. M.; Utsunomiya, M.; Incarvito, C. D.; Hartwig, J. F. A Highly Active Palladium Catalyst for Intermolecular Hydroamination. Factors that Control Reactivity and Additions of Functionalized Anilines to Dienes and Vinylarenes. *J. Am. Chem. Soc.* **2006**, *128*, 1828-1839.
(57) Norrby, P. O., Organotransition Metal Chemistry: From Bonding to Catalysis. John Hartwig. Wiley Online Library: 2010.
(58) Aylward, G. F., T., *SI Chemical Data*. 3rd ed.; Wiley: New York, 1994.
(59) Harris, R. K.; Jackson, P. High-resolution fluorine-19 magnetic resonance of solids. *Chem. Rev.* **1991**, *91*, 1427-1440.
(60) Determined experimentally using 19F ssNMR spectroscopy.
(61) Breitfeld, S.; Scholz, G.; Emmerling, F.; Kemnitz, E. BaF-benzenedicarboxylate: the first mechanochemical synthesis of a new coordination polymer with a direct Ba–F bond. *J. Mater. Sci.* **2018**, *53*, 13682-13689.
(62) Zheng, A.; Liu, S.-B.; Deng, F. 19F Chemical Shift of Crystalline Metal Fluorides: Theoretical Predictions Based on Periodic Structure Models. *J. Phys. Chem. C.* **2009**, *113*, 15018-15023.
(63) Zhang, J.; Stanciu, C.; Wang, B.; Hussain, M. M.; Da, C.-S.; Carroll, P. J.; Dreher, S. D.; Walsh, P. J. Palladium-Catalyzed Allylic Substitution with (η6-Arene–CH2Z)Cr(CO)3-Based Nucleophiles. *J. Am. Chem. Soc.* **2011**, *133*, 20552-20560.
(64) Zeng, W.-L.; Yuan, Y.-F.; Wang, M.-Y.; Li, W. Chromium-Mediated Dearomative Allylic Addition to Arenes. *Eur. J. Org. Chem.* **2024**, *27*, e202400826.
(65) Merlic, C. A.; Miller, M. M.; Hietbrink, B. N.; Houk, K. N. Reactivity of (η6-Arene)tricarbonylchromium Complexes toward Additions of Anions, Cations, and Radicals. *J. Am. Chem. Soc.* **2001**, *123*, 4904-4918.
(66) Trahanovsky, W. S.; Wells, D. K. Arene-metal complexes. I. Thermodynamic stabilities of substituted benzyl cations complexed with tricarbonylchromium. *J. Am. Chem. Soc.* **1969**, *91*, 5870-5871.
(67) Holmes, J. D.; Jones, D. A. K.; Pettit, R. Electronic effects in group VIB arene-metal carbonyl complexes and related species. *J. Organomet. Chem.* **1965**, *4*, 324-331.
(68) Thum, K.; Martin, J.; Elsen, H.; Eyselein, J.; Stiegler, L.; Langer, J.; Harder, S. Lewis Acidic Cationic Strontium and Barium Complexes. *Eur. J. Inorg. Chem.* **2021**, *2021*, 2643-2653.
(69) Shi, X.; Cheng, J. Reversible addition and hydrogenation of 1,1-diphenylethylene with a barium complex. *Dalton Trans.* **2019**, *48*, 8565-8568.
(70) Gärtner, M.; Görls, H.; Westerhausen, M. Synthesis and structural variations of substituted phenylamide complexes of the heavy alkaline earth metals calcium, strontium and barium. *Dalton Trans.* **2008**, 1574-1582.
(71) Wilson, A. S. S.; Hill, M. S.; Mahon, M. F.; Dinoi, C.; Maron, L. Organocalcium-mediated nucleophilic alkylation of benzene. *Science* **2017**, *358*, 1168-1171.
(72) Yanagisawa, A.; Yoshida, K. Recent Advances in Selective Reactions Promoted by Barium Reagents. *Synlett* **2011**, *2011*, 2929-2938.
(73) Yang, K. S.; Nibbs, A. E.; Türkmen, Y. E.; Rawal, V. H. Squaramide-Catalyzed Enantioselective Michael Addition of Masked Acyl Cyanides to Substituted Enones. *J. Am. Chem. Soc.* **2013**, *135*, 16050-16053.

(74) Yang, K. S.; Rawal, V. H. Synthesis of α-Amino Acid Derivatives and Peptides via Enantioselective Addition of Masked Acyl Cyanides to Imines. *J. Am. Chem. Soc.* **2014**, *136*, 16148-16151.
(75) Hethcox, J. C.; Shockley, S. E.; Stoltz, B. M. Enantioselective Iridium-Catalyzed Allylic Alkylation Reactions of Masked Acyl Cyanide Equivalents. *Org. Lett.* **2017**, *19*, 1527-1529.
(76) Shockley, S. E.; Hethcox, J. C.; Stoltz, B. M. Enantioselective Synthesis of Acyclic α-Quaternary Carboxylic Acid Derivatives through Iridium-Catalyzed Allylic Alkylation. *Angew. Chem. Int. Ed.* **2017**, *56*, 11545-11548.
(77) Lu, G.; Liu, R. Y.; Yang, Y.; Fang, C.; Lambrecht, D. S.; Buchwald, S. L.; Liu, P. Ligand–Substrate Dispersion Facilitates the Copper-Catalyzed Hydroamination of Unactivated Olefins. *J. Am. Chem. Soc.* **2017**, *139*, 16548-16555.
(78) Xi, Y.; Su, B.; Qi, X.; Pedram, S.; Liu, P.; Hartwig, J. F. Application of Trimethylgermanyl-Substituted Bisphosphine Ligands with Enhanced Dispersion Interactions to Copper-Catalyzed Hydroboration of Disubstituted Alkenes. *J. Am. Chem. Soc.* **2020**, *142*, 18213-18222.
(79) Qiu, Y.; Thomas, V. C. J. X.; Fantoni, T.; Chen, R.; Jiang, X.; He, Z.-T.; Butcher, T. W.; Nomura, D. K.; Hartwig, J. F. Convergent synthesis and protein binding of vicinal difluorides by stereodivergent C–C bond formation. *Chem* **2024**, *10*, 3709-3721.
(80) Yang, K. S.; Nibbs, A. E.; Turkmen, Y. E.; Rawal, V. H. Squaramide-catalyzed enantioselective Michael addition of masked acyl cyanides to substituted enones. *J Am Chem Soc* **2013**, *135*, 16050-3.
(81) Sakamoto, S.; Butcher, T. W.; Yang, J. L.; Hartwig, J. F. gem-Difluoroallylation of Aryl Halides and Pseudo Halides with Difluoroallylboron Reagents in High Regioselectivity. *Angew. Chem. Int. Ed.* **2021**, *60*, 25746-25752.
(82) Xia, J.-B.; Zhu, C.; Chen, C. Visible Light-Promoted Metal-Free C–H Activation: Diarylketone-Catalyzed Selective Benzylic Mono- and Difluorination. *J. Am. Chem. Soc.* **2013**, *135*, 17494-17500.
(83) Gaussian 16, R. C., M. J. Frisch, G. W. Trucks, H. B. Schlegel, G. E. Scuseria, M. A. Robb, J. R. Cheeseman, G. Scalmani, V. Barone, G. A. Petersson, H. Nakatsuji, X. Li, M. Caricato, A. V. Marenich, J. Bloino, B. G. Janesko, R. Gomperts, B. Mennucci, H. P. Hratchian, J. V. Ortiz, A. F. Izmaylov, J. L. Sonnenberg, D. Williams-Young, F. Ding, F. Lipparini, F. Egidi, J. Goings, B. Peng, A. Petrone, T. Henderson, D. Ranasinghe, V. G. Zakrzewski, J. Gao, N. Rega, G. Zheng, W. Liang, M. Hada, M. Ehara, K. Toyota, R. Fukuda, J. Hasegawa, M. Ishida, T. Nakajima, Y. Honda, O. Kitao, H. Nakai, T. Vreven, K. Throssell, J. A. Montgomery, Jr., J. E. Peralta, F. Ogliaro, M. J. Bearpark, J. J. Heyd, E. N. Brothers, K. N. Kudin, V. N. Staroverov, T. A. Keith, R. Kobayashi, J. Normand, K. Raghavachari, A. P. Rendell, J. C. Burant, S. S. Iyengar, J. Tomasi, M. Cossi, J. M. Millam, M. Klene, C. Adamo, R. Cammi, J. W. Ochterski, R. L. Martin, K. Morokuma, O. Farkas, J. B. Foresman, and D. J. Fox, Gaussian, Inc., Wallingford CT, 2016.
(84) Marenich, A. V.; Cramer, C. J.; Truhlar, D. G. Universal Solvation Model Based on Solute Electron Density and on a Continuum Model of the Solvent Defined by the Bulk Dielectric Constant and Atomic Surface Tensions. *J. Phys. Chem. B.* **2009**, *113*, 6378–6396.
(85) R. Dennington, T. A. K., J. M. Millam, GaussView, Version 6.1; Semichem Inc., Shawnee Mission, KS (USA), 2016.
(86) Perdew, J. P.; Burke, K.; Ernzerhof, M. Generalized Gradient Approximation Made Simple. *Phys. Rev. Lett.* **1996**, *77*, 3865–3868.
(87) Adamo, C.; Barone, V. Toward reliable density functional methods without adjustable parameters: The PBE0 model. *J. Chem. Phys.* **1999**, *110*, 6158–6170.

(88) Grimme, S.; Ehrlich, S.; Goerigk, L. Effect of the damping function in dispersion corrected density functional theory. *J. Comput. Chem.* **2011**, *32*, 1456–1465.
(89) Falivene, L.; Credendino, R.; Poater, A.; Petta, A.; Serra, L.; Oliva, R.; Scarano, V.; Cavallo, L. SambVca 2. A Web Tool for Analyzing Catalytic Pockets with Topographic Steric Maps. *Organometallics* **2016**, *35*, 2286-2293.

5.7 Experimental Information

5.7.1 General Information

All reactions were conducted under inert atmosphere in a nitrogen-filled glovebox or with standard Schlenk techniques, unless otherwise specified. All reagents and solvents were purchased from commercial sources and used as received, unless otherwise noted. All glassware was flame-dried or dried overnight at 120 °C, allowed to cool under vacuum, and stored in a N_2-atomsphere drybox until use unless otherwise noted. Tetrahydrofuran, toluene, and diethyl ether were purified by passing the degassed solvents (N_2) through a column of activated alumina (solvent purification system purchased from Innovative Technologies, Newburyport, MA). All other solvents were stored over 4 Å molecular sieves for at least 24 h prior to use. Compounds **1a-1g**, **1i**, **1j**, **1l-1o**, **2a**, **2c-2k**, **2m-2u** are commercially available. Compounds **1s**,[38] **2b**,[80] and **2l**[79] were prepared by methods previously reported in the literature. $Ba(OTf)_2$ purchased from Sigma-Aldrich was flame-dried before use. $Ba(OTf)_2$ from Strem was used as received. All reagents purchased from commercial suppliers were stored in the glove box and used as received. Racemic samples were obtained using racemic DTBM-SEGPHOS as the ligand, which was prepared by mixing equal amounts of (*S*)-DTBM-SEGPHOS and (*R*)-DTBM-SEGPHOS.

Deuterated solvents were purchased from Cambridge Isotope Laboratories and used as received.

^1H, ^{13}C, and ^{19}F NMR spectra were recorded on Bruker AV-300, AVQ-400, AV-500, AV-600, NEO-500, NEO-501 and AV-700 spectrometers at the University of California, Berkeley NMR facility. Chemical shifts are reported relative to residual solvent peaks ($CDCl_3$ = 7.26 ppm for ^1H NMR spectra and 77.16 ppm for $^{13}C\{^1H\}$ NMR spectra, DMSO-*d6* = 2.50 ppm for ^1H NMR spectra and 39.52 ppm for $^{13}C\{^1H\}$ NMR spectra). For ^{19}F NMR spectra, chemical shifts are reported relative to the δ –113.15 resonance of fluorobenzene used as an external reference or the δ –63.72 resonance of α,α,α-trifluorotoluene. The following abbreviations are used in reporting NMR data: s, singlet; d, doublet; t, triplet; q, quartet; AB, AB quartet; p, pentet; hept, heptet; m, multiplet.

HPLC analyses were carried out on an Agilent Infinity II chiral HPLC system with Chiralpak columns. High-resolution mass spectra were recorded on an Agilent Time of Flight (Q-TOF) mass spectrometer in ESI mode operated by the Catalysis Center at the University of California, Berkeley or were obtained from the QB3 Mass Spectrometry Facility at UC Berkeley. Analytical thin layer chromatography (TLC) was performed on Kieselgel 60 F254 glass plates precoated with a 0.25 mm thickness of silica gel. The TLC plates were visualized with UV light. Preparatory TLC was performed on AnalTech preparatory TLC plates with a 1000 μm-thick silica coating and visualized by UV. Column chromatography was generally performed on a Teledyne Isco Combiflash® Rf system with RediSep Gold™ columns.

5.7.2 Preliminary Examination of Reaction Parameters

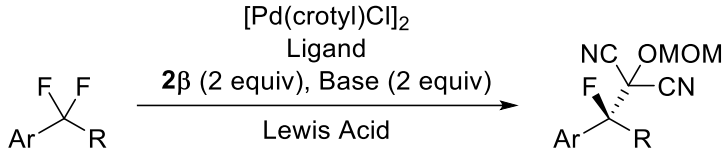

To a vial equipped with magnetic stir bar was added, sequentially, 100 µL aliquots of stock solutions of electrophile (0.01 mmol), dichlorobis(1-methylallyl)dipalladium (0.10–5.00 mol%, 0.01–0.50 µmol), and ligand (0.30–15.0 mol%, 0.03–1.50 µmol) in THF. The solvent was then evaporated, and 100 uL stock solutions of Lewis acid (1.0–3.0 equiv, 0.01–0.03 mmol), **2b** (2.00 equiv, 0.02 mmol), and base (2.00 equiv, 0.02 mmol) in THF were added sequentially (final volume 300 µL, 0.03 M). The vial was then sealed with a Teflon-lined cap and electrical tape and stirred at 650 rpm for 48 h at 65 °C. Once cooled to rt, internal standard (monofluorobenzene, 100 mol% in 1 mL $CDCl_3$) was added to the reaction mixture, the resulting solution was passed through a syringe filter, and the filtered crude mixture was analyzed using ^{19}F NMR Spectroscopy.

5.7.3 Examination of the Effect of the Manner of Addition on the Reaction

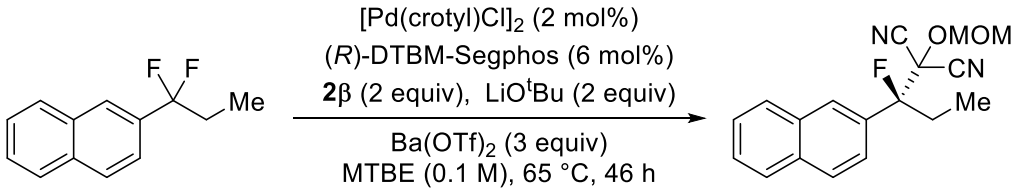

To a vial equipped with magnetic stir bar was added, sequentially, 2-(1,1-difluoropropyl)naphthalene (31.0 mg, 0.15 mmol), dichlorobis(1-methylallyl)dipalladium (1.20 mg, 2.00 mol%, 3.00 µmol), (*R*)-DTBM-SEGPHOS (11.0 mg, 6.00 mol%, 9.00 µmol), 2-(methoxymethoxy)malononitrile (38.0 mg, 2.00 equiv, 0.30 mmol). MTBE (1.50 mL, 0.10 M) was then added, followed by LiO*t*Bu (24.0 mg, 2.00 equiv, 0.30 mmol). The vial was then sealed with a Teflon-lined cap and electrical tape and stirred at 650 rpm for 46 h at 65 °C. Once cooled to ambient temperature, internal standard was added (100 mol%) and the reaction mixture was diluted with ethyl acetate, filtered through celite using ethyl acetate and hexanes as eluent, and the filtrate was concentrated *in vacuo*. Conversion was determined by ^{19}F NMR spectroscopy.

5.7.4 Examination of the Effect of Pre-Mixing Pronucleophile and Base on the Reaction

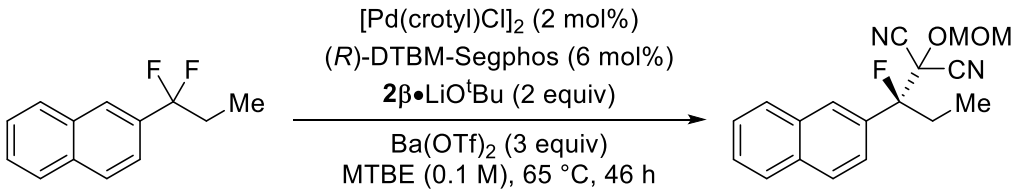

To a vial equipped with magnetic stir bar was added, sequentially, 100 µL aliquots of a stock solution of 2-(1,1-difluoropropyl)naphthalene (21.0 mg , 0.10 mmol) in MTBE and a pre-mixed

stock solution of dichlorobis(1-methylallyl)dipalladium (0.78 mg, 2.00 mol%, 2.00 μmol) and ligand (7.10 mg, 6.00 mol%, 6.00 μmol) in MTBE. MTBE (700 μL) was added, followed by solid $Ba(OTf)_2$ (130 mg, 3.00 equiv, 0.30 mmol). The contents of the vial were stirred briefly, then 100 μL of a pre-mixed stock solution of 2-(methoxymethoxy)malononitrile (25.0 mg, 2.00 equiv, 0.20 mmol) and Li*O*t*Bu* (16.0 mg, 2.00 equiv, 0.20 mmol) in MTBE was added (total volume 1.00 mL) and the vial was sealed with a Teflon-lined cap and electrical tape and stirred at 650 rpm for 48 hour at 65 °C. Once cooled to ambient temperature, internal standard was added (100 mol%) and the reaction mixture was diluted with ethyl acetate, filtered through celite using ethyl acetate and hexanes as eluent, and concentrated *in vacuo*. Conversion was determined by ^{19}F NMR spectroscopy.

5.7.5 General Procedure: Palladium-Catalyzed Desymmetrization of Benzylic Difluoromethylene Units

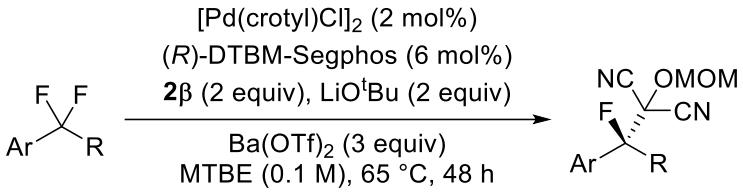

To a vial equipped with magnetic stir bar was added, sequentially, 100 μL of a stock solution of electrophile (0.10 mmol) in MTBE and 100 μL of a pre-mixed stock solution of dichlorobis(1-methylallyl)dipalladium (2.00 mol%, 2.00 μmol) and (*R*)-DTBM-SEGPHOS (6.00 mol%, 6.00 μmol) in MTBE. MTBE (700 μL) was added, followed by solid $Ba(OTf)_2$ (3.00 equiv, 0.30 mmol). The contents of the vial were stirred briefly, then 100 μL of a stock solution of 2-(methoxymethoxy)malononitrile (2.00 equiv, 0.20 mmol) in MTBE (total volume 1 mL) and powdered Li*O*t*Bu* (2.00 equiv, 0.20 mmol) were added sequentially. The vial was then sealed with a Teflon-lined cap and electrical tape and stirred at 650 rpm for 48 h at 65 °C. Once cooled to ambient temperature, the reaction mixture was diluted with ethyl acetate, filtered through celite using ethyl acetate and hexanes as eluent, and concentrated *in vacuo*. The residue was then purified by column chromatography to afford the desired product.

5.7.6 Evaluation of Commercial Ligands

Table S1. Effect of Lewis acids on the Desymmetrization Reaction with Difluoromethylbenzene.[a]

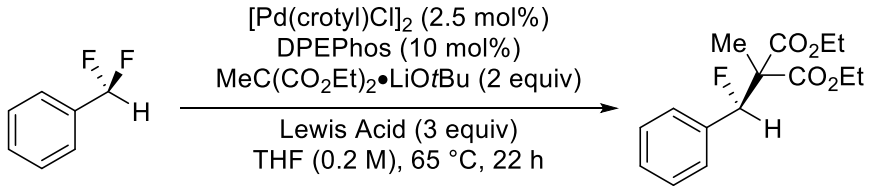

Entry	Lewis acid	Yield (1 equiv)	Yield (3 equiv)
1	LiOTf	0%	<1%
2	$Mg(OTf)_2$	0%	0%
3	$Mg(OtBu)_3$	0%	0%
4	$Al(OtBu)_3$	0%	0%
5	$Ba(OTf)_2$	0%	3%
6	$BiCl_3$	0%	0%
7	$MgBr_2$	0%	0%
8	$CeCl_3$	0%	0%
9	$Zn(OTf)_2$	0%	0%
10	$TiCl_2(OiPr)_2$	0%	0%
11	$In(OTf)_3$	0%	0%
12	$Bi(OTf)_3$	0%	0%
13	$La(OTf)_3$	<1%	<1%
14	$Yb(OAc)•_3H_2O$	0%	0%
15	$Sc(NO_3)•_3H_2O$	0%	0%
16	$Ni(OTf)_2$	<1%	0%
17	$Cu(OTf)_2$	0%	0%
18	$Ce(OTf)_3$	0%	0%
19[b]	$Ba(OTf)_2$	-	83%

[a]Conversion determined using ^{19}F qNMR spectroscopy. Enantiomeric ratio determined using chiral HPLC analysis. [b]DTBM-SEGPHOS used as ligand.

Table S2. Evaluation of the Effect of Ligands on the Desymmetrization Reaction.[a]

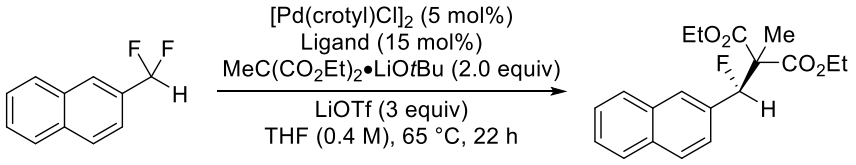

Yield[a] (e.r.)[b]

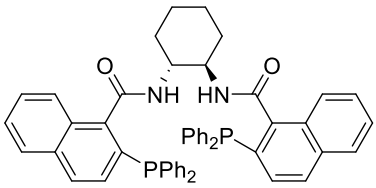

0% (n.d.)

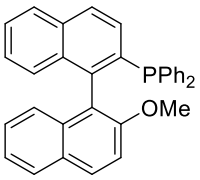

0% (n.d.)

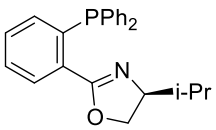

0% (n.d.)

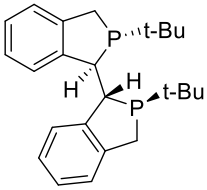

0% (n.d.)

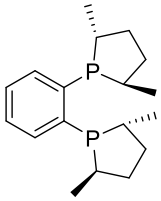

0% (n.d.)

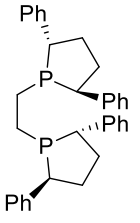

0% (n.d.)

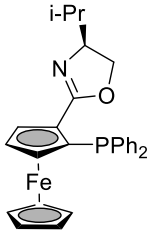

0% (n.d.)

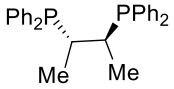

0% (n.d.)

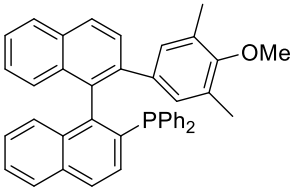

2% (n.d.)

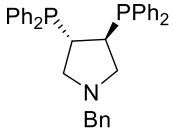

2% (n.d.)

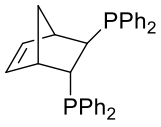

6% (n.d.)

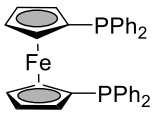

20% (n.d.)

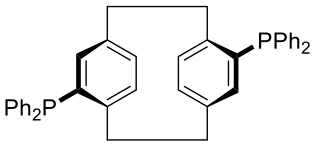

33% (n.d.)

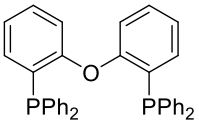

>95% (n.d.)

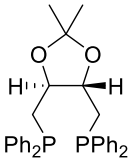

74% (54:46)

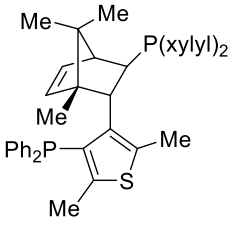

100% (26:74)

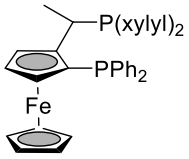

10% (n.d.)

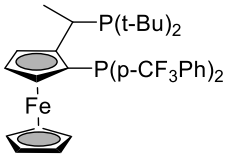

100% (22:78)

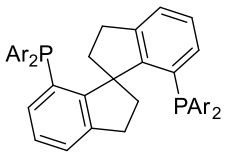

Ar = p-Tol: 18% (n.d.)

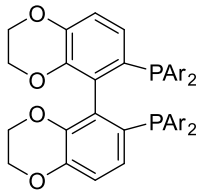

Ar = Ph: 92% (15:85)
Ar = DMM: 76% (20:80)

[a]Yield determined by ^{19}F NMR spectroscopy with either PhF or trifluorotoluene as internal standard. [b]Determined using HPLC analysis. n.d. = not determined. Xylyl = 3,5-MePh; DTBM = 3,5-tBu-4-OMePh; DMM = 3,5-Me-4-OMePh; BTMS = 3,5-TMSPh; TMP = 3,4,5-OMePh; BTFM = 3,5-CF3Ph; DIDMA = 3,5-iPr-4-NMe_2Ph; Cy = cyclohexyl; o-Tol = 2-MePh; Ad = 1-adamantyl. [c]Conversion (%) determined by ^{19}F NMR spectroscopy. [d]Reaction conducted with the MAC nucleophile (2.0 equiv), LiOtBu (2.0 equiv), Ba(OTf)2 (3 equiv), THF (0.03 M), 65 °C, 48 h.

Table S3. Evaluation of the Effect of Ligands on the Desymmetrization Reaction.[a]

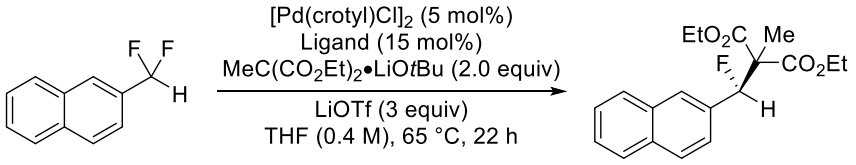

Yield[a] (e.r.)[b]

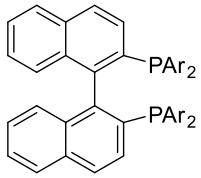

Ar = Ph: 100% (82:18)
Ar = Xylyl: 97% (27:73)
Ar = p-Tol: 82% (80:20)
Ar = DTBM: 100% (54:46)

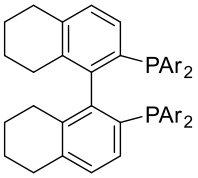

Ar = Ph: 96% (78:22)
Ar = Xylyl: 88% (34:66)

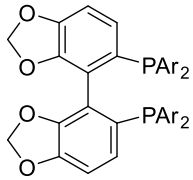

Ar = Ph: 3% (n.d.)
Ar = Xylyl: 93% (26:74)
Ar = DTBM: 100% (40:60)
Ar = DMM: 83% (18:82)

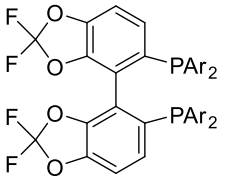

Ar = Ph: 99.5% (55:45)
Ar = BTMS: 100% (51:49)

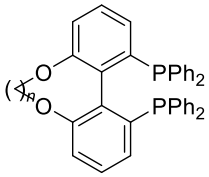

n = 1: 44% (68:32)
n = 3: 83% (14:86)

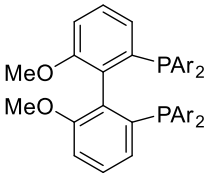

Ar = Xylyl: 10% (n.d.)
Ar = DTBM: 100% (58:42)
Ar = TMP: 100% (67:33)
Ar = Ph: 53% (82:18)
Ar = BTFM: 8% (n.d.)
Ar = 2-furyl: 22% (n.d.)
Ar =DIDMA: 100% (69:31)

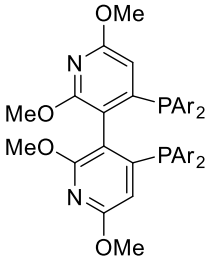

Ar = Xylyl: 100%
(24:76)

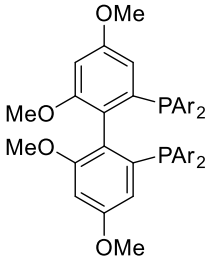

Ar = Ph: 100% (16:84)
Ar = Xylyl: 84% (21:79)
Ar = DTBM: 100% (56:44)
Ar = DMM: 97% (20:80)
Ar = BTFM: 14% (n.d.)

Conversion[c]

6%

0%

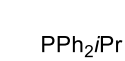

33%

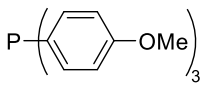

12%

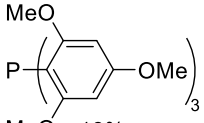

18%

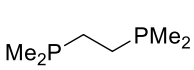

0%

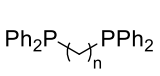

n = 1: 0%
n = 2: 13%
n = 3: 15%
n = 4: 0%
n = 5: 4%

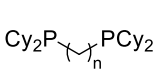

n = 1: 1%
n = 2: 0%
n = 3: 0%

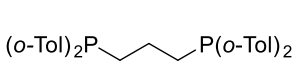

77%

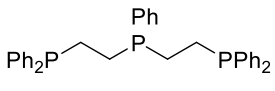

0%

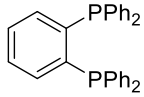

14%

[a]Yield determined by ^{19}F NMR spectroscopy with either PhF or trifluorotoluene as internal standard. [b]Determined using HPLC analysis. n.d. = not determined. Xylyl = 3,5-MePh; DTBM = 3,5-tBu-4-OMePh; DMM = 3,5-Me-4-OMePh; BTMS = 3,5-TMSPh; TMP = 3,4,5-OMePh; BTFM = 3,5-CF3Ph; DIDMA = 3,5-iPr-4-NMe_2Ph; Cy = cyclohexyl; o-Tol = 2-MePh; Ad = 1-adamantyl. [c]Conversion (%) determined by ^{19}F NMR spectroscopy. [d]Reaction conducted with the MAC nucleophile (2.0 equiv), LiOtBu (2.0 equiv), Ba(OTf)2 (3 equiv), THF (0.03 M), 65 °C, 48 h.

Table S4. Evaluation of the Effect of Ligands on the Desymmetrization Reaction.[a]

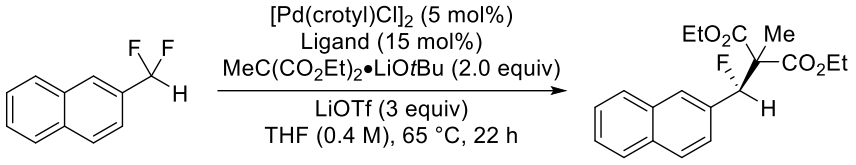

Conversion[c]

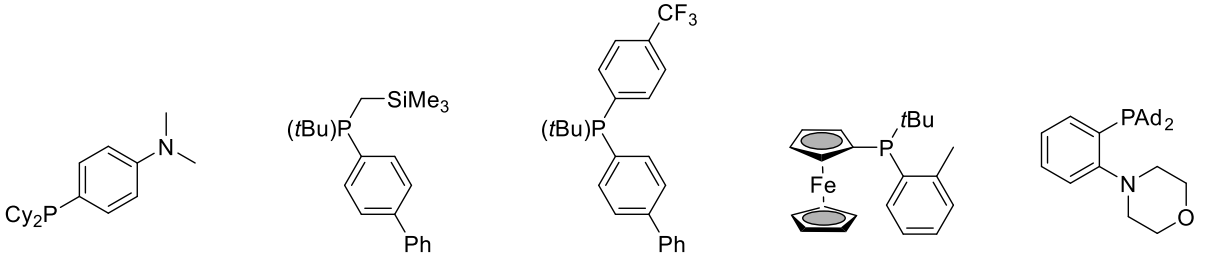

10% 13% 6% 1% 11%

Yield[a] (e.r.)[b]

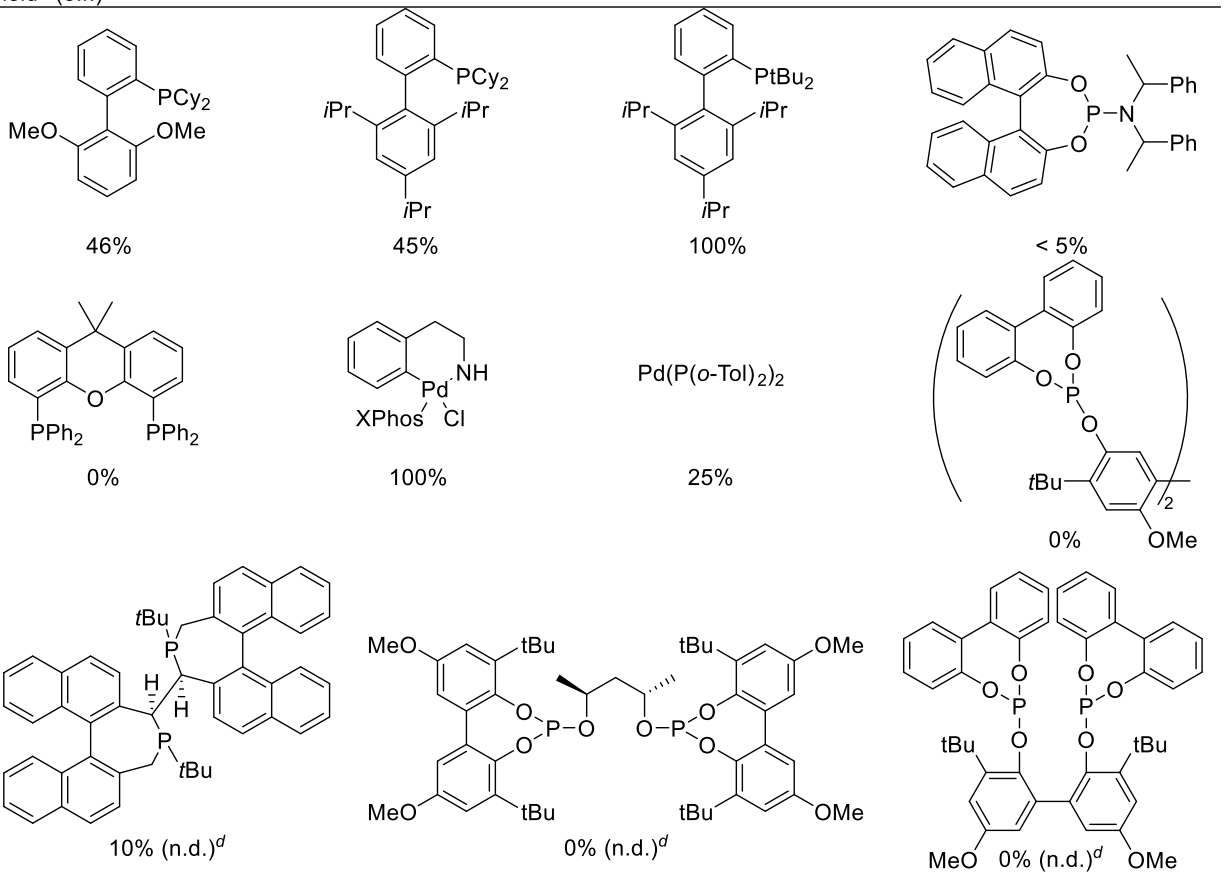

46% 45% 100% < 5%

0% 100% 25% 0%

10% (n.d.)[d] 0% (n.d.)[d] 0% (n.d.)[d]

[a]Yield determined by ^{19}F NMR spectroscopy with either PhF or trifluorotoluene as internal standard. [b]Determined using HPLC analysis. n.d. = not determined. Xylyl = 3,5-MePh; DTBM = 3,5-tBu-4-OMePh; DMM = 3,5-Me-4-OMePh; BTMS = 3,5-TMSPh; TMP = 3,4,5-OMePh; BTFM = 3,5-CF3Ph; DIDMA = 3,5-iPr-4-NMe_2Ph; Cy = cyclohexyl; o-Tol = 2-MePh; Ad = 1-adamantyl. [c]Conversion (%) determined by ^{19}F NMR spectroscopy. [d]Reaction conducted with the MAC nucleophile (2.0 equiv), LiOtBu (2.0 equiv), Ba(OTf)2 (3 equiv), THF (0.03 M), 65 °C, 48 h.

Table S5. Evaluation of the Effect of Ligands on the Desymmetrization Reaction.[a]

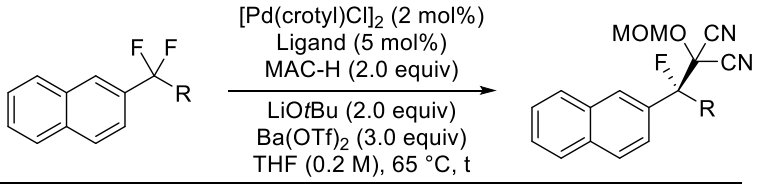

Entry	R	Ligand	t (h)	Yield (%)[a]	e.r.[b]
1	H	(*R*)-I	48	0	n.d.
2	H	XPhos	48	0	n.d.
3	H	*t*BuXPhos	48	0	n.d.
4	H	(*R*)-II	48	14	n.d.
5	H	(*R*)-III	48	57	n.d.
6	Et	(*R*)-IV	48	77	87:13
7	Et	(*R*)-III	48	76	88:12
8	Et	(*R*)-V	48	0	n.d.
9	Et	(*R*)-VI	48	1	n.d.
10	Et	(*R*)-VII	48	5	n.d.
11	Et	(*R*)-VIII	48	12	84:16
12	Et	(*R*)-IX	48	83	87:13
13	Et	(*R*)-X	48	0	n.d.
14	Et	(*R*)-XI	48	1	n.d.
15	Et	(*R*)-XII - XIV	48	0	n.d.
16	Et	(*R*)-XV	48	12	63:37
17	Et	(*R*)-XVI	48	0	n.d.
18	Et	(*rac*)-XVII	48	85	n.d.
19	Et	(*rac*)-XIV	48	32	n.d.
20	Et	(*rac*)-XVIII	4	85	n.d.
21[c]	Et	(*rac*)-XVIII	48	85	n.d.

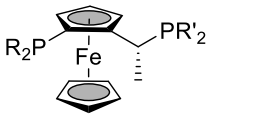

I: R = Cy; R' = *t*Bu
XII: R = *1*-nap; R' = Xyl
XIII: R = *2*-furanyl; R' = *o*-Tol
XIV: R = DMM; R' = *o*-Tol
XV: R = Ph; R' = Xyl

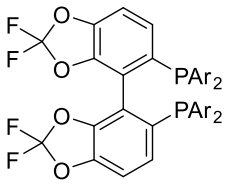

XVI: Ar = Ph

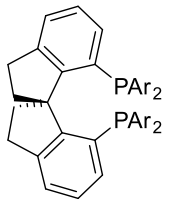

X: Ar = Xyl
XI: Ar = DTBM

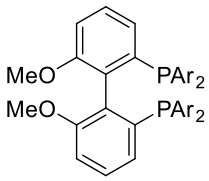

V: Ar = 2-furanyl
VI: Ar = TMP
VII: Ar = DTB
VIII: Ar =DIDMA
IX: Ar = DTBM

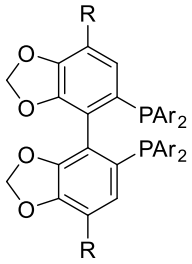

III: R = H; Ar = DTBM
XVII: R = H; Ar = DTMSM
XVIII: R = H; Ar = DTMGM
XIV: R = Ad; Ar = DTBM

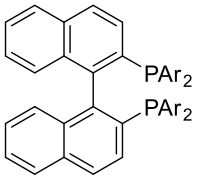

II: Ar = Ph
IV: Ar = DTBM

[a]Yields determined by ^{19}F NMR spectroscopy with either PhF or PhCF3 as internal standard; [b]Enantiomeric ratio was found using chiral HPLC; [c]Reaction conducted at rt. DMM = 3,5-Me-4-OMePh; TMP = 3,4,5-OMePh; DTB = 3,5-tBuPh; DIDMA = 3,5-iPr-4-NMe_2Ph; DTBM = 3,5-tBu-4-OMePh; DTMGM = 3,5-$(GeMe_3)_2$-4-OMePh; DTMSM = 3,5-$(SiMe_3)_2$-4-OMePh; DPM = 3,5-Ph-4-OMePh; Xyl = 3,5-MePh.

5.6.7 Evaluation of Additional Reaction Parameters

Table S6. Effect of base and Lewis acid on Conversion.[a]

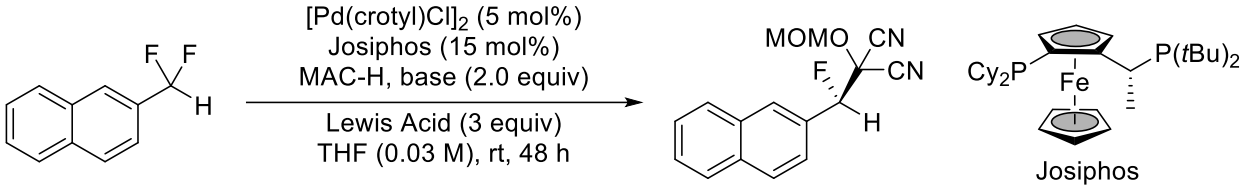

Entry	Base	Conversion w/ LiOTf (%)	Conversion w/ $Ba(OTf)_2$ (%)
1	DIPEA	0	1
2	pyridine	0	0
3	DBU	<1%	0
4	Cs_2CO_3	0	6
5	Li_2CO_3	0	0
6	$BaCO_3$	0	0
7	LiO*t*Bu	10	52
8	$Ba(OtBu)_2$	26	0
9	LiHMDS	16	49

[a]Conversion determined using ^{19}F qNMR spectroscopy. Enantiomeric ratio determined using chiral HPLC analysis.

Table S7. Effect of LiX on the Reaction e.r.[a]

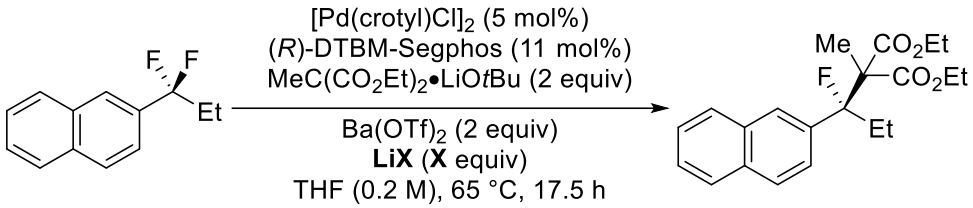

Entry	LiX	X (equiv)	Yield (%)	e.r.
1	LiCl	5.0	93	87:14
2	LiBr	5.0	26	97:3
3	LiI	5.0	0	n.d.
4	LiOTf	5.0	93	88:12
5	$LiBF_4$	5.0	0	n.d.
6	$LiNO_3$	5.0	93	86:14
7	LiOAc	5.0	79	89:11
8	$LiClO_4$	5.0	0	n.d.
9	Li_3PO_4	5.0	93	90:10
10	LiOTFA	5.0	41	93:7
11	LiBr	2.0	92	90:10
12	LiBr	1.0	92	90:10
13	LiBr	0.5	92	90:10
14	LiBr	0.1	92	91:9

[a]Conversion determined using ^{19}F qNMR spectroscopy. Enantiomeric ratio determined using chiral HPLC analysis.

Table S8. Effect of solvent on the Reaction e.r.[a]

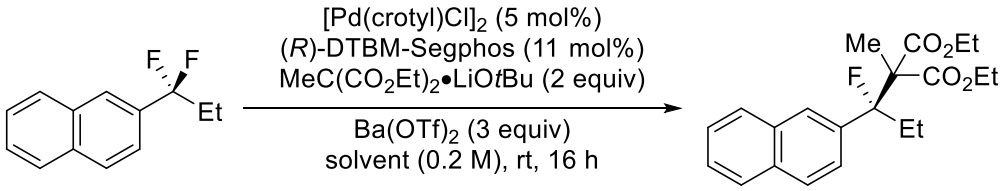

Entry	solvent	Yield (%)	e.r.
1	1,4-dioxane	91	90:10
2	THF	98	93:7
3	4Me-THF	98	92:8
4	CPME	>99	91:9
5	Et_2O	98	92:8

[a]Conversion determined using ^{19}F qNMR spectroscopy. Enantiomeric ratio determined using chiral HPLC analysis.

Table S9. Effect of $Ba(OTf)_2$ Loading on Reaction Yield and e.r., and the Formation of 2.[a]

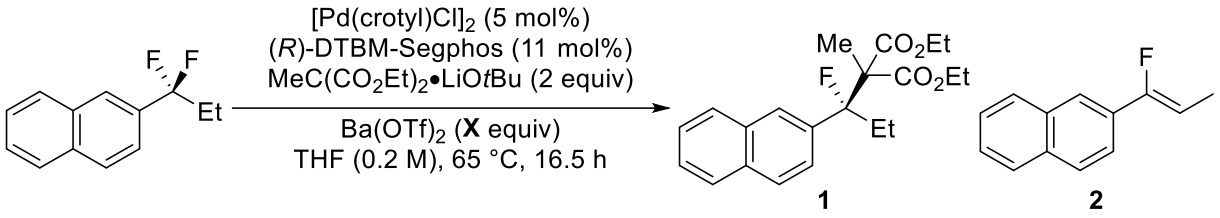

Entry	**X** (equiv)	Yield **1** (%)	**2** (%)	**1** e.r.
1	0.0	40	60	95:05
2	0.1	96	4	87:13
3	0.5	95	5	86:14
4	1.0	97	3	88:12
5	2.0	94	6	90:10
6	3.0.	93	7	91:09

[a]Conversion determined using ^{19}F qNMR spectroscopy. Enantiomeric ratio determined using chiral HPLC analysis.

Table S10. Effect of The equivalents of Malonate Nucleophile on e.r.[a]

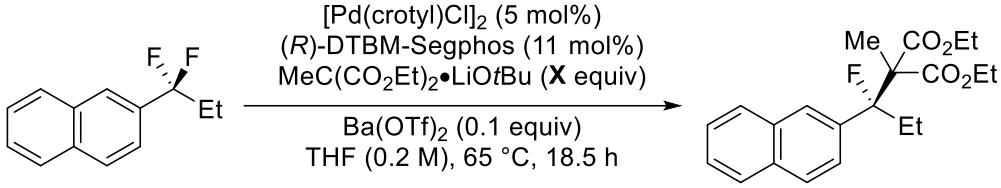

Entry	**X** (equiv)	Yield (%)	e.r.
1	0.5	28	90:10
2	1.0	63	87:13
3	1.5	87	87:13
4	2.0	95	88:12
5	3.0	94	88:12
6	5.0	93	89:11

[a]Conversion determined using ^{19}F qNMR spectroscopy. Enantiomeric ratio determined using chiral HPLC analysis.

Table S11. Metal and Ligand Loading and its Effect on the Product Distribution.[a]

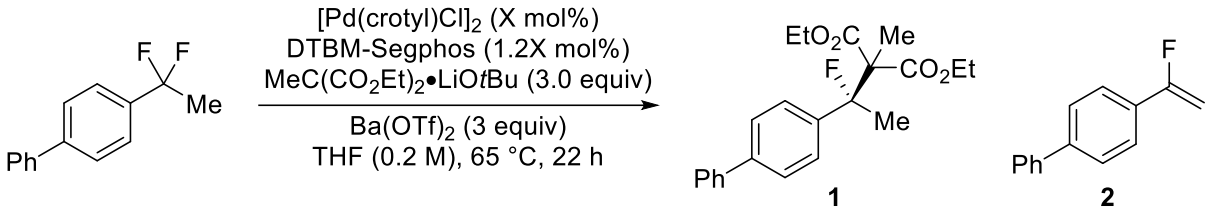

Entry	X (mol%)	Yield **1** (%)	Yield **2** (%)
1	5.0	44	7
2	7.5	57	9
3	10.0	62	9
4	15.0	55	7
5	20.0	53	7
6	25.0	37	5

[a]Conversion determined using ^{19}F qNMR spectroscopy. Enantiomeric ratio determined using chiral HPLC analysis.

Table S12. Reaction Concentration and Nuclophile Loading and its Effect on the Product Distribution.[a]

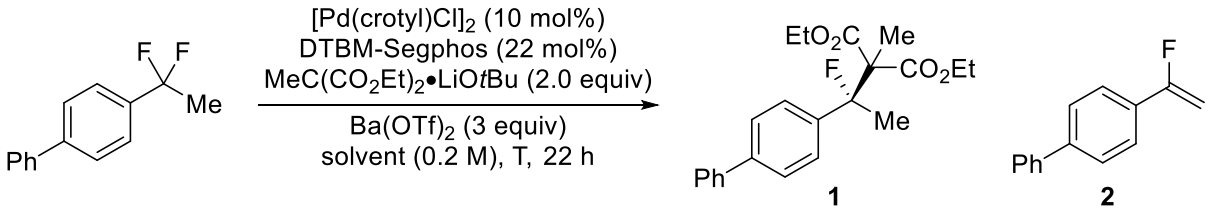

		concentration (M)				
	NMR yield:	0.4	0.2	0.1	0.05	0.01
MeC(CO$_2$Et)$_2$•LiO*t*Bu	10 equiv	-	-	65% **1** 6% **2**	7% **1** 1% **2**	0% **1** 0% **2**
	5 equiv	-	80% **1** 3% **2**	19% **1** 10% **2**	5% **1** 1% **2**	0% **1** 0% **2**
	3 equiv	59% **1** 7% **2**	31% **1** 5% **2**	7% **1** 1% **2**	7% **1** 1% **2**	-

[a]Conversion determined using ^{19}F qNMR spectroscopy. Enantiomeric ratio determined using chiral HPLC analysis.

Table S13. Effect of the Reaction Temperature and of the Pd:L Ratio on Conversion and Product Distribution.[a]

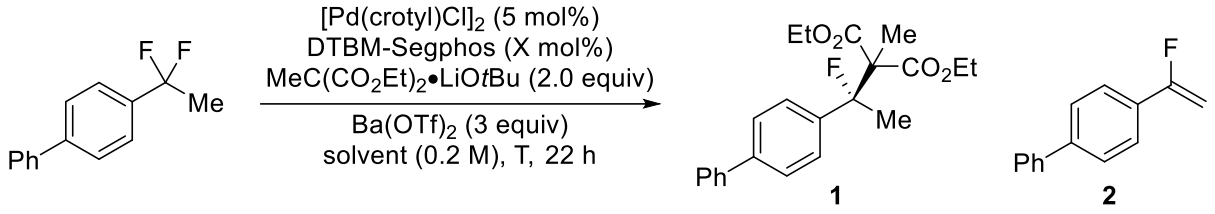

Entry	Solvent	T (°C)	X (mol%)	Conversion (%)	Ratio **1**:**2**
1	CPME	rt	15	19	6.5:1
2	CPME	65	15	49	6:1
3	CPME	80	15	11	2:1
4	CPME	100	15	9	3:1
5[b]	CPME	120	15	15	8:1
6	THF	65	9	<1	3:1
7	THF	65	10	8	3:1
8	THF	65	11	17	3:1
9	THF	65	12	14	3:1
10	THF	65	15	15	3:1
11	THF	65	20	14	3:1

[a]Conversion determined using ^{19}F qNMR spectroscopy. [b]Palladium black formed.

Table S14. Effect of the Reaction Solvent on Conversion and Product Distribution.[a]

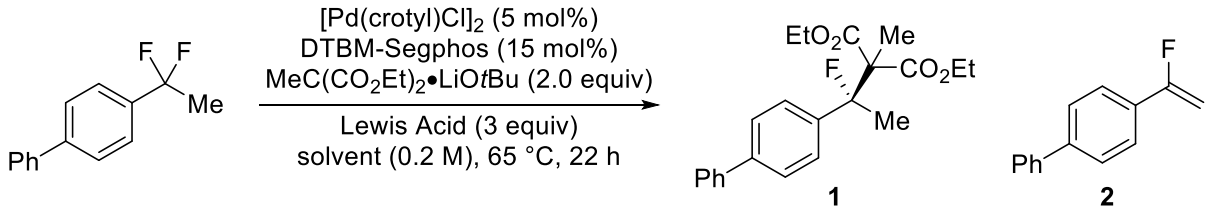

Entry	Solvent	Lewis Acid	Conversion (%)	Ratio **1**:**2**
1	THF	LiOTf	10	3:1
2	THF	$Ba(OTf)_2$	28	5:1
3[b]	DCM	LiOTf	0	n.d.
4[b]	DCM	$Ba(OTf)_2$	0	n.d.
5[b]	toluene	LiOTf	6	1:3
6[b]	toluene	$Ba(OTf)_2$	6	1:0
7[b]	1,4-dioxane	LiOTf	17	3:1
8[b]	1,4-dioxane	$Ba(OTf)_2$	21	6:1
9[b]	Et_2O	LiOTf	10	3:1
10[b]	Et_2O	$Ba(OTf)_2$	13	11:1
11	DME	LiOTf	11	2:1
12	DME	$Ba(OTf)_2$	26	5:1
13[b]	MTBE	LiOTf	5	3:1
14[b]	MTBE	$Ba(OTf)_2$	31	11:1
15[b]	CPME	LiOTf	17	1:2
16[b]	CPME	$Ba(OTf)_2$	23	5:1

[a]Conversion determined using ^{19}F qNMR spectroscopy. [b]Significant solubility issues of the lewis acid in these solvents.

Table S15. Effect of Catalyst Loading on Yield, e.r., and Product Distribution.[a]

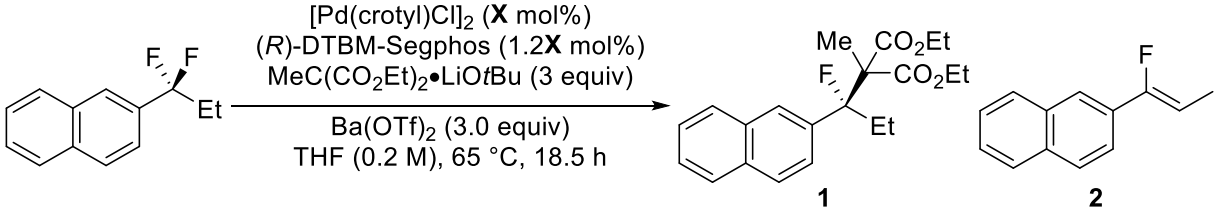

Entry	**X** (mol%)	Yield **1** (%)	**2** (%)	e.r.
1	0.0	0	0	n.d.
2	0.1	37	5	90:10
3	0.5	90	10	90:10
4	2.0	90	10	90:10
5	5.0	89	11	93:7
6	10.0	86	14	95:5
7	25.0	47	41	97:3

[a]Conversion determined using ^{19}F qNMR spectroscopy.

5.7.7 Synthesis of Benzylic Difluorides

2-(1,1-difluoropropyl)naphthalene

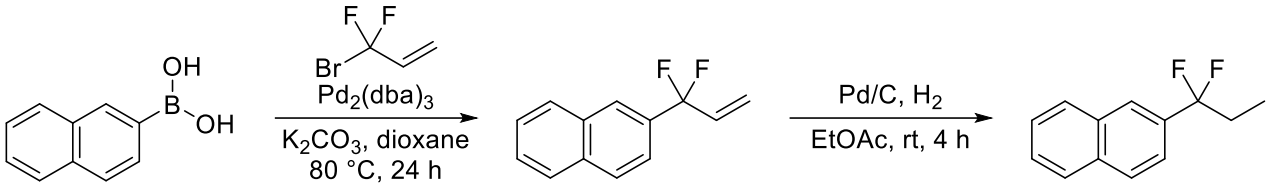

Step 1: This compound was prepared according to a literature procedure.[81] To a Schlenck bomb was added 2-naphthaleneboronic acid (1.46 g, 1.00 equiv, 8.49 mmol), tris(dibezylideneacetone)dipalladium (31.1 mg, 0.40 mol%, 34.0 μmol), and potassium carbonate (3.52 g, 3.00 equiv, 25.5 mmol), followed by dioxane (freshly distilled) (42.4 mL, 0.20 M) and water (76.5 μL, 0.50 equiv, 4.24 mmol) while stirring. 3-Bromo-3,3-difluoro propene (1.30 mL, 1.50 equiv, 12.7 mmol) was then added in one portion, and the tube was sealed and heated to 80 °C for 24 h. After this time, the reaction mixture was cooled to room temperature, diluted with THF, filtered through a pad of magnesium sulfate, and the filtrate was concentrated under reduced vacuum. The crude residue was purified by flash column chromatography (SiO_2, 100% pentanes) to afford 2-(1,1-difluoroallyl)naphthalene (569 mg, 33%) as a clear oil. The spectral data matched those in the literature.

^{1}H NMR (500 MHz, $CDCl_3$) δ 8.06 (s, 1H), 7.96 – 7.85 (m, 3H), 7.63 – 7.53 (m, 3H), 6.28 (ddt, *J* = 17.2, 10.6, 9.6 Hz, 1H), 5.66 (dt, *J* = 17.3, 2.8 Hz, 1H), 5.55 (d, *J* = 10.9 Hz, 1H).

^{19}F NMR (471 MHz, $CDCl_3$) δ -93.09 (dd, *J* = 9.8, 2.6 Hz).

Step 2: This compound was prepared according to a literature procedure.[81] Outside of the glovebox, to a 25 mL round-bottom flask was loaded with 2-(1,1-difluoroallyl)naphthalene (550 mg, 1.00 equiv, 2.69 mmol) in EtOAc (9.00 mL) was added Pearlman's catalyst (158 mg, 0.55 equiv, 1.48 mmol). The headspace was purged with H_2 briefly, and the round-bottom flask was fitted with three H_2 balloons. The suspension was stirred vigorously at rt for 4 h. The resulting suspension was filtered through celite, concentrated, and subjected directly to column chromatography (SiO_2, 1% EtOAc in pentanes) to afford 2-(1,1-difluoropropyl)naphthalene (435 mg, 78%) as a clear oil that solidified in the freezer. NOTE: this compound decomposes slowly at room temperature and should be stored in the freezer. The spectral data agreed with those in the literature.

^{1}H NMR (500 MHz, $CDCl_3$) δ 7.99 (s, 1H), 7.90 (ddd, *J* = 12.3, 7.4, 3.8 Hz, 3H), 7.59 – 7.50 (m, 3H), 2.25 (ttd, *J* = 16.2, 7.4, 1.4 Hz, 2H), 1.03 (td, *J* = 7.5, 1.5 Hz, 3H).

^{19}F NMR (471 MHz, $CDCl_3$) δ -97.08 (td, *J* = 16.0, 3.2 Hz).

4-(1,1-difluoroethyl)-1,1'-biphenyl (3p)

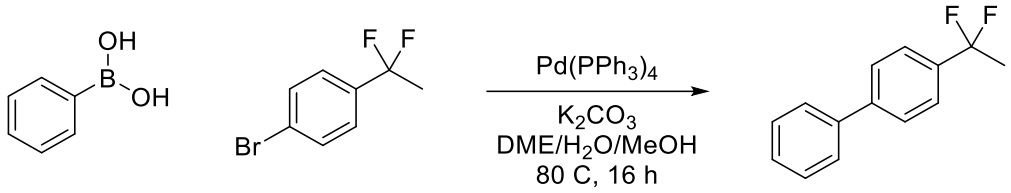

To a flame-dried round-bottom flask was added tetrakis(triphenylphosphine)palladium (327 mg, 5.00 mol%, 283 μmol), benzeneboronic acid (1.10 g, 1.60 equiv, 9.05 mmol), and potassium carbonate (1.56 g, 2.00 equiv, 11.3 mmol). This was dissolved in 2:1:0.8 DME:H_2O:MeOH (14.0 mL), then 1-(4-bromophenyl)-1,1-difluoroethane (940 μL, 1.00 equiv, 5.66 mmol) was added. The resulting suspension was stirred at 80 °C for 16 h. After this time, the suspension was diluted with DCM, washed with $NaHCO_3$ (sat. aq.), the aqueous extracted with DCM (2x), dried over magnesium sulfate, and the solid filtered off. The combined organic materials were concentrated *in vacuo*, and the resulting residue was purified by flash column chromatography (SiO_2, 0 - 5% EtOAc in hexanes) to afford 4-(1,1-difluoroethyl)-1,1'-biphenyl (788 mg, 64 %) as a white solid. The spectral data match those in the literature.[82]

^{1}H NMR (500 MHz, $CDCl_3$) δ 7.64 (d, *J* = 8.1 Hz, 2H), 7.62 – 7.57 (m, 4H), 7.46 (dd, *J* = 8.4, 6.8 Hz, 2H), 7.41 – 7.36 (m, 1H), 1.97 (t, *J* = 18.1 Hz, 3H).

^{19}F NMR (471 MHz, $CDCl_3$) δ -87.26 (q, *J* = 18.1 Hz).

5.7.8 Synthesis of Nucleophiles

2-(methoxymethoxy)malononitrile (2b)

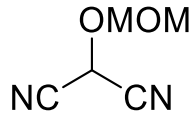

Compound **2b** was synthesized using a known method.[80] To a solution of acetylmalononitrile (4.99 g, 46.3 mmol) in water (110 mL) was added a 9.6% solution of peracetic acid (30.0 mL) in acetic acid slowly using a glass pipette. The resulting solution was stirred at rt for 2 h. The stir bar was then removed, and the reaction mixture was concentrated on a rotary evaporator until most of the volatiles were removed. A stir bar was then added, and the residual oil was stirred under high vacuum for 4 h (NOTE: a blast shield was used during the concentration of the peracetic acid). The resulting residue was suspended in DCM (275 mL), and dimethoxymethane (40.6 mL, 46.3 mmol) was added in one portion, followed by P_2O_5 (23.6 g, 83.3 mmol) in one portion. The heterogeneous mixture was stirred for 14 h, and the liquid was decanted from the P_2O_5 into a separatory funnel. The P_2O_5 was washed with DCM (2x), and the combined organic layers were washed with $NaHCO_3$ (sat. aq.) (2x) and brine (1x), dried over magnesium sulfate, filtered, and the filtrate was concentrated *in vacuo*. The crude residue was further purified by flash chromatography (SiO_2, 10% ethyl acetate in hexanes) to afford **2b** as a white powder (3.17 g, 54% yield). The spectral data agreed with the literature.

^{1}H NMR (400 MHz, $CDCl_3$) δ 5.32 (s, 1H), 4.89 (s, 2H), 3.51 (s, 3H).

5.7.9 Functionalization of Masked Acyl Cyanide Products

2-Fluoro-1-morpholino-2-(naphthalen-2-yl)butan-1-one (4c)

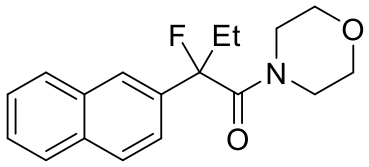

A dry vial equipped with a dry magnetic stir bar was charged with 3bβ (10.0 mg, 0.03 mmol), dry DME (64.0 µL, 0.50 M), and glacial acetic acid (3.80 µL, 8.50 M). Camphorsulfonic acid (15.0 mg, 2.00 equiv, 0.64 mmol) was then added, the headspace was replaced with N_2, the vial was sealed with a Teflon-lined cap, and the mixture was stirred at 70 °C for 2.5 h. This was then cooled to rt, diluted with dry DME (213 µL, final concentration 0.15 M), the cap was replaced with a Teflon-lined septum cap, the headspace was filled with N_2, and the vial was cooled to –40 °C. A 1:1 mixture of dry DME: dry morpholine (14.0 µL, 2.50 equiv morpholine) was added, followed by dropwise addition of a 1:1 solution of dry DME: dry NEt_3 (62.0 µL, 7.00 equiv NEt_3). After complete addition, the reaction was stirred and allowed to slowly warm to rt overnight for a total stir time of 20 h. NH_4Cl (sat. aq.) was then added dropwise, and the reaction mixture was transferred to a separatory funnel containing NH_4Cl (sat. aq). The aqueous layer was extracted with DCM (3x) and the combined organic materials were dried over magnesium sulfate. The product was purified by column chromatography (SiO_2 5% to 30% EtOAc in hexanes) to give 5 (8.4 mg, 87 %) as a white solid.

^{1}H NMR (500 MHz, $CDCl_3$) δ 7.89 – 7.80 (m, 4H), 7.52 (m, 2H), 7.47 (dd, *J* = 8.5, 1.9 Hz, 1H), 3.77 – 3.55 (m, 5H), 3.41 (d, *J* = 10.0 Hz, 1H), 3.34 – 3.26 (m, 1H), 3.03 (t, *J* = 9.4 Hz, 1H), 2.54 – 2.38 (m, 1H), 2.25 – 2.08 (m, 1H), 0.92 (t, *J* = 7.3 Hz, 3H).

^{13}C NMR (126 MHz, $CDCl_3$) δ 168.2 (d, *J* = 21.2 Hz), 136.9 (d, *J* = 20.7 Hz), 133.0, 128.8, 128.3, 127.9, 126.7 (d, *J* = 19.3 Hz), 122.8 (d, *J* = 8.3 Hz), 121.7 (d, *J* = 7.4 Hz), 100.8 (d, *J* = 190.3 Hz), 66.8 (d, *J* = 48.9 Hz), 60.5, 47.0, 43.7, 33.8 (d, *J* = 25.1 Hz), 29.8, 14.3, 7.8 (d, *J* = 5.4 Hz).

^{19}F NMR (470 MHz, $CDCl_3$) δ –163.5 (t, *J* = 24.5 Hz).

HRMS (ESI): *m/z* for $C_{10}H_9F_2NOH^+$ $[M+H]^+$ calc'd.: 198.0730, found: 198.0492.

5.7.10 Characterization Data of Isolated Products

(*S*)-2-(1-Fluoro-1-(naphthalen-2-yl)propyl)-2-(methoxymethoxy)malononitrile (3q)

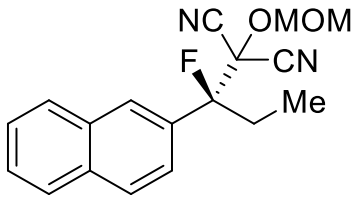

According to desymmetrization procedure A, 2-(1,1-difluoropropyl)naphthalene (21.0 mg, 0.10 mmol) afforded **3q** (23.6 mg, 76% yield) as a white solid after purification by flash chromatography (SiO_2, 0% to 5% to 10% to 30% EtOAc in hexanes).

The e.r. was determined to be 87:13 by HPLC analysis with t_R = 10.397 min (minor) and t_R = 13.04 min (major) [IC, 1.0% iPrOH in hexanes, 1 mL/min, 210 nm, 25 °C].

^{1}H NMR (500 MHz, $CDCl_3$) δ 8.05 (d, *J* = 1.9 Hz, 1H), 7.95 – 7.86 (m, 3H), 7.60 – 7.51 (m, 3H), 5.08 – 5.01 (AB, *J* = 8.7 Hz, 2H), 3.43 (s, 3H), 2.63 – 2.46 (AB, *J* = 10.2 Hz, 2H), 0.88 (t, *J* = 7.4 Hz, 3H).

^{13}C{^{1}H} NMR (126 MHz, $CDCl_3$) δ 138.2, 133.2 (d, *J* = 111.2 Hz), 130.6 (d, *J* = 20.8 Hz), 129.9, 128.9, 128.4, 127.8, 127.4, 127.2 (d, *J* = 11.9 Hz), 126.9, 123.6 (d, *J* = 9.2 Hz), 112.0, 111.4, 96.9, 72.7, 57.6, 27.0 (d, *J* = 20.7 Hz), 7.3 (d, *J* = 3.7 Hz).

^{19}F NMR (470 MHz, $CDCl_3$) δ –161.7 – –162.0 (m).

HRMS (ESI): *m/z* for $C_{18}H_{17}FN_2O_2Na^+$ $[M+Na]^+$ calc'd.: 335.1172, found: 335.1149

5.7.11 Determination of the Stereochemistry of the Coupled Product

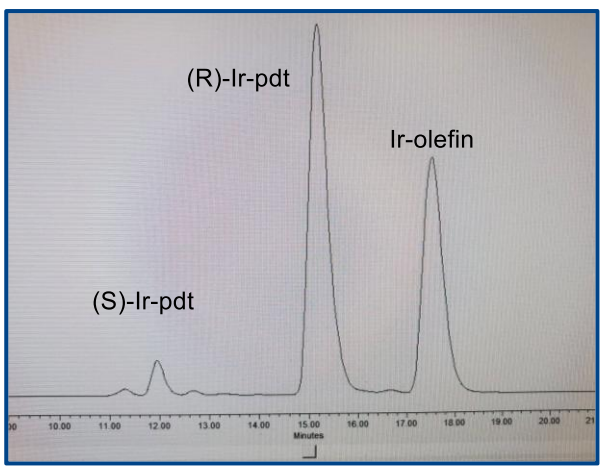

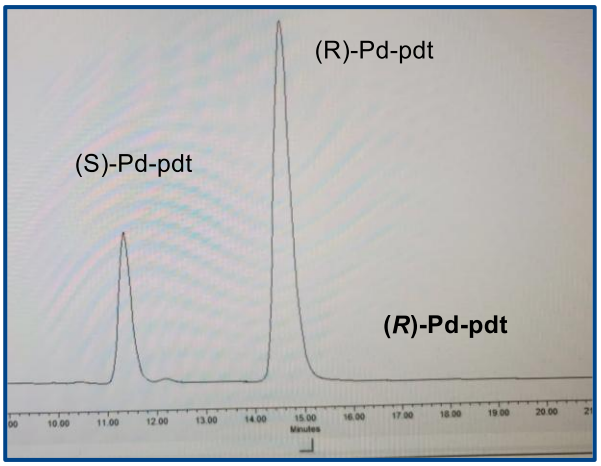

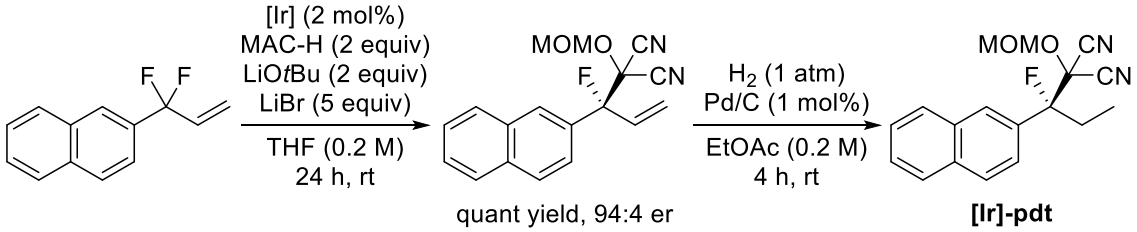

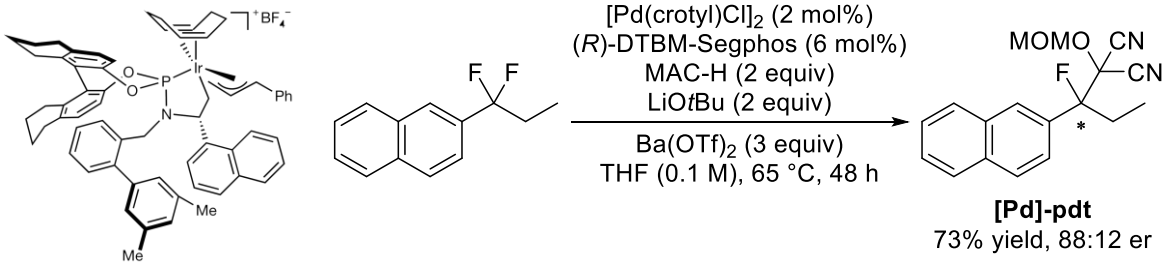

5.7.12 Example Racemic and Chiral HPLC Traces

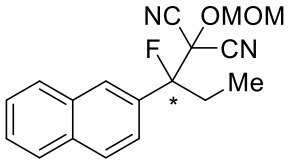

Racemic (0.10 mmol 3q, 2.00 equiv 2b, 2.00 equiv LiO*t*Bu, 2.0 mol% $[Pd(crotyl)Cl]_2$, 6.00 mol% (*rac*)-DTBM-SEGPHOS, THF (0.10 M), 65 °C, 46 h)

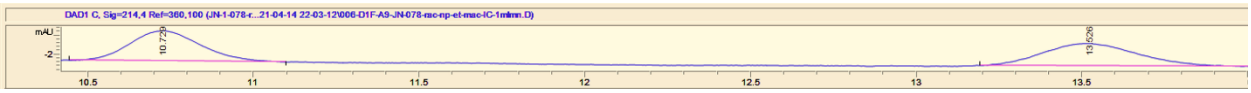

Signal: DAD1 C, Sig=214,4 Ref=360,100

RT [min]	Type	Width [min]	Area	Height	Area%
10.729	BB	0.1793	23.4414	1.5645	0.2440
13.526	BB	0.2364	23.2414	1.1591	0.2420

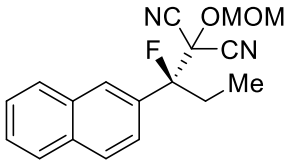

86:14 e.r. (0.10 mmol 3q, 2.00 equiv 2b, 2.00 equiv LiO*t*Bu, 2.00 mol% $[Pd(crotyl)Cl]_2$, 6.00 mol% (*R*)-DTBM-SEGPHOS, MTBE (0.10 M), 65 °C, 46 h)

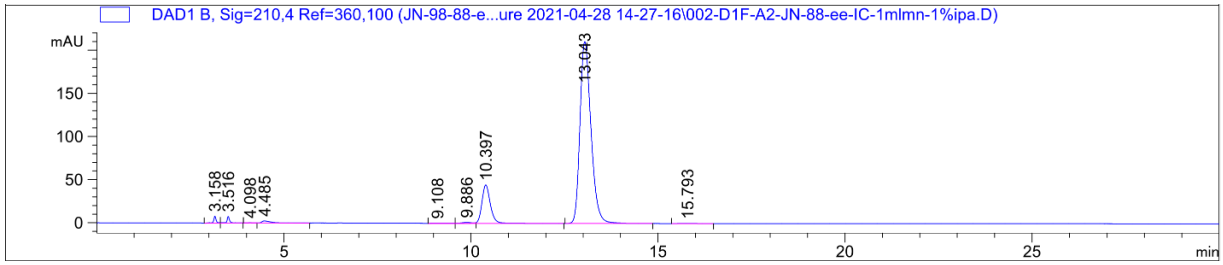

Signal 2: DAD1 B, Sig=210,4 Ref=360,100

Peak #	RetTime [min]	Type	Width [min]	Area [mAU*s]	Height [mAU]	Area %
1	3.158	BV	0.0734	36.02380	7.86510	0.7026
2	3.516	VB	0.0782	38.10804	7.63405	0.7432
3	4.098	BV E	0.1139	2.50481	3.40037e-1	0.0489
4	4.485	VB R	0.2599	41.70966	2.38638	0.8135
5	9.108	BV E	0.3124	5.04820	2.19423e-1	0.0985
6	9.886	VV E	0.2446	17.44811	1.07920	0.3403
7	10.397	VB R	0.2414	690.61981	44.41070	13.4694
8	13.043	BB	0.3138	4290.47021	210.51120	83.6784
9	15.793	BB	0.3448	5.40171	1.96418e-1	0.1054
Totals :				5127.33437	274.64251	

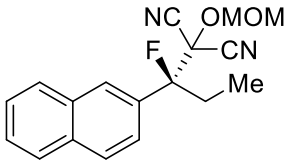

78:22 e.r. (0.10 mmol 3q, 2.00 equiv 2b, 2.00 equiv LiO*t*Bu, 5.00 mol% $[Pd(crotyl)Cl]_2$, 15.0 mol% (*R*)-DTBM-SEGPHOS, MTBE (0.10 M), 65 °C, 46 h)

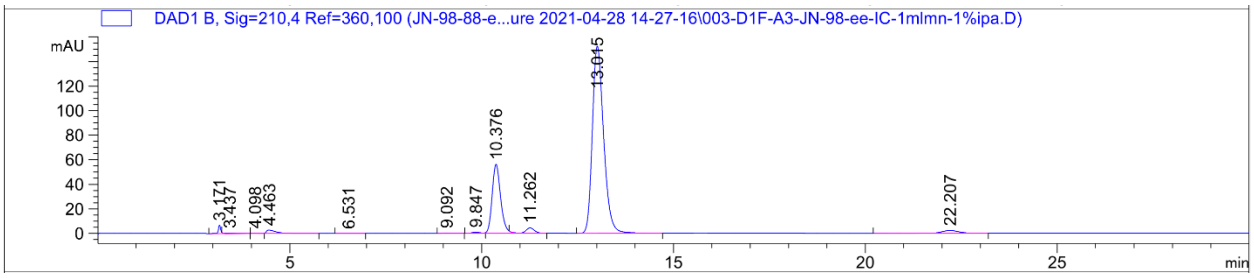

Signal 2: DAD1 B, Sig=210,4 Ref=360,100

Peak #	RetTime [min]	Type	Width [min]	Area [mAU*s]	Height [mAU]	Area %
1	3.171	BV R	0.0710	30.12729	6.89674	0.7134
2	3.437	VB E	0.2181	8.58798	5.16296e-1	0.2034
3	4.098	BV E	0.1128	2.45388	3.37594e-1	0.0581
4	4.463	VB R	0.2720	51.20290	2.76532	1.2125
5	6.531	BB	0.1942	1.66992	1.17246e-1	0.0395
6	9.092	BB	0.2489	5.73938	3.26860e-1	0.1359
7	9.847	BV E	0.2361	12.62765	8.36764e-1	0.2990
8	10.376	VV R	0.2357	863.44403	56.06880	20.4462
9	11.262	VB E	0.2362	68.22461	4.41824	1.6155
10	13.015	BB	0.3139	3105.81348	152.28632	73.5452
11	22.207	BB	0.4815	73.10984	2.30867	1.7312
Totals :				4223.00095	226.87884	

5.7.13 Computational Details

DFT calculations were conducted at the Molecular Graphics and Computational Facility (MGCF) at the University of California, Berkeley, using the Gaussian 16[83] software package. All calculations, including geometry optimizations, were performed in THF solvent using the SMD solvent continuum model reported by Truhlar and co-workers according to the Solvent-Accessible Surface (scrf=smd, surfrace=sas, SC=Qconv=VeryTight).[84] Initial geometries were constructed in GaussView[85] and optimized to stationary points (either minima or first-order saddle points) using the PBE0 functional (the hybrid functional based on the Perdew-Burke-Ernzerhof functional [PBE][86] as described by Adamo[87]) with Grimme's D3 dispersion correction with Becke-Johnson damping (GD3BJ)[88] and the basis sets SDD (with effective core potential) for Pd and Ge, and 6-311G(2d,2p) for all other atoms. The nature of each stationary point was evaluated by accompanying frequency calculations (all positive eigenvalues for minima and exactly one negative eigenvalue for transition states). Several isomers were considered, but only those representing the minimum-energy paths are presented here. Percent buried volume ($\%V_{bur}$) plots were generated using SambVca.[89] All other parameters were left as their defaults.

5.7.14 XYZ Coordinates of Optimized Geometries

[(*R*)-SEGPHOS)$PdCl_2$]

C	-1.40820	-2.80830	0.48660
C	-1.34120	-1.43390	0.39280
C	-0.13230	-0.75080	0.15420
C	1.03990	-1.54690	0.01180
C	-0.12970	0.72380	0.09100
C	-0.37790	1.46930	1.26050
C	-0.41120	2.84810	1.26580
C	-0.19870	3.59250	0.09850
C	0.05330	2.87890	-1.09290
C	0.08790	1.46040	-1.10820
P	2.69500	-0.79150	-0.33480
P	0.45610	0.61930	-2.71700
H	-0.22650	4.67200	0.11500
H	0.22390	3.42770	-2.00810
C	-0.78010	-0.74420	-2.98610
C	-0.53600	-2.01400	-2.47640
C	-1.94780	-0.49330	-3.69680
C	-1.45970	-3.03280	-2.67750
H	0.37310	-2.20940	-1.92310

C	-2.87150	-1.51210	-3.89780
H	-2.13780	0.49530	-4.09360
C	-2.62740	-2.78190	-3.38820
H	-1.26970	-4.02140	-2.28070
H	-3.78060	-1.31670	-4.45120
H	-3.34660	-3.57510	-3.54470
C	0.18210	1.82550	-4.10610
C	-0.80450	2.79830	-3.99720
C	0.96390	1.75400	-5.25300
C	-1.00930	3.69960	-5.03520
H	-1.41320	2.85400	-3.10440
C	0.75910	2.65530	-6.29090
H	1.73200	0.99660	-5.33770
C	-0.22750	3.62810	-6.18200
H	-1.77740	4.45700	-4.95040
H	1.36780	2.59960	-7.18380
H	-0.38690	4.32980	-6.99010
C	2.98520	0.60970	0.85350
C	3.04080	0.36190	2.21990
C	3.14640	1.90450	0.37490
C	3.25760	1.40890	3.10780
H	2.91520	-0.64630	2.59240
C	3.36320	2.95160	1.26280
H	3.10320	2.09750	-0.68890
C	3.41880	2.70370	2.62920
H	3.30080	1.21590	4.17160
H	3.48880	3.95970	0.89030
H	3.58760	3.51890	3.32050
C	4.02130	-2.04360	0.02980
C	5.20170	-2.03920	-0.70380
C	3.83180	-2.98360	1.03580
C	6.19270	-2.97480	-0.43140
H	5.34920	-1.30730	-1.48700

C	4.82280	-3.91920	1.30830
H	2.91280	-2.98710	1.60700
C	6.00330	-3.91480	0.57470
H	7.11180	-2.97130	-1.00250
H	4.67540	-4.65110	2.09150
H	6.77480	-4.64320	0.78680
C	0.96110	-2.96040	0.10750
C	-0.26830	-3.61050	0.34860
H	-0.33310	-4.68600	0.42300
H	1.85650	-3.55460	-0.00620
Pd	2.64650	-0.11180	-2.55060
Cl	3.01170	-1.79100	-3.89780
Cl	4.02400	1.55670	-2.85880
O	-0.66720	3.29760	2.52000
O	-0.61000	1.01230	2.51910
O	-2.58550	-0.91370	0.55870
O	-2.68890	-3.19200	0.71760
C	-0.80320	2.15030	3.31680
H	-0.06080	2.16780	4.11550
H	-1.80240	2.12370	3.75290
C	-3.43880	-2.00680	0.77270
H	-4.21050	-2.02460	0.00230
H	-3.90860	-1.91600	1.75280

[((*R*)-DBTM-SEGPHOS)$PdCl_2$]

C	-1.39550	-2.83160	0.49650
C	-1.33600	-1.45690	0.40150
C	-0.13020	-0.76710	0.16600
C	1.04690	-1.55670	0.02780
C	-0.13580	0.70730	0.10140
C	-0.39180	1.45250	1.26950
C	-0.43280	2.83110	1.27330
C	-0.22110	3.57560	0.10600

C	0.03850	2.86240	-1.08400
C	0.08120	1.44410	-1.09780
P	2.69870	-0.79240	-0.31460
P	0.45900	0.60360	-2.70480
H	-0.25500	4.65490	0.12140
H	0.20880	3.41130	-1.99920
C	-0.76860	-0.76710	-2.97630
C	-2.12170	-0.47410	-3.09820
C	-0.33280	-2.08440	-3.05720
C	-3.03900	-1.49840	-3.30100
H	-2.46100	0.55140	-3.03510
C	-1.25010	-3.10860	-3.26010
H	0.72070	-2.31250	-2.96230
C	-2.60320	-2.81560	-3.38200
C	0.18230	1.80690	-4.09580
C	0.96800	1.73880	-5.24020
C	-0.81010	2.77430	-3.99080
C	0.76120	2.63800	-6.27960
H	1.74060	0.98570	-5.32200
C	-1.01690	3.67340	-5.03020
H	-1.42180	2.82730	-3.09980
C	-0.23120	3.60530	-6.17460
C	2.97740	0.61160	0.87330
C	3.13270	1.90690	0.39400
C	3.03030	0.36530	2.24010
C	3.34090	2.95590	1.28160
H	3.09150	2.09860	-0.67010
C	3.23850	1.41440	3.12760
H	2.90930	-0.64310	2.61320
C	3.39380	2.70970	2.64840
C	4.03090	-2.03660	0.05520
C	3.84380	-2.97670	1.06150
C	5.21350	-2.02610	-0.67490

C	4.83930	-3.90640	1.33780
H	2.92310	-2.98490	1.62990
C	6.20900	-2.95580	-0.39860
H	5.35920	-1.29420	-1.45840
C	6.02190	-3.89600	0.60770
C	0.97580	-2.97060	0.12460
C	-0.25060	-3.62740	0.36260
H	-0.30950	-4.70320	0.43780
H	1.87480	-3.55980	0.01410
C	1.60920	2.56440	-7.51480
C	1.71930	3.98940	-8.08430
H	2.17520	4.66910	-7.36350
H	2.32650	4.01160	-8.99020
H	0.73710	4.39220	-8.33430
C	0.90500	1.61780	-8.50210
H	0.78520	0.62070	-8.07670
H	-0.09010	1.98310	-8.75870
H	1.46960	1.51620	-9.42980
C	2.98560	2.01830	-7.09760
H	2.89870	1.02760	-6.65000
H	3.65900	1.93760	-7.95190
H	3.46160	2.66690	-6.36120
C	-2.08800	4.71740	-4.91680
C	-3.38230	4.11440	-5.48940
H	-3.67880	3.22030	-4.93990
H	-4.20970	4.82350	-5.43890
H	-3.25630	3.82690	-6.53390
C	-1.62920	5.93930	-5.73130
H	-0.68620	6.33540	-5.35280
H	-1.47540	5.68060	-6.77960
H	-2.36500	6.74370	-5.69350
C	-2.24050	5.06170	-3.42520
H	-1.30720	5.44390	-3.01020

H	-3.00830	5.82030	-3.26690
H	-2.51900	4.18260	-2.84300
C	-4.49940	-1.18210	-3.43260
C	-0.77970	-4.53030	-3.34750
C	-0.47340	-4.82480	-4.82610
H	0.29790	-4.15650	-5.21070
H	-0.12380	-5.84860	-4.96530
H	-1.35930	-4.69020	-5.44780
C	-1.91470	-5.42500	-2.81990
H	-2.16240	-5.18100	-1.78620
H	-2.82340	-5.29990	-3.40990
H	-1.64030	-6.48010	-2.85440
C	0.48290	-4.65280	-2.47700
H	0.27310	-4.39660	-1.43790
H	0.88250	-5.66760	-2.49350
H	1.26930	-3.98180	-2.82450
C	-5.28360	-2.39250	-2.89700
H	-5.04130	-2.58970	-1.85210
H	-6.36040	-2.23140	-2.96230
H	-5.04940	-3.29630	-3.46080
C	-4.78680	-0.94210	-4.92480
H	-4.19330	-0.11380	-5.31350
H	-4.54480	-1.82290	-5.52070
H	-5.83770	-0.70530	-5.09600
C	-4.77510	0.08010	-2.59730
H	-4.18140	0.92460	-2.94920
H	-5.82540	0.37030	-2.64700
H	-4.52480	-0.07790	-1.54760
C	7.48530	-2.94450	-1.18650
C	4.63730	-4.92110	2.42390
C	3.98220	-6.15740	1.78420
H	4.61250	-6.57730	0.99940
H	3.80480	-6.94180	2.52120

H	3.02270	-5.90630	1.33060
C	3.72160	-4.28570	3.48440
H	4.16770	-3.38210	3.90170
H	2.75800	-4.00490	3.05770
H	3.53060	-4.97220	4.31020
C	6.02170	-5.25640	3.00520
H	6.50410	-4.36820	3.41490
H	5.95080	-5.99370	3.80600
H	6.68430	-5.66200	2.23970
C	7.74760	-1.49160	-1.61920
H	7.84130	-0.83260	-0.75530
H	8.66660	-1.40770	-2.20070
H	6.93150	-1.10850	-2.23300
C	7.28490	-3.86530	-2.40260
H	7.05150	-4.88460	-2.09260
H	6.46150	-3.51970	-3.02880
H	8.17980	-3.90540	-3.02500
C	8.60120	-3.46620	-0.26480
H	8.38860	-4.47920	0.07910
H	9.56480	-3.48550	-0.77550
H	8.70840	-2.83850	0.62060
C	3.50860	4.35390	0.76430
C	3.29560	1.14860	4.60280
C	2.78020	2.40890	5.31890
H	1.75560	2.63970	5.02480
H	2.79370	2.28620	6.40270
H	3.39140	3.27910	5.07670
C	4.76290	0.85830	4.96280
H	5.14010	-0.00720	4.41700
H	5.40550	1.70400	4.71500
H	4.88000	0.65460	6.02800
C	2.39630	-0.06670	4.88770
H	2.73610	-0.94690	4.34070

H	2.38980	-0.31870	5.94900
H	1.36560	0.12490	4.58680
C	2.97310	5.31200	1.84240
H	3.51890	5.19730	2.77970
H	3.06410	6.35370	1.53180
H	1.92050	5.12050	2.05400
C	2.69740	4.46420	-0.53820
H	3.04820	3.75010	-1.28420
H	1.64040	4.25930	-0.36430
H	2.77390	5.46160	-0.97320
C	5.00990	4.57530	0.51160
H	5.39730	3.86300	-0.21770
H	5.20730	5.57850	0.13150
H	5.58790	4.44900	1.42780
O	7.01030	-4.81910	0.88210
C	6.92270	-5.99690	0.16820
H	5.97200	-6.48360	0.38560
H	6.98480	-5.78070	-0.89840
H	7.74220	-6.65650	0.45350
O	3.60060	3.75130	3.52970
O	-3.51400	-3.83260	-3.58340
O	-0.43650	4.49810	-7.20670
C	-3.76120	-4.14080	-4.90560
H	-4.15630	-3.26230	-5.41570
H	-2.83360	-4.45290	-5.38550
H	-4.48880	-4.95050	-4.96010
C	-1.34560	4.08800	-8.16050
H	-1.00110	3.15920	-8.61510
H	-2.31580	3.92480	-7.69130
H	-1.43790	4.85600	-8.92840
C	4.92340	4.01380	3.82230
H	5.37850	3.13060	4.27060
H	5.45430	4.27050	2.90560

H	4.98220	4.84760	4.52190
Pd	2.65300	-0.11500	-2.53110
Cl	3.03170	-1.79320	-3.87560
Cl	4.02190	1.56100	-2.83680
O	-0.69520	3.28030	2.52640
O	-0.62510	0.99540	2.52770
C	-0.82700	2.13290	3.32380
H	-0.08720	2.15540	4.12470
H	-1.82740	2.10110	3.75700
O	-2.58370	-0.94360	0.56320
O	-2.67470	-3.22230	0.72390
C	-3.43140	-2.04130	0.77570
H	-4.20070	-2.06420	0.00300
H	-3.90460	-1.95230	1.75430

[((*R*)-DTMGM-SEGPHOS)PdCl$_2$]

C	-1.40520	-2.80760	0.47580
C	-1.33880	-1.43300	0.38460
C	-0.12980	-0.74880	0.14980
C	1.04320	-1.54390	0.00830
C	-0.12780	0.72590	0.08940
C	-0.37900	1.46910	1.25980
C	-0.41300	2.84790	1.26750
C	-0.19850	3.59450	0.10210
C	0.05640	2.88330	-1.09020
C	0.09180	1.46490	-1.10800
P	2.69860	-0.78710	-0.33340
P	0.46380	0.62690	-2.71770
H	-0.22690	4.67400	0.12050
H	0.22860	3.43390	-2.00400
C	-0.77100	-0.73670	-2.99180
C	-2.12270	-0.43650	-3.11160
C	-0.34200	-2.05590	-3.07690

C	-3.04550	-1.45540	-3.31650
H	-2.45680	0.59060	-3.04540
C	-1.26470	-3.07490	-3.28170
H	0.71030	-2.28970	-2.98360
C	-2.61640	-2.77460	-3.40150
C	0.19200	1.83560	-4.10510
C	-0.79540	2.80770	-3.99640
C	0.97620	1.76660	-5.25040
C	-0.99850	3.71080	-5.03310
H	-1.40600	2.86130	-3.10470
C	0.77310	2.66980	-6.28710
H	1.74490	1.00980	-5.33500
C	-0.21430	3.64180	-6.17840
C	2.98550	0.61210	0.85810
C	3.03840	0.36170	2.22410
C	3.14700	1.90790	0.38230
C	3.25280	1.40720	3.11440
H	2.91260	-0.64710	2.59450
C	3.36140	2.95340	1.27260
H	3.10580	2.10280	-0.68130
C	3.41430	2.70310	2.63860
C	4.02480	-2.03910	0.03160
C	3.83380	-2.98110	1.03550
C	5.20670	-2.03260	-0.69950
C	4.82470	-3.91660	1.30820
H	2.91350	-2.98610	1.60470
C	6.19770	-2.96820	-0.42680
H	5.35540	-1.29920	-1.48110
C	6.00670	-3.91020	0.57710
C	0.96490	-2.95770	0.10130
C	-0.26460	-3.60890	0.33860
H	-0.32890	-4.68460	0.41090
H	1.86090	-3.55120	-0.01170

C	-3.07890	5.51490	-6.66330
H	-3.85330	6.27720	-6.57870
H	-2.26600	5.89010	-7.28500
H	-3.49990	4.61820	-7.11800
C	-1.63240	6.69320	-4.06190
H	-2.40640	7.45600	-3.97640
H	-1.24940	6.45160	-3.07040
H	-0.81970	7.06830	-4.68390
C	-3.85190	4.40710	-3.76080
H	-4.62610	5.16960	-3.67560
H	-4.27330	3.51040	-4.21510
H	-3.46850	4.16630	-2.76920
C	0.84470	3.20940	-9.44050
H	1.45930	3.15550	-10.33910
H	-0.03970	2.58500	-9.56720
H	0.53920	4.24180	-9.27060
C	3.46900	3.69600	-7.67530
H	4.04430	3.34280	-6.81950
H	4.08370	3.64160	-8.57380
H	3.16320	4.72850	-7.50630
C	2.42950	0.71640	-8.20810
H	1.54540	0.09160	-8.33530
H	3.04450	0.66310	-9.10650
H	3.00460	0.36230	-7.35250
C	-1.50720	-5.98960	-1.98320
H	-1.23150	-5.57950	-1.01160
H	-2.59030	-5.95120	-2.09970
H	-1.17110	-7.02430	-2.04940
C	1.28790	-5.00260	-3.19220
H	1.56320	-4.59260	-2.22050
H	1.62500	-6.03700	-3.25880
H	1.75860	-4.41560	-3.98080
C	-1.15430	-5.67210	-5.14930

H	-0.81780	-6.70670	-5.21580
H	-2.23730	-5.63400	-5.26630
H	-0.68280	-5.08520	-5.93760
C	-6.01580	-2.53770	-2.82050
H	-7.07600	-2.30280	-2.91420
H	-5.78820	-3.42940	-3.40450
H	-5.77490	-2.71830	-1.77290
C	-5.36160	0.57080	-2.43450
H	-5.12140	0.38960	-1.38680
H	-4.76950	1.40840	-2.80330
H	-6.42170	0.80590	-2.52880
C	-5.38550	-0.70640	-5.36890
H	-4.79360	0.13090	-5.73860
H	-5.15860	-1.59800	-5.95340
H	-6.44570	-0.47100	-5.46210
C	4.64710	-7.04560	1.95500
H	4.49730	-7.78480	2.74190
H	3.87030	-7.15770	1.19860
H	5.62470	-7.19560	1.49680
C	2.79730	-4.97390	3.54690
H	2.64690	-5.71240	4.33440
H	2.74660	-3.97220	3.97380
H	2.02070	-5.08620	2.79040
C	5.95150	-5.04250	4.08460
H	5.90000	-4.04090	4.51170
H	5.80160	-5.78130	4.87180
H	6.92930	-5.19250	3.62690
C	9.32810	-3.62610	-0.33770
H	9.10490	-4.64340	-0.01620
H	10.25530	-3.62130	-0.91070
H	9.43790	-2.98460	0.53660
C	7.66790	-4.11340	-3.02970
H	8.59520	-4.10790	-3.60270

H	7.44570	-5.13080	-2.70780
H	6.85370	-3.74330	-3.65260
C	8.26610	-1.13010	-2.03700
H	8.37640	-0.48820	-1.16300
H	9.19310	-1.12580	-2.61030
H	7.45200	-0.75920	-2.65980
C	4.75480	5.78190	1.81840
H	5.72670	5.29190	1.87580
H	4.88180	6.79840	1.44580
H	4.30410	5.81230	2.81040
C	4.40060	4.72670	-1.18170
H	4.52700	5.74320	-1.55440
H	5.37280	4.23740	-1.12380
H	3.75310	4.16940	-1.85870
C	1.84170	5.66250	0.49740
H	1.96920	6.67870	0.12420
H	1.19360	5.10560	-0.17920
H	1.39070	5.69360	1.48920
C	4.51420	2.35770	5.89750
H	5.51460	2.27200	5.47310
H	4.13210	3.36410	5.72680
H	4.55610	2.16180	6.96890
C	1.52890	1.20910	5.80460
H	0.86820	0.48490	5.32810
H	1.57100	1.01270	6.87600
H	1.14740	2.21590	5.63450
C	4.01370	-0.75570	5.34870
H	3.35360	-1.48050	4.87210
H	5.01420	-0.84180	4.92490
H	4.05490	-0.95140	6.42020
O	6.99060	-4.83910	0.84790
C	7.55020	-5.43670	-0.26300
H	6.77480	-5.95800	-0.82450

H	8.00600	-4.67440	-0.89480
H	8.31170	-6.14980	0.05280
O	3.62710	3.74110	3.52260
O	-3.53260	-3.78640	-3.60490
O	-0.41590	4.53860	-7.20780
C	-3.78250	-4.08960	-4.92780
H	-4.17370	-3.20770	-5.43510
H	-2.85700	-4.40520	-5.40940
H	-4.51440	-4.89550	-4.98380
C	0.73430	5.08790	-7.73650
H	1.27260	5.62500	-6.95560
H	1.36690	4.29400	-8.13360
H	0.47200	5.77860	-8.53790
C	2.48270	4.36360	3.97770
H	1.93530	4.78080	3.13240
H	1.85500	3.63750	4.49430
H	2.75370	5.16430	4.66580
Pd	2.65420	-0.10330	-2.54800
Cl	3.02310	-1.77970	-3.89760
Cl	4.03140	1.56660	-2.85030
Ge	1.87910	2.57250	-7.90230
Ge	-2.39090	5.08160	-4.87990
Ge	3.58920	4.78080	0.60160
Ge	3.32730	1.05420	5.04090
Ge	7.86450	-2.95910	-1.45790
Ge	-0.65970	-4.93530	-3.40160
Ge	-4.95170	-1.03200	-3.48540
Ge	4.55540	-5.24510	2.72390
O	-0.67190	3.29490	2.52200
O	-0.61340	1.00960	2.51700
C	-0.80880	2.14600	3.31640
H	-0.06820	2.16250	4.11670
H	-1.80900	2.11800	3.75040

O	-2.58370	-0.91380	0.54890
O	-2.68620	-3.19250	0.70330
C	-3.43680	-2.00780	0.75910
H	-3.90870	-1.91910	1.73830
H	-4.20700	-2.02460	-0.01290

[((*R*)-Ad-DTMGM-SEGPHOS)PdCl$_2$]

C	2.23500	-0.91140	-3.07650
C	0.99970	-0.29770	-2.91880
C	0.57840	0.26830	-1.73870
C	1.51890	0.22950	-0.68790
C	-0.78670	0.81020	-1.62620
C	-1.23560	1.79200	-2.47710
C	-2.55020	2.26440	-2.50180
C	-3.52530	1.75270	-1.67350
C	-3.05540	0.78370	-0.77160
C	-1.75560	0.31230	-0.71960
P	1.17900	1.11980	0.86390
P	-1.34360	-0.88030	0.60060
H	-3.77630	0.37270	-0.08430
C	-2.99280	-1.45890	1.09700
C	-3.62850	-2.46070	0.37350
C	-3.70630	-0.76780	2.07260
C	-4.95930	-2.77800	0.61100
H	-3.08580	-2.98620	-0.40120
C	-5.03530	-1.06670	2.35290
H	-3.21070	0.02920	2.61180
C	-5.63600	-2.08550	1.61260
C	-0.53400	-2.29310	-0.17830
C	0.38300	-3.03050	0.56240
C	-0.84950	-2.69350	-1.47580
C	0.95450	-4.19380	0.05710
H	0.65350	-2.67490	1.55160

C	-0.31540	-3.85870	-2.00620
H	-1.52370	-2.08670	-2.06900
C	0.55140	-4.60770	-1.21070
C	2.81780	1.14400	1.64200
C	3.84000	1.92710	1.12010
C	3.12120	0.21910	2.63680
C	5.16010	1.80190	1.54480
H	3.61230	2.62200	0.32350
C	4.41070	0.09680	3.12670
H	2.33020	-0.40000	3.04060
C	5.41550	0.89140	2.57370
C	0.77600	2.77510	0.25850
C	-0.28330	3.48850	0.80570
C	1.47340	3.30960	-0.82390
C	-0.62520	4.73910	0.30880
H	-0.84710	3.04340	1.61690
C	1.18210	4.56960	-1.32940
H	2.23930	2.71240	-1.30350
C	0.13770	5.27360	-0.72780
C	2.74140	-0.40550	-0.85460
C	3.15250	-1.01310	-2.04870
H	3.42840	-0.41300	-0.02540
C	3.45650	-6.38560	0.18900
H	3.69920	-6.00250	-0.80040
H	4.37940	-6.53080	0.75310
H	2.95900	-7.34850	0.08340
C	1.38360	-5.98630	2.67420
H	0.81400	-5.24600	3.23750
H	0.69780	-6.74840	2.30320
H	2.10810	-6.45600	3.34110
C	3.49860	-3.68200	1.91020
H	4.34670	-3.53080	1.24510
H	2.96370	-2.74080	2.02150

H	3.86880	-3.99950	2.88420
C	-1.63500	-6.16360	-3.95990
H	-2.05460	-6.27620	-4.96130
H	-0.93410	-6.97820	-3.78290
H	-2.44630	-6.21900	-3.23560
C	-1.90140	-3.04230	-4.65050
H	-2.89030	-3.09620	-4.19370
H	-1.50220	-2.03930	-4.50700
H	-2.00760	-3.23280	-5.71970
C	0.97880	-4.55360	-4.88630
H	1.51550	-5.44480	-4.56240
H	0.76120	-4.63800	-5.95220
H	1.61150	-3.68490	-4.71480
C	-5.18120	1.84060	3.66010
H	-5.60260	2.43610	4.47160
H	-4.09850	1.81610	3.77940
H	-5.43010	2.31560	2.71270
C	-5.51360	-0.72810	5.53050
H	-5.92990	-1.72620	5.66420
H	-4.43010	-0.78220	5.64200
H	-5.91540	-0.07220	6.30440
C	-7.90050	0.14240	3.48210
H	-8.12940	0.40050	2.44890
H	-8.39600	-0.79450	3.73020
H	-8.28730	0.92740	4.13460
C	-7.18320	-3.01690	-1.66760
H	-7.78510	-3.69000	-2.27970
H	-7.84150	-2.45170	-1.00860
H	-6.65120	-2.32630	-2.32200
C	-4.49950	-4.82660	-1.76730
H	-4.04440	-4.05510	-2.38790
H	-3.72380	-5.31330	-1.17550
H	-4.96130	-5.56920	-2.41940

C	-6.80450	-5.52170	0.36040
H	-6.13690	-5.99030	1.08320
H	-7.69410	-5.15860	0.87260
H	-7.10450	-6.27150	-0.37370
C	-1.76130	7.36590	1.89930
H	-1.45040	8.12330	1.18060
H	-2.63450	7.73380	2.44060
H	-0.95530	7.19430	2.61300
C	-3.09520	4.44820	2.25970
H	-3.23650	3.46790	1.80780
H	-2.47900	4.33920	3.15290
H	-4.06830	4.84330	2.55310
C	-3.42340	6.06270	-0.55390
H	-3.05490	6.93730	-1.08850
H	-3.43180	5.21440	-1.23650
H	-4.43910	6.25560	-0.20730
C	1.18650	6.27620	-4.16420
H	1.87900	6.77600	-4.84350
H	0.51640	5.65090	-4.75370
H	0.59950	7.02610	-3.63800
C	3.83260	6.19190	-2.30400
H	4.68810	5.91510	-2.92130
H	3.65880	7.26290	-2.41060
H	4.06380	5.97400	-1.26180
C	2.81780	3.53160	-3.85440
H	3.50570	2.93900	-3.25270
H	1.95020	2.92210	-4.10540
H	3.32820	3.82400	-4.77360
C	3.12790	-1.96870	5.19680
H	2.44450	-1.20800	5.57620
H	2.63950	-2.49860	4.38080
H	3.33540	-2.68020	5.99780
C	6.18630	-2.45440	4.10270

H	7.17920	-2.02740	4.24120
H	6.09520	-3.35040	4.71820
H	6.06640	-2.73040	3.05620
C	5.49910	-0.04300	6.15040
H	6.49540	0.34150	5.93650
H	4.82570	0.79350	6.33970
H	5.54540	-0.66390	7.04660
C	8.10060	1.54390	0.17810
H	9.01870	2.09220	0.39000
H	8.04120	0.67760	0.83490
H	8.12970	1.20220	-0.85680
C	5.65400	2.97910	-1.34270
H	5.28730	2.02810	-1.72920
H	4.82560	3.68090	-1.26560
H	6.38580	3.38510	-2.04290
C	6.99060	4.50990	1.11500
H	6.07910	5.09740	1.23210
H	7.50040	4.45680	2.07580
H	7.64070	5.01160	0.39650
O	-0.22320	6.51600	-1.18920
C	0.66840	7.55150	-0.80200
H	0.23490	8.48740	-1.15110
H	0.77850	7.58420	0.28520
H	1.65630	7.42750	-1.25210
O	6.66630	0.67400	3.07790
O	-6.95610	-2.40530	1.81550
O	1.03570	-5.77700	-1.74360
C	-7.16860	-3.22710	2.95430
H	-6.87330	-2.72160	3.87650
H	-8.23420	-3.44700	2.99300
H	-6.60570	-4.16050	2.87260
C	0.41990	-6.93320	-1.19310
H	0.86480	-7.79540	-1.68670

H	0.59000	-7.00800	-0.11620
H	-0.65800	-6.92320	-1.37590
C	7.39460	1.80990	3.51830
H	6.73070	2.54670	3.97470
H	8.10370	1.45300	4.26460
H	7.95950	2.27380	2.70860
Ge	-0.71160	-4.41540	-3.86770
Ge	2.32890	-5.09870	1.17740
Ge	4.82130	-1.12020	4.63360
Ge	6.51980	2.71860	0.41630
Ge	2.23790	5.16960	-2.90750
Ge	-5.94690	0.02160	3.74940
Ge	-5.88640	-4.05230	-0.58890
Ge	-2.23480	5.67990	0.98020
Pd	-0.25780	0.13590	2.30530
C	-1.31710	3.51760	-3.84810
H	-1.00260	4.41920	-3.31340
H	-1.25170	3.63840	-4.92700
O	-2.65560	3.20070	-3.48600
O	-0.51390	2.41800	-3.44230
O	0.27780	-0.42280	-4.06500
O	2.31460	-1.41970	-4.33980
C	1.20940	-0.86080	-5.04380
H	0.75230	-1.62330	-5.67150
H	1.55190	-0.00290	-5.63230
C	4.47380	-1.73740	-2.17930
C	5.36360	-1.54360	-0.94360
C	5.25690	-1.23550	-3.40650
C	4.19540	-3.24500	-2.33840
H	5.57640	-0.47930	-0.80030
H	4.84270	-1.88910	-0.04810
C	6.67250	-2.31740	-1.09290
H	5.46680	-0.16790	-3.28370

H	4.65160	-1.34630	-4.30690
C	6.56190	-2.01510	-3.56160
H	3.65010	-3.59670	-1.45800
H	3.54930	-3.41500	-3.20320
C	5.50420	-4.01520	-2.49820
H	7.27700	-2.16080	-0.19500
C	7.42850	-1.81350	-2.32030
C	6.37000	-3.80690	-1.25690
H	7.09140	-1.64880	-4.44580
C	6.24770	-3.50250	-3.73170
H	5.27920	-5.07890	-2.61790
H	8.37460	-2.35360	-2.42730
H	7.67140	-0.75290	-2.20070
H	5.85040	-4.18530	-0.37140
H	7.30400	-4.37000	-1.35000
H	5.63650	-3.65580	-4.62680
H	7.17540	-4.06640	-3.87090
C	-5.00620	2.08080	-1.65940
C	-5.80180	0.79380	-1.96610
C	-5.41400	3.14590	-2.68520
C	-5.40800	2.57890	-0.25800
H	-5.52490	0.43100	-2.96130
H	-5.53510	0.01040	-1.25180
C	-7.30400	1.05860	-1.89500
H	-5.14630	2.81280	-3.69080
H	-4.86700	4.07190	-2.49850
C	-6.91790	3.41290	-2.61240
H	-5.12960	1.83610	0.49300
H	-4.85320	3.49210	-0.02880
C	-6.91050	2.83780	-0.18710
H	-7.83820	0.12940	-2.11180
C	-7.68330	2.12690	-2.91850
C	-7.66280	1.54220	-0.49020

H	-7.17430	4.17860	-3.35000
C	-7.28710	3.90480	-1.21340
H	-7.16390	3.18440	0.81920
H	-8.76130	2.31360	-2.88610
H	-7.44390	1.77950	-3.92870
H	-7.39800	0.77530	0.24420
H	-8.74210	1.70720	-0.41350
H	-6.75860	4.83770	-0.99280
H	-8.35950	4.11750	-1.16120
Cl	0.42450	1.68480	3.98660
Cl	-1.14220	-1.34980	3.94790